

Simon J Lorentzen

# Understanding Energy Conversion in Combustion

A Detailed Analysis of Entropy Production in Flames

Master's thesis in Energy and the Environment Engineering

Supervisor: Ivar Ståle Ertesvåg

Co-supervisor: Ning Guo

June 2021



Simon J Lorentzen

# **Understanding Energy Conversion in Combustion**

A Detailed Analysis of Entropy Production in Flames

Master's thesis in Energy and the Environment Engineering  
Supervisor: Ivar Ståle Ertesvåg  
Co-supervisor: Ning Guo  
June 2021

Norwegian University of Science and Technology  
Faculty of Engineering  
Department of Energy and Process Engineering



Norwegian University of  
Science and Technology



## Preface

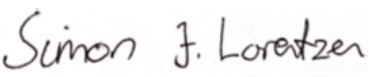
This project concludes the two-year MSc program *Energy and Environment Engineering*, at the Department of Energy and Process Engineering, at the Norwegian University of Science and Technology. The master thesis have been written in conjunction with the subject TEP920, and accounts for 30 ECTS credits.

First and foremost, a deep gratitude is owed to Ivar Ståle Erstesvåg for his immense help with the project. The project could not have been completed without his guidance, as well as all the numerous and long email threads. Furthermore, the extensive help received from Stefanie Tomasch in regard to the modeling tool and debugging of codes have been much appreciated. Great feedback and guidance on writing the thesis from co-supervisor Ning Guo were also highly valued.

Moreover, special thanks are owed to co-student Henriette Skaret-Kjos Hanssen for the mental support through the writing process, and Martin Sande for the assistance in keeping a strong and rigorous study, and workout routine, and both for the strong solidarity the last two years.

The love, support, and assistance from my brother Tomas Mikal Lorentzen, as well as my Girlfriend Lili Lan Nguyen have also been an essential factor in the completion of this masters degree. Finally, the rest of my fellow students in *Energy and Environment Engineering*, and at B430 have had a great impact on my two year period at NTNU.

Trondheim, June 11<sup>th</sup>, 2021

Signature: 

---

Department of Energy- and Process Engineering  
Norwegian University of Science and Technology

## Sammendrag

I dette prosjektet har tre forskjellige modeller for flammer blitt undersøkt: forblandet vel-blandet reaktor, forblandet fritt-spredene flamme, og ikke-forblandet motstrøms flamme. Målet med prosjekter var å først bestemme en måte å beregne entropiproduksjonen i flammer, samt hvordan den fordeles seg i rom, og deretter utføre en slik analyse på modellene nevnt over, med metan og syntese gass (syngas) som brensel. For hvert brensel ble det brukt detaljert, redusert, og globale mekanismer. GRI-mech 3.0 [41] ble brukt som den detaljerte mekanismen for begge brenslene, mens DRM19 [24] og Davis et al. [15] var de reduserte mekanismene brukt for metan og syngas, respektivt. For metan ble det bruke en global mekanisme med en reaksjon, laget av Westbrook og Dryer [47]. I midlertid ble det brukt to globale mekanismer for syngas. For den vel-blandete reaktoren, og motstrøms flammen ble en global mekanisme presentert av Cuoci [11] brukt. En annen mekanisme presenter av Marzouk og Huckaby [32] ble brukt for den fritt-spredene flammen. I tillegg til variasjon av forenkling i den kjemiske mekanismen var trykket variert mellom 1 atm, 10 atm og 20 atm. Dette resulterte i totalt 54 forskjellige tilfeller som skulle simuleres.

Entropi produksjonen ble beregnet i en post-prosess analyse i en separat kode for den fritt-utvidende flammen og motstrøms flammen, mens den var inkludert i koden for den vel-blanda reaktoren. For å validere koden ble entropi produksjonen beregnet for metan ved bruk av den detaljerte og redusert mekanismen, sammenlignet med Nishida et al. [35]. Dermed ble kodene for, den fritt-spredene flammen, entropi produksjonen, samt bruken av GRI-mech 3.0 [41] og DRM19 [24] for metan validert. Videre ble koden for motstrømsflammen, samt bruken av GRI-mech 3.0 [41] og Davis et al. [15] for syngas, validert mot Som et al. [42]. Den vel-blandete reaktoren var antatt å være såpass enkel at en omgående validering ikke var nødvendig. Den var derfor kun sammenlignet med manuelle beregninger.

To større hindre, blant flere små, ble møtt i prosjekt. Den ene var at Cantera [16] ikke gir ut flerkomponent diffusjons koeffisientene, nødvendig for entropi produksjon fra diffusjon, i hvert punkt i løsningen. Derfor ble i stedet stoffenes molare diffusjon hentet ut i hvert punkt og brukt i utregningene. Den andre var entropi produksjon fra intern varmeoverføring fra reaksjonene til luft-brensel blandingen måtte tas med for reaktoren, i tillegg til produksjonen fra reaksjonene som først var antatt å være den eneste kilden. Når hindrene var overkomne ble flammene simulert, og entropi produksjonen og dens distribusjon i rommet ble beregnet.

Fra resultatene ble det oppdaget at både for den vel-blandete reaktoren og den fritt-spredene flammen, økte den integrerte entropi produksjonen med trykket for begge brenselene, ved bruk av alle mekanismene. I motsetning sank produksjonen for begge brenselene, ved bruk av alle mekanismer i motstrøms flammen. Grafene som viste den lokale produksjonen ble høyere og smalere for begge stoffene, og alle mekanismene i den fritt-spredene flammen. Profilen for den lokale produksjonen i motstrøms flammen var mindre avhengig av trykket.

Videre ble det oppdaget at den redusert mekanismen for metan fungerte bra for å beregne den integrerte og den lokale produksjonen for den fritt-spredene flammen, men hadde noen avvik for motstrøms flammen. Den reduserte mekanismen for syngas fungerte bra i begge modellene. Den globale mekanismen for methan fungerte bra for å beregne den integrerte produksjonen i alle modellene. Den hadde noe avvik ved 1 atm for den fritt-spredene flammen, og ved 10 atm og 20 atm for motstrøms flammen. Den globale mekanismen brukt for syngas i den fritt-spredene flammen fungerte ikke bra. Den globale mekanismen brukt i de andre modellene fungerte derimot overraskende bra.

## Abstract

In this project, three different flame models have been investigated, namely premixed well-stirred reactor, premixed freely-propagating flame, and non-premixed counterflow flame. The objective of the project was to figure out a way to analyse the entropy production in flames, and how it is distributed in space, and thereafter perform such an analysis on the flame models mentioned. In the analyses, methane and syngas were used as fuels. For each fuel it was used one detailed, one reduced and one global mechanism. GRI-mech 3.0 [41] was used as the detailed mechanism for both fuels, while DRM19 [24] and [15] was used as the reduced mechanisms for methane and syngas, respectively. For methane, a global mechanism consisting of one equation created by Westbrook and Dryer [47] was used. Meanwhile, for syngas two global mechanisms were used. For the well-stirred reactor, and the non-premixed counterflow flame, a global mechanism presented by Cuoci et al. [11] was used. Another global mechanism presented by Marzouk and Huckaby [32] was used for the last model. In addition to varying the chemical mechanism, in degree of simplification, the pressure was varied between 1 atm, 10 atm, and 20 atm. This resulted in a total of 54 individual cases to be simulated.

The entropy production was estimated in a post-process analysis in a separate code for the freely-propagating and counterflow flames, while it was included in the code for the well-stirred reactor. To validate the codes, the entropy production estimated for methane using both the detailed, and reduced mechanisms were compared with results obtained by Nishida et al. [35]. Thus, the code for the freely-propagating flame, the use of GRI-mech [41] and DRM19 [24] for methane, as well as the post-process analysis code were validated. The code written for the counterflow flame, as well as the use of GRI-mech [41] and Davis et al. [15] for syngas, were validated against Som et al. [42]. The well-stirred reactor was considered to be of such simplicity that an extensive validation was unnecessary. The values obtained for entropy was however crosschecked with manually. This was also done for the freely-propagating flame.

Two larger obstacles, amongst more less time-demanding obstacles, were met during the project. Firstly, the multi-component diffusion coefficient necessary for the calculation of entropy production due to mass diffusion was not given by Cantera [16]. Therefore, the species mole fluxes were retrieved rather than the coefficients. Secondly, it was discovered that the entropy change in the reactor was not caused by the chemical reactions alone, as initially thought. The entropy production due to internal heat transfer from the reactions to the fuel-air mixture also had to be accounted for. With all obstacles sorted, the flames were simulated, and the entropy production, with its distribution in space was estimated.

It was discovered that both in the well-stirred reactor model, and the freely-propagating flame model the integrated entropy production increased with pressure for both fuels, with all mechanisms. In contrast, the production decreased for both fuels, with all mechanisms in the counterflow model. The profiles of the local entropy production got thinner and taller for both fuels in the freely-propagating flame. The counterflow model was less pressure dependent.

Furthermore, the reduced mechanism for methane worked well for the integrated entropy production and the local production in the freely-propagating flame, but had some discrepancies in the counterflow flame. The reduced mechanism for syngas worked well in both models. The global mechanism for methane worked well to calculate the integrated production in both models, but had discrepancies for the local production at 1 atm for the freely-propagating flame, and at 10 atm, and 20 atm for the counterflow model. The global mechanism used for syngas in the freely-propagating model did not work, and was not appropriate to use. The global mechanism used in the reactor and counterflow flame models worked well.

## Nomenclature

$D_i^T$	thermal diffusion coefficient i (kg/ms)
$D_{ij}$	multicomponent diffusion coefficient, relating species i to species j ( $\text{m}^2/\text{s}$ )
$J_i$	diffusive mass flux of species i ( $\text{kg}/\text{s} \cdot \text{m}^2$ )
$N_R$	number of reactions (—)
$N_S$	number of species (—)
$Q$	heat transfer across boundary ( $\text{W}/\text{m}^2$ )
$R_u$	universal gas constant ( $\text{J}/\text{kmol} \cdot \text{K}$ )
$T$	temperature (K)
$V_i$	mass diffusion velocity of species i (m/s)
$W_i$	molar mass of species i (kg/kmol)
$X_i$	molar fraction (—)
$Y_i$	mass fraction (—)
$\Delta G_j$	change in Gibbs free energy for each reaction ( $\text{J}/\text{kmol}$ )
$\lambda$	thermal conductivity ( $\text{J}/\text{s} \cdot \text{m} \cdot \text{K}$ )
$\mu$	viscosity ( $\text{Pa} \cdot \text{s}$ )
$\overline{AF}$	Molar air-fuel ratio
$\phi$	equivalence ratio
$\rho$	mass density ( $\text{kg}/\text{m}^3$ )
$\sigma$	volumetric entropy generation rate ( $\text{J}/\text{s} \cdot \text{m}^3 \cdot \text{K}$ )
$\tau$	viscous stress tensor (Pa)
$d_j$	diffusion driving force of species j ( $\text{m}^{-1}$ )
$k_{fj}, k_{rj}$	forward, reversed rate coefficient of reaction j ( $\text{m}^{-1}$ )
$p$	pressure (Pa)
$q_j$	net rate of progress of elementary reaction j ( $\text{mol}/\text{m}^3 \cdot \text{s}$ )
$u$	velocity (m/s)



$v'_{ij}, v''_{ij}$  stoichiometric coefficients of species  $i$  in reaction  $j$ , of the reactants, and products

$x$  spatial coordinates (m)

# Table of Contents

<b>Preface</b>	<b>I</b>
<b>Sammendrag</b>	<b>II</b>
<b>Abstract</b>	<b>III</b>
<b>Nomenclature</b>	<b>IV</b>
<b>1 Introduction</b>	<b>1</b>
1.1 Motivation and Background . . . . .	1
1.2 Previous Work . . . . .	1
1.2.1 Premixed Flames . . . . .	2
1.2.2 Non-Premixed Flames . . . . .	3
1.2.3 Reactor . . . . .	3
1.2.4 Chemical Mechanism . . . . .	4
1.3 Present Contributions . . . . .	5
1.3.1 Objectives . . . . .	5
1.3.2 Scope . . . . .	5
1.3.3 Research Questions . . . . .	6
<b>2 Theory</b>	<b>7</b>
2.1 Chemical Kinetics . . . . .	7
2.2 Diffusive Mass Flux . . . . .	7
2.3 Viscous Forces . . . . .	8
2.4 Radiation . . . . .	8
2.5 Equivalence Ratio . . . . .	9
2.6 Entropy . . . . .	9
2.6.1 The Second Law of Thermodynamics . . . . .	9
2.6.2 Definition . . . . .	10
2.6.3 Reacting Systems . . . . .	12
2.6.4 Gibbs Function . . . . .	12
2.6.5 Entropy Production . . . . .	13
2.7 Exergy . . . . .	14
2.8 Flame Models . . . . .	15
2.8.1 Freely-Propagating Laminar Premixed Flame . . . . .	15
2.8.2 Counterflow Laminar Non-Premixed Flame . . . . .	16
2.8.3 Governing Equations . . . . .	17
2.8.4 Boundary Conditions . . . . .	18
2.9 Reactor Model . . . . .	20
2.9.1 Continuously Stirred Tank Reactor . . . . .	20
2.9.2 Governing Equations . . . . .	20

<b>3</b>	<b>Methodology and Case Configuration</b>	<b>22</b>
3.1	Cantera . . . . .	22
3.1.1	Usage . . . . .	22
3.1.2	Reaction Rates . . . . .	22
3.1.3	Reacting Medium . . . . .	23
3.1.4	Grid Refinement Criteria . . . . .	23
3.1.5	Solver . . . . .	23
3.2	Varying Conditions . . . . .	24
3.2.1	Fuel Type and Oxidizer . . . . .	24
3.2.2	Models . . . . .	24
3.2.3	Chemical Mechanism . . . . .	24
3.2.4	Inlet Pressure . . . . .	26
3.2.5	Overview of Cases . . . . .	27
3.3	Model Setup . . . . .	27
3.3.1	Laminar, Premixed, Freely-Propagating Flame . . . . .	27
3.3.2	Laminar, Non-Premixed, Counterflow Flame . . . . .	28
3.3.3	Continuously Stirred Tank Reactor . . . . .	28
3.4	Entropy Production . . . . .	29
3.4.1	Flame Models . . . . .	29
3.4.2	Reactor Model . . . . .	29
<b>4</b>	<b>Validation</b>	<b>32</b>
4.1	Laminar, freely-propagating, premixed flame . . . . .	32
4.2	Laminar, counterflow, diffusion flame . . . . .	34
4.3	Entropy Change . . . . .	36
<b>5</b>	<b>Results and Discussion</b>	<b>37</b>
	<b>Well-Stirred Reactor</b>	<b>37</b>
5.1	Methane . . . . .	37
5.2	Syngas . . . . .	38
5.3	Comparisons . . . . .	39
	<b>Premixed, Freely-Propagating</b>	<b>41</b>
5.4	Methane . . . . .	41
5.4.1	Comparison of Cases. . . . .	41
5.4.2	1 atm . . . . .	42
5.4.3	10 atm . . . . .	48
5.4.4	20 atm . . . . .	55
5.4.5	Solution Grid . . . . .	62
5.5	Syngas . . . . .	63
5.5.1	Comparison of Cases. . . . .	63
5.5.2	1 atm . . . . .	64
5.5.3	10 atm . . . . .	75

5.5.4	20 atm . . . . .	82
5.5.5	Solution Grid . . . . .	89
<b>Non-premixed, Counterflow Flame</b>		<b>90</b>
5.6	Methane . . . . .	90
5.6.1	Comparison of Cases. . . . .	90
5.6.2	1 atm . . . . .	92
5.6.3	10 atm . . . . .	99
5.6.4	20 atm . . . . .	106
5.6.5	Solution Grid . . . . .	113
5.7	Syngas . . . . .	113
5.7.1	Comparison of Cases. . . . .	114
5.7.2	1 atm . . . . .	116
5.7.3	10 atm . . . . .	124
5.7.4	20 atm . . . . .	132
5.7.5	Solution Grid . . . . .	138
<b>6</b>	<b>Conclusion</b>	<b>139</b>
6.1	Objective . . . . .	139
6.2	Entropy Production . . . . .	139
6.3	Effect of Chemical Mechanism . . . . .	139
6.4	Effect of Pressure . . . . .	140
<b>References</b>		<b>141</b>
<b>Appendices</b>		<b>145</b>
	Spatial resolution . . . . .	146

# 1 Introduction

## 1.1 Motivation and Background

For centuries humanity has relied on combustion to help satisfy its energy usage. In the early years, combustion was used to cook food and give warmth in the form of bonfires. Through the years, the use of combustion has been extended beyond what was imaginable when the first flame was lit many millenniums ago. In modern times, combustion is used in far more complicated processes such as engines in cars, or electricity production.

The International Energy Agency (IEA) claim in their report the world energy outlook 2020 [18], that even though the COVID-19 pandemic caused a decrease in energy demand in 2020, it is predicted to rise and surpass the previous energy demand by 2023. IEA also has statistical data on the world energy balance [17], and it shows that despite the growth in renewable energy usage, fossil fuels still are the dominate source of energy. Since fossil fuel sources are limited, in addition to the consequences from emissions of greenhouse gases, renewable energy usage will further increase in the future. However, combustion of fossil fuels have some advantages like higher reliability, as it is not weather dependent, and are therefore ensured a continued share in the energy balance.

Fossil fuels are used in combustion to generate electricity, heat, and movement. By devoting time and resources to improve combustion technology, efficiency can be increased and thereby decrease emissions. When combustion efficiency is investigated, exergy analysis has over time become a well employed tool used by thermal engineers [44], because entropy and exergy are physical properties that are used to describe how useful energy is.

Bejan [5] shows that maximum power out of a power plant, is directly related to minimum entropy production. Consequently, exergy or entropy analysis combined with numerical simulation tools can be a crucial tool in the improvement of combustion, as it can give valuable analysis results without conducting experiments. Accordingly, studying entropy production in laminar flames can give a valuable insight into entropy production in combustion, and is therefore the main objective of this project, which is further specified in the Section 1.3.

## 1.2 Previous Work

The range of problems to study regarding flames is broad. Many investigations and analyses have been performed, studying different fuels with varying configurations and conditions. The conditions are defined by parameters that differ in degree of importance, and some have greater impact on the simulations than others. Deciding to include or neglect turbulence has a significant impact on the simulations. In the current project, turbulence is not included, and it is therefore focused on previous works with laminar systems. Whether the fuel and air are mixed before (premixed), or after (non-premixed/diffusion) ignition is another example of an important decision. Furthermore, the choice of model for the system will have a great impact on the simulations. Other parameters can be variations in the inlet condition such as equivalence ratio, temperature, or pressure. Moreover, which chemical mechanism to use to simulate the flame is a parameter of great significance. These are some common parameters in analyses, and below it is presented a variety of previous

works considering some of them. The section is divided into parts according to what is presumed to be the parameters of most importance, that is premixed and non-premixed flames, reactors, and chemical kinetics. These parameters are selected as they have great impact on the simulation, and their results differ notably.

### 1.2.1 Premixed Flames

Firstly presented are previous works on premixed flames, with various configurations. Two examples of entropy analyses performed on a configuration not considered in this project are executed by Jejurkar with various co-authors [19][20]. In the first article, the effects of wall thermal conductivity in a  $H_2$ -air flame was investigated. As a conclusion it is stated that irreversibilities due to combustion decreased when the conductivity was increased, and that entropy production due to diffusion was most affected. The second analysis considered the effects of using a multistep kinetics. It was discovered that schemes neglecting  $HO_2$  did not simulate the combustion accurately, as reactions containing this species had a high contribution to entropy production. Porous media is another possible configuration that is not considered in the present project. Mohammadi [33] investigated the effect that the degree of porosity has on entropy production. At higher degrees of porosity the contribution from chemical reactions and heat transfer decreased, while contributions from mass diffusivity increased.

One example of an analysis considering the same premixed configuration as the present project is conducted by Nishida et al. [35]. The effects that changing the fuel between methane and hydrogen has on entropy productions was investigated. Additionally, the equivalence ratio and inlet temperature was varied. One of the conclusion was that chemical reactions had the highest contribution to entropy production using both fuels. Furthermore, it was concluded that increasing the inlet temperature made the entropy production decrease, while decreasing the equivalence ratio increased it.

Another example using the same configuration as in the present project with syngas is done by Acampora and Marra [4], where entropy production with different values of hydrogen molar fraction was analysed. The analysis was executed with different equivalence ratios for both atmospheric pressure, as well as ten and fifty times the atmospheric pressure. The study concluded that with an increase in the molar fraction of hydrogen, the entropy production increased, but as the exergy in the outlet decreased it balanced out. Both the contributions from chemical reaction and heat conduction were strongly dependent on pressure, and the contribution from the former decreased as the contribution from the latter increased. Higher temperatures also lead to lower entropy production.

As can be seen from this section some possible parameters to study are factors of the configurations such as wall thermal conductivity and porosity. Other parameters can be: temperature, equivalence ratio, inlet pressure, fuel type, molar fraction or kinetics. There exists many more combinations of laminar flame configurations and parameters that are possible to study. However, as time and resources are limited it is necessary to limit the parameters to investigate. The selected articles also show that the combination of the parameters chosen for consideration in this report have not been done before.

### 1.2.2 Non-Premixed Flames

Secondly, some examples are presented of articles where non-premixed flames are studied. In the same manner as with premixed flames, there are many alternative configurations. As an example, Puri [38] considers the entropy production in spray combustion to optimize the working conditions. It was found that large droplets, with large Reynolds numbers are optimal. Another example is flames where the fuel and oxidizer flows are co-flowing instead of counter-flowing as they are in this project. Datta [13] has performed an analysis on entropy generation in a co-flowing flame with methane and air. The inlet air temperature, and fuel ratio was considered. The results showed that irreversibilities due to heat transfer was the dominant contributor to entropy production, while contributions due to fluid friction could be neglected. Increasing the inlet temperatures was shown to decrease entropy production, while decreasing the air-fuel ratio increased it. Also, the walls had an effect on the production and adiabatic walls lead to less production. Additionally, Datta [14] studied the effects of gravity on a confined, co-flowing, methane-air flame. The study found that the flame got wider in structure and less intense at lower gravity. The contribution from heat transfer was very dependent on gravity, and increased with increased gravity. Meanwhile, the contribution due to chemical reactions and mass transfer was insensitive to changes in gravity.

As mentioned above, this project considers counterflow flames. Chen et al. [10] have conducted a first- and second-law analysis on a hydrogen-air counterflow flame. The inlet air temperature and equivalence ratio is varied over a wide range of values. One innovative feature of the analysis is that the results are mapped with regard to equivalence ratio and inlet air temperature. In this way, it is easier to decide the final combustion regime. Using the same configuration Chen et al. [9] have studied the effects of hydrogen addition in a ultra lean methane-air flame. Increasing hydrogen addition is shown to decrease the contribution from heat transfer, but increased contribution from mixing. The entropy generation is nearly insensitive to changes in the equivalence ratio.

Additionally, Chen et al. [8] have investigated the entropy production in a counterflow hydrogen-air flame. Here, it was concluded that the molar fraction of hydrogen had little impact on the entropy production, while it was heavily dependent on inlet Reynolds number. Liu et al. [28] have also used a counterflow configuration, but have looked into MILD combustion with biogas. The two most common ways of establishing such combustion is with  $\text{CO}_2$  or  $\text{H}_2\text{O}$  and oxygen, and the study by Liu et al. compared the two options. One of the conclusions stated that the  $\text{CO}_2\text{--O}_2$  environment, in all cases, was better than the  $\text{H}_2\text{O--O}_2$  environment in regard to entropy production.

There are an abundance of articles with varying fuels, configurations and analysing parameters, that have not been included in this report. From the ones included it can be seen that Reynolds number, inlet temperature, fuel-air ratio, gravity, equivalence ratio, dilution, molar composition, and fuel type are some common parameters to analyse in counterflow diffusion flows.

### 1.2.3 Reactor

The last configuration that is considered in this project is a reactor, and some examples of studies using reactors will be presented in this section. In the first example, Acampora with various co authors [2][3] have investigated the effects of changing the chemical mechanism on combustion in reactors. In the first study the chemical mechanism varied between a global, two-step, reduced, and detailed mechanism for batch and perfectly stirred reactors. It was concluded that by studying

the entropy production it could be decided whether a mechanism was capable of replicating the dynamics of a batch reactor. Also, the stability of a perfectly stirred reactor could be illustrated. In the second article, the same four mechanisms were used for a perfectly stirred reactor with methane-air combustion, to see which mechanisms could adequately replicate the dynamics of the reactor. It was discovered that when the detailed mechanism was used as the reference mechanism, only the reduced mechanism was adequate.

Reactor models have been used to minimize entropy production in combustion, as exemplified by the articles presented next. Nummedal et al. [36] developed a method for minimizing the entropy generation in an exothermic reactor, using only the ammonia reaction with a fixed production. It was discovered that by allowing the reactor to vary in length, the entropy production could decrease by 16%. Zuo et al. [49] investigated a modified micro reactor to reduce entropy production, by varying the chamber diameter. The flame consisted of premixed hydrogen-air, and the results showed that the modified reactor had a lower entropy production. The parameters that were varied in the investigation were the flow rate, equivalence ratio, the diameter of the inlet and outlet, and the solids. Johannessen and Kjelstrup [21] studied a plug flow reactor, and developed a method for minimizing the entropy production. Optimal control theory was used, and as a conclusion it was found that by varying the length, the entropy production could be reduced by 24.7% for oxidation of  $\text{SO}_2$ .

Marra et al. [31] have conducted an analysis on methane-air combustion in a continuously stirred tank reactor to map the extinction line in regard to equivalence ratio and residence time. The response of the systems to periodically forcing the residence time was also considered. One of the conclusions was that two frequencies could be defined, one high where the system is insensitive to oscillations, and one low where the oscillations result in extinction. Also, to be adequate under oscillating conditions, it was discovered that a mechanism should be adequate under non-oscillating conditions.

The articles presented stands to show that the reactor configuration can be used in several types of investigations. studies can consider the effects of chemical mechanisms, reactor length, flow rate, equivalence ratio, diameters and residence time, amongst other parameters.

#### 1.2.4 Chemical Mechanism

As chemical mechanism plays an important role in the current project, some articles regarding entropy production are included. Slattery et al. [40] states in an article that the entropy inequality often is ignored. A theorem is derived, stating that if all reactions are both reversible and conform to the law of mass action, the entropy inequality is automatically satisfied. The article also gives three examples where the inequality is violated, and emphasizes that the inequality must be imposed. Jones et al. [22] continue the research, and show how to modify chemical mechanisms, by using the theorem, so that the entropy inequality is not violated. The method is tested, and the results are closer to the experimental results when the mechanism is reduced using the proposed method.

Kooshkbaghi [26] proposes another systematic approach for the reduction of mechanisms to avoid this issue. In this approach the contributions to the entropy production, from all the reactions are considered to see which ones should be included. An advantage with this approach is that the amount of equations included are flexible. Acampora et al. [1] continues and presents a generalized method for mechanism reduction. Finally Porras et al. [37] uses another approach, where the local



timescales are used in combination with the local entropy production. The method is shown to have great potential to adequately simulate the dynamics of a system.

The selected articles shows that entropy production in regards to chemical mechanisms have been investigated. However, it has not been studied in the same extent as in the current project, with the combination of parameters chosen.

## 1.3 Present Contributions

The collection of previous studies presented above stands to show that there have been conducted studies considering many different sets of parameters. However, to the extent of the authors knowledge it has not been presented any studies or previous works considering the combinations of configurations and conditions as presented in the following section.

### 1.3.1 Objectives

The main objective is to be able to analyse combustion, and investigate the entropy production and its spatial distribution. Part of the objective is to figure out a suitable method to calculate the entropy production. Furthermore, the purpose is to compare different approaches such as variations in the conditions, or the degree of simplification.

The entropy production will be compared with the total change in entropy in the system, where this is appropriate. This will give insight into how well the chemical mechanisms can replicate the systems, and especially the entropy production. In addition to this, by comparing the entropy production in the different cases, with different conditions, factors causing increased or decreased production may be elucidated. Moreover, if the characteristics are only valid for certain cases or in a more general sense.

### 1.3.2 Scope

In Section 1.2, it is given examples of previous works considering various parameters. Due to limited time and resources the parameters that are varied in the current analysis must be carefully selected. First of all, the simulations will be executed using two different fuels, methane and synthetic gas (syngas). The chemical mechanism will vary between a detailed, reduced and global mechanism. The three different configurations to be examined are a premixed, laminar, freely-propagating flame, a non-premixed, laminar, counterflow flame, and a premixed, laminar, constant volume and pressure, well-stirred reactor. The entropy production, due to the five irreversible processes (heat conduction, mass diffusion, viscous dissipation, thermal radiation, and chemical reactions) will be calculated.

Furthermore, the Soret flux is taken into account as a multicomponent formulation is used for the transport model. Radiation is included, but only for the counterflow diffusion flame. It does not make sense to include it for the reactor as it is adiabatic. It attempted to include radiation for the premixed, freely-propagating flame. However, it is common to not include it ([35], [1]), and the model used for radiation [29] is designed for counterflow flames. Even though there are changes in the inlet pressure, it is constant in the axial and radial direction, and mass diffusion due to pressure difference are therefore also excluded. Inlet temperature will not be varied and are kept

constant in all cases. The equivalence number is not varied, and is equal to one for the premixed well-stirred reactor, and freely-propagating flame, while it is decided by the mass flow rate for the non-premixed, counterflow flame. The mass flow rate will also not be varied.

### 1.3.3 Research Questions

To ensure that it is explicitly clear what the research in the current project is about, the following research questions may be formulated:

- *How is the entropy production calculated for premixed well-stirred reactor, premixed freely-propagating flame, and non-premixed counterflow flame affected by changes in pressure when it is varied between 1 atm, 10 atm, and 20 atm? and degree of simplification in the chemical mechanism, when methane and syngas are used as fuels?*
- *How is the entropy production calculated for premixed well-stirred reactor, premixed freely-propagating flame, and non-premixed counterflow flame affected by changes in the degree of simplification in the chemical mechanism, when it is varied between detailed, reduced, and global mechanisms?*
- *How does the effect of the pressure change, and variation of chemical mechanism, differ when syngas and methane are used as fuels?*

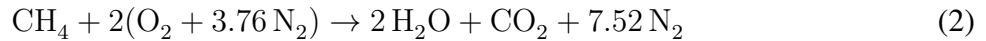
## 2 Theory

### 2.1 Chemical Kinetics

Chemical kinetics is defined in Turns [45](Chapter 4), as the study of elementary reactions and their rates. It is an important part of combustion as the chemical reaction rate controls the rate of combustion. The net production rate of an equation is the forward reaction rate, subtracted by the backward reaction rate, and is calculated as shown in Equation 1.  $\nu'_{ij}$  and  $\nu''_{ij}$  are the stoichiometric coefficients of species  $i$ , in reaction  $j$  of the reactants and products, respectively.  $k_{fj}$  and  $k_{rj}$  are the forward and reverse rate coefficients of reaction  $j$ , respectively. Furthermore,  $N_s$  is the number of species,  $Y_i$  is the mass fraction and  $W_i$  is the molar weight of species  $i$ .

$$q_j = k_{fj} \prod_{i=1}^{N_s} \left( \frac{\rho Y_i}{W_i} \right)^{\nu'_{ij}} - k_{rj} \prod_{i=1}^{N_s} \left( \frac{\rho Y_i}{W_i} \right)^{\nu''_{ij}} \quad (1)$$

To simulate combustion it is necessary to collect information regarding the species, and a set of equations describing the various reaction. Such collections are called chemical mechanisms. The simplest form of a chemical mechanism is when only a global reaction is utilized. An example of a global reaction is presented in Equation 2, which describe stoichiometric combustion of methane in air, where the air is assumed to be a 21/79 mixture of oxygen and nitrogen. Methane is destroyed through oxidation and creates water and carbon dioxide. Nitrogen does not react and is a so-called inert gas. Realistically, when combustion occurs it is in multiple steps called elementary reactions. There exist more complex mechanism considering these reactions called detailed mechanisms which can contain hundreds, or even thousands of equations. Sometimes the detailed mechanisms are not necessary, and a reduced mechanism can be used that contain only the equations regarded as most important.



### 2.2 Diffusive Mass Flux

In Kee [25] Chapter 4.3 diffusive mass flux is explained, with basis in Fick's law. If there is a solution containing different species and the composition is not homogeneous, meaning the concentration of a certain species is higher in one location than another, molecular diffusion will transport that species to even out the differences. Furthermore, the diffusive mass flux of that species will depend on a diffusion coefficient.

In this project a multicomponent transport formulation is used, and therefore the coefficient is a multicomponent diffusion coefficient denoted  $D_{ij}$ , relating species  $i$  to species  $j$ . This coefficient is used to calculate the mass diffusion velocity  $V_i$  for species  $i$  as shown in Equation 4. In this equation  $d_j$  represents the gradients in the concentration and pressure field, and is calculated according to Equation 5. The pressure gradient term is also referred to as the Dufour flux. The last term in Equation 4, containing the thermal diffusion coefficient  $D_i^T$  represents the Soret flux. With the species diffusion velocity and mass fraction, in addition to the solution density, the diffusive mass flux can be calculated according to Equation 3. In the equations presented below  $Y_i$  and  $X_i$  are the

mass and molar fraction of species  $i$ , respectively.  $W_i$  is the molar weight of species  $i$ , while  $\bar{W}$  is the average molar weight of the solution.  $N_s$  stand for number of species,  $T$  is temperature,  $x$  is spatial position,  $p$  is pressure, and  $\rho$  is the solution density.

- Species mass flux

$$J_i = \rho Y_i V_i \quad (3)$$

- Mass diffusion velocity

$$V_i = \frac{1}{X_i \bar{W}} \sum_{j \neq i}^{N_s} W_j D_{ij} d_j - \frac{D_i^T}{\rho Y_i} \frac{\partial \ln T}{\partial x} \quad (4)$$

- Diffusion driving force

$$d_i = \frac{\partial X_i}{\partial x} + (X_i - Y_i) \frac{\partial}{\partial x} (\ln p) \quad (5)$$

## 2.3 Viscous Forces

Viscous forces relate to the viscosity of a solution. In many systems and calculations it is considered to be negligibly small and not accounted for. In this project the normal viscous stress is included, but only in the flame models as these are one-dimensional. It would not be logical to include it in the reactor model, as it is zero-dimensional. The equation used for the viscous stress is obtained from Turns [45](Chapter 7), and is presented in Equation 6. Here  $\mu$  denotes the viscosity of the solution,  $u$  is flame speed and  $x$  is the spatial position.

$$\tau = \mu \left( \frac{\partial u}{\partial x} + \frac{\partial u}{\partial x} \right) - \frac{2}{3} \mu \frac{\partial u}{\partial x} \quad (6)$$

## 2.4 Radiation

In Turns [45], Chapter 13, flame radiation is explained for jet flames. It is stated that turbulent non premixed flames can be highly radiating. Further, Turns state that the radiation in some cases is wanted, and other times unwanted as it can decrease efficiency. In Turns [45], Chapter 8, it is also stated under the physical description of laminar premixed flames that hydrocarbon flames are recognizable for their visible radiation. On the basis of these arguments it was decided that radiation should be included in the simulations. The model used for radiation in the tool utilized in this project is that of Liu and Rogg [29]. Here, the expression for radiation flux is given by the equation below.

$$\frac{\partial q_R}{\partial x} = 2k_p (2\sigma T^4 - B_w - B_e) \quad (7)$$

In this equation,  $x$  is spatial position,  $k_p$  denotes the Planck mean absorption coefficient,  $\sigma$  is the Stefan-Boltzmann constant, and  $B = \epsilon \sigma T^4$ , where  $\epsilon$  denotes the mean emissivity.

## 2.5 Equivalence Ratio

A short description of equivalence ratio is appropriate, as it is an important parameter in combustion. The global equation representing methane combustion in air presented in Equation 2 describes stoichiometric complete combustion, where all the air and fuel are used to produce water and carbon dioxide. The amount of air required to obtain complete combustion is called the theoretical amount of air. The fuel-air ratio is the number of moles fuel, divided by the total number of reactants as illustrated in Equation 8. If a combustion process has any other amount of air than the theoretical air, the actual fuel-air ratio divided by the theoretical fuel-air ratio is called the equivalence ratio  $\phi$ . Accordingly, the equivalence ratio for Equation 2 has a value of one.

$$\overline{AF} = \frac{n_{fuel}}{n_{reactants}} \quad (8)$$

$$\phi = \frac{\overline{AF}_{actual}}{\overline{AF}_{theoretical}} \quad (9)$$

## 2.6 Entropy

### 2.6.1 The Second Law of Thermodynamics

Entropy is a thermodynamic property, which is closely related to the second law of thermodynamics. The second law is introduced in Chapter 5 of Moran and Shapiro [34], and has many applications such as establishing guidelines for the direction of a process. The first law of thermodynamics states that energy cannot be created or destroyed, only transformed from one form to another, however it does not state the direction of the energy transfer. In some cases this may be intuitive, take for example a mug with coffee, if left alone the temperature of the coffee will adjust to the surroundings. In more complex, and less intuitive systems, the second law gives indications on the direction of the process in situations that are not as simple as the example given, by using entropy which will be explained in Section 2.6.2.

Additionally, the second law can be used in determining the best theoretical performance of various systems such as combustion. Returning to the previous example, when the coffee reacts with its surrounding, and the temperature decreases until equal temperatures are reached, the heat released could in theory have been used in a more useful way than merely heating up the surroundings. For example, considering combustion as illustrated in Figure 1, the heat released can either be released to the surroundings as shown in system 1, or it can be used to evaporate water and the steam can be used to produce electricity in a turbine, as illustrated by system 2. The second law can be used to estimate the theoretical maximum of heat, or work that can be extracted from such a system and thereby determine the best theoretical performance of that system.

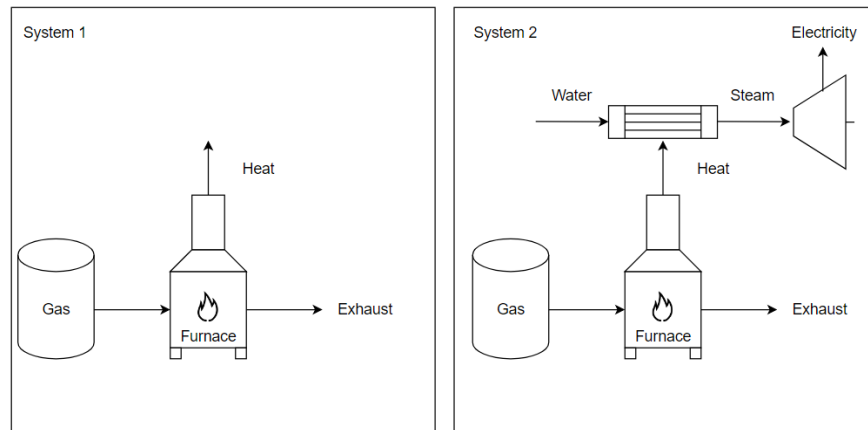


**Figure 1:** Example of system of combustion with, and without utilization of the heat released.

The main reason that the theoretical maximum of work or heat cannot be extracted from a system is the presence of irreversibilities in the system. Irreversibilities are processes where it is not possible to restore the system and its surroundings to its respective initial states. Revisiting the coffee mug example, the reversed process where the temperature of the mug suddenly increases, cannot occur spontaneously without an additional device. The irreversible processes considered in this project are heat conduction, viscous dissipation, mass diffusion and chemical reactions.

### 2.6.2 Definition

The Kelvin-Planck statement of the second law of thermodynamics is given in Chapter 5 of Moran and Shapiro [34] as below.

*It is impossible for any system to operate in a thermodynamic cycle and deliver a net amount of energy by work to its surroundings while receiving energy by heat transfer from a single thermal reservoir.*

The significance of the statement above is that it is impossible to design a system produces positive work, while receiving heat from a single reservoir. This statement has resulted in many corollaries, one being the Clausius inequality. The inequality is derived using the energy balance combined with the Kelvin-Planck statement and is presented in Equation 10, as in Chapter 6 of Moran and Shapiro [34].

$$\oint \left( \frac{\delta Q}{T} \right)_b \leq 0 \quad (10)$$

In Equation 10  $\delta Q$  is the heat transferred over a part of the boundary  $b$ , with the temperature  $T$ . The circle on the integral indicate that the integral is to be calculated over the entire thermodynamic cycle. Accordingly, all heat transfer over every part of the boundary are summed up and that the total must be less than, or equal to zero. The integral will have a negative value if there are irreversibilities in the system, and zero if the system is composed of reversible processes. It is impossible for the integral to have a positive value.

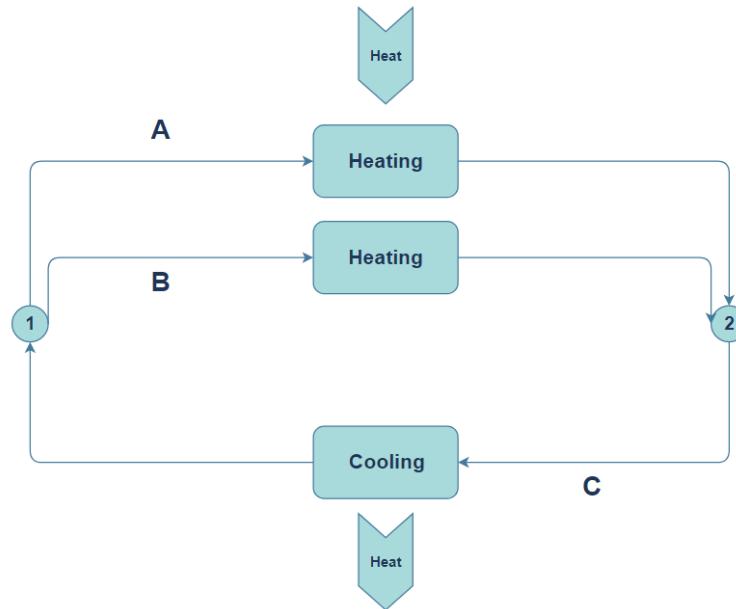


**Figure 2:** Example of system with three processes in two cycles.

In Chapter 6 of Moran and Shapiro [34] an arbitrary closed system with two cycles is used to define entropy change. In the same manner, the system in Figure 2 can be used to define entropy change. The system also consist of two cycles, made up of three adiabatic, reversible processes. From state 1, an arbitrary medium is heated through either process A or B to state 2. From the second state the medium cooled to state 1 through process C. Since all the processes are reversible the integral in Equation 10 from state 1 to state 2 and back will have a value of zero for both the cycles.

Furthermore, the integrals have equal value indicating that it represents the change in a property of the system, as the change is independent of the process. This property is denoted entropy, and from this conclusion the definition for entropy change is given in Equation 11. Here the subscript stands as a reminder that the integral applies for internally reversible processes. In practical systems there will always be irreversibilities, and it is therefore somewhat confusing that the entropy change is defined by an integral over reversible processes. However, since a property is independent of the process, the change in entropy is equal regardless if the process is internally reversible or not.

$$S_2 - S_1 = \left( \int_1^2 \frac{\delta Q}{T} \right)_{internally\ reversible} \quad (11)$$

Equation 11 can be rearranged to obtain Equation 12, where it becomes evident that processes always proceed in the direction of increasing entropy. Therefore, studying the entropy change gives an indication of the direction of a process, similarly to the second law. Moreover, looking at Figure 1, in system 1 the heat released by combustion will have a higher temperature which results in a higher entropy according to Equation 12. Contrary, in system 2 the heat is transferred to the water and the energy is utilized to produce heat. As a result the temperature, and thereby the entropy will be lower at the exit of the turbine. This difference in entropy at the exit indicates a

higher thermodynamic efficiency in the second system, and the figure serves as an example of how entropy can be used.

$$S_2 = S_1 + \left( \int_1^2 \frac{\delta Q}{T} \right)_{internally\ reversible} \quad (12)$$

Equation 12 calculates the entropy change for an internally reversible process. When there are irreversibilities present the entropy balance must be expanded. For open systems such as the models considered in the current project, the new balance is presented in Equation 13. This equation gives the entropy change over a control volume. The first term is the entropy transferred to or from the control volume over boarder  $j$  due to heat transfer with temperature  $T_j$ . The second term is the entropy accompanying mass transfer at inlet  $i$ , while the last term is the entropy accompanying mass transfer at the exit  $e$ .

$$\frac{dS_{cv}}{dt} = \sum_j \frac{\dot{Q}_j}{T_j} + \sum_j \dot{m}_i s_i - \sum_e \dot{m}_e s_e + \dot{\sigma}_{cv} \quad (13)$$

### 2.6.3 Reacting Systems

In systems where there are no chemical reactions, so-called non-reacting systems, the value for the entropy in a state can be extracted in numerous ways such as tables, graphs or integrals. Additionally, when the change in entropy is interesting, the reference point from which the entropy is calculated can be arbitrary as it cancels out. Contrary, when reacting systems are considered it is important to have a predetermined common datum from which the entropy is calculated. The datum is determined by using the third law of thermodynamics, which in Moran and Shapiro [34](Chapter 13) is stated as below.

*The entropy of a pure crystalline substance is zero at the absolute zero of temperature, 0 K. Substances not having a pure crystalline structure at absolute zero have nonzero value of entropy at absolute zero.*

The entropy calculated from this datum is referred to as the absolute entropy and can be calculated using Equation 14. Equipped with this equation it is possible to calculate the entropy change in a reacting system such as combustion.

$$s = s_{ref}^\circ + \int_{T_{ref}}^T C_p \frac{dT}{T} - R_u \cdot \ln \left( X_i \cdot \frac{p}{p_{ref}} \right) \quad (14)$$

### 2.6.4 Gibbs Function

Another parameter related to entropy, necessary for the calculation of the entropy production due to chemical reactions is the Gibbs function which is defined as in Equation 15. As mentioned above, this project considers reacting systems and it is therefore necessary with a predetermined common datum. This issue is already taken care of for the entropy in Section 2.6.3, but also needs to be resolved for the enthalpy. The common datum is ensured by using the enthalpy of formation, and



the total enthalpy is calculated according to Equation 16. In this equation the first term on the left hand side denoted  $h_f^\circ$  is the enthalpy of formation, while the integral is the definition of enthalpy change with constant pressure.

$$g = h - Ts \quad (15)$$

$$h = h_f^\circ + \int_{T_{ref}}^T C_p dT \quad (16)$$

In this project the total change in Gibbs function of a reaction is required, and is calculated as shown in Equation 17. The letters on the right hand side are in uppercase, which indicates that the term consist of the sum of changes for each of the product species, subtracted the reactant species. In other words, Equation 14 and Equation 16 are firstly used to calculate the total entropy and enthalpy of the products, respectively. secondly, the same equations are used for the reactants and these values are then subtracted from the total entropy and enthalpy of the products giving the total change of Gibbs function.

$$\Delta G = \Delta H - T\Delta S \quad (17)$$

### 2.6.5 Entropy Production

As stated in Section 1.3.1, viscous dissipation, heat conduction, mass diffusion, chemical reactions, and thermal radiation are the irreversible processes considered in the present project. These are the reason for the entropy production that leads to changes in the entropy. The integrated value of their respective contributions summed up should therefore equal the total change in entropy in the system. Their equations are given as Equations 18-22, in the same order as the processes were mentioned. In Equation 20 and Equation 21 for mass diffusion and chemical reactions, the contributions are the accumulated contributions from every species and reaction, respectively. The equations used for the entropy production due to the four first processes were taken from a thesis submitted for a PhD, written by Salimath and Ertesvåg [39], with the title "*Numerical simulations of combustion at solid and hydrogen permeable walls*". In this project, as in the project cited above, the Dufour flux is neglected in the entropy generation calculations. Equation 22 was obtained in cooperation with the supervisor, from the radiation model [29].

$$\sigma_{visc} = \frac{\tau}{T} \frac{\partial u}{\partial x} \quad (18)$$

$$\sigma_{cond} = \frac{\lambda}{T^2} \left( \frac{\partial T}{\partial x} \right)^2 \quad (19)$$

$$\sigma_{diff} = \sum_{i=1}^{N_s} (-J_i) \left( \frac{1}{T} \frac{\partial h_i}{\partial x} - \frac{\partial s_i}{\partial x} \right) \quad (20)$$

$$\sigma_{chem} = \sum_{j=1}^{N_R} -\frac{\Delta G_j}{T} \cdot q_j \quad (21)$$

$$\sigma_{rad} = \frac{Q_R}{T^2} \cdot \frac{\partial T}{\partial x} \quad (22)$$

In Equation 20, the last term including enthalpy and entropy can be rewritten. As the gas is assumed to be an ideal gas, the following relations applies, which allow the term to be rewritten as shown in Equation 23.

$$\begin{aligned} dh_i &= C_{p,i}dT & ds_i &= (C_{p,i})dT - (R_i/p_i)dp_i \\ R_i &= R_u/W_i & p_i &= X_i p \\ \left( \frac{1}{T} \frac{\partial h_i}{\partial x} - \frac{\partial s_i}{\partial x} \right) &= \frac{R_i}{p_i} \frac{\partial p_i}{\partial x} = \frac{R_u}{W_i} \left( \frac{1}{X_i} \frac{\partial X_i}{\partial x} + \frac{1}{p} \frac{\partial p}{\partial x} \right) \end{aligned} \quad (23)$$

## 2.7 Exergy

Exergy is explained in detail in Chapter 7 of Moran and Shapiro [34]. As exergy is not the main focus in this project it is only described briefly. It has many similarities to entropy, and is also defined with basis in the second law of thermodynamics. Considering an arbitrary system and a suitable predefined environment, the thermomechanical exergy is the maximum theoretical work obtainable from the interactions between the system and the environment until equilibrium is reached. The exergy balance gives the change in exergy between two states, and can be derived from the entropy and energy balance and is presented in Equation 24. In this equation,  $Q$  is the heat transferred over the boundary with temperature  $T_b$ , while  $T_0$  and  $p_0$  are the temperature and pressure of the environment, respectively. Furthermore,  $W$  is the work done by, or on the system,  $\sigma$  denotes the entropy production,  $V_1$  is the volume of the system in the first state, and  $V_2$  is the volume in the second state.

$$E_2 - E_1 = \int_1^2 \left( 1 - \frac{T_0}{T_b} \right) \delta Q - [W - p_0(V_2 - V_1)] - T_0\sigma \quad (24)$$

The first term, and second term in Equation 24 accounts for the exergy transferred to or from the system by heat and work, respectively. The last term including  $\sigma$  determine the exergy destroyed by irreversibilities, and is the term most relevant for the current project. In many thermal systems, such as the system in the present project that considers combustion, the exergy supplied to the system mainly originates from the exergy of the fuel. Because the system considered in the present project is a reacting system, it is necessary to introduce the chemical exergy in addition to the thermomechanical exergy. The chemical exergy is defined in Chapter 13.6 of Moran and Shapiro [34] as the maximum theoretical work obtainable by allowing the system to react with the environment by oxidation. Equation 25 shows how the chemical exergy of the fuel is calculated. Here,  $a$  and  $b$  are the number of moles of carbon and hydrogen in the fuel, respectively.  $\bar{h}$  is the total specific enthalpy, and  $\bar{s}$  is the total specific entropy of the various species at  $T_0$  and  $P_0$ .  $\bar{R}$  is the universal gas constant, and  $X^e$  is the molar fraction of the species in the environment.

$$\begin{aligned} \bar{e}^{ch} = & \left[ \bar{h}_F + \left( a + \frac{b}{4} \right) \bar{h}_{O_2} - a\bar{h}_{CO_2} - \frac{b}{2}\bar{h}_{H_2O} \right] (T_0, p_0) \\ & - T_0 \left[ \bar{s}_F + \left( a + \frac{b}{4} \right) \bar{s}_{O_2} - a\bar{s}_{CO_2} - \frac{b}{2}\bar{s}_{H_2O} \right] (T_0, p_0) \\ & + \bar{R} \ln \left[ \frac{\left( X_{O_2}^e \right)^{a+\frac{b}{4}}}{\left( X_{CO_2}^e \right)^a \left( X_{H_2O}^e \right)^{\frac{b}{2}}} \right] \end{aligned} \quad (25)$$

## 2.8 Flame Models

In this project, two different flame configurations will be investigated. These two configurations are premixed freely-propagating and non-premixed counterflow flames. The simulations are done using the same governing equations for both, presented in Section 2.8.3. The flames are distinguished by their boundary conditions presented in Section 2.8.4.

### 2.8.1 Freely-Propagating Laminar Premixed Flame

Freely-propagating flame is explained in Turns, Chapter 8 [45]. A typical freely propagating flame would be initiated in a tube, where the fuel and air are mixed. For the freely-propagating, premixed, flame model the temperature profile is a crucial characteristic. An example of such a profile is presented in Figure 3, where the dashed line shows the temperature variation. The other lines represent the species molar fraction profiles for the reactants and products in the global equation of methane combustion in air shown in Equation 2. The graph illustrates that as the temperature rise, the reactants in the equation is destroyed while products are created.

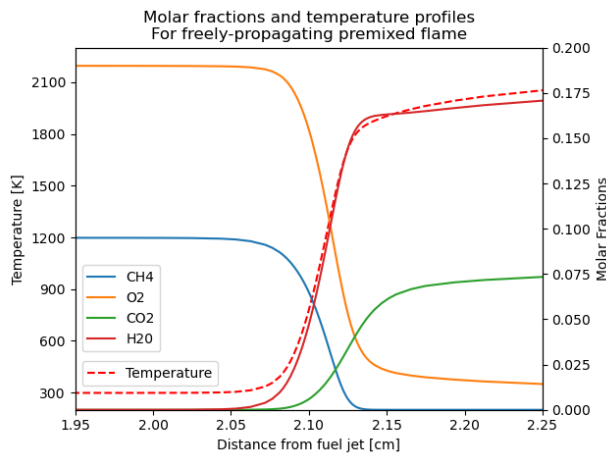


**Figure 3:** Illustration of the characteristics of a premixed, laminar, freely-propagating flame. The molar fractions of selected species are compared with the temperature over the spatial position.

At atmospheric pressure the flame region is quite thin, as stated by Turns in Chapter 8 [45]. It is also indicated that the flame thickness is inversely proportional to pressure, meaning that when the pressure increases the flame thickness is expected to decrease. The general thin structure results in large temperature and species concentration gradients. The governing equations are presented in Section 2.8.3, with boundary conditions as explained in Section 2.8.4.

### 2.8.2 Counterflow Laminar Non-Premixed Flame

When a counterflow flame is non-premixed, it is created by two opposing jets where one consists of fuel and the other of oxidizer, as explained by Turns [45] in Chapter 9, and illustrated in Figure 4. When the two jets meet, they create a stagnation plane indicated with a dashed line in the figure. If the jet initial momentum fluxes are equal, the plane will exist at the center between the jets. If one flux is larger than the other, the plane will shift towards the jet with the lower initial momentum flux. If a flame is ignited it will stabilize where the streams meet in near stoichiometric conditions. Furthermore, as shown in the figure and explained in detail in Kee et al. [25], Chapter 7, the flame appears to be flat. There seems to be no variations in the radial direction, which is a strong indication that the flame is only dependent on the axial position and can be treated as one dimensional. The governing equations are the same as for the freely-propagating flame, and are presented in Section 2.8.3, with accompanying boundary conditions presented in Section 2.8.4.

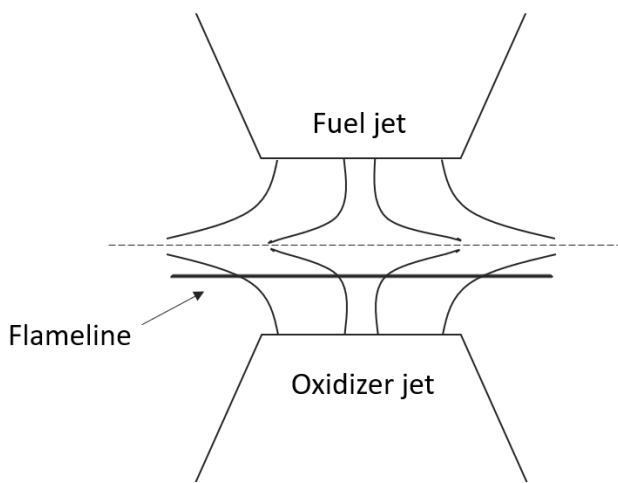


**Figure 4:** Illustration of a laminar, diffusion, counterflow flame, where the initial jet momentum of the fuel jet is higher than the oxidizer jet.

Figure 5 illustrates a normal characteristic profile for a laminar, counterflow, diffusion flame. Here, the flame is stationed where the temperature profile has its peak. The oxidizer and fuel are consumed in the flame, while products such as H<sub>2</sub>O and CO<sub>2</sub> are created.

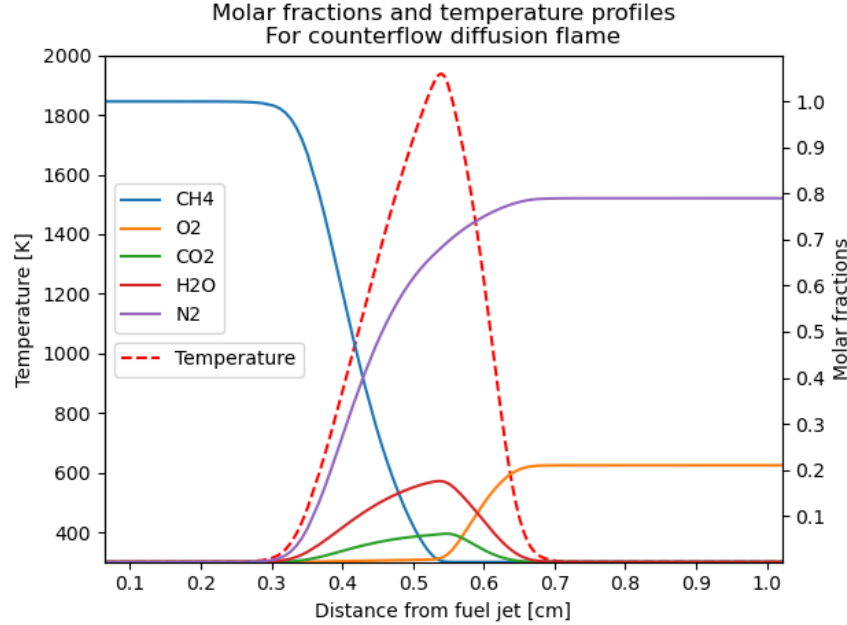


**Figure 5:** Illustration of the characteristics of a diffusion, laminar, counterflow flame. The molar fractions of selected species are compared with the temperature over the spatial position.

### 2.8.3 Governing Equations

The governing equations used in the present project, for both the freely-propagating and counterflow flame are derived from the three-dimensional steady state Navier-Stokes equations, confined to the  $z$ - $r$  plane, as done by Kee et al., Chapter 7 [25]. A similarity solution, which involves a principal assumption, is used to reduce the equations to one-dimensional. The assumption is that there exist a boundary layer, in which the temperature and species composition depend on only one parameter.

Further, the derivation make use of two conjectures. The first being that a stream function, with the separable form given in equation 26, is used to describe the velocity field. In the equation,  $U(x)$  is an unspecified function of  $x$  alone. The function is later specified by using the definition of stream functions. The second conjecture states that temperature, species composition and density only varies in the axial direction. However, the pressure may vary, but only according to a constant  $\Lambda_r$  as shown in equation 27.

$$\Psi(x, r) = r^2 U(z) \quad (26)$$

$$\frac{1}{r} \frac{\partial p}{\partial r} = \lambda_r \quad (27)$$

By using the conjectures and assumption mentioned above, in addition to the definition of stream functions, the complete set of governing equation shown below is obtained. Here, the equation regarding the axial momentum is decoupled from the rest. Meaning that the velocity, temperature and composition fields can be estimated without considering this equation.

- Continuity

$$\frac{\partial \rho u}{\partial x} + 2\rho V = 0 \quad (28)$$

- Axial momentum

$$\rho u \frac{\partial u}{\partial x} = -\frac{dp}{dx} + \frac{4}{3} \frac{\partial}{\partial x} \left[ \mu \frac{\partial u}{\partial x} - \mu V \right] + 2\mu \frac{dV}{dx} \quad (29)$$

- Radial momentum

$$\rho u \frac{dV}{dx} + \rho (V^2 - W^2) = -\Lambda_r + \frac{d}{dx} \left( \mu \frac{dV}{dx} \right) \quad (30)$$

- Energy

$$\rho c_p u \frac{\partial T}{\partial x} = \frac{\partial}{\partial x} \left( \lambda \frac{\partial T}{\partial x} \right) - \sum_i J_i c_{p,i} \frac{\partial T}{\partial x} - \sum_i h_i W_i \dot{\omega}_i \quad (31)$$

- Species

$$\rho u \frac{\partial Y_i}{\partial x} = -\frac{\partial J_i}{\partial x} + W_i \dot{\omega}_i \quad (32)$$

- Equation of state

$$p = \rho R T \sum_{i=1}^{N_s} \frac{Y_i}{W_i} \quad (33)$$

In the governing equations presented in Equations 28-33,  $u$  is the flame speed in x-direction,  $V$  is the scaled vertical velocity equal to  $v/r$ , and  $W$  is the scaled velocity in the z-direction equal to  $w/r$ .  $\rho$  is the solutions density,  $p$  is pressure,  $x$  is spatial position,  $\mu$  is the viscosity of the solution, and  $T$  is temperature.  $-\Lambda_r$  is a constant representing the changes in pressure along  $r$ .  $c_p$ , and  $c_{p,i}$  denotes the specific heat capacity of the solution and species  $i$  at constant pressure, respectively.  $\lambda$  is the thermal conductivity of the solution, and  $J_i$  is the species mass flux of species  $i$ .  $h_i$ ,  $W_i$ ,  $\dot{\omega}_i$ , and  $Y_i$  are the enthalpy, molar weight, molar production rate, and mass fraction of species  $i$ . Lastly,  $N_s$  is the number of species, and  $R$  is the universal gas constant.

#### 2.8.4 Boundary Conditions

The flame models use the same set of equations, and only differ in the boundary conditions used [7]. When the premixed, freely-propagating flame model is used it will use the inlet boundaries in Equation 34, and the outlet boundaries presented in Equation 35. For the non-premixed, counter-flow flame there are one fuel inlet, and one oxidizer inlet. Accordingly, the boundary conditions presented in Equation 34 is applied on both inlets.

**Inlet Boundary and Assumptions** If there is an inlet at  $x_0$ , the following equations are solved. Here,  $T_0$  is temperature,  $V_0$  is the scaled radial velocity while  $Y_{i,0}$  is the species mass fractions.  $\dot{m}_0$  denoted the mass flow rate, and if it is specified, the second to last equation is solved. Otherwise the last equation is solved.

$$\begin{aligned}T(x_0) &= T_0 \\V(x_0) &= V_0 \\ \dot{m}_0 Y_{i,0} - J_i(x_0) - \rho(x_0)u(x_0)Y_i(x_0) &= 0 \\ \rho(x_0)u(x_0) &= \dot{m}_0 \\ \Lambda(x_0) &= 0\end{aligned}\tag{34}$$

**Outlet Boundary** If there is an outlet at the boundary at  $x_0$ , the following equations are solved.

$$\begin{aligned}\Lambda(x_0) &= 0 \\ \left(\frac{\partial T}{\partial x}\right)_{x_0} &= 0 \\ \left(\frac{\partial Y_i}{\partial x}\right)_{x_0} &= 0 \\ V(x_0) &= 0\end{aligned}\tag{35}$$

Furthermore, it is important to remember that certain assumptions have been made. For the sake of order, the most important assumptions are considered below.

- Laminar
- Ideal gas
- Steady axisymmetric stagnation flows
- Combustion in infinite reservoir
- Constant pressure
- Kinetic and potential energies are neglected
- Radiation only accounted for by the non-premixed, counterflow flame
- For the non-premixed, counterflow flame only diffusion in the axial direction is considered

## 2.9 Reactor Model

In Turns, Chapter 6 [45], reactors are used to explain how chemical kinetics can be used together with with fundamental conservation principles, such as the conservation of mass or energy. There are many different reactors of interest, and Turns mentions constant-pressure fixed-mass, constant-volume fixed-mass, well-stirred and plug-flow reactors. These systems are simple due to assumptions made about them, for example it is assumed in the first three systems that all state variables are spatially uniform, as the systems are perfectly mixed. This assumption also applies for the current project, as the reactor used here is a continuously stirred tank reactor.

### 2.9.1 Continuously Stirred Tank Reactor

Reactors can interact with the surroundings in various ways, such as heat and mass transfer, or expansion and compression. In this project the continuously stirred tank reactor (CSTR) is considered, where the only interaction with the surroundings is the transfer of mass. This kind of reactor is also known as well-stirred reactor or perfectly-stirred reactor, and Figure 6 serves as an illustration for the model. In Kee et al., Chapter 9.5 [25], such idealized reactors are explained as reactors where gas enters at a certain mass flow rate, with a temperature and composition. As soon as the gas enters the reactor it mixes perfectly, thus there are no spatial gradients for the temperature or composition. The outlet condition is also assumed to be equal to the condition within the tank. Since there are no gradients it does not make sense to graph any temperature, or species molar profiles as previously done in Figure 3 and Figure 4.

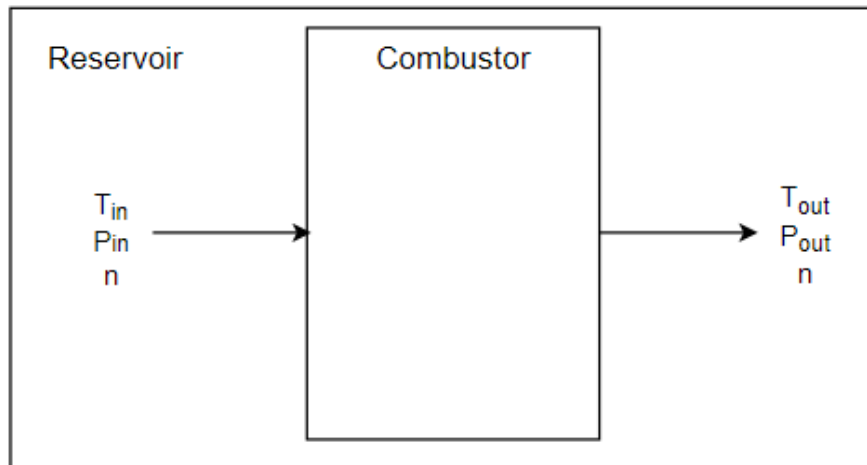


Figure 6: Model Illustration, Single Reactor

### 2.9.2 Governing Equations

The governing equations used were those derived by Kee et al. in Chapter 9.5 [25]. The terms resulting from wall interaction have been omitted as wall reactions are not considered in this project. The summation signs are included in case there are multiple inlets and, or outlets. In the equations presented below  $m$  is the mass in the reactor, while  $\dot{m}$  is mass flow rate.  $Y_i$ ,  $\omega_i$ , and  $W_i$  denotes the



mass fraction, volumetric molar reaction rate, and molar weight of species  $i$ , respectively. In the energy equations,  $c_v$  denotes the constant volume heat capacity inside the reactor.  $T$ ,  $V$ , and  $p$  are temperature, volume, and pressure in the reactor.  $\dot{Q}$  is heat transfer in or out of the reactor, while  $h$  is enthalpy and  $u_i$  is the internal energy of species  $i$  transferred to the reactor by mass.

- Mass Conservation

$$\frac{dm}{dt} = \sum_{in} \dot{m}_{in} - \sum_{out} \dot{m}_{out} \quad (36)$$

- Species Conservation for Homogeneous Phase Species

$$m \frac{dY_i}{dt} = \sum_{in} \dot{m}_{in} (Y_{i,in} - Y_i) + V \dot{\omega}_i W_i \quad (37)$$

- Energy Conservation (Ideal Gas Reactor)

$$m c_v \frac{dT}{dt} = -p \frac{dV}{dt} - \dot{Q} + \sum_{in} \dot{m}_{in} \left( h_{in} - \sum_i u_i Y_{i,in} \right) - \frac{pV}{m} \sum_{out} \dot{m}_{out} - \sum_i V \dot{\omega}_i W_i \quad (38)$$

Since the governing equations make up a complete system of equations it is not necessary with any boundary conditions. However, it is important to remember that there have been made some assumptions. The most important ones are listed below.

- Ideal gas
- Constant volume
- Constant pressure
- Adiabatic
- Well stirred - Homogeneous solution inside reactor

## 3 Methodology and Case Configuration

The project can for the sake of order be divided into two parts. The first part concerns the simulations of the selected combustion models, using the pre-determined conditions explained in Section 3.2. The second part considers the post-process analysis with the codes written for this project, on the results obtained from the simulations. This section begins by explaining the tools that was utilized in project in Section 3.1. Further, as mentioned above, Section 3.2 presents the different cases and variation in conditions. Section 3.3 explains in more detail the methodology for simulating the various cases in Cantera [16]. Lastly, Section 3.4 explains the details of the post-process analysis.

### 3.1 Cantera

#### 3.1.1 Usage

Python is the programming language used to write the codes that make up the program utilized in the simulations and post process analysis. Cantera [16] can be thought of as a package or a toolbox that can be incorporated into such programs. By doing so, the program can make use of all the functions and tools that comes with Cantera. These functions are applicable in various problems, especially where chemical kinetics or transport properties are important. Since turbulence is excluded, Cantera is an appropriate, well-employed tool and is considered to be adequate to use rather than more complex computational fluid dynamics (CFD) programs. Additionally, it is open-source which is advantageous.

Cantera is often used to simulate combustion or flames, and it is possible to operate with different models. These models can either be zero- or one-dimensional. The zero-dimensional models are reactors, such as ideal gas reactor, constant pressure reactor or flow reactor. Meanwhile, freely propagating, counterflow, and burner stabilized flat flames are examples of the one-dimensional laminar flame models.

To initialize a simulation, an input file is required. The file must contain the chemical mechanism with the relevant properties for the reactions and species included in the mechanism. The phase, content and condition of the reacting medium can be specified as desired. With the input file, model, and condition, the simulations can be executed and Cantera can solve the governing equations of the selected model. In the following sections, some of the aspects of Cantera relevant to the current project will be explained.

#### 3.1.2 Reaction Rates

In Cantera the forward reaction coefficient is estimated by using the Arrhenius function, as shown in Equation 39. Meanwhile, the reversed rate coefficient is estimated from the relation with the equilibrium constant, illustrated in Equation 40. In these equations  $k_{fj}$  and  $k_{rj}$  denotes the forward, and reverse reaction rate coefficients of equation  $j$ , respectively.  $A$  is the pre-exponential factor,  $T$  is temperature,  $b$  is the temperature exponent,  $E_a$  is the activation energy,  $R$  the universal gas constant, and lastly  $K_{Cj}$  is the equilibrium constant of reaction  $j$ . As can be seen from the lack of pressure terms, the coefficients depend on temperature alone.

$$k_{fj} = AT^b \exp\left(\frac{-E_A}{RT}\right) \quad (39)$$

$$k_{rj} = \frac{k_{fj}}{K_{Cj}} \quad (40)$$

### 3.1.3 Reacting Medium

The reacting medium can be determined in different ways, and can be in various phases. For example, it is possible to use a pure fluid consisting of purely  $\text{CO}_2$ . Another example is the interface representing reacting two-dimensional interfaces, or dusty gas which models gas in a stationary, solid, porous medium. In this project, the reacting medium is modeled as a solution. This models a chemically reacting solution which can be a mixture of gases, liquids or solids.

### 3.1.4 Grid Refinement Criteria

For the flame models, where there is a spatial extent, Cantera can perform grid refinements. If this is activated, the criteria for refinement can be specified. The parameters to specify are ratio, slope, curve, and prune. The first parameter add a point in the grid if the spacing on either side of the grid point exceeds its value. The slope adds points in the regions where the maximum difference in value between two points beside each other, scaled by the maximum difference in the profile exceeds the constraint. Curve uses the maximum difference in slope between two adjacent points, scaled by the maximum difference in the profile, to decide if a new point is required. Lastly, prune removes points where the slope and curve criteria are sufficiently satisfied.

### 3.1.5 Solver

For Cantera to solve the equations for the desired model with the specified conditions, the solve statement must be called. When the solver is called it is also possible to pass additional statements. One such statement is the grid refinement mentioned in Section 3.1.4. The default is on, and it has to specified if it is not desired. Also when the solver is called, the amount of logical output can be determined. The output can be varied on a scale from one to 8 for the flame models, and to 5 for the reactor model.

Another statement that is possible to pass with the solver is an auto statement. If the auto statement is set to True, the solver will first try to solve the equations using the initial width with the energy equation enabled. Then, if it does not converge to a solution, the solver will systematically try a fixed-temperature solution, with grid refinement enabled, and if it succeeds the energy equation is enabled again. A small inconvenience with the auto statement is that if the multi-component transport model is used, the solver will change it to mixture averaged. This only had a consequence for the flame models, and the issue was solved by first solving the equations using the mixture-averaged model, with the auto statement, and afterwards solving the system using the multi-component model without the auto statement.

When the equations are solved and the simulations are finished, Cantera returns various results such as temperature, flame speed, and species composition. These results can be further utilized in

the post-process analysis. If a one-dimensional model is used, the results are given along the axial extent of the flame. When a zero-dimensional model is used, the results have no spatial or temporal extent. The results are therefore given as homogeneous results valid for the entire volume of the reactor. The convergence criteria, and time steps were not changes and had the default values set by Cantera [16].

## 3.2 Varying Conditions

In the following sections, the values for the parameters that were varied for the different cases are presented.

### 3.2.1 Fuel Type and Oxidizer

Methane and syngas were the fuel types chosen for investigation in the current project. All subsequent variations and simulations will be done for both these fuels. Methane was chosen because it is a well-employed fuel in simulations as can be seen in Section 1.2. Additionally, natural gas can consist of 64-98% methane, according to a study by Dagaut [12]. Therefore, methane can be used as a surrogate fuel to investigate, instead of natural gas which is more complex.

Synthesis gas is mainly composed of a carbon monoxide and hydrogen mixture, but can also contain other species such as  $\text{CO}_2$ ,  $\text{H}_2\text{O}$ , or  $\text{N}_2$ . The gas can be produced from coal, natural gas, or biomass amongst other sources, and the primary application is electricity production [27]. Furthermore, Turns [45] enunciate in Chapter 5 that the oxidation of carbon monoxide is extremely important for the oxidation of hydrocarbons. These two statements make two compelling arguments as to why synthesis gas should be investigated.

The air was modeled as a 21/79 mixture of oxygen and nitrogen. The synthetic gas was modeled as a 50/50 mixture of carbon monoxide ( $\text{CO}$ ) and hydrogen ( $\text{H}_2$ ) mixture. The composition of syngas can vary greatly, and industrial syngas often consist of 66.7%  $\text{CO}$  and 33.3%  $\text{H}_2$ . However, 50/50 mixture is often used in the literature, and as a base case for comparison [27]. When methane was used it was considered to be pure without dilution.

### 3.2.2 Models

The models used in the present project were the ideal gas reactor, laminar freely-propagating premixed flame, and laminar counterflow diffusion flame. Choosing three different configurations with clear distinctions can give an indication for whether a result is characteristic for that particular configuration, or is relevant to all of them. The configurations mentioned were chosen because the reactor model is premixed and zero-dimensional, the freely-propagating model is premixed and one-dimensional, and the counterflow diffusion model is non-premixed and one-dimensional. They are therefore models with very clear differences, and can make similarities or dissimilarities in the results evident. Specifications regarding the models are given in Section 3.3

### 3.2.3 Chemical Mechanism

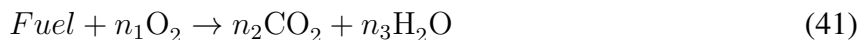
For all three of the selected models, with both the selected fuel types, simulations were run using three different chemical mechanisms. One detailed, one reduced, and one global reaction mech-

anism. The results obtained from the reduced and global mechanism can be compared with the results from the detailed mechanism to elucidate any loss in information.

The mechanism chosen as the detailed mechanism for both of the fuels was Gri-Mech 3.0 [41], which contains 325 reactions involving 53 different species. Gri-Mech 3.0 is a common mechanism to use for modeling methane combustion. The mechanism is optimized for modeling natural gas flames and ignition [41]. As stated in Section 3.2.1, natural gas consist mostly of methane and the detailed mechanism is therefore considered to be an appropriate mechanism. Furthermore, syngas can be obtained from natural gas and Gri-Mech 3.0 [41] is therefore assumed to be an appropriate detailed mechanism for syngas as well. Additionally, it was stated in Section 3.2.1 that the oxidation of CO is an important part of the oxidation of hydrocarbons. It stands to reason then, that a well-employed mechanism for methane combustion, which is a hydrocarbon, should be suitable for the combustion of syngas as well.

The reduced mechanism used for methane was DRM 19 [24]. It is a mechanism reduced from Gri-Mech 1.2, and contains 19 species (21 counting argon and nitrogen) and 84 reactions. As the mechanism is reduced from Gri-Mech 1.2 it is considered to be a good choice for methane. A reduced mechanism optimized for H<sub>2</sub>/CO combustion has been developed by Davis et al. [15]. This mechanism contains 14 species and 38 reactions and was used as the reduced mechanism for syngas.

The global mechanism used for methane combustion was obtained from Westbrook and Dryer [47]. Here, a single-step mechanism for the combustion of hydrocarbon is presented as in Equation 41, where  $n_1, n_2, n_3$  are decided depending on the hydrocarbon chosen as the fuel. For methane the equation turns into Equation 2, if nitrogen is included. If nitrogen is not included the coefficients are still the same. The values required for the Arrhenius function in Cantera was chosen from Westbrook and Dryer, Table 2, Set 3. Unlike the reduced and detailed mechanisms, for which files were readily available online, the file containing the global mechanisms had to be created. This was done using a copy of the file containing the detailed mechanism, Gri-Mech 3.0 [41]. The file was kept the same, keeping the information about the species thermodynamics. Only the 325 reactions where changed with the global reaction. The reason for keeping the information regarding all the species was to ensure that air was still modeled properly as a 21/79 mixture of N<sub>2</sub> and O<sub>2</sub>, amongst other reasons.



For the combustion of syngas, two mechanisms where utilized. One mechanism was used for the reactor, and counterflow flame model, while another mechanism was used for the premixed, freely-propagating flame model. The first model is presented by Cuoci et al. in a conference paper [11]. In the paper the authors present optimized versions of a global mechanism created by Dryer and Westbrook [48], and Jones and Lindstedt [23]. The Dryer-Westbrook mechanism was chosen as it contains no reversible reactions, in contrast to Jones and Lindstedt's which have one reversible and two irreversible reactions. The Dryer-Westbrook mechanism is as presented below. Note that the third reactions appear to have been added by Cuoci et al. [11].



The corresponding forward reaction rates are as presented below. Note that the order of the pre-exponential factors are not according to the article, as they are transformed to ensure appropriate units. The units for the reaction rates are cm, mol, cal, and s.

$$\begin{aligned}k_1 &= 2.30 \cdot 10^{14} e^{\frac{-31700}{RT}} [\text{CO}][\text{H}_2\text{O}] \\ k_2 &= 4.45 \cdot 10^9 e^{\frac{-41300}{RT}} [\text{CO}_2] \\ k_3 &= 1.35 \cdot 10^{11} e^{\frac{-6900}{RT}} [\text{H}_2]^{0.87} [\text{O}_2]^{1.10}\end{aligned}\tag{43}$$

The second mechanism used for syngas combustion if created by Watanabe and Otaka [46], as presented in the comparative study by Marzouk and Huckaby [32], Appendix B, Table 4. The reason for using this version rather than the original source is that Marzouk and Huckaby presents the mechanism in the same units used in this project, that is, cm, mol, cal, and s. Additionally, they corrected some smaller errors in conversation with Dr Watanabe. The mechanism is shown below.



The corresponding forward reaction rates are as shown below.

$$\begin{aligned}k_1 &= 1.209 \cdot 10^{18} T^{-1} e^{\frac{-40000}{RT}} [\text{H}_2]^{0.25} [\text{O}_2]^{1.5} \\ k_2 &= 3.981 \cdot 10^{14} e^{\frac{-40000}{RT}} [\text{CO}][\text{O}_2]^{0.25} [\text{H}_2\text{O}]^{0.5} \\ k_3 &= 2.75 \cdot 10^{12} e^{\frac{-20000}{RT}} [\text{CO}][\text{H}_2\text{O}]\end{aligned}\tag{45}$$

### 3.2.4 Inlet Pressure

Finally, the pressure was varied between the atmospheric pressure (atm) as well as 10 atm and 20 atm. 20 atm was chosen as the maximum pressure, because the ideal gas assumption was employed, and it is not valid with exceeding pressures. Three different pressure values were considered sufficient, as more could yield an unnecessary amount of results. 1 atm, 10 atm and atm was chosen to ensure a good range of pressure values.

### 3.2.5 Overview of Cases

Figure 7 shows an overview for all the individual cases that were simulated for each model. It was executed a total of nine simulations per model, with three different models this results in 27 simulations. Since both methane and syngas was used in all models the total number of simulations was 54.

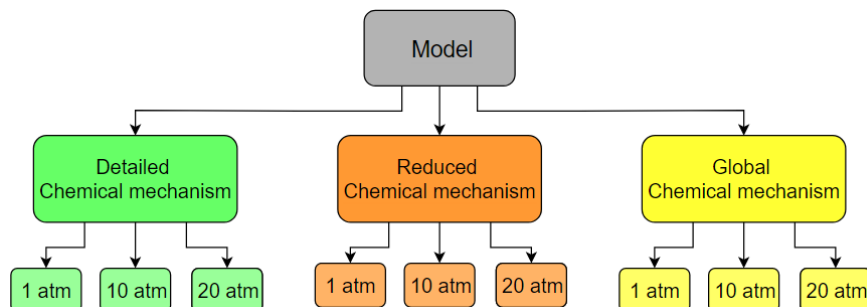


**Figure 7:** Overview of the individual cases for each model.

## 3.3 Model Setup

In this section a more detailed description of how the different cases were set up is presented. For all the models the mechanism, inlet pressure, and fuel were allowed to vary so that a separate code was not necessary for each case. The inlet temperature were in all cases set to be 300 K. The level of logical output was set to one for all cases, as an higher number only resulted in unnecessary information in this project. In all cases the reacting medium was created as a solution, made up of the specified fuel or a fuel-air mixture depending on the model.

Regarding the extractions of the relevant results after the simulations there is an important note to be made. For the freely-propagating and counterflow flame models, some values can be extracted either with basis in the defined solution, or the flame. The difference is that when the basis is in the solution, the results do not account for the spatial changes or any other gradients. It is therefore important to keep in mind which parameters are a property of the solution, or the flame.

### 3.3.1 Laminar, Premixed, Freely-Propagating Flame

For this model, the solution consisted of a fuel-air mixture with equivalence ratio equal to one. For methane, the initial width of the computational domain was set to 0.03 m. When syngas was used as fuel, some of the cases could not be solved with 0.03 m as the domain width without expanding it to 0.06 m. Therefore, to ensure equal domain width for all cases, the initial width was increased to 0.06 m. Note that the mass flow rate was not specified, as this is decided by Cantera, as explained in Kee et al. Chapter 15 [25]. The mass flow rate is estimated by specifying the temperature in one mesh point. The temperature must be equal to the temperature of the fuel-air mixture, and satisfy the energy balance, which allows Cantera to solve the energy equation with regards to the mass flow rate.

Furthermore, the flame was created as a free flame, using the gas mixture and width specified in the previous paragraph. Since it was desirable to use a multi-component transport model this

was also specified, and the Soret diffusion was enabled. The entropy before and after solving the flame was extracted and used to estimate the entropy change. The inlet chemical exergy was also calculated, and used as a control measure. For the premixed, freely-propagating flame the grid refinements criteria was decided as follows, ratio was set to two, slope and curve was set to 0.2, while prune was set to zero.

### 3.3.2 Laminar, Non-Premixed, Counterflow Flame

The counterflow flame was initiated as a counterflow diffusion flame using a solution with the desired chemical mechanism, temperature and pressure but without any specifications regarding its composition. The width between the jets was set to 0.03 m. After the flame was initiated, the conditions at the fuel- and oxidizer jet was decided. The fuel jet contained pure fuel, and the oxidizer jet contained pure air. The temperature of both inlets were equal, radiation and Soret flux was enabled, while boundary emissivities were neglected. The grid refinement criteria was kept the same as for the freely-propagating flame for 10 atm and 20 atm. However, when simulating with the global mechanism for 1 atm, using methane as the fuel it was necessary with a finer grid. The criteria was changed to the following, ratio was set to 2, slope and curve to 0.08 while prune was kept at zero.

The mass flow rates were set to  $2 \text{ kg/m}^2/\text{s}$  and  $1 \text{ kg/m}^2/\text{s}$  for the oxidizer and fuel jet, respectively. This was decided from a try-and-fail method to avoid the flame stabilizing too close to the fuel inlet, and to ensure that the flame ignited properly. For methane, the mass flow rates corresponds to an equivalence ratio of approximately 0.116, while the equivalence ratio for syngas was approximately 0.435.

### 3.3.3 Continuously Stirred Tank Reactor

In Cantera, reactors are the simplest form of reacting systems. In this system, all the states are a function of time and the state variables are homogeneously distributed over the system volume. Furthermore, it is assumed that at all instants of time, thermodynamic equilibrium exist and changes in transient state can only be caused by chemical reactions. Also included in Cantera are various components used with the reactors. Reservoir is a component which functions as an infinitely large volume, and is normally used to define the gas or liquid solution before entering the reactor. Walls are used for separation, or to define expansion and compression work. Valves are flow devices that can be used to define mass flow rate as a function of pressure drop across themselves. Lastly, there are controllers such as mass flow or pressure controllers. These components are combined with the reactors in reactor networks.

The reactor from Figure 6 was modeled using a single ideal gas reactor as the combustor with a volume of  $0.01\text{m}^3$ . A reservoir was created and filled with a fuel-air mixture with equivalence ratio equal to one. This served as the inlet for the reactor, and the conditions of the reservoir determines the inlet conditions of the reactor. When reactor models such as the one used in the current project are used, problems with the ignition might arise. Therefore, it is suggested that the reactor is initiated with a high temperature. Furthermore, it is recommended that the gas inside the reactor can be in chemical equilibrium as an initial state [7]. Chemical equilibrium was ensured by a function in Cantera [16] called equilibrate.



The function minimizes the total Gibbs free energy in the mixture by using an element potential method. If the function do not converge to a solution, it uses Gibbs minimization which is more robust. A mass flow and pressure controller was attached to the inlet and outlet of the reactor, respectively. These controllers ensured constant mass flow and pressure. A second reservoir was also created for the exhaust from the reactor. The reactor was modeled at adiabatic conditions and radiation therefore have no effect on the model, and was disabled. The same goes for multicomponent diffusion, and Soret flux. To initiate the simulation the reactor was first put in a reactor network, which is common even when there is only one reactor in the system. The whole system was then advanced to steady state before the required properties for the post-process analysis were extracted. Cantera [16] has a function named `advance to steady state`, which approaches steady step by time stepping, and checking the changes in condition at each step against a tolerance. The default value for tolerance was used, which is approximately ten times the relative error tolerance for the time stepping.

## 3.4 Entropy Production

### 3.4.1 Flame Models

A separate code was written for the calculation of the entropy production for the flame models. The code uses the results obtained from the simulations to preform post-process calculations. The relevant results from the simulations were obtained according to the Cantera documentation [6], and used according to Equations 18-22.

While most of the necessary results were obtained in a straightforward manner, the multicomponent diffusion coefficients were more complicated to extract. The coefficients were necessary for calculations of the mass diffusion velocity in Equation 4. Since it is one coefficient for each pair of species, and the detailed mechanism contains 53 species [41], it would require a large matrix to hold all the coefficients. This can be one of the reasons Cantera [16] does not provide the coefficients in each point of the flame. As a consequence, it had to be obtained in a different way as a part of the post-process procedure.

The solution was to use the obtained profiles for molar fractions, pressure, and temperature. The results were iterated, and at each spatial position the current state was imposed onto a dusty gas object. This object was used because Cantera calculates the species molar fluxes directly. With this solution, Equations 3-5 were left obsolete. The molar species fluxes were multiplied with the molecular weights to get the species mass flux, which was then used directly in Equation 20.

The local entropy production due to all the irreversible reactions were calculated in each point, and the total integrated value was calculated. This value was then compared with the total change in entropy for the premixed, freely-propagating flame. As the counterflow, diffusion flame actually is two-dimensional and is here only solved in one dimension it did not make sense to do the same for this model.

### 3.4.2 Reactor Model

Because the reactor model is zero-dimensional there are no temperature or composition gradients, as well as no mass fluxes for the species. This leaves the contribution from the chemical reactions

as the only source of entropy production. However, early in the project it was discovered that the entropy production from the chemical reactions did not equal the change in entropy between the reservoir and the outlet of the reactor. This indicated that there was some other source of entropy production or transfer.

After some investigation it was formed a hypothesis that the entropy production resulted from internal heat transfer. Meaning that the heat released from the combustor heated up the fuel-air mix before reactions started to occur. Theoretically the reactor could be divided into two zones as illustrated in Figure 8. In the figure, heating occurs in the first zone, while the chemical reactions are restricted to the second zone. The theory was first tested in an Excel sheet to determine if it was plausible. The entropy production due to heating the fuel-air mix to the temperature and the partial pressures of the combustor, with constant composition was estimated.

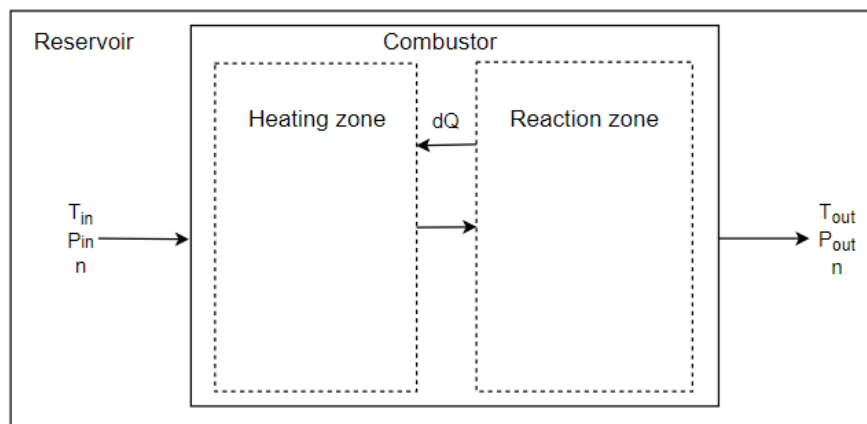


**Figure 8:** Model illustration, single reactor with two zones.

The values obtained from Excel was promising, and summed with the entropy production in the combustor it was equal to the change in entropy between the reservoir and the outlet of the reactor. Therefore, it had to be included into the program to automatically account for the issue in the simulations. A new function was written and incorporated in the program. The function estimates the entropy production due to the internal heat transfer as explained next.

The entropy production due to internal heat transfer was estimated from the entropy balance given in Equation 13. However, in the current project the combustor worked in steady state, with only one inlet and outlet, and the specific entropies were calculated on a molar basis. Therefore, the version presented in Equation 46 was more appropriate. In this equation  $n$  is molar flow,  $\frac{dS_{12}}{dt}$  is set to zero since it is steady state, and the entropy at the inlet and outlet are the weighted sum of the total entropy of each species according to Equation 14. The last term is the entropy transferred from the second state to the first with heat, at the temperature in state two.

$$\dot{\sigma}_{12} = \sum_i^{NS} \dot{n}_{i,2} \bar{s}_{i,2} - \sum_i^{NS} \dot{n}_{i,1} \bar{s}_{i,1} - \frac{\dot{Q}_{12}}{T_2} \quad (46)$$

Since it was desirable that no chemical reaction occurred in the heating zone  $n_{i,2}$  was assumed to be equal to  $n_{i,1}$ . The heat transfer between the zones was calculated according to Equation 47,

which is the energy balance for a rigid, adiabatic system in steady state, without potential and kinetic energy.

$$Q_{12} = H_2 - H_1 \quad (47)$$

As already mentioned, the total specific entropy for each species was calculated according to Equation 14. Cantera can calculate the absolute entropy for a certain species at a given temperature. The absolute entropy at the reference state was obtained by Cantera at the reference temperature 298.15 K. Furthermore, the integral in the second term was calculated by subtracting the absolute entropy at the reference state, from the current state. Lastly, the third term was calculated using the partial pressure of the relevant species in state 1 and 2.

With the total entropy of each species, the species molar flows, and the heat transferred between the zones the function calculated the entropy production due to the internal heat transfer. The values that was obtained for the entropy production were considered to be reasonable, and the program for the reactor model could be used in further simulations.

## 4 Validation

An extensive amount of time was spent validating the various models to ensure correct behaviour, before the final simulations were performed. The freely-propagating and counterflow models were validated against results in the literature. The reactor model was considered to be of such simplicity that an extensive verification was not necessary. Additionally, the global mechanisms used were not validated.

### 4.1 Laminar, freely-propagating, premixed flame

The current project is based on a previous project assignment [30]. In the assignment a laminar, premixed, freely-propagating methane-air flame was considered. The model was simulated using both GriMech 3.0 [41], and DRM19 [24] as detailed and reduced mechanisms, respectively. The model was compared with Nishida et al. [35], where a premixed, freely-propagating flame is simulated using a mechanism based on GRI-mech 3.0 [41]. However, the NO<sub>x</sub>-related mechanism is excluded, and therefore only 32 species and 186 elementary reactions are included.

The model in the project assignment performed sufficiently with both mechanisms. However, it is important to mention that the model did not account for radiation, and used a mixture-averaged transport model. Additionally, the entropy production calculated using the code written for the previous assignment agreed with the results in the article. The code was therefore considered to work properly, and used in the master thesis without further verification. This was also partly because of lack of similar analyses to compare with.

To further investigate the effects of including radiation, and using the multicomponent transport model, the results from the project assignment are compared with results from the master thesis at the same conditions. For Figure 9 and Figure 10 GriMech 3.0 [41] mechanism was used, and the conditions were as stated in Nishida et al. [35]. The first figure is included from the project assignment [30], and as mentioned earlier, mixture-averaged transport model was used, and radiation was neglected. The next figure is obtained with the code written for the master thesis. As stated previously, this model considers radiation and uses a multicomponent transport model. As can be seen by comparing the figures they are near identical. The graph in Figure 10 is however slightly shifted to the left, which may be caused by the difference in diffusion models.

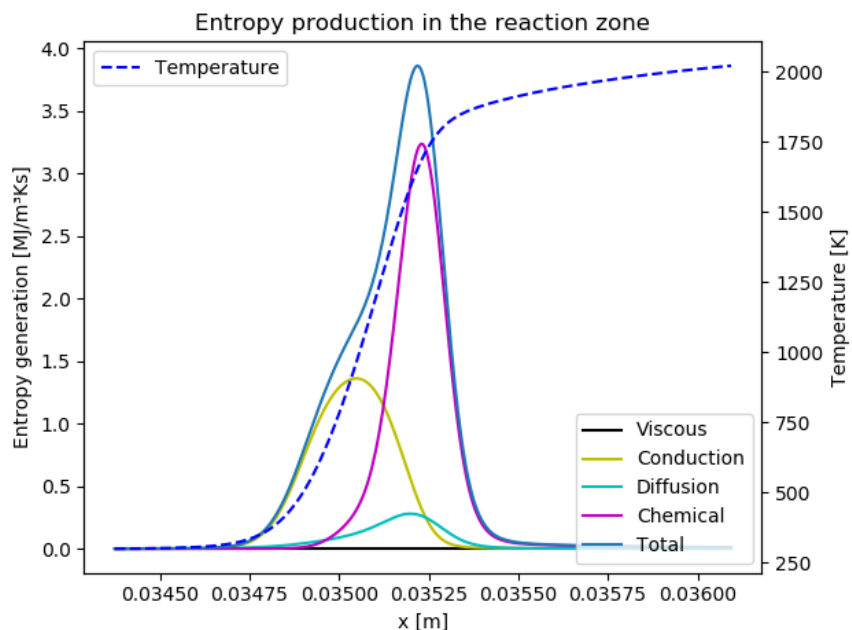


**Figure 9:** Results for entropy production from previous project assignment. Without radiation and with mixture-averaged transport. Condition from Nishida et al. [35], and GriMech 3.0 [41] mechanism.

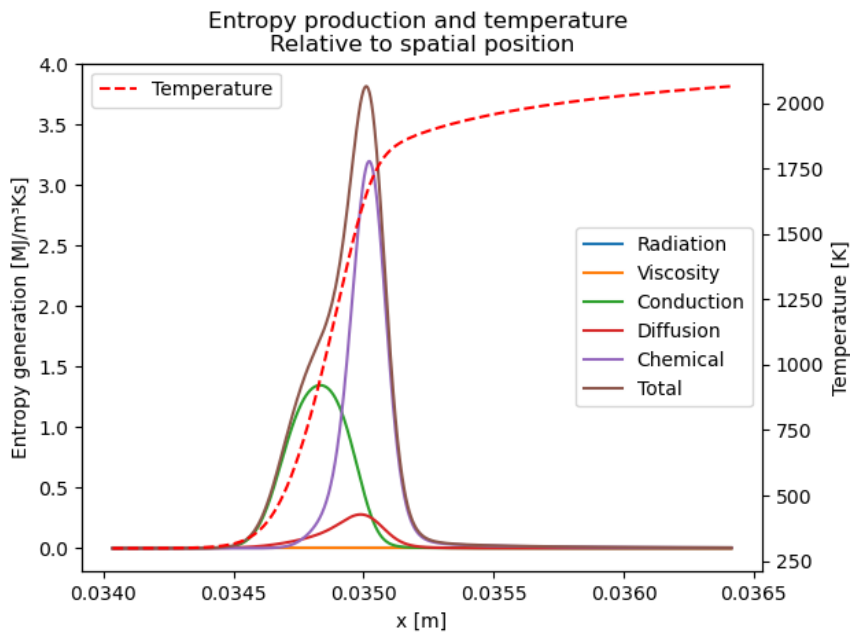


**Figure 10:** Results for entropy production from current project. With radiation and with multicomponent-averaged transport. Condition from Nishida et al. [35], and GriMech 3.0 [41] mechanism.

Furthermore, the results for the total, integrated entropy production due to the irreversible processes in the project assignment [30] can be compared those in the master thesis. As it can be seen from Table 1 some of the results agree more than others. However, an important result to elucidate is that for both the master thesis, and project assignment, chemical reactions make up approximately 55% of the total entropy production. Furthermore, heat conduction accounts for approximately 36% in the project, and 37% in the thesis, of the total entropy production. This is the same results as obtained by Nishida et al. [35]. The freely-propagating, premixed model was considered to be properly validated. As was the use of GriMech 3.0 [41] and DRM19 [24] as detailed and reduced mechanism, respectively, for methane combustion. Based on this, the entropy model was considered sufficiently validated for use in both flame models.

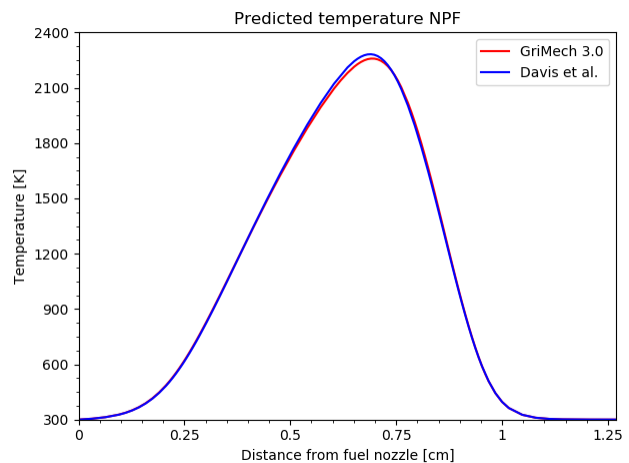
**Table 1:** Comparison of total integrated entropy production between the master thesis and project assignment [30]. The units are in  $\text{J}/\text{K}/\text{m}^2/\text{s}$ . Note: The vertical lines at the bottom are unintentional.

	Master thesis	Project assignment
Entropy change	1013.56	1119.96
Entropy production	1088.03	1096.58
Radiation	0.189	0.0
Viscosity	$4.46 \cdot 10^{-4}$	$4.70 \cdot 10^{-4}$
Conduction	409.83	406.96
Diffusion	79.46	79.54
Chemical	598.93	610.09

## 4.2 Laminar, counterflow, diffusion flame

The laminar, counterflow, diffusion flame model was validated against an article written by Som et al. [42]. In Section 5.1 of their article they compare three mechanisms against results from an experiment. Two of the mechanisms investigated were GriMech 3.0 [41] and Davis et al. [15]. These two were also chosen for the current project as the detailed and reduced mechanism used for syngas combustion. The mechanisms were validated against Figure 2 in said section. Furthermore, the model in the current project was also compared with Figure 8, and 11 in Som et al. [42].

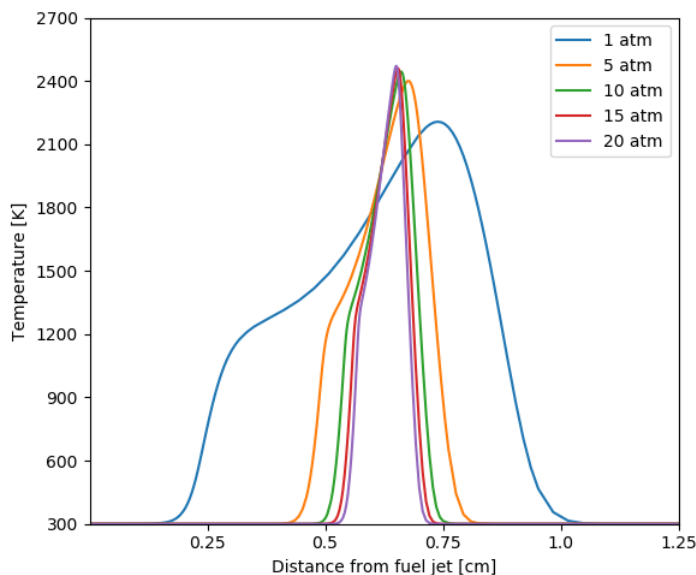
Figure 2 in Som et al. [42] Section 5.1 display the measured and predicted temperature profile for a counterflow, non-premixed syngas/air flame. Syngas is modeled as 50% CO



**Figure 11:** Replication of Figure 2, Section 5.1 [42]. Temperature profile using the GriMech 3.0 [41] and Davis et al. [15] mechanisms. Non-premixed counterflow flame.

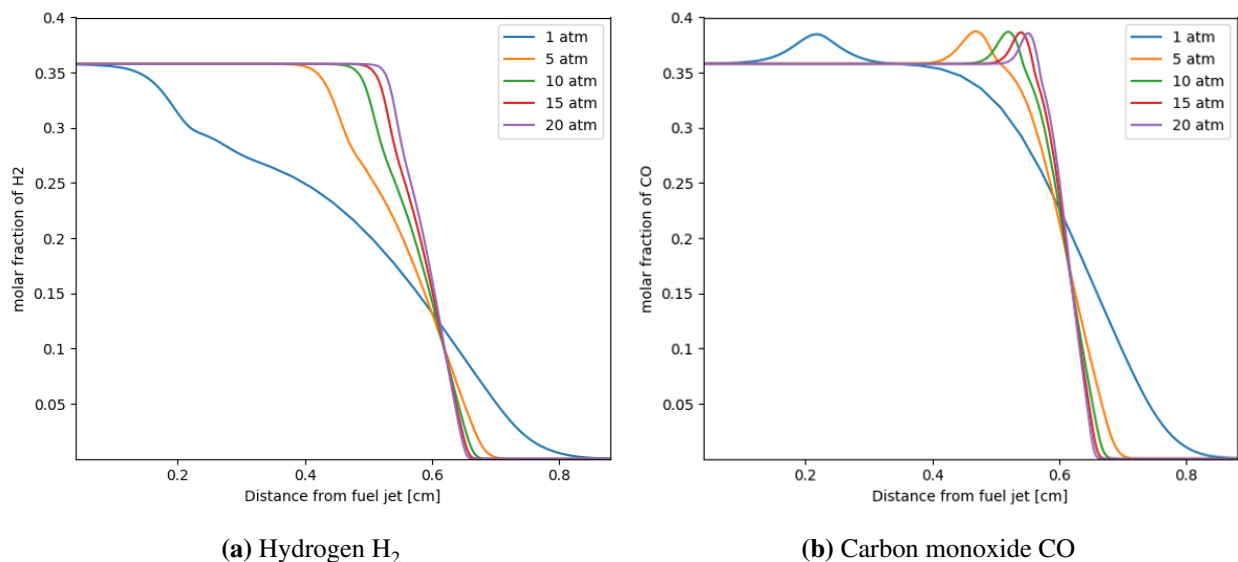
and 50%  $H_2$ , the pressure is atmospheric pressure, temperature at both inlets are 300 K and the inlet velocities are 13.84 cm/s. In Figure 11, Figure 2 is replicated by imposing the conditions in the article on the model from the current project. The graphs are near-identical to the graphs of the results using GriMech 3.0 [41] and Davis et al. [15] in the article [42]. The predicted temperature profiles, in the article and the current project, are left-shifted approximately 0.18 cm. This is caused by the suction of excess fuel in the experiment set up in Som et al. [42]. The predicted peak temperature from the model in this project were 2258 K and 2281 K, by GriMech [41] and Davis et al. [15], accordingly. Both profiles reach their peak 0.69 cm from the fuel inlet. For comparison, the profiles predicted by the same mechanisms in Som et al. [42] peak at 0.70 cm, and reach a temperature of 2252 K and 2279 K, respectively. This small difference in peak value may come from the fact that it was used different radiation models for this project, and the project described in the article.

Figure 8a in Section 5.3 in Som et al. [42] display the effect of varying the pressure from 1 atm to 20 atm on a partially premixed counterflow flame. Syngas is still modeled as a 50%  $CO/50\% H_2$  mixture, with inlet temperatures of 300 K. The fuel is now partially premixed with air, with equivalence ratio 6, and the inlet velocities are now 31.75 cm/s and 38.07 cm/s for the oxidizer and fuel inlets, respectively. The mechanism used is Davis et al. [15]. The graph contains the temperature profiles for 1, 5, 10, 15, and 25 times the atmospheric pressure. In Figure 12 the condition have been imposed on the model of the current project. The profiles are near-identical for all of the five cases.



**Figure 12:** Replication of Figure 8a, Section 5.3 [42]. Temperature profile along distance from jet fuel, with the effects of varying pressure, partially-premixed counterflow flame.

In Section 5.3 of Som et al. [42] Figure 11a and Figure 11b display the molar species profiles for  $H_2$  and CO, respectively. The profiles are predicted using the Davis et al. [15] mechanism, and the same conditions as mentioned in the previous paragraph. In Figure 13 the molar species profiles are replicated. The same conditions as used in the article was imposed on the current model, with the same mechanism. Again, the graphs compare well and the counterflow diffusion model was concluded to be adequate. Furthermore, GriMech 3.0 [41] and Davis et al. [15] were considered sufficiently validated for further use.



**Figure 13:** Replication of Figure 11a and Figure 11b, Section 5.3 [42]. Molar species profiles of  $H_2$ (a) and CO(b) along the distance from the jet fuel, with effects of varying pressure, partially premixed counterflow flame

### 4.3 Entropy Change

The values for the change in entropy in the reactor, and freely-propagating, premixed flame models were verified against manual estimations. Using the results from Cantera [16] for mole fractions and temperatures the change of entropy was estimated with Equation 14 in an excel sheet. Values to calculate the integral were gathered from Table A.9 in Sonntag and VanWylen [43]. Furthermore, the absolute entropy at  $T_{ref} = 298K$  was taken from Table A-25 in Moran and Shapiro [34]. These values was used without attempting to find the values used by Cantera. This was to save time, as the excel sheet was readily available. The pressure, temperature, number of moles and mole fractions before and after combustion were extracted from Cantera. It should be mentioned that the excel sheet did not contain data on all the species. However, it was confirmed that the species that lacked data had considerable lower molar fractions than the ones with available data. The results for entropy change calculated by Cantera [16], and in the excel sheet was determined to be adequately similar.



## 5 Results and Discussion

### Premixed, Well-Stirred Reactor

#### 5.1 Methane

Figure 14 presents the peak temperatures in the reactor when the pressure is 1 atm, 10 atm, and 20 atm while using detailed, reduced, and global mechanisms. As the state inside the reactor is uniform the peak temperature is the temperature in the whole reactor volume, when it has been advanced to steady state. The peak temperature is seen to increase as the pressures is increased. From the graphs one can also see that the global mechanism overestimated the temperature. However, the overestimation is less significant for 10 atm and 20 atm. The calculated peak temperature using the detailed and reduced mechanisms are approximately equal. The calculations get more similar with pressure, and improves from 0.5% to 0.005 % in deviation from 1 atm to 20 atm.

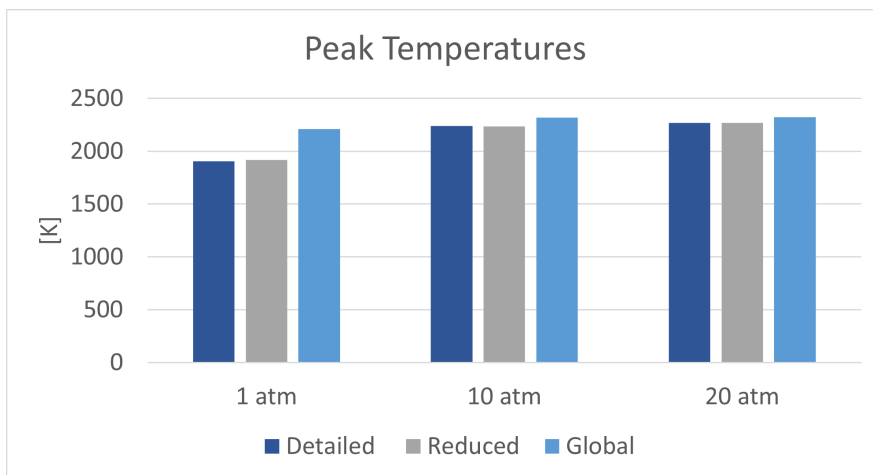


**Figure 14:** Comparison of calculated peak temperatures for detailed, reduced and global mechanisms. Pressure range: 1 atm, 10 atm, and 20 atm. Fuel type is methane in premixed, well-stirred reactor model.

In Figure 15 the total entropy production by heating and chemical reactions are presented. In addition, the entropy change is given for each case as a small circle. As mentioned in Section 3.3.3, the reactor had a constant volume of  $0.001 \text{ m}^3$ , and the units on the y-axis in Figure 15 are therefore  $\text{kJ/K/s}$ . From the graphs it is seen that all the mechanisms are capable of predicting the total entropy production very well. As the pressure increases, the entropy production due to chemical reactions decreases while the production due to heating increases.

The increase in entropy production due to the internal heating is cancelled by the decrease in production due to chemical reactions, making the total production near independent of the pressure changes. The entropy change calculated by the reduced and global mechanisms are close to that of the detailed mechanism. The proximity in estimations indicate that the reduced and global mechanisms are capable of correctly simulating the system.

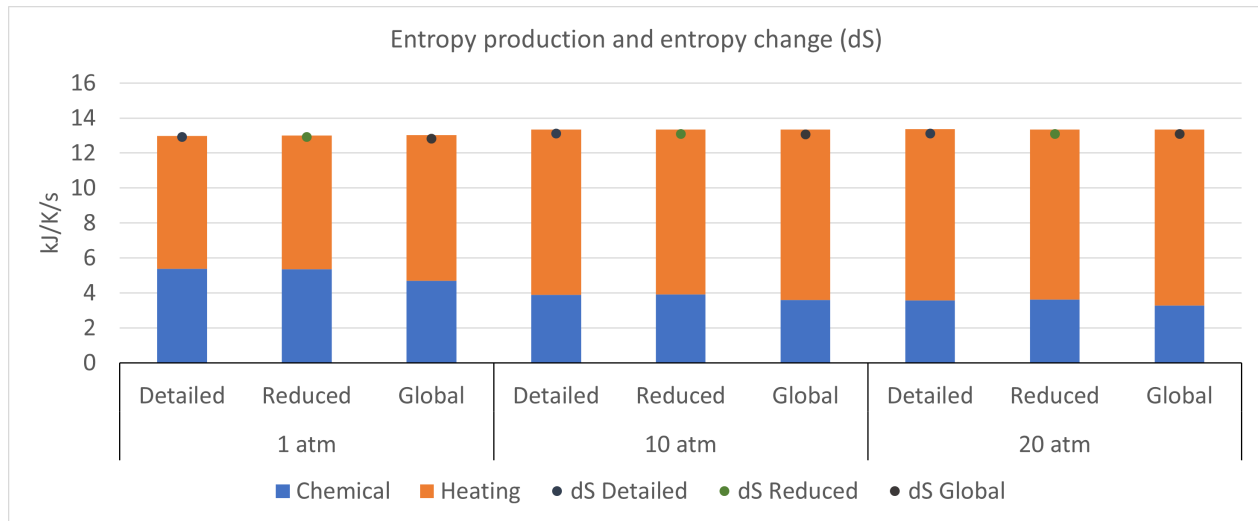


**Figure 15:** Comparison of the entropy production by source and the entropy change, for detailed, reduced, and global mechanisms. Pressure range: 1 atm, 10 atm, and 20 atm. Fuel type is methane in premixed, well-stirred reactor model.

## 5.2 Syngas

Figure 16 compares the calculated peak temperatures for 1 atm, 10 atm, and 20 atm using the detailed, reduced, and global mechanisms. It can be seen that the reduced mechanism slightly over-predicts the temperature, while the global mechanism under-predicts it, compared with the detailed mechanism at all pressures. This is in contrast with the results obtained with methane where the global mechanism overestimates it, and the reduced mechanism were closer as well. Furthermore, the temperature increases with pressure, which could also be seen for the use of methane in Figure 14.

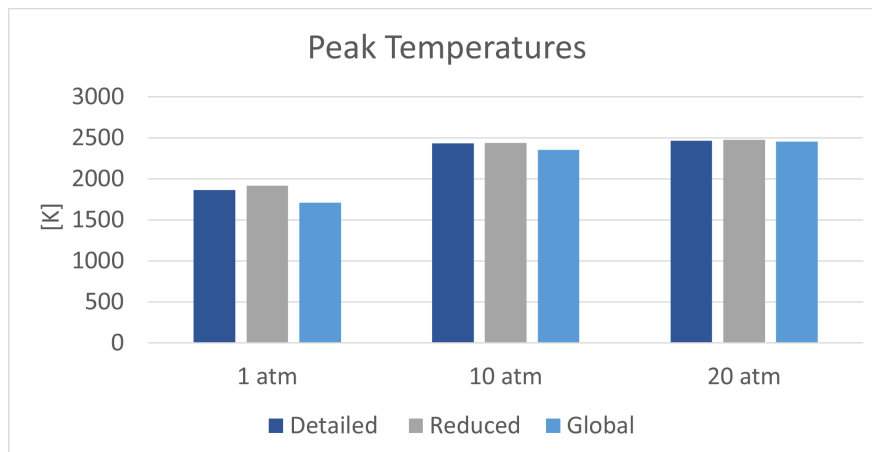


**Figure 16:** Comparison of calculated peak temperatures for detailed, reduced and global mechanisms. Pressure range: 1 atm, 10 atm, and 20 atm. Fuel type is syngas in premixed, well-stirred reactor model.

In Figure 17, the entropy production due to chemical reactions and heating are compared with

the change in entropy. Included in the figure are the results using the detailed, reduced, and global mechanisms for 1 atm, 10 atm, and 20 atm. The entropy production due to heating increases with the increase in pressure, while the entropy production due to the chemical reactions decrease. However, the increase in entropy production due to heating is larger and therefore the total entropy production are increasing with pressure for all mechanisms. Additionally, the entropy change also increases with pressure.

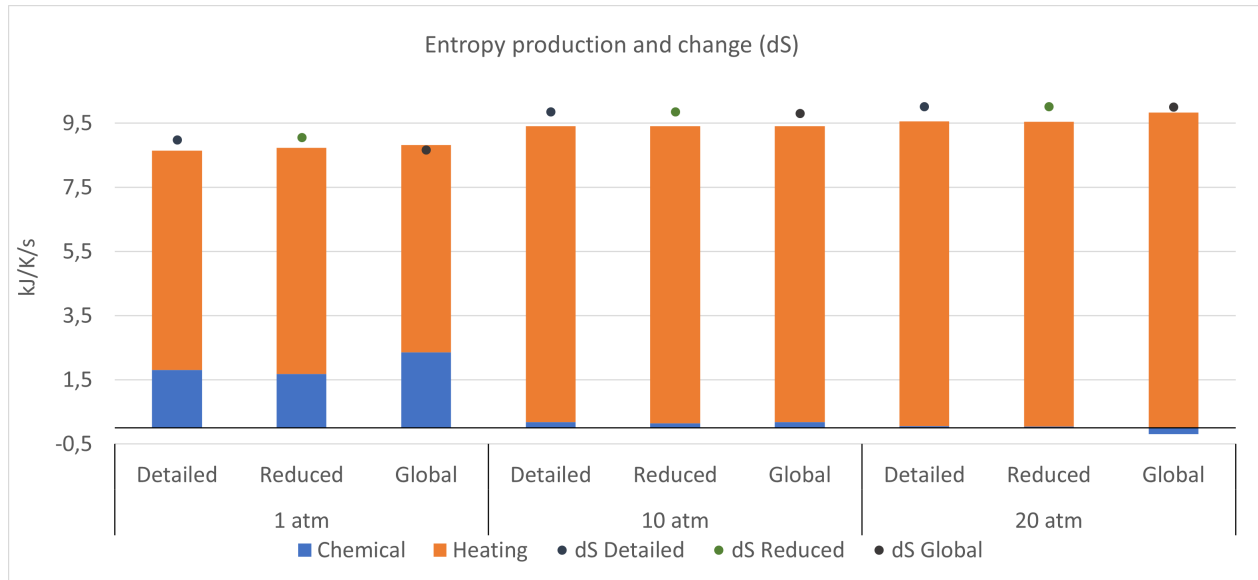


**Figure 17:** Comparison of the entropy production by source and the entropy change, for detailed, reduced, and global mechanisms. Pressure range 1 atm, 10 atm, and 20 atm. Fuel type is syngas in premixed, well-stirred reactor model.

### 5.3 Comparisons

The contribution from the internal heating when methane, and syngas are used as fuels are similar. The increase in the contribution has the same explanation for both fuels. The density of the gas is seen to increase with a factor of approximately the same order as the pressure increase. When the density increases, and since the volume is kept constant, the mass inside the reactor increases. With more mass inside the reactor more internal heat transfer is required to increase the temperature of the gas, and thereby the entropy production due to heating increases. Additionally, the temperature increases with pressure which again lead to more internal heat transfer and entropy production.

Moreover, the entropy production due to heating is slightly higher when methane is used, which may seem strange since the temperature is higher when syngas is used. This may be because methane has a higher specific heat capacity than CO and H<sub>2</sub> ([34], Table A-21), and therefore requires more energy to heat up.

Furthermore, since the mass flow rate is also kept constant the residence time inside the reactor will increase with the same factor as the density. With a higher residence time the gas is allowed to react more, and is therefore closer to chemical equilibrium at higher pressures. When the gas is closer to the equilibrium state the Gibbs free energy is lower, and therefore the entropy production

due to chemical reactions is also lower.

By comparing Figure 15 and Figure 17, it can be seen that the entropy production due to the chemical reactions are lower when syngas is used than when methane is used. One explanation is that methane has a higher chemical exergy than CO and H<sub>2</sub>, and therefore releases more energy in reactions ([34], Table A-26).

Finally, it is important to discuss the entropy production due to chemical reactions when syngas is used at 20 atm. In Figure 17 it can be seen that the contribution is negative. This might be a consequence of the reactions selected for the global mechanism presented in Equation 42. Here, it can be seen that the last equation does not have any reversed reaction. Therefore, it is reasonable to assume that this may lead to problems when chemical equilibrium is approached.

This argument is reinforced by Table 2, where  $\Delta G$ , and  $q_j$  are compared for the reactions in the global mechanism presented in Equation 42. From the table it can be seen that  $\Delta G$  is identical for Reaction 1 and Reaction 2, for all pressures. Reaction 1, the forward reaction has a higher net rate of progress than the reversed reaction, Reaction two. Additionally,  $q_j$  increases faster for the forward reaction, indicating that more CO<sub>2</sub> is produced at the higher pressures. However, due to the negative sign in the equation for entropy production due to chemical reactions given in Equation 21, the entropy production due to these two equations are positive at all pressures. Reaction 3 also has an increased  $q_j$  at higher pressures but  $\Delta G$  is increasing, in contrast to Reaction 1 and Reactions 2 where  $\Delta G$  is decreasing. Therefore, at 20 atm the contribution from Reaction 3 will surpass the combined contribution of Reaction 1 and Reaction 2, and since the reaction has a positive  $\Delta G$ , the total entropy production due to all the chemical reactions will be negative.

**Table 2:** Comparison of  $\Delta G$  and  $q_j$  for reaction 1, 2, and 3 in the global mechanism for syngas presented in Equation 42, in the premixed, well-stirred reactor at pressure 1 atm, 10 atm, and 20 atm.

Reaction	1 atm			10 atm			20 atm		
	1	2	3	1	2	3	1	2	3
$\Delta G$ [J/kmol]	-124487840	124487840	-108456266	-40265413	40265413	5007838	-18741405	18741405	32483778
$q_j$ [kmol/m <sup>3</sup> /s]	10,31	9,28	2,54	4416,25	4413,92	2,97	13747,09	13744,49	2,98

## Premixed, Freely-Propagating

### 5.4 Methane

To focus on the reaction zone the graphs displayed throughout this section only show parts of the domain. The domain width for all pressures were 3 cm. The reason is to highlight small scale variations between cases, and avoid unnecessary information.

#### 5.4.1 Comparison of Cases.

Figure 18 shows the peak temperatures at 1 atm, 10 atm, and 20 atm, using the detailed, reduced, and global mechanisms. The peak temperatures were the highest temperatures estimated in the flames by Cantera [16]. Since the premixed, freely-propagating flame model has an outlet boundary condition that sets the gradients to zero (Equation 35), the highest temperature was also the outlet temperature for all cases. The peak temperatures are close to independent of the changes in pressure. The peak temperature calculated by the detailed and reduced mechanisms is seen to increase with pressure. When the global mechanism is used, the peak temperature is slightly over-estimated. Moreover, the temperature increases from 1 atm to 10 atm, but then decreases with 1 K from 10 atm to 20 atm.

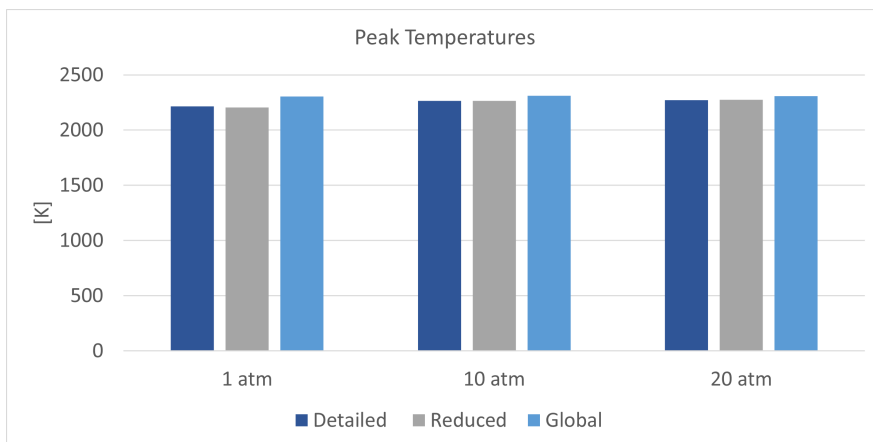


**Figure 18:** Comparison of calculated peak temperatures for detailed, reduced and global mechanisms. Pressure range: 1 atm, 10 atm, and 20 atm. Fuel type is methane in premixed, freely-propagating model.

Figure 19 shows the integrated entropy production by source at 1 atm, 10 atm, and 20 atm, using the detailed, reduced, and global mechanisms. In contrast to the peak temperatures in Figure 18, and the reactor model in Section 5.1 the entropy production for this model is pressure dependent. From the figure it is clear that both the change in entropy, and entropy production increase as the pressure increases.

Compared with the detailed mechanism, the global mechanism underestimates the entropy production while the reduced mechanism calculates approximately the same production for 1 atm. When the pressure is increased to 10 atm the global mechanism still underestimates, while the

reduced mechanism now slightly overestimating the entropy production. Finally, at 20 atm both the reduced, and global mechanism overestimates the entropy production.

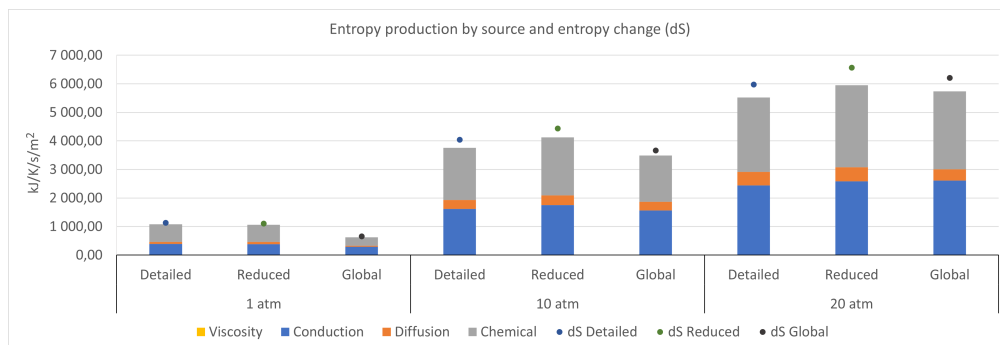


**Figure 19:** Comparison of the integrated entropy production by source and the entropy change, for detailed, reduced, and global mechanisms. Pressure range: 1 atm, 10 atm, and 20 atm. Fuel type is methane in premixed, freely-propagating model.

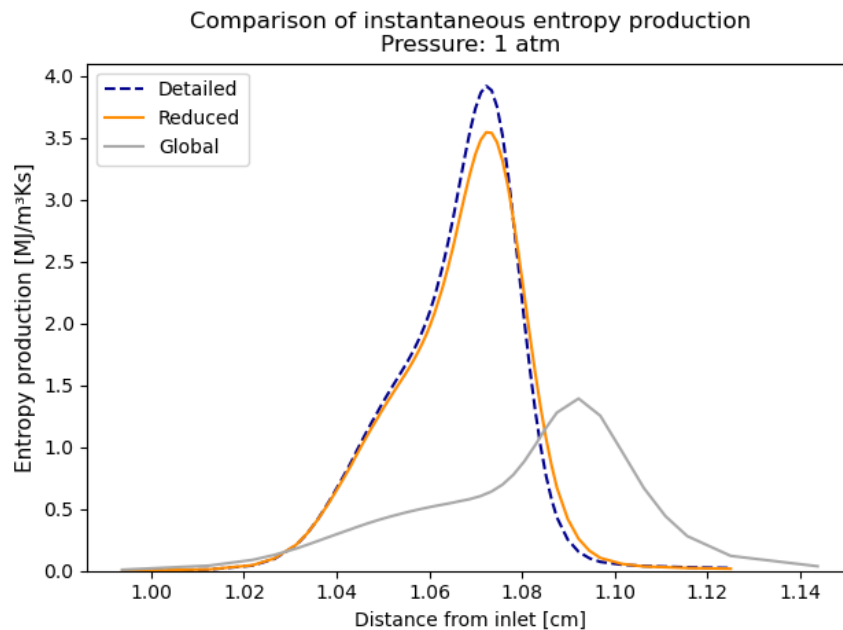
### 5.4.2 1 atm

The integrated entropy production by source is given in Table 3. Here it can be seen that chemical reactions and conduction are the main contributors, followed by diffusion, while viscosity has a negligible contribution. The table also further shows how the reduced and global mechanisms underestimate the entropy production due to all the irreversible processes.

**Table 3:** Integrated entropy production by source for the premixed, freely-propagating methane flame at 1 atm pressure.

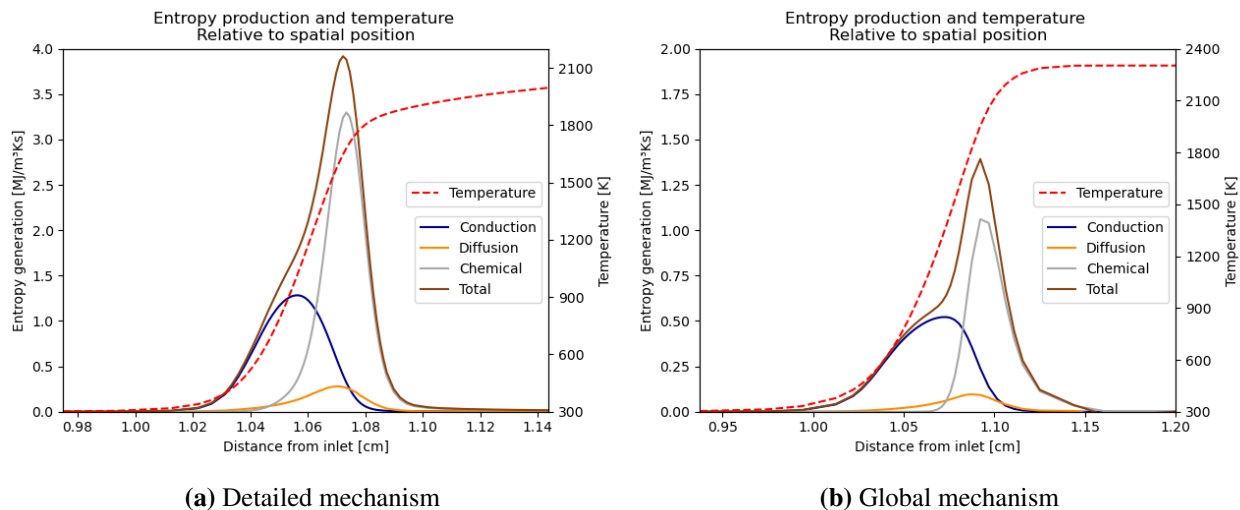
	Integrated entropy production by source [ $\text{kJ/K/s/m}^2$ ]		
	Detailed	Reduced	Global
Viscosity	4,67E-04	4,48E-04	1,25E-04
Conduction	388,20	385,41	288,60
Diffusion	77,55	74,12	36,59
Chemical	616,89	598,48	297,30

Figure 20 displays the total instantaneous entropy production at 1 atm. Since the system is in steady state, the production does not change with time, and local entropy production may therefore be a better term than instantaneous. From the figure it can be seen, as stated in Section 5.4.1, that the reduced and global mechanisms underestimate the entropy production. In addition to underestimating the total local entropy production, the global mechanism is delayed by approximately 0.01 cm. The shape of the profile also has some clear discrepancies. The graph of the reduced mechanism is also delayed slightly. This may be due to the reduced number of reactions. Some of the reactions that are neglected in the reduced and global mechanisms may be more active, with lower activation energies  $A$  in their Arrhenius functions. Therefore, these reactions occur at a lower temperature, allowing the detailed mechanism to precede the reduced, and global mechanisms.



**Figure 20:** Comparison of the entropy production using detailed, reduced, and global mechanism. Fuel type is methane in premixed, freely-propagating model with 1 atm pressure.

Figure 21 shows the local entropy production by source for detailed (Figure 21a), and global (Figure 21b) mechanisms. The reduced mechanism is not included, as it is adequately similar to the detailed mechanism in Figure 20. The contributions from viscosity and radiation are not included as they were not visible on the graph. Figure 21a gives an explanation for the shape of the profiles of the detailed, and reduced mechanisms in Figure 20. The shape is similar to the profiles in Nishida et al. [35] (Figure 2a), which was also stated in Section 4.1. It can be seen that in the left part of the graph the entropy production is mainly due to conduction. The contribution from conduction has a peak where the temperature gradient is at its steepest, because it is dependent on the temperature gradient squared (Equation 19). Then, the chemical reactions start to occur when the temperature is sufficiently high, which also causes the entropy production due to diffusion to increase. The entropy production due to diffusion is dependent on the species mole fraction gradients (Equation 20). Therefore, the increase in contribution comes as a result of intermediate species being created and destroyed by the elementary reactions. Figure 21b is included for comparison, and it can be seen that the profiles possess some of the same characteristics as for the detailed mechanism in Figure 21a. For example, the entropy production is initiated by the temperature gradient, which causes an entropy production due to conduction. However, the profile for the conduction is both lower and wider. This feature is the main reason for the skewed shape of the profile in Figure 20. Moreover, the profiles are much lower which becomes clear by noting the difference in scale on the vertical axis.



**Figure 21:** Instantaneous entropy production by source for detailed (a), and global (b) mechanisms. Model is premixed, freely-propagating methane flame at 1 atm.

To further investigate the difference in entropy production due to conduction seen in Table 3, the temperature profiles, for all mechanisms are displayed in Figure 22. First, it is clearly shown again that the global mechanism overestimates the peak temperature, as shown in Figure 18. Second, it should be noted that as the figure is only a section of the complete graphs the reduced mechanism does not overestimate the temperature as it may appear. More important are the shape of the profiles, as the global mechanism does not have a profile as steep as the detailed, and reduced mechanisms. This is the main reason for the lower contribution from conduction when the global mechanism is used.

Another possible reason may be the thermal conductivity  $\lambda$  included in Equation 19. Cantera [16] calculate the solutions conductivity based on all the species included at each location. Furthermore, because of the fewer reactions, there may be species that are produced by the detailed mechanism in specific locations, but not by the reduced and global mechanisms. If these species have a high thermal conductivity, it would result in a higher entropy production for the detailed mechanism. However, this argument works both ways. If the species produced by the detailed mechanism have low thermal conductivity, they would cause the species with high thermal conductivity to have lower mole fractions, thus cause a decrease in entropy production. Regardless, there was not enough time to investigate this

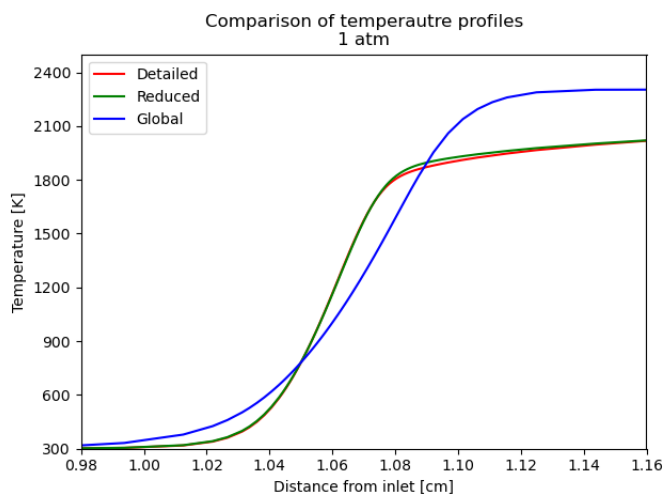


**Figure 22:** Comparison of temperature profiles for detailed, reduced, and global mechanisms for premixed, freely-propagating methane flame at 1 atm.



hypothesis.

To better understand why the reduced and global mechanisms estimate lower entropy production due to diffusion and chemical reactions than the detailed mechanism, Figure 23 can be studied. Here the mole fraction profiles for reactants ( $\text{CH}_4$ ), oxidants ( $\text{O}_2$ ,  $\text{N}_2$ ), and products ( $\text{CO}_2$ ,  $\text{H}_2\text{O}$ ), are included. The graphs clearly show how the reduced mechanism closely follow the detailed mechanism, while the global mechanism has a much more flat, and delayed profile. The profiles for the reactants, oxidants, and products using the detailed and reduced mechanisms have steeper gradients, than the profiles using the global mechanism. The lesser gradients are the main reason for the lower entropy production using the global mechanism.

Additionally, the argument considering the lower number of reactions can be reviewed here. Since Equation 20 and Equation 21 are summed over the number of species and reactions, respectively, it is reasonable to assume that fewer reactions will lead to lower entropy production. This argument may work both ways, as mentioned regarding the thermal conductivity. If the species that are produced by the detailed mechanism, but not by the reduced and global mechanisms, have low mass flux  $J_i$ , species with high mass flux may have lower mole fractions which will result in a lower entropy production. However, this is normally accounted for in the reduced mechanisms if they are created properly. Due to time restrictions this was not further investigated.

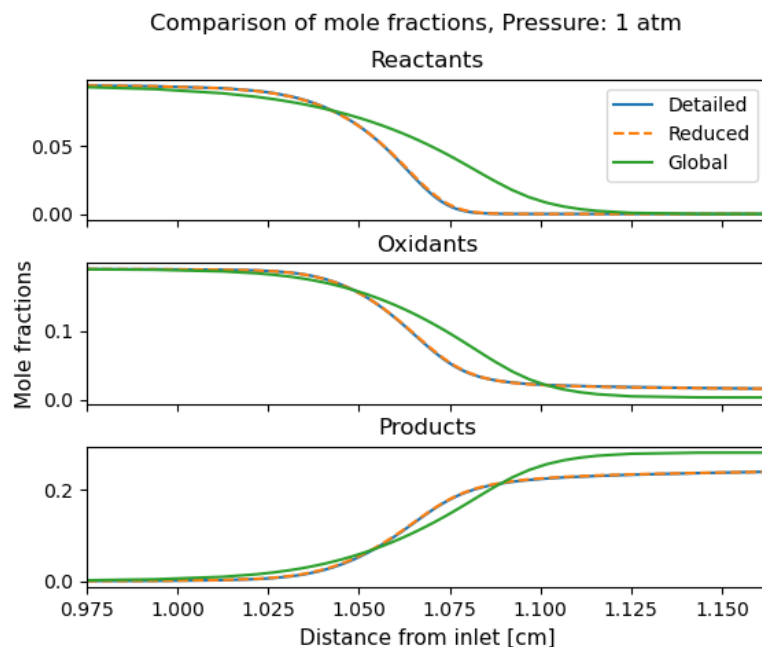


**Figure 23:** Comparison of mole fraction profiles for reactants ( $\text{CH}_4$ ), oxidants ( $\text{O}_2$ ,  $\text{N}_2$ ), and products ( $\text{CO}_2$ ,  $\text{H}_2\text{O}$ ), using detailed, reduced, and global mechanisms. Model is premixed, freely propagating flame with methane as fuel at 1 atm.

The difference in contribution from viscosity may be a consequence of two things. First, the viscosity  $\mu$  of the solution is, like the thermal conductivity calculated by considering all the species in the solution at every point. Therefore, it is reasonable to assume that with fewer equations there will be fewer species in the grid points. Some of these species may have high viscosity, and by neglecting them the viscosity of the solution decreases, which again decrease the entropy production. The investigation of this hypothesis was excluded due to time restrictions. Second, the velocity profile is important for the viscous contribution (Equation 18). As shown in Figure 24, the velocity profiles using the detailed and reduced mechanisms are much steeper than that of the global mechanism. Which is the main reason for the higher entropy production due to viscosity.

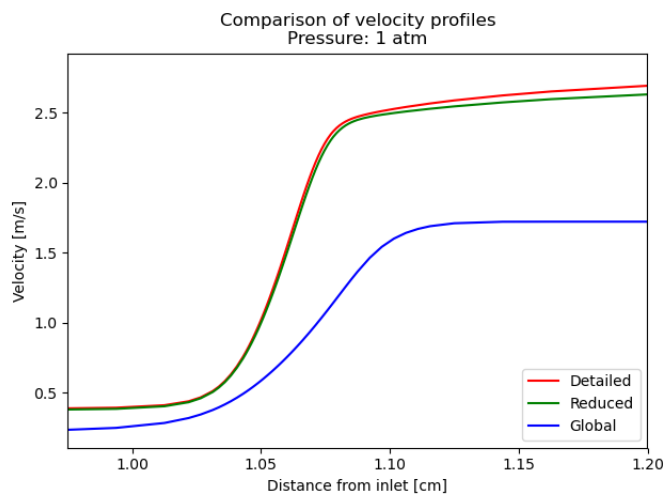


**Figure 24:** Comparison of velocity profiles for detailed, reduced, and global mechanisms for the premixed, freely-propagating, methane flame at 1 atm.

Regarding the entropy production from the chemical reactions, it is possible to further investigate it by looking at the highest contributing reactions. Figure 25 compares the seven reactions with highest local entropy production, when the detailed (Figure 25a), and reduced (Figure 25b) mechanisms are used. Seven reactions was considered an appropriate number of reactions, as more only reduced the readability. When the figures are studied it is important to keep in mind that the colors of the graphs do not necessarily refer to the same reactions. For example, the second highest reaction is not the same in the legends in Figure 25a and Figure 25b, as it is included in the detailed [41], but not in the reduced mechanism [24].

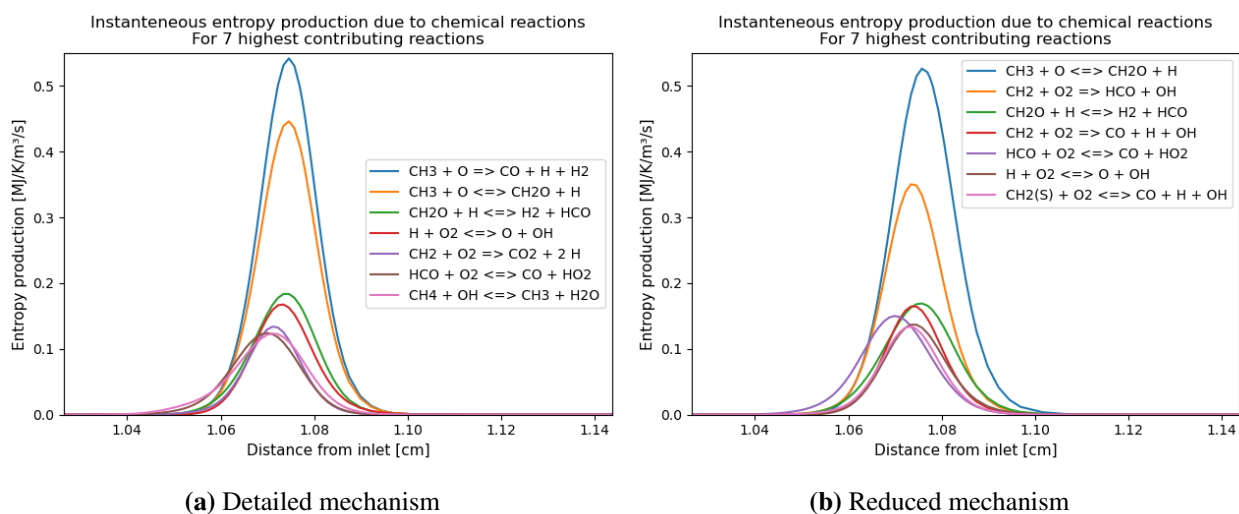


**Figure 25:** Local entropy production from the seven highest contributing reactions using the detailed (a), and reduced (b) mechanisms. Fuel type is methane in premixed, freely-propagating model at 1 atm.

In Figure 26, the integrated entropy production from the 25 reactions with the highest contributions using the detailed mechanism are presented. In addition, the contribution from the remaining reactions are summed up and included at the bottom. What can be interesting to see from this bar chart, is that the reactions with the highest local contribution does not necessarily have the highest integrated contribution. In this particular case, the ranking between the integrated and local values (Figure 25a) match until the fifth highest contributing reaction.

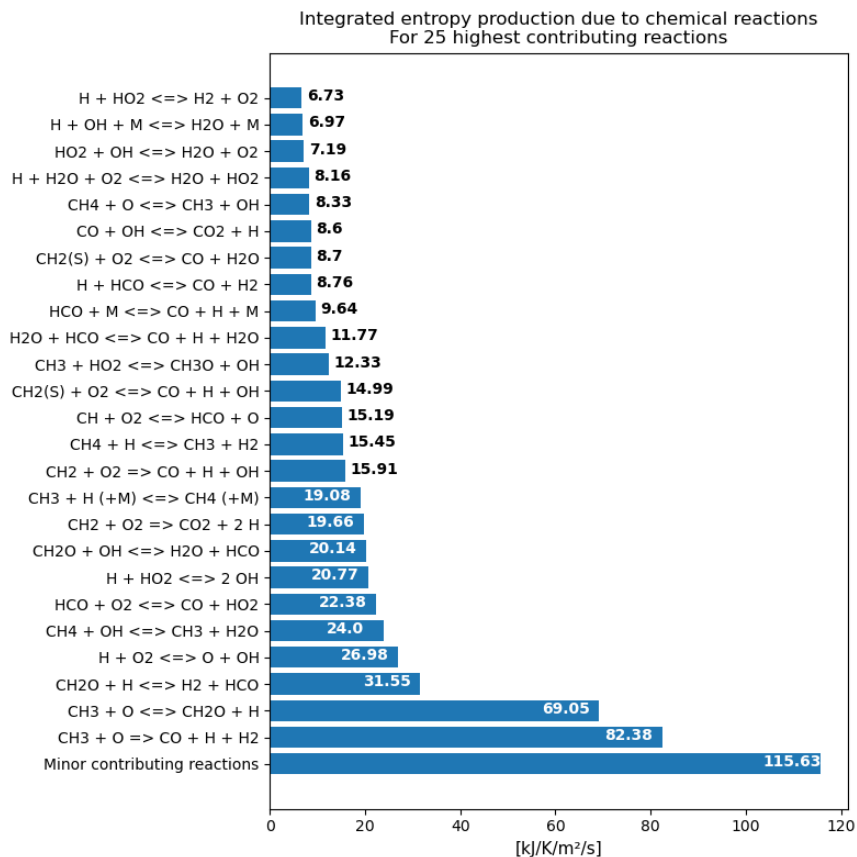


**Figure 26:** Integrated entropy production due to the highest contributing reactions, for detailed mechanism in premixed, freely-propagating methane flame at 1 atm

The 25 reactions with the highest integrated contribution, in addition to the sum of the minor contributing reactions using the reduced mechanism are presented in Figure 25a. Again, the second highest reaction using the detailed mechanism is not included in the reduced, and is therefore not in the chart. Compared with the local entropy production only the three highest contributing reactions are the same.

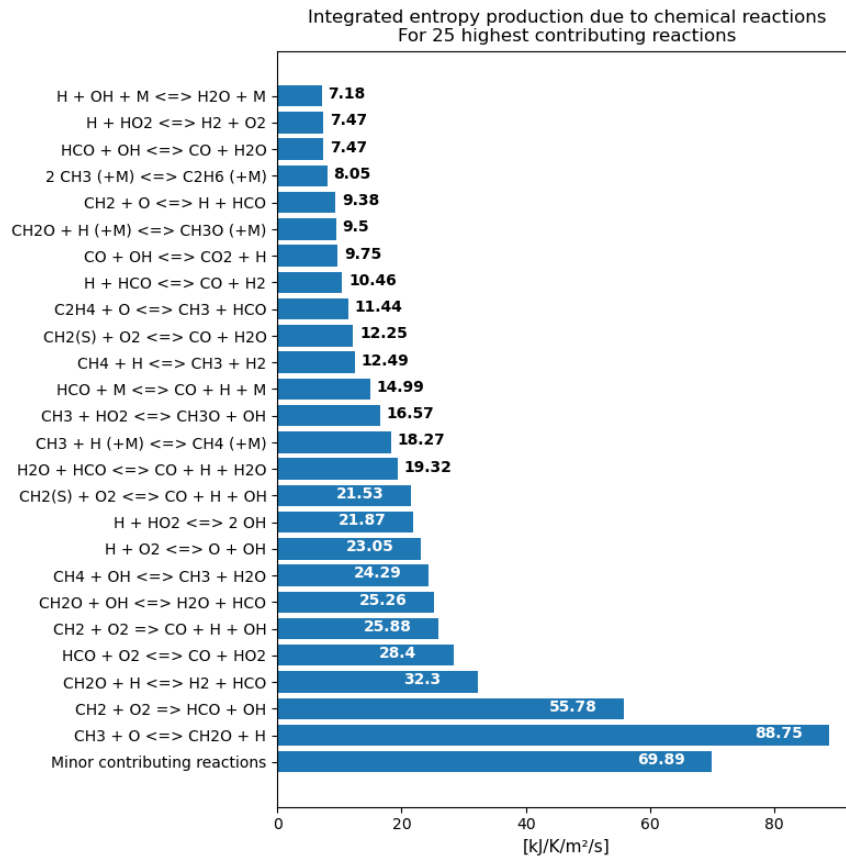


**Figure 27:** Integrated entropy production due to the highest contributing reactions, for reduced mechanism in premixed, freely-propagating methane flame at 1 atm

### 5.4.3 10 atm

Table 4 shows the integrated entropy production by source at 10 atm. As it can be seen, the chemical reactions and conduction are still the main contributors, again followed by diffusion, and viscosity is still negligible. Additionally, the reduced mechanism have now surpassed the detailed mechanism in entropy production due to all the irreversible processes. The global mechanism still underestimates the entropy production from all sources. Another interesting change from 1 atm, is that for the detailed and reduced mechanisms the contribution from viscosity have decreased, while it has increased for the global mechanism. This will be discussed later in this section. The specific contribution from conduction, diffusion, and chemical reactions have increased for all mechanisms.

**Table 4:** Integrated entropy production by source for the premixed, freely-propagating methane flame at 10 atm.

	Integrated entropy production by source [kJ/K/s/m <sup>2</sup> ]		
	Detailed	Reduced	Global
Viscosity	2,62E-04	3,40E-04	2,09E-04
Conduction	1616,03	1754,61	1562,62
Diffusion	316,75	332,55	309,22
Chemical	1825,10	2038,39	1613,90

Figure 28 shows the total local entropy productions using the detailed, reduced, and global mechanisms, at 10atm. The reduced mechanism still follows the detailed mechanism closely, but has now a higher peak and wider profile. An important change from Figure 20 is that the profile of the reduced mechanism now is initiated before the detailed mechanism. The global mechanism is still much lower, but is not as delayed as for 1 atm, and have a shape that is more similar to that of the detailed and reduced mechanisms. The profiles indicate that the flame in general has become much thinner, and the peaks have moved towards the inlet. The thinner profiles are expected, as explained in Section 2.8.1. The peaks have moved approximately 0.01 cm for the detailed and reduced mechanisms, and close to 0.03 cm for the global mechanism. At 1 atm the profile was approximately 0.08 cm wide, while they are now approximately 0.02 cm for the detailed and reduced mechanisms. The profile of the global mechanism was slightly more than 0.12 cm, but has reduced to a width of 0.03 cm. One consequence of a more narrow flame, with higher peak values, is steeper gradients which leads to higher entropy production.

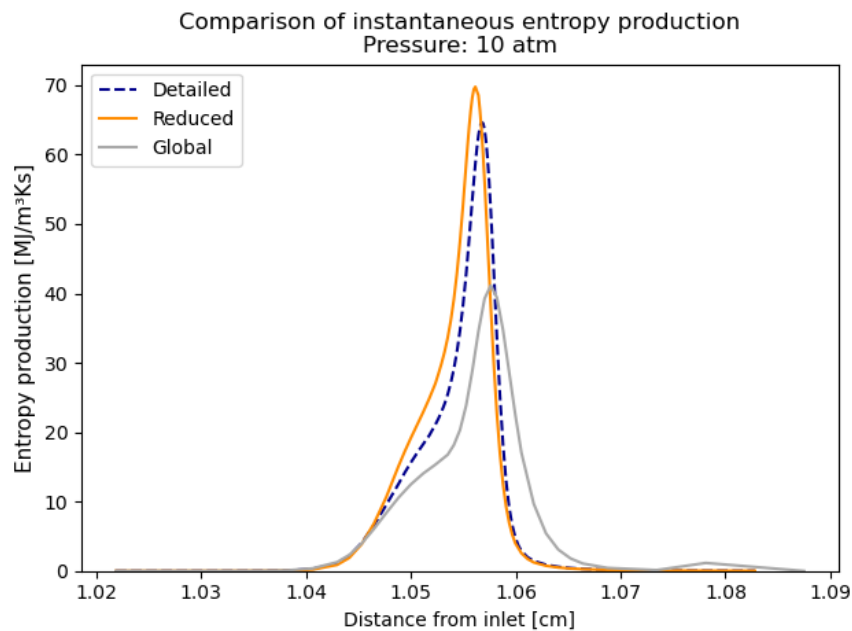
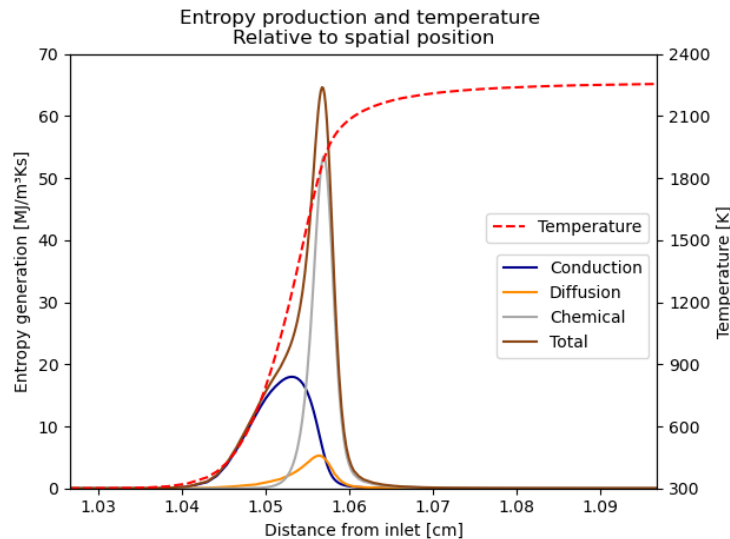
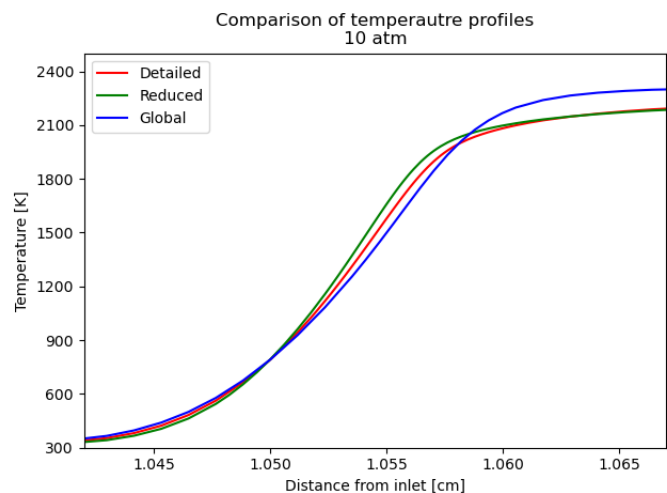
**Figure 28:** Comparison of the entropy production using detailed, reduced, and global mechanism. Fuel type is methane in premixed, freely-propagating model with 10 atm pressure.

Figure 29 shows the local entropy production by source for the detailed mechanism at 10 atm. Considering that all the graphs included in Figure 20 have similar shapes and characteristics, only the graph for the detailed mechanism is included in this section. It can be seen that the profiles for all the contributions are thinner, however the dimension on the y-axis is much higher than that of Figure 20. Therefore, the effects of thinner profiles are outweighed by the effects of taller peaks. In fact, the dimensions on the y-axis are higher by a factor of ten, which is the same as the factor of pressure increase.



**Figure 29:** Instantaneous entropy production by source using detailed mechanism, for premixed, freely-propagating methane flame at 10 atm.

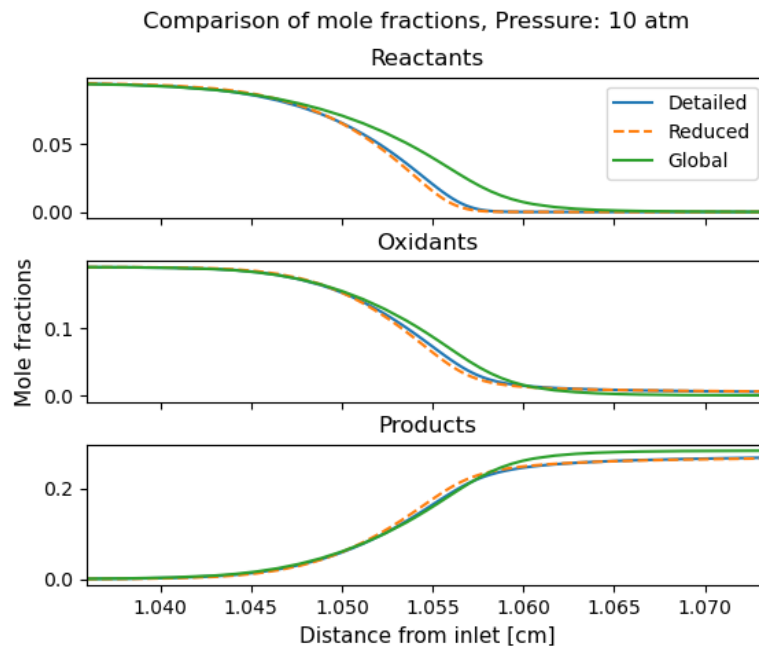
To further investigate the reason for the changes, the temperature profiles for all mechanisms presented in Figure 30, are investigated. From the figure it can be seen that the profile for the detailed mechanism starts to increase before the profile for the reduced mechanism. However, the reduced mechanism exceeds the detailed mechanism around 1.05 cm from the inlet. The peak temperatures calculated by the detailed, and reduced mechanism are almost identical at 2265 K and 2266 K, respectively. Nevertheless, the steeper temperature gradient of the reduced mechanism is sufficient to exceed the entropy production from conduction, calculated by the detailed mechanism.



**Figure 30:** Temperature profiles for detailed, reduced, and global mechanisms for premixed, freely-propagating, methane flame at 10 atm.

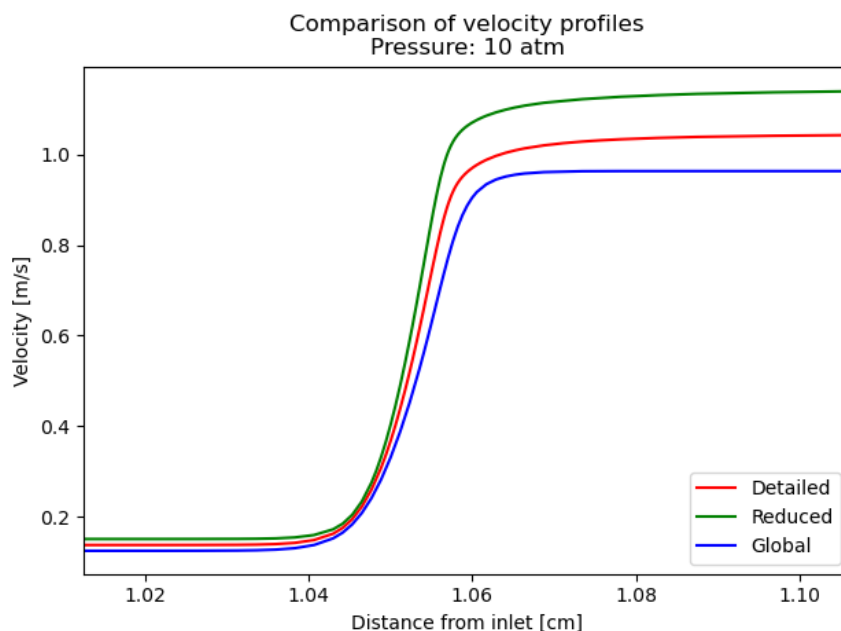
Additionally, it may also be the reason for the higher contribution from chemical reactions, as a faster increase in temperature allows the chemical reactions to occur at a location closer to the inlet. The profiles clearly show that the global mechanism overestimates the temperature. However, the effect of the higher temperature is outweighed by the lesser temperature gradient which result in a lower entropy production due to conduction calculated by the global mechanism.

To further investigate the changes in entropy production from 1 atm to 10 atm, the mole fraction profiles for the reactants ( $\text{CH}_4$ ), oxidants ( $\text{O}_2$ ,  $\text{N}_2$ ), and products ( $\text{CO}_2$ ,  $\text{H}_2\text{O}$ ), can be studied. For 10 atm the profiles are presented in Figure 31. It can clearly be seen that the profiles for the reactants, oxidants, and products using the reduced mechanism are steeper than the profiles using the detailed mechanism. In other word, the oxidants reacts with the reactants to create the products faster. Why the contribution from the chemical reactions calculated by the reduced mechanism precede the contribution calculated by the detailed mechanism was not further investigated due to time limitations. Nevertheless, the steeper gradients result in a higher contribution from diffusion and chemical reactions, when the reduced mechanism is used rather than the detailed. The global mechanism is now closer to the other profiles, but still has some discrepancy and flatter profiles. On another note, Figure 31 indicates that more oxidants and reactants are used, and more  $\text{CO}_2$  and  $\text{H}_2\text{O}$  are produced, indicating a cleaner combustion.



**Figure 31:** Comparison of mole fraction profiles for reactants ( $\text{CH}_4$ ), oxidants ( $\text{O}_2$ ,  $\text{N}_2$ ), and products ( $\text{CO}_2$ ,  $\text{H}_2\text{O}$ ), using detailed, reduced, and global mechanisms. Model is premixed, freely propagating flame, with methane as fuel at 10 atm.

As mentioned in the beginning of this sections, the contribution from viscosity is increased from 1 atm to 10 atm for the global mechanism. To understand why, the velocity profiles are presented in Figure 32. Here, it is clear how the velocity is lower but the velocity gradient is steeper than they were at 1 atm, for all mechanisms. For the detailed and reduced mechanisms this leads to a lower entropy production due to the viscous forces. In contrast, the contribution using the global mechanism is increased. For the detailed, and reduced mechanisms the calculated maximum velocity decreases from approximately 2.8 m/s, to 1m/s and 1.15 m/s, respectively. Meanwhile, the maximum velocity decreased from 1.7 m/s to 0.96 m/s, using the global mechanism. Since the decrease is smaller for the global mechanism, the effects of the steeper gradients outweighs the effects of the lower velocity, and therefore the entropy production increases.



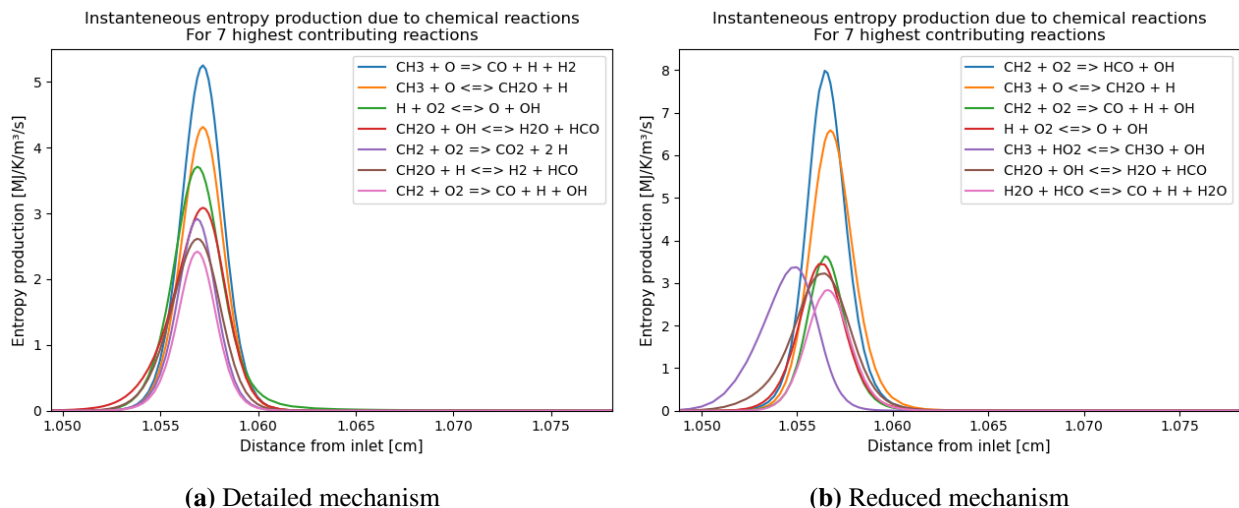
**Figure 32:** Comparison of velocity profiles for detailed, reduced, and global mechanisms for the premixed, freely-propagating, methane flame at 10 atm.

Figure 33 presents the profiles for the locale entropy production due to the seven reactions with the highest local contribution. Figure 33a shows the results using the detailed mechanism, and by comparing the profiles with those presented in Figure 25a, it can be seen that the scale on the vertical axis have increased with one order of magnitude. Furthermore, the first two reactions in the legend are the same in both cases. The next two have switched places, while the third to last are the same, and the two last are different reactions. Additionally, the profiles are shifted left-wards, closer to the inlet.

Figure 33b, shows the results using the reduced mechanism and can be compared with Figure 25b. Here, the scale on the vertical axis have been increased by more than one order of magnitude. Again, the profiles have shifted towards the inlet. The first two reactions in the legend have switched places. Meanwhile, there has been a higher exchange for the other reactions for the reduced mechanism, than the detailed mechanism. Furthermore, the reaction with the third lowest



contribution seems to be the reason for the earlier increase in entropy production calculated by the reduced mechanism, compared with that calculated by the detailed mechanism.



**Figure 33:** Comparison of the entropy production due to chemical reactions, from the seven highest contributing reactions using the detailed (a), and reduced (b) mechanisms. Fuel type is methane in premixed, freely-propagating model at 10 atm.

The integrated contribution from the 25 highest contributing reactions, using the detailed mechanism at 10 atm are presented in Figure 34. The bar at the bottom represents the summed contribution from the remaining reactions. By comparing it with the results at 1 atm it can be seen that the highest contributing reaction remain the same, and the reaction with the fourth highest contribution at 1 atm is now the second highest.

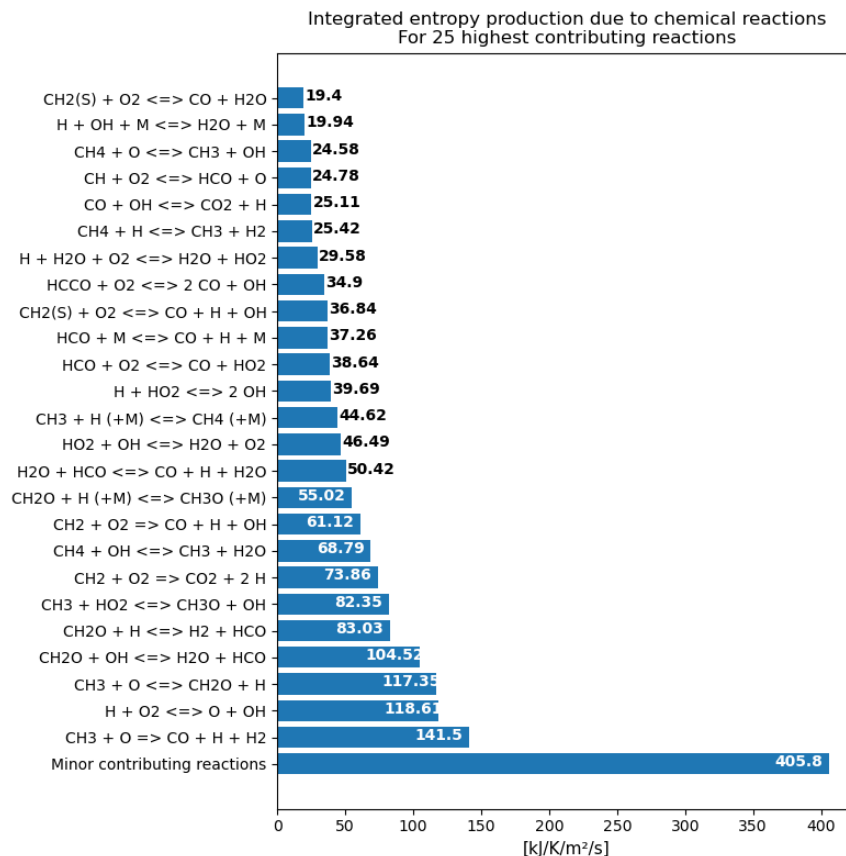


**Figure 34:** Integrated entropy production due to the highest contributing reactions, for detailed mechanism in premixed, freely-propagating methane flame at 10 atm

Figure 35 shows the integrated contribution from the the 25 highest contributing reactions, and the sum of the remaining reactions. Comparing with the results at 1 atm, the two highest contributing reactions have switched places. In regards to the following reactions, there have been a higher exchange in the included reaction from 1 atm to 10 atm for the reduced mechanism, than the detailed mechanism.

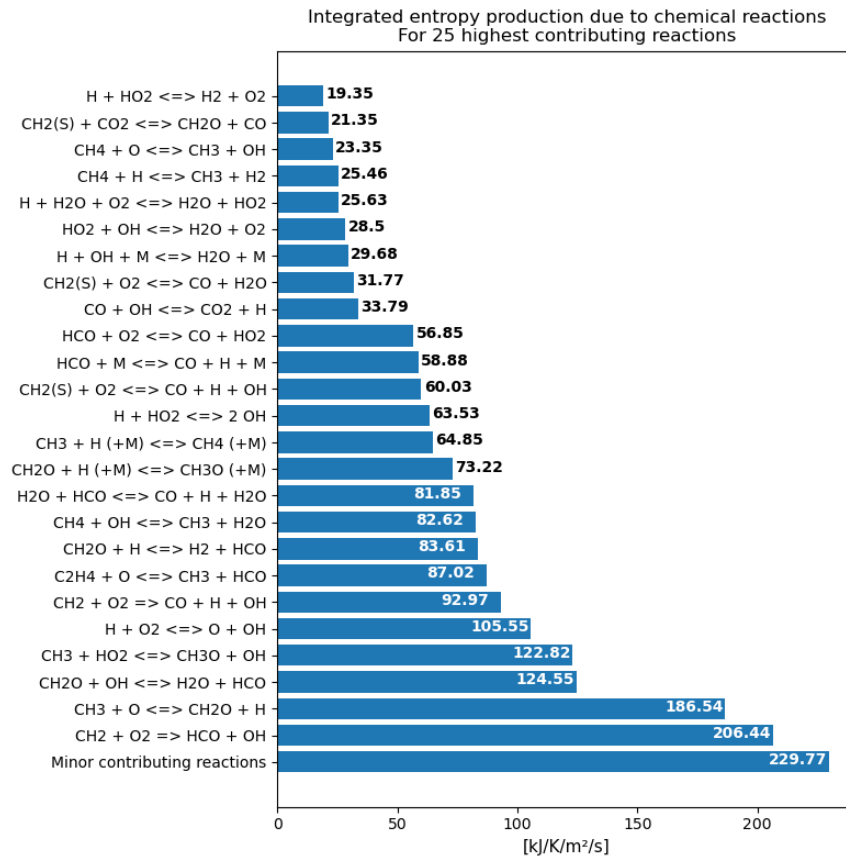


**Figure 35:** Integrated entropy production due to the highest contributing reactions, for reduced mechanism in premixed, freely-propagating methane flame at 10 atm

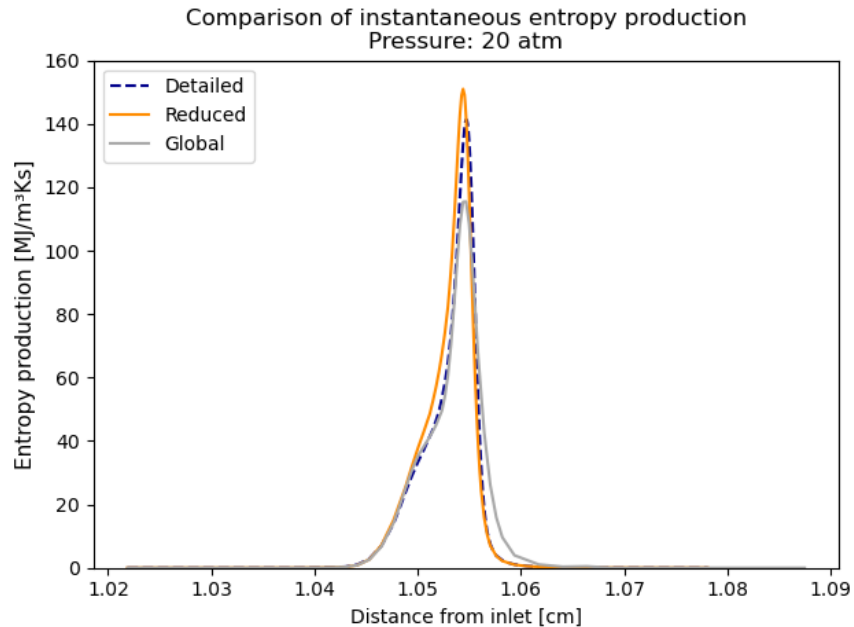
#### 5.4.4 20 atm

Table 5 includes the integrated entropy production by source at 20 atm. The contributions from chemical reactions, conduction, and diffusion have increased again for all mechanisms. For the detailed, and reduced mechanisms the entropy production due to viscous forces have decreased again, while for the global mechanism it has increased more. The reduced mechanism still overestimates the entropy production due to all the irreversible processes. The global mechanism now overestimates the entropy production due to viscosity, conduction and chemical reactions, when it is compared with the detailed mechanism.

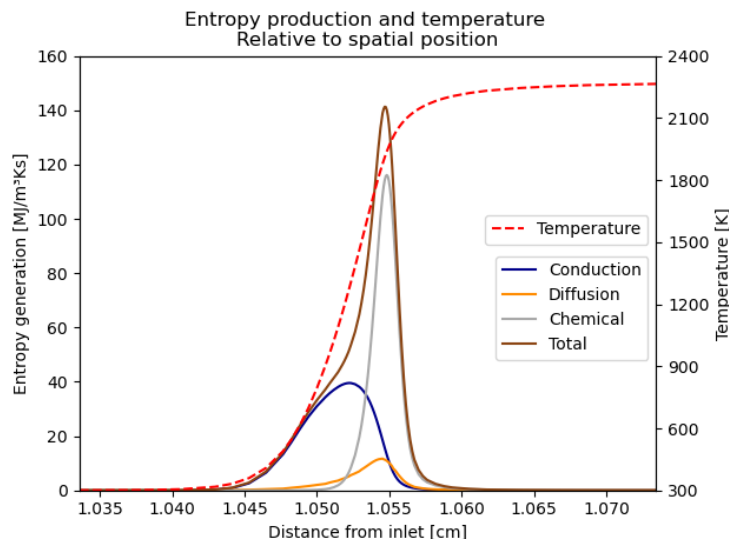
**Table 5:** Integrated entropy production by source for the premixed, freely-propagating methane flame at 20 atm.

	Integrated entropy production by source [kJ/K/s/m <sup>2</sup> ]		
	Detailed	Reduced	Global
Viscosity	2,18E-04	2,79E-04	2,52E-04
Conduction	2438,10	2585,52	2614,73
Diffusion	472,85	492,74	394,01
Chemical	2607,40	2873,79	2722,33

At 20 atm, the local total entropy production for the detailed, reduced, and global mechanism looks as presented in Figure 36. The reduced, and global mechanisms are now only slightly delayed. The profile of the reduced mechanism precedes that of the detailed mechanism, and has a higher peak value which lead to a higher integrated entropy production. The profile of the global mechanism also precedes the detailed mechanism over a short distance in the beginning, but is surpassed by the profile of the detailed mechanism right after a distance of 1.05 cm from the inlet. Even though the profile has a lower peak than that of the detailed mechanism, it is visibly wider, which leads to a higher integrated entropy production. The profiles have become even thinner, and is now approximately 0.015 cm wide for the detailed and reduced mechanism, and slightly wider for the global mechanism. The reduction in width has approximately the same factor as for the reduction in pressure. Since the reaction zone was reduced by a larger factor from 1atm to 10 atm, than from 10 atm to 20 atm the effect was not as large.

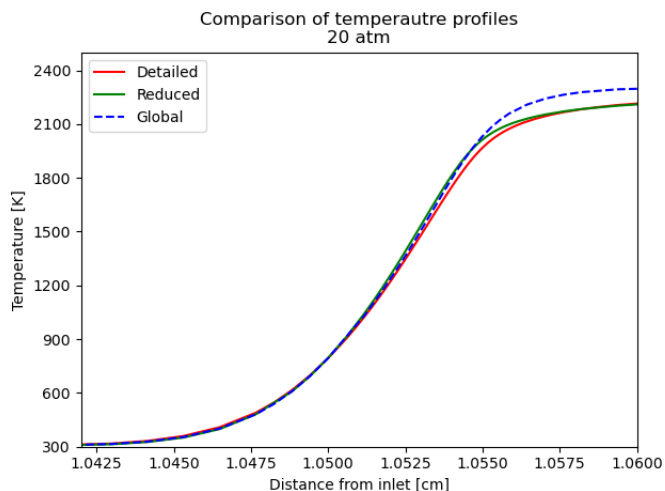
**Figure 36:** Comparison of the entropy production using detailed, reduced, and global mechanisms. Fuel type is methane in premixed, freely-propagating model at 20 atm.

As for 10 atm, the profiles in Figure 36 are assumed to adequately similar, and therefore only the local entropy production by source calculated by the detailed mechanism is displayed in Figure 37. Again the profiles for the different contributions are more narrow, but much taller. The dimensions on the y-axis have been increased by a factor of 2, which is the same as the factor of pressure change.



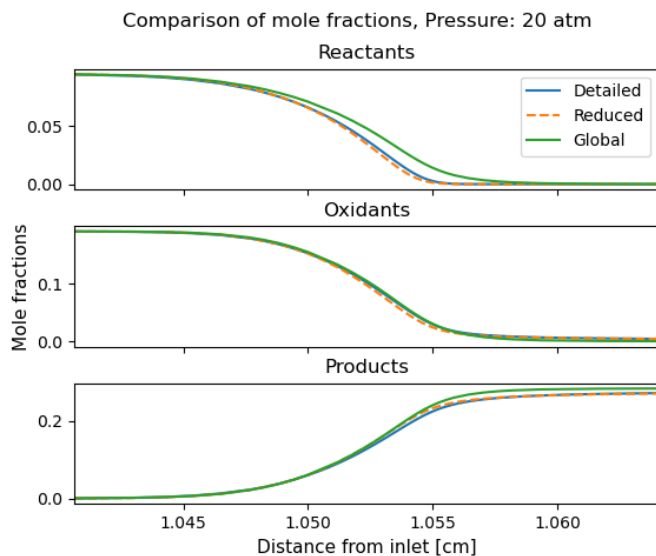
**Figure 37:** Instantaneous entropy production by source using detailed mechanism, for premixed, freely-propagating methane flame at 20 atm.

In Figure 38 the temperature profiles for all mechanisms at 20 atm are presented. All profiles are steeper than the profiles at 10 atm presented in Figure 30, which is the main reason for the increase in contribution from conduction. Furthermore, the profiles of the reduced and global mechanisms now precedes the profile of the detailed mechanism. The global mechanism still overestimates the peak temperature, and even though it is not visible on the graph the reduced mechanism now overestimates the peak temperature by 1 K. Therefore, the entropy production due to conduction is higher when the reduced, and global mechanisms are used rather than the detailed mechanism.



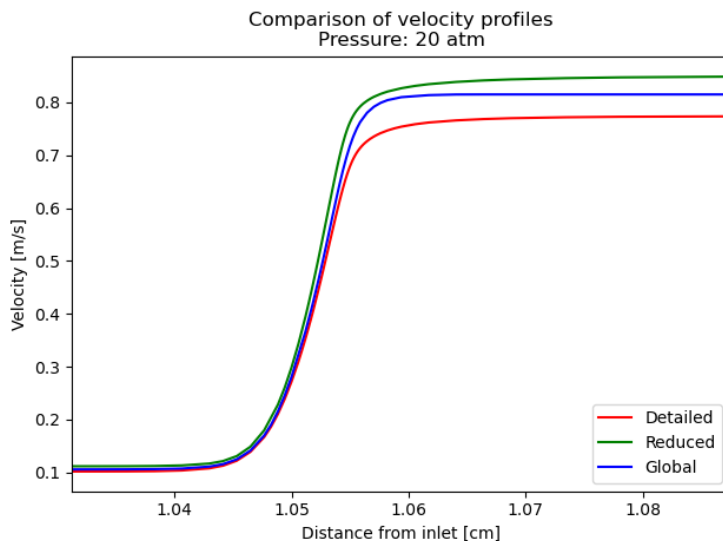
**Figure 38:** Comparison of temperature profiles for detailed, reduced, and global mechanisms for premixed, freely-propagating, methane flame at 20 atm.

Since the temperature profiles using the reduced, and global mechanisms precede the profile using the detailed mechanism it is natural to assume a similar characteristic in the species mole fraction profiles. Figure 39 displays the mole fractions for the reactants ( $\text{CH}_4$ ), oxidants ( $\text{O}_2$ ,  $\text{N}_2$ ), and products ( $\text{CO}_2$ ,  $\text{H}_2\text{O}$ ), using detailed, reduced, and global mechanisms at 20 atm. Comparing the results at 10 atm, Figure 31, with the results at 20 atm it is seen that the gradients are steeper for all mechanisms. This is because of the thinner profiles. As a consequence, the chemical reactions occur closer to the inlet, and faster. Furthermore, it can be seen that the profiles using the reduced mechanism still precede the profiles using the detailed mechanism, which is the reason for the higher contribution from diffusion using the reduced mechanism. The global mechanism is still somewhat delayed, with flatter profiles, and calculates therefore a lower production due to diffusion.



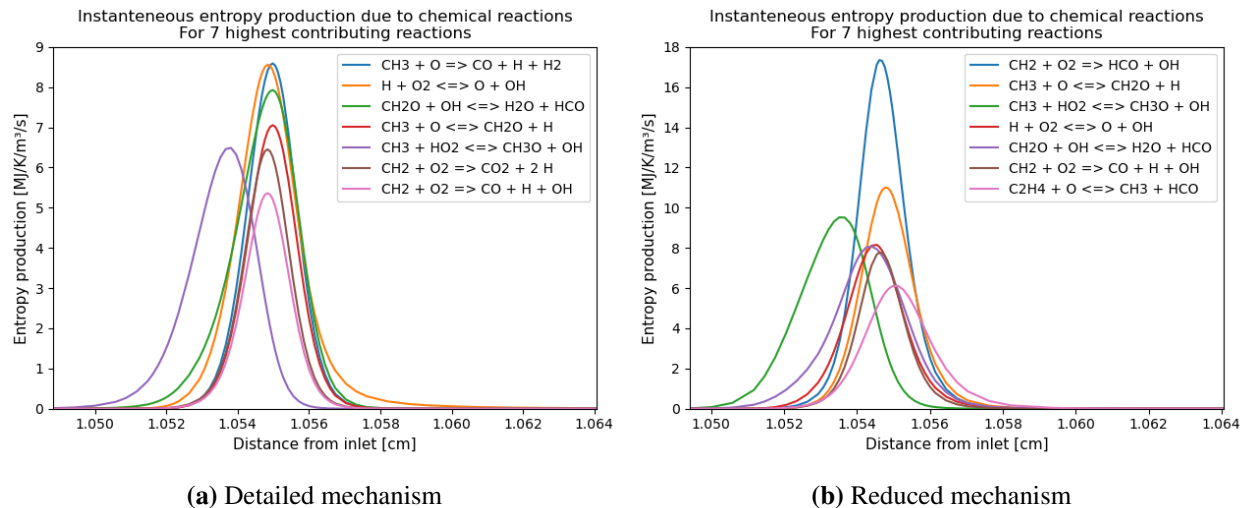
**Figure 39:** Comparison of mole fraction profiles for reactants ( $\text{CH}_4$ ), oxidants ( $\text{O}_2$ ,  $\text{N}_2$ ), and products ( $\text{CO}_2$ ,  $\text{H}_2\text{O}$ ), using detailed, reduced, and global mechanisms. Model is premixed, freely propagating flame, with methane as fuel at 20 atm pressure.

Figure 40 show the velocity profiles for all mechanisms at 20 atm. It almost cannot be detected any differences between Figure 40, and Figure 32. However, the gradients are steeper, and the velocities are lower. As for 10 atm, the effects of steeper gradients at 20 atm exceeds the effects of lower velocity, causing a higher entropy production due to viscous forces for the global mechanism. In contrast, the effects of a lower velocity outweighs the effects of steeper gradients, resulting in a lower entropy production, when the detailed and reduced mechanisms are used.



**Figure 40:** Velocity profiles for detailed, reduced, and global mechanisms for the premixed, freely-propagating, methane flame at 20 atm.

Figure 41 compares the local entropy production due to the seven reactions with highest contribution at 20 atm. The detailed mechanism is used in Figure 41a, and the reduced mechanism is used in Figure 41b. The scales on the vertical axis in both figures have increased from 10 atm to 20 atm, as they did from 1 atm to 10 atm. Additionally, the scales in the figure for the reduced mechanism is larger than the scale in the figure for the detailed mechanism. This was also seen at 10 atm, and is explained by the lower number of reactions included in the reduced mechanism. Since the same amount of fuel is used with both mechanism, the released energy is distributed over fewer reactions, thus giving each reaction an increased contribution. In Figure 41a it can be seen that the reaction causing the reduced mechanism to precede the detailed mechanism in Figure 28 is included now. However, the same reaction has a higher contribution when the reduced mechanism is used which causes it to still precede the detailed mechanism.



**Figure 41:** Comparison of the entropy production due to chemical reactions, from the highest contributing reactions using the detailed (a), and reduced (b) mechanisms. Fuel type is methane in premixed, freely-propagating model at 20 atm pressure.

Figure 42 shows the integrated entropy production due to the 25 reactions with highest contributions. The bottom column represents the sum of the remaining reactions. More reactions have been exchanged from 10 atm to 20 atm, than from 1 atm to 10 atm. And the highest contributing reaction is no longer the same.



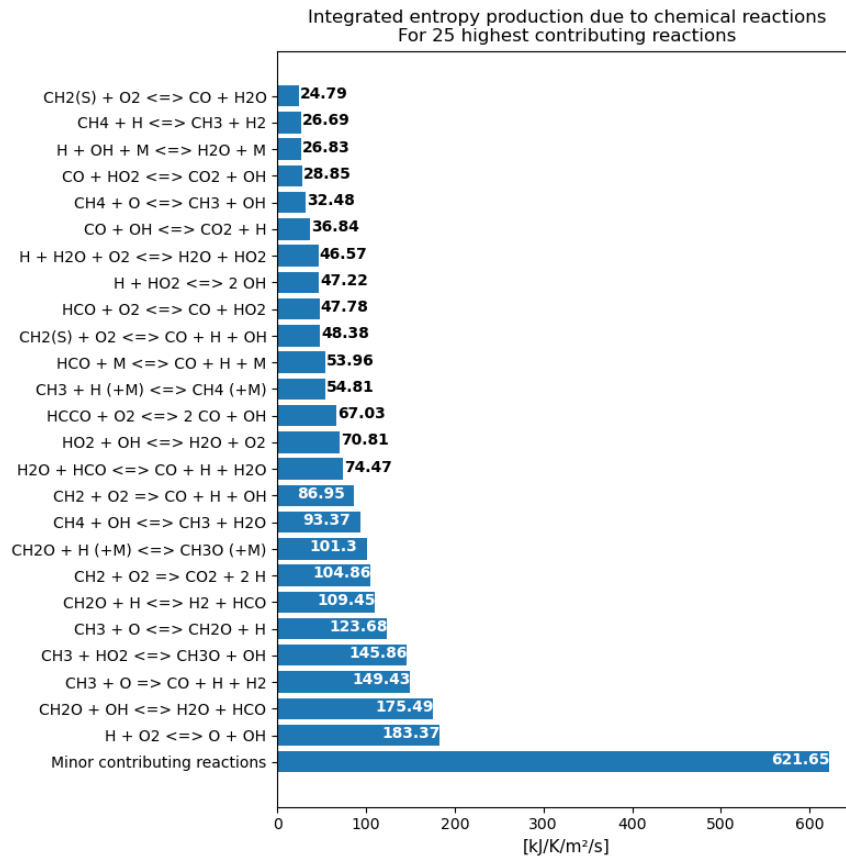


**Figure 42:** Integrated entropy production due to the highest contributing reactions, for detailed mechanism in premixed, freely-propagating methane flame at 20 atm

In Figure 43 the 25 highest contributions to entropy production due to reactions are included, using the reduced mechanism. Additionally, the sum from the remaining reactions are included in the column in the bottom. It appears to be less exchange of reactions for the reduced mechanism, than the detailed mechanism when the pressure is increased from 10 atm to 20 atm. The reaction causing the reduced mechanism to precede the detailed mechanism has now the second highest integrated production.

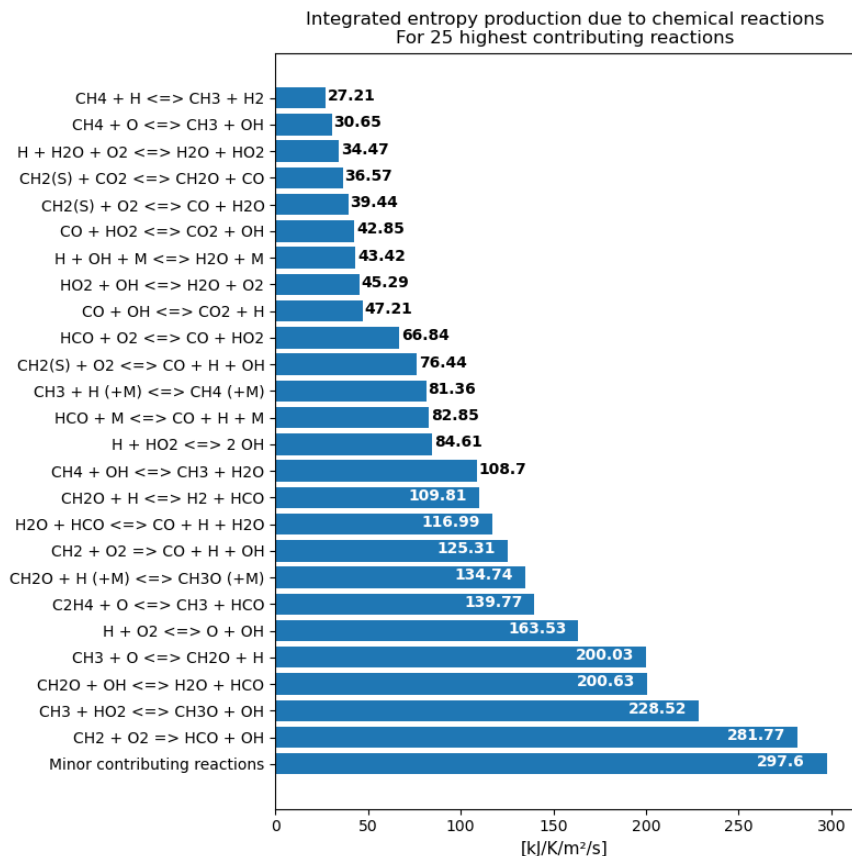


**Figure 43:** Integrated entropy production due to the highest contributing reactions, for reduced mechanism in premixed, freely-propagating methane flame at 20 atm

### 5.4.5 Solution Grid

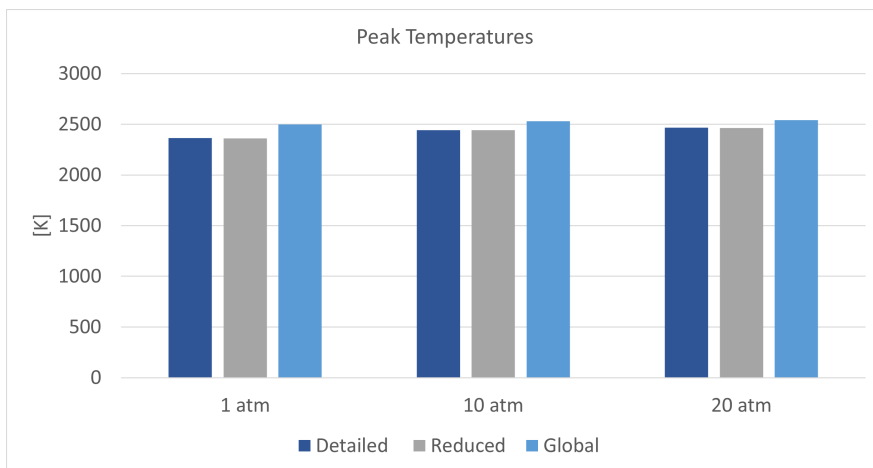
The solution grid was determined by the grid refinement criteria defined in Section 3.3.1. At 1 atm, the numerical grid for the solution was identical for the detailed, and reduced mechanisms (115 grid points), while the global mechanism had fewer grid points (69 grid points). The resolution, spacing between the grid points increased when the gradients increased and had an order of magnitude ranging from  $10^{-3}$  to  $10^{-6}$ , for all mechanisms. At 10 atm the detailed mechanism had the most grid points (97), followed by the reduced (90), and the global mechanisms (59). The spacing varied in order of magnitude between  $10^{-3}$  and  $10^{-6}$  for all mechanisms. When the pressure was increased to 20 atm, the detailed mechanism still had most grid points (99), followed by the reduced (86), and the global mechanisms (63). The grid spacing now varied between  $10^{-3}$  to  $10^{-7}$  for the detailed and reduced mechanism, and  $10^{-3}$  to  $10^{-6}$  for the global mechanism. The spacing in each point is given in the appendix.

## 5.5 Syngas

The graphs in the the following section are limited parts of the complete numerical domain. The complete domain was 6 cm wide for this model, at all pressures, using the various chemical mechanisms. This was necessary because Cantera could not solve the governing equations on a 3 cm wide domain, at 1 atm. Therefore, to ensure equal domain sizes for the different cases, the initial width of the domain was increased. The graphs are limited to focus on the reaction zone where the changes are more distinct.

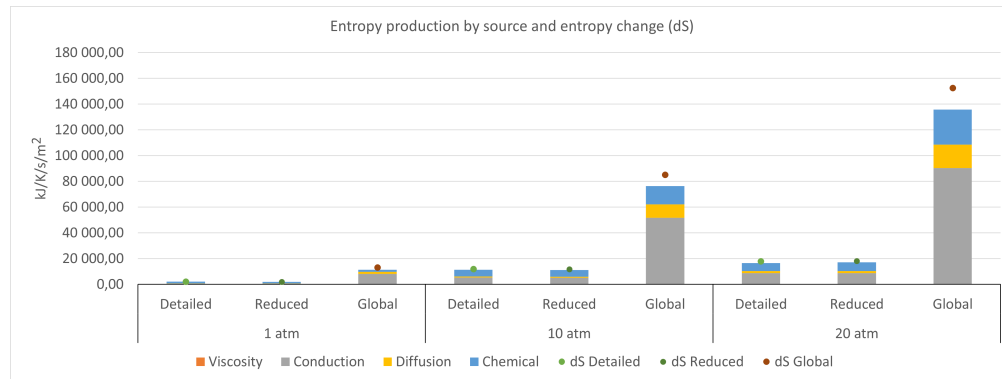
### 5.5.1 Comparison of Cases.

In Figure 44 the peak temperatures calculated by the detailed, reduced, and global mechanisms are presented. At all pressures, the detailed and reduced mechanisms calculate approximately the same temperature, while the global mechanism overestimate it. For all mechanisms the peak temperature increases with the pressure.



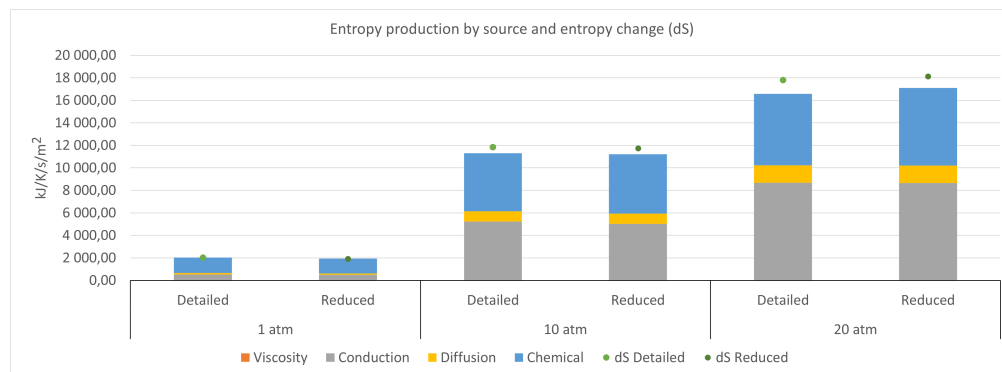
**Figure 44:** Comparison of the peak temperatures at 1 atm, 10 atm, and 20 atm using detailed, reduced, and global mechanisms for the premixed, freely-propagating syngas flame.

Figure 45 presents the integrated entropy production by source, and entropy change in the system for the detailed, reduced, and global mechanisms with the variation in pressure. The most striking aspect of this figure is how the global mechanism overestimates both the entropy change, and entropy production. The total integrated entropy production using the global mechanism is an order of magnitude higher than those of the detailed and reduced mechanisms. As a consequence, it is hard to separate the contributions from the different irreversible processes from each other. Nevertheless, the total integrated entropy production calculated by the global mechanism increases with pressure.



**Figure 45:** Comparison of the integrated entropy production by source, and entropy change, at 1 atm, 10 atm, and 20 atm using detailed, reduced, and global mechanisms for the premixed, freely-propagating syngas flame.

In Figure 46 the entropy production calculated by the global mechanism is excluded. For both the detailed and reduced mechanisms the total integrated entropy production increases with pressure. At 1 atm and 10 atm, the reduced mechanism underestimated the entropy production compared with the detailed mechanism, while it overestimates it at 20 atm. The entropy change calculated by both mechanisms are similar. Furthermore, as the pressure increase, the difference between the calculated entropy production, and entropy change increases. When syngas is used as the fuel the entropy production due to the chemical reactions are higher, which is in contrast to the results for the reactor model where methane had a higher entropy production.



**Figure 46:** Comparison of the integrated entropy production by source, and entropy change, at 1 atm, 10 atm, and 20 atm using detailed and reduced mechanisms for the premixed, freely-propagating syngas flame.

### 5.5.2 1 atm

Table 6 presents the integrated entropy production by source for the detailed, reduced, and global mechanisms at 1 atm. The table highlights the difference between the mechanisms. For the detailed and reduced mechanisms, chemical reactions are the main contributor to entropy production, followed by conduction, diffusion and viscosity. The detailed mechanism calculates a higher production from all the sources. When the global mechanism is used, conduction is the main contributor, followed by diffusion, chemical reactions and viscosity. The entropy production due to all the

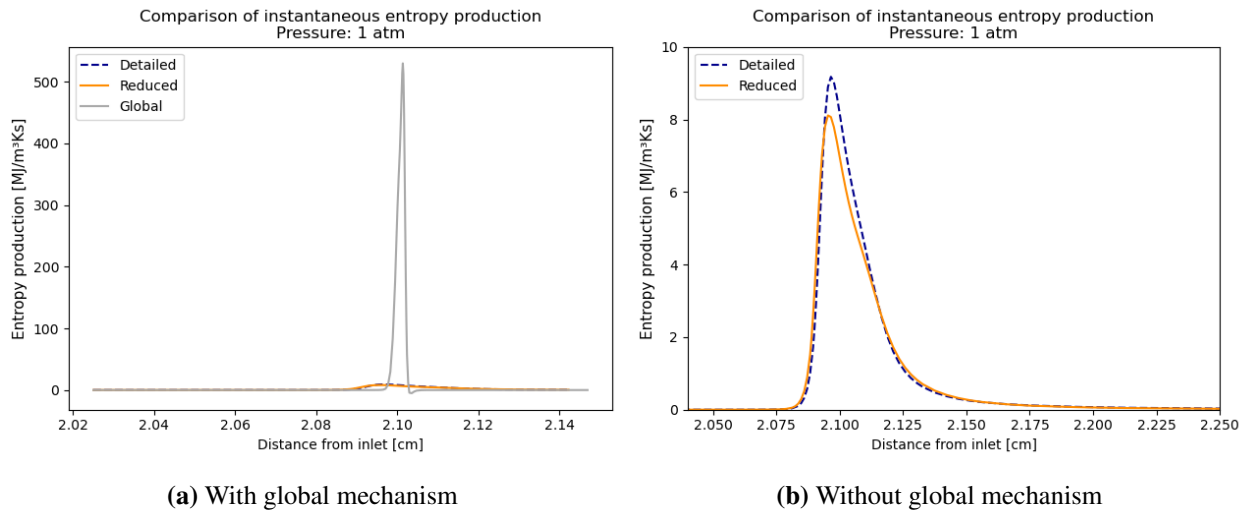
irreversible processes calculated by the global mechanism, are also considerably larger than those calculated by the detailed and reduced mechanisms.

**Table 6:** Integrated entropy production by source for the premixed, freely-propagating syngas flame at 1 atm.

	Integrated entropy production by source [kJ/K/s]		
	Detailed	Reduced	Global
Viscosity	3,10E-03	2,66E-03	2,56E+00
Conduction	532,29	499,02	8184,71
Diffusion	116,50	109,20	1562,42
Chemical	1381,61	1334,36	1538,73

Figure 47 contains two graphs. The first, in Figure 47a, shows the total instantaneous entropy production using the detailed, reduced, and global mechanisms. Again, it is reminded that the system is in steady state, meaning the entropy production will not change with time, and local entropy production would therefore be a more suitable term. It is evident that the entropy production calculated by the global mechanism is erroneous both in the integrated value, as well as the local. Figure 45 and Table 6 also indicated that a direct comparison between the detailed, reduced, and global mechanisms would be nonsensical. Therefore, Figure 47b only includes the graphs for the detailed, and reduced mechanisms. All graphs in the following sections where the total local entropy production is shown will also exclude the results from the global mechanism. Nonetheless, Figure 47b shows that the flame is thin and around 0.75 cm wide. The reduced mechanism follows the detailed mechanism closely, but underestimates the entropy production, which was also shown in Figure 46.

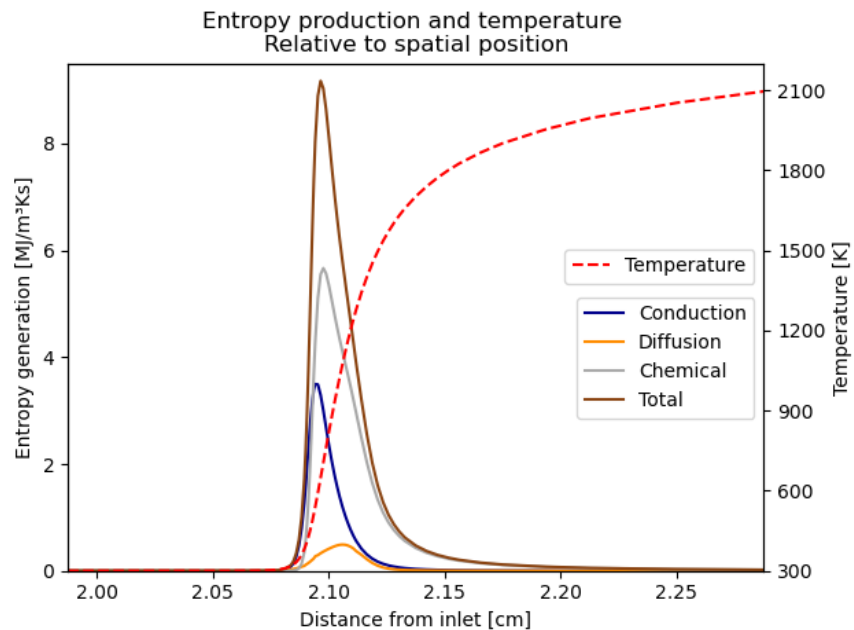
Interestingly, the graphs in Figure 47b almost appear to be the graphs in Figure 20 reversed, in that it has a steep gradient on the left side, and a more gradual gradient on the right side. This might be because syngas is a more reactive fuel and therefore the main entropy production due to the reactions occur earlier, while more time is needed for methane.



**Figure 47:** Comparison of the entropy production using detailed, reduced, and global mechanism. Fuel type is syngas in premixed, freely-propagating model with 1 atm. Figure 47a includes the global mechanism, while it is excluded in Figure 47b

Figure 48 shows the local entropy production by source for the detailed mechanism. Since the profile using the reduced mechanism follows the profile using the detailed mechanism closely in Figure 47b, it is not presented as it is assumed that the detailed mechanism is representative for both mechanisms. The profiles in Figure 48 agree well with the profiles in Figure 5 in Acampora and Marra [4], mentioned in Section 1.2.1. The result presented in their figure was obtained at the same conditions as in Figure 48.

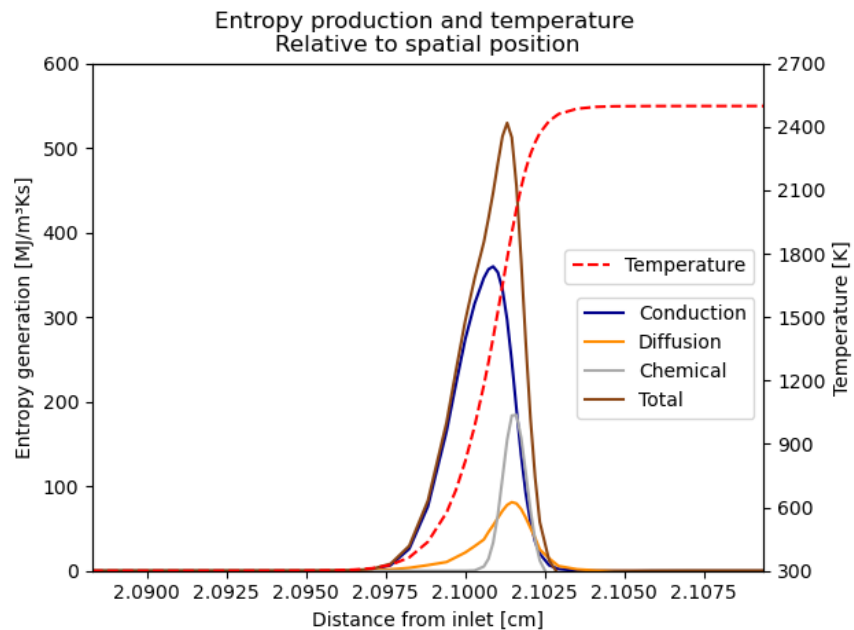
It can be seen that the entropy production is initiated by conduction, which again is initiated by an increase in temperature. The chemical reactions start to occur closely after, and has its peak shortly after the conduction. The contribution from diffusion increases when the the reactions are initiated, and peaks close to the peak in contribution from chemical reactions. This is a similar pattern seen when methane is used as the fuel, and the same explanation given in Section 5.4.2 therefore applies here. However, as mentioned in brief above, the gradients are much steeper on the left side of the graph, compared with the local entropy production with the detailed mechanism with methane presented in Figure 29. This is because syngas is a more reactive fuel, that reacts at lower temperatures.



**Figure 48:** Instantaneous entropy production by source using the detailed mechanism on a premixed, freely-propagating syngas flame at 1 atm.

In Figure 49 the local entropy production by source, using the global mechanism is shown. The profile is similar to that of the detailed mechanism, but with some distinct differences. The graph possesses the same patterns, where the entropy production due to conduction is initiated by the increase in temperature, and peaks where the temperature gradient is largest. The chemical reactions start to occur when the temperature is sufficient, and peaks slightly after the conduction does. However, in contrast to Figure 48 the contribution from the chemical reactions are considerably lower relative to conduction.

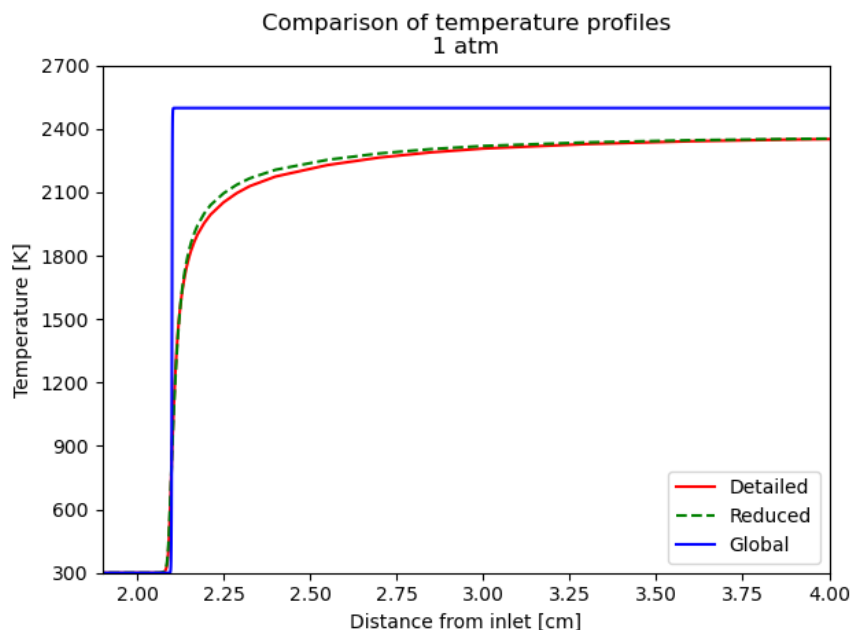
Furthermore, the profiles in Figure 49 are thinner, which is a result of steep gradients, such as the temperature gradient. When the global mechanism is used, the temperature increases from 300 K to approximately 2500 K, over a distance of right above 0.005 cm. In contrast, when the detailed mechanism is used, the temperature increase more gradually from 300 K to 2364 K. This is better shown in Figure 50.



**Figure 49:** Instantaneous entropy production by source using the global mechanism on a premixed, freely-propagating syngas flame at 1 atm.

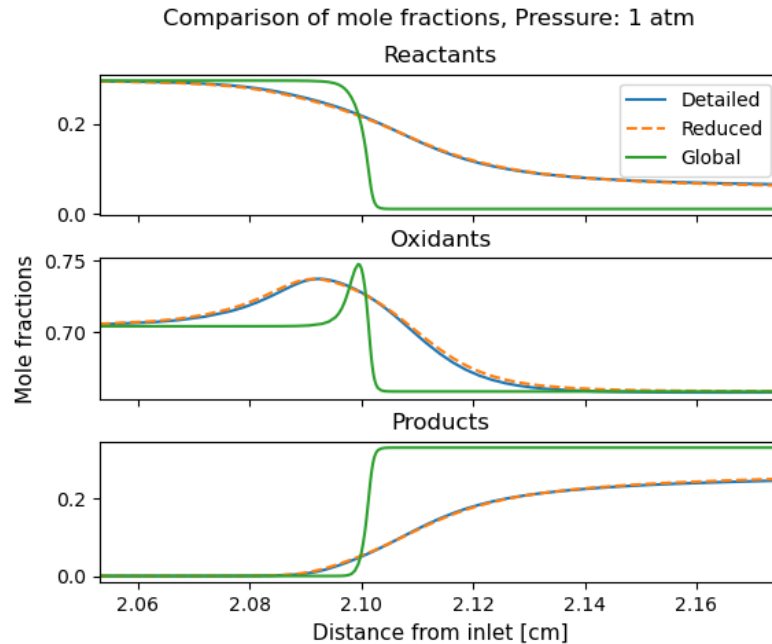
Figure 50 shows the temperature profile for all mechanisms at 1 atm. Here, it is shown clearly how the temperature profile for the global mechanism is much steeper, and calculates a higher peak temperature than the detailed and reduced mechanisms. As explained in Section 5.4.2, the contribution from conduction is very dependent on the temperature gradient (Equation 19), and the steep temperature profile is therefore the main reason for the overestimation done by the global mechanism regarding the entropy production. Furthermore, it may seem like the temperature profile of the reduced mechanism is steeper than the detailed mechanism, which would indicate that it should calculate a higher contribution from conduction. However, this is not the case and it can be assumed that if the figure is further zoomed in the detailed mechanism would have a steeper profile.





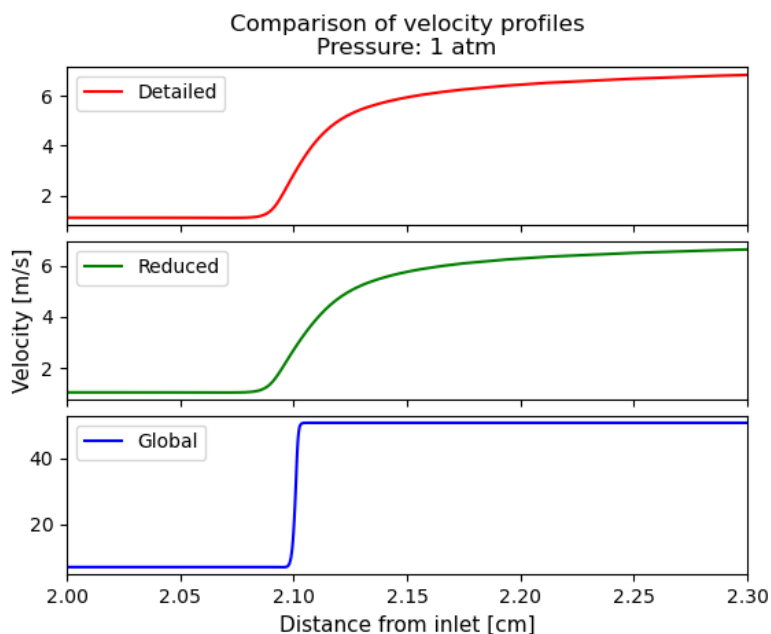
**Figure 50:** Comparison of temperature profiles using detailed, reduced, and global mechanisms for pre-mixed, freely-propagating syngas flame at 1 atm

To further understand the entropy production due to the chemical reactions and diffusion, the mole fraction profiles can be studied. Figure 51 shows the mole fraction profiles for reactants ( $\text{CO}$ ,  $\text{H}_2$ ), oxidants ( $\text{O}_2$ ,  $\text{N}_2$ ), and products ( $\text{CO}_2$ ,  $\text{H}_2\text{O}$ ) for all mechanisms. The small increase in mole fraction for the oxidants around 2.9 cm from the inlet, is because the oxygen is used in the reactions before the nitrogen, which increase the mole fraction of nitrogen. It should be noted that even though it looks like the fraction of oxidants falls to zero, it does not in reality as nitrogen is not completely used. Again it is seen that the profiles for the global mechanism have a much steeper profiles than the detailed and reduced mechanisms. For the detailed, and reduced mechanisms, the profiles are steepest between 2.1 cm, and 2.12 cm from the inlet, which is coherent with the entropy production profile of the chemical reactions and diffusion in Figure 48. For the global mechanism, the mole fraction profiles in Figure 51 are not coherent with the entropy production in Figure 49. The gradients are centered at 2.1 cm from the inlet, which is where the contribution from the chemical reactions is initiated. This indicates that Reaction 3, in the chemical mechanism presented in Equation 44 is the main contributor to the entropy production, since the first two equations produce  $\text{CO}_2$ , and  $\text{H}_2\text{O}$ , which is produced mainly around 2.1 cm from the inlet. This possible reason was not further investigated due to time limitations.



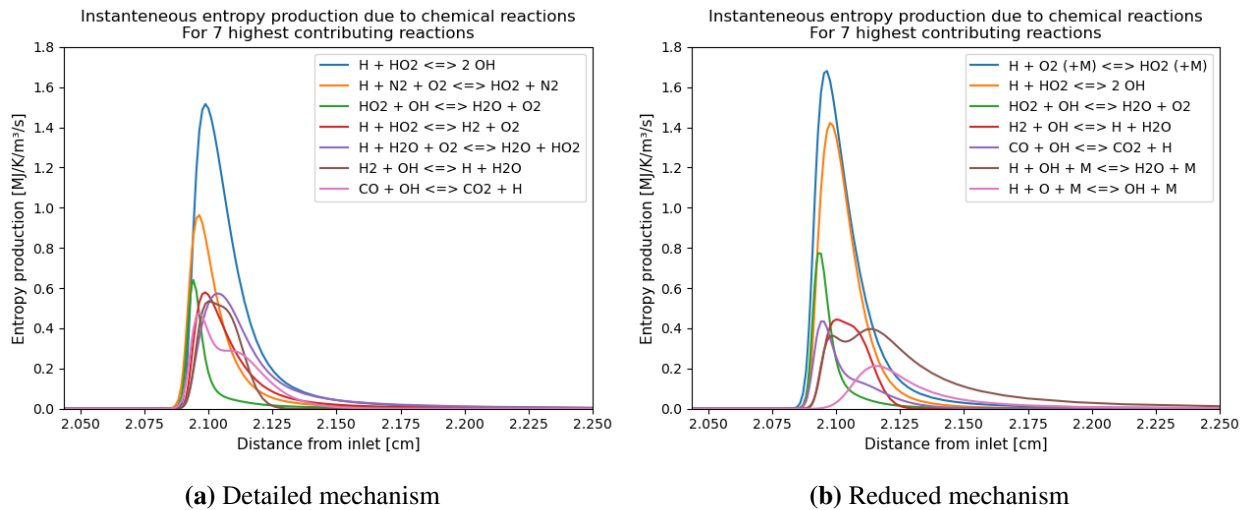
**Figure 51:** Comparison of mole fraction profiles for reactants ( $\text{CO}$ ,  $\text{H}_2$ ), oxidants ( $\text{O}_2$ ,  $\text{N}_2$ ), and products ( $\text{CO}_2$ ,  $\text{H}_2\text{O}$ ), using detailed, reduced, and global mechanisms for premixed, freely-propagating syngas flame at 1 atm

Figure 52 presents the velocity profiles for all the mechanisms. The velocity profile of the global mechanism is both steeper, and one order of magnitude higher than the detailed, and reduced mechanisms. This is the main reason for the high contribution from viscosity, and is also related to the steep temperature gradients. It is natural that as diffusion increases, the velocity must increase to transport the species. Since the graphs in Figure 52 only show a section of the complete domain, the profiles for detailed and reduced mechanisms is seen to further increase. Because of the boundary conditions the velocity profiles flattens out with a zero gradient further from the inlet.



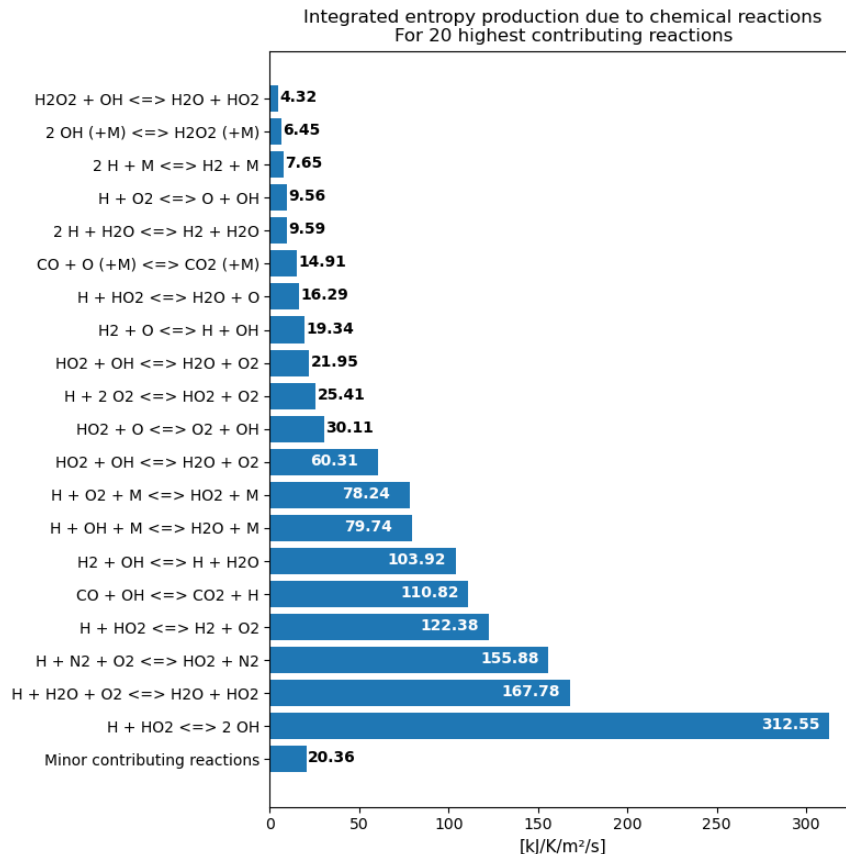
**Figure 52:** Comparison of velocity profiles using detailed, reduced, and global mechanisms for premixed, freely-propagating syngas flame at 1 atm

Figure 53 compares the seven reactions with highest local entropy production, using the detailed (Figure 53a), and reduced (Figure 53b) mechanisms. It can be seen that the highest contributing reaction in Figure 53a, is the second highest in Figure 53b. Furthermore, the second highest contributing reaction for the detailed mechanism is similar to the highest contributing reaction for the reduced mechanism. The only difference is that in the reduced mechanism, the reaction contains a variable species M that is included to represent inert species. Species that are not active in the reaction, but can contribute through collisions.  $N_2$  included in the corresponding reaction in the detailed mechanism often act as such inert species. However, since the reaction in the reduced mechanism also accounts for other species, it is reasonable that it has a higher contribution.



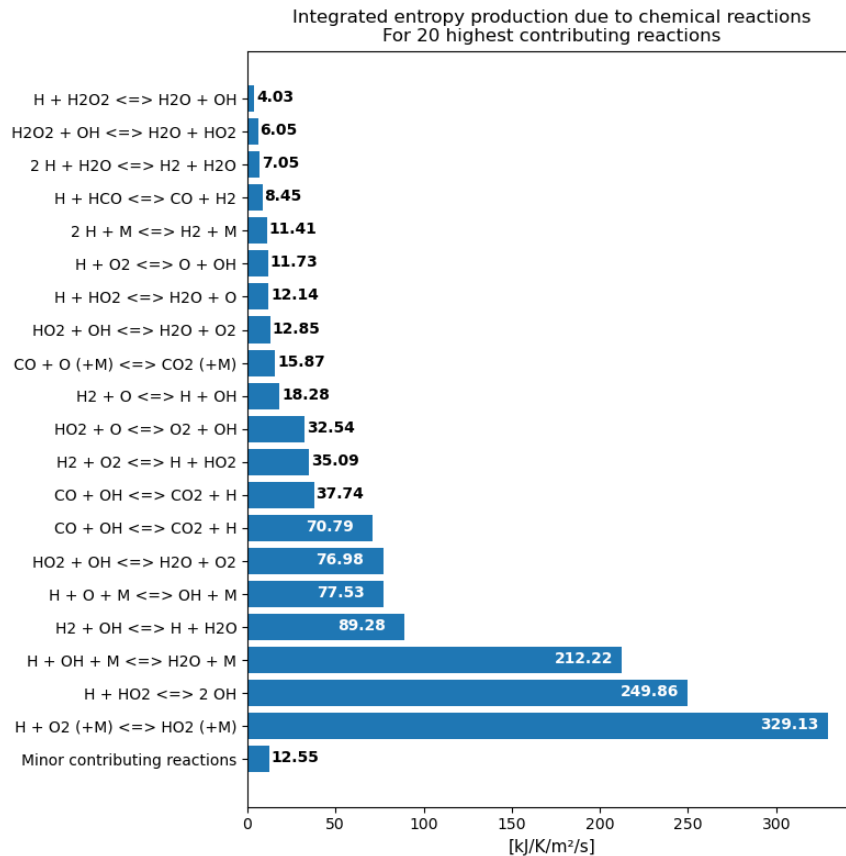
**Figure 53:** Comparison of the entropy production due to chemical reactions, from the highest contributing reactions using the detailed (a), and reduced (b) mechanisms. Fuel type is syngas in premixed, freely-propagating model at 1 atm pressure.

Figure 54 contains the 20 reactions with the highest contributions to the integrated entropy production. The number of reactions included has been reduced compared with the results for methane, since the remaining reactions had minor contributions. Furthermore, the entropy production appears to be distributed over fewer reactions with higher contributions, when syngas is used. It should be repeated that GRI-mech 3.0 [41] is used as the detailed mechanism for both fuels. By comparing Figure 53a with Figure 54, it can be seen that the reaction with the highest local entropy production, also has the highest integrated contribution.



**Figure 54:** Integrated entropy production due to the highest contributing reactions, for detailed mechanism in premixed, freely-propagating syngas flame at 1 atm

Figure 55 shows the highest contributing reactions when the reduced mechanism is used. By comparing with the local production in Figure 53b it can be seen that both the highest, and second highest contributing reactions are the same for the local and integrated production.



**Figure 55:** Integrated entropy production due to the highest contributing reactions, for reduced mechanism in premixed, freely-propagating syngas flame at 1 atm

In Figure 56, the local (Figure 56a), and integrated (Figure 56b) entropy production, using the global mechanism, are displayed. This was not included for methane, as it would not make sense because the global mechanism for methane only has one reaction, and therefore all entropy production originates from this reaction.

In Figure 56a it appears that the third reaction has no contribution. However, in Figure 56b it is clear that it has a contribution to the integrated value. This is because the third reaction has a small, but constant contribution around  $0.8 \text{ MJ/K/M}^3/\text{s}$  starting around 2.1 cm from the inlet, and lasts for the entire domain.

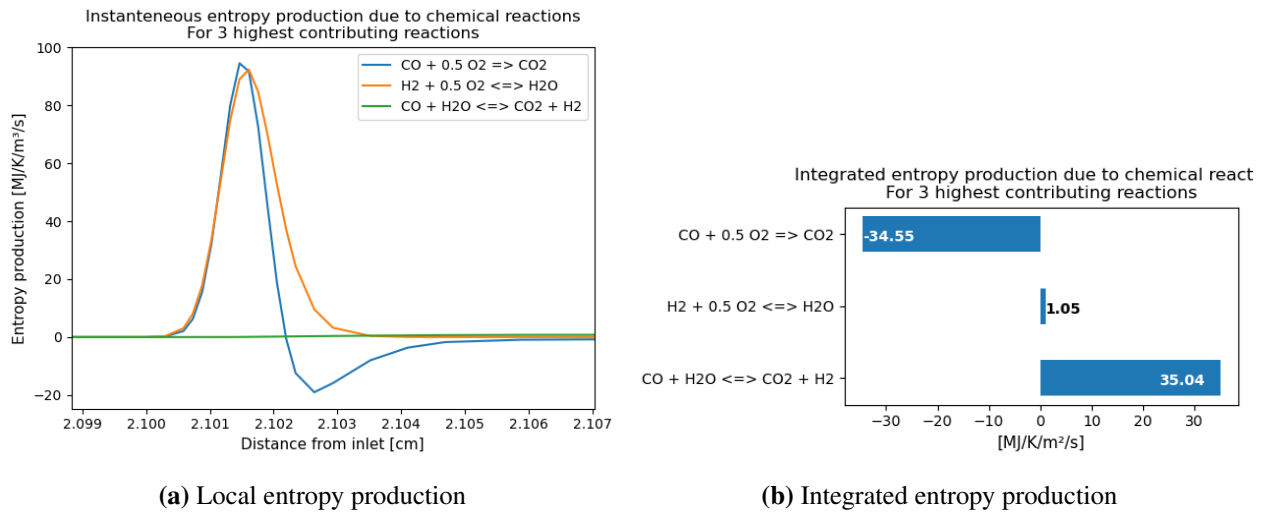


**Figure 56:** Comparison of the local (a), and integrated (b) entropy production due to the chemical reactions, using the global mechanism. Fuel type is syngas in premixed, freely-propagating model at 1 atm.

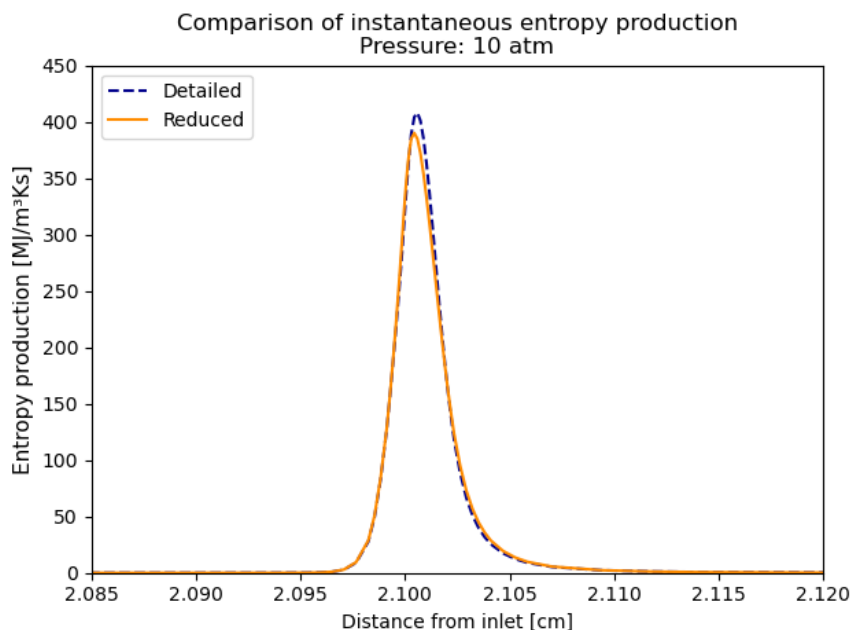
### 5.5.3 10 atm

Table 7 shows the detailed information on the integrated entropy production by source at 10 atm. For the detailed and reduced mechanisms, the entropy production due to conduction, diffusion and chemical reactions have increased, while the contribution from viscosity has decreased. The contribution from conduction calculated by the reduced mechanism has surpassed that of the detailed mechanism, but not sufficient for the total entropy production to surpass. For the global mechanism, the entropy production due to all the irreversible processes have increased. Now, the contribution from the chemical reactions is also considerably larger than for the detailed and reduced mechanism.

**Table 7:** Integrated entropy production by source for the premixed, freely-propagating syngas flame at 10 atm.

	Integrated entropy production by source [kJ/K/s]		
	Detailed	Reduced	Global
Viscosity	1,10E-02	1,03E-02	6,10E+00
Conduction	5221,35	5024,84	51791,79
Diffusion	928,50	905,11	10373,69
Chemical	5153,32	5271,23	14157,51

In Figure 57 the local total entropy production is presented for the detailed and reduced mechanisms. It can be seen that it is less discrepancy for the reduced mechanism for 10 atm than it was for 1 atm. Furthermore, both of the profiles are more narrow, and span approximately 0.012 cm. The width of the profiles have decreased by a factor of 10, which is the same as the factor of increase in pressure. The reason for the thinner flames was explained for the methane flame in Section 5.4.3, and was expected, as mentioned in Section 2.8.1.



**Figure 57:** Comparison of the entropy production using detailed, reduced, and global mechanism. Fuel type is syngas in premixed, freely-propagating model with 10 atm pressure.

Figure 58 contains the local entropy production by source, for the detailed (Figure 58a) and global (Figure 58b) mechanisms at 10 atm. It is clear that both profiles have become more narrow, with higher peaks. Furthermore, in Figure 58a it can be seen how the entropy production due to conduction surpasses that of chemical reactions. This is mainly because the contribution from conduction is dependent on the temperature gradient squared. The profile for the global mechanism in Figure 47b is similar in shape to the profile presented in Figure 58a. The global mechanism shows a reversed trend where the entropy production due to chemical reactions has a higher relative entropy production, compared to conduction.



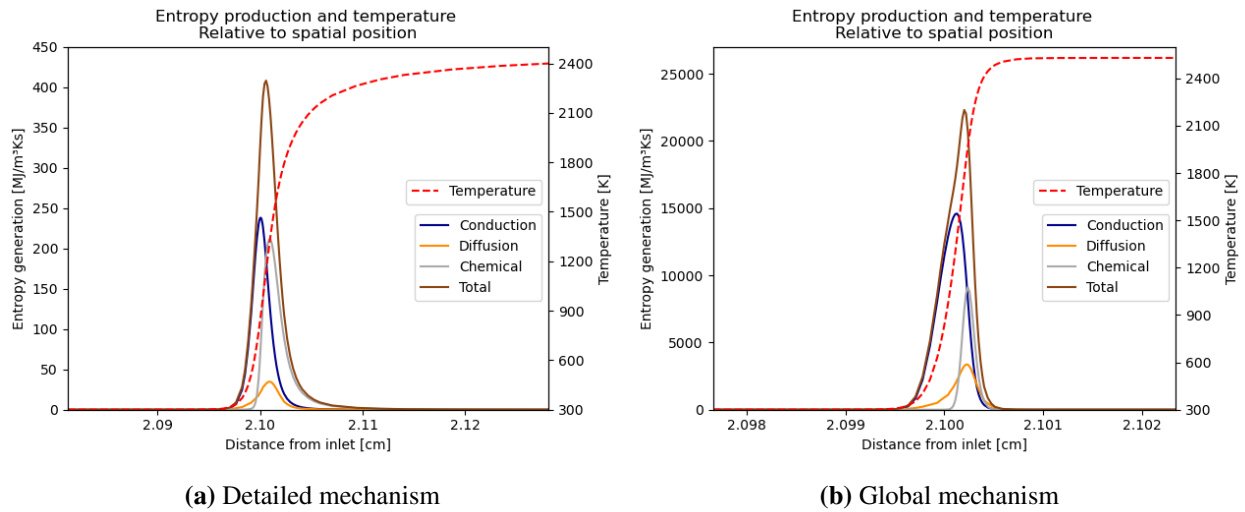


**Figure 58:** Instantaneous entropy production by source using the detailed (a), and global (b) mechanism on a premixed, freely-propagating syngas flame at 10 atm.

In Figure 59 the temperature profiles for all the mechanisms are included. Regarding the profile for the global mechanism it is difficult to see any changes from Figure 50. The profile remain steeper, which causes the overestimation of entropy production. For the detailed and reduced mechanism it can be seen clearly that the temperature increases over a shorter distance, resulting in a higher gradient and an increased contribution from conduction.

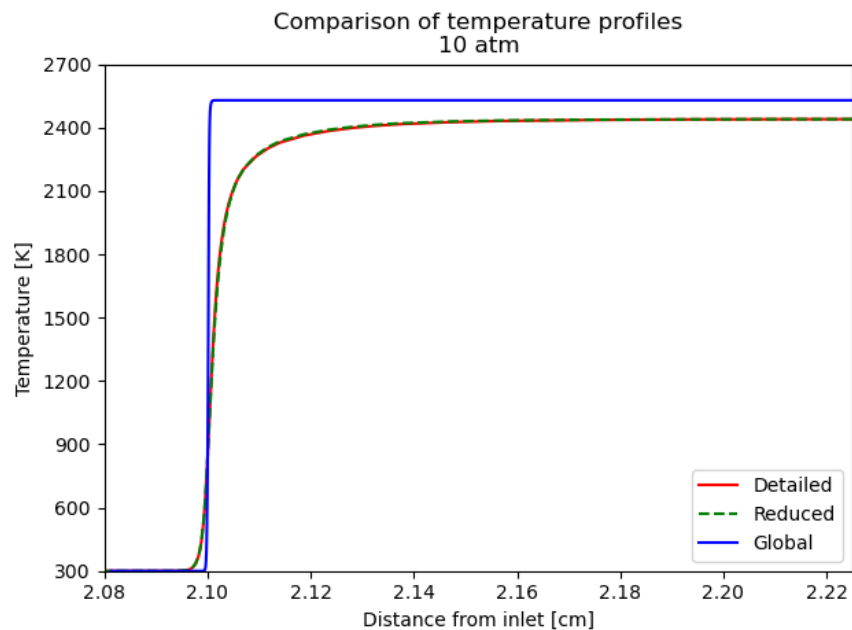


**Figure 59:** Comparison of temperature profiles using detailed, reduced, and global mechanisms for premixed, freely-propagating syngas flame at 10 atm

Because the reaction zone is more narrow at 10 atm, it is expected that the mole fraction profiles also show a similar development as the temperature profiles. This is seen to be true in Figure 60, where the mole fraction profiles for reactants ( $\text{CO}$ ,  $\text{H}_2$ ), oxidants ( $\text{O}_2$ ,  $\text{N}_2$ ), and products ( $\text{CO}_2$ ,  $\text{H}_2\text{O}$ ), using detailed, reduced, and global mechanisms are presented. The gradients of the profiles are steeper than they are in Figure 51. Additionally, it can be seen that more of the reactants are used to produce more products, which indicates a more complete combustion. The steepest gradients are still located around 2.1 cm, but the peak in entropy production due to chemical reactions for the detailed mechanism is slightly moved to the right. Regarding the global mechanism, the gradients are still located where the entropy production due to chemical reactions is initiated.

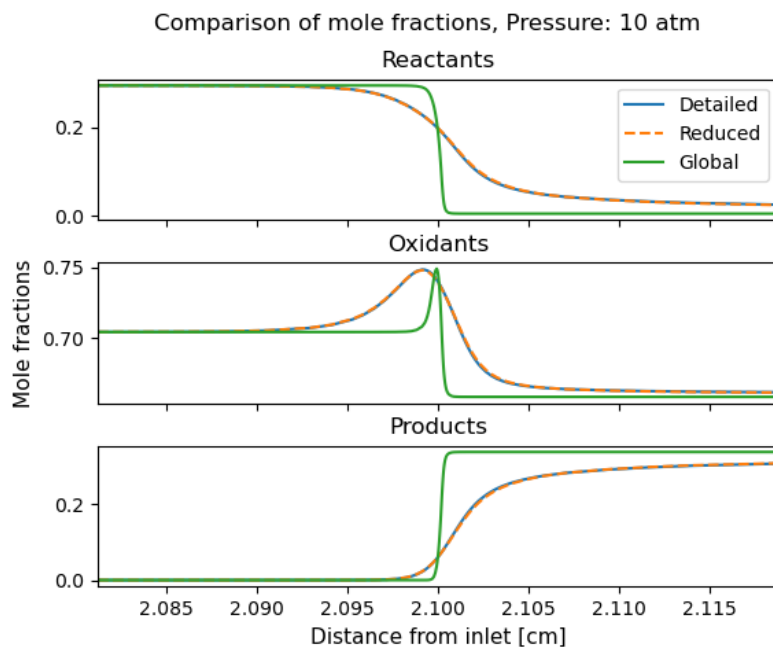


**Figure 60:** Comparison of mole fraction profiles for reactants ( $\text{CO}$ ,  $\text{H}_2$ ), oxidants ( $\text{O}_2$ ,  $\text{N}_2$ ), and products ( $\text{CO}_2$ ,  $\text{H}_2\text{O}$ ), using detailed, reduced, and global mechanisms for premixed, freely-propagating syngas flame at 10 atm

The velocity profiles are compared in Figure 61. The velocity calculated by the global mechanism have decreased from 1 atm to 10 atm. Even so, the gradient is steeper which leads to a higher contribution from the viscosity. The detailed and reduced mechanism have also gotten steeper gradients, but the effects of lower magnitude outweighs the effects of steeper gradients, which results in a lower entropy production due to viscosity. Regarding the velocities and diffusion, it was said in Section 5.5.2 that more diffusion requires higher velocities. However, the entropy production due to diffusion increased from 1 atm to 10 atm for all mechanisms.

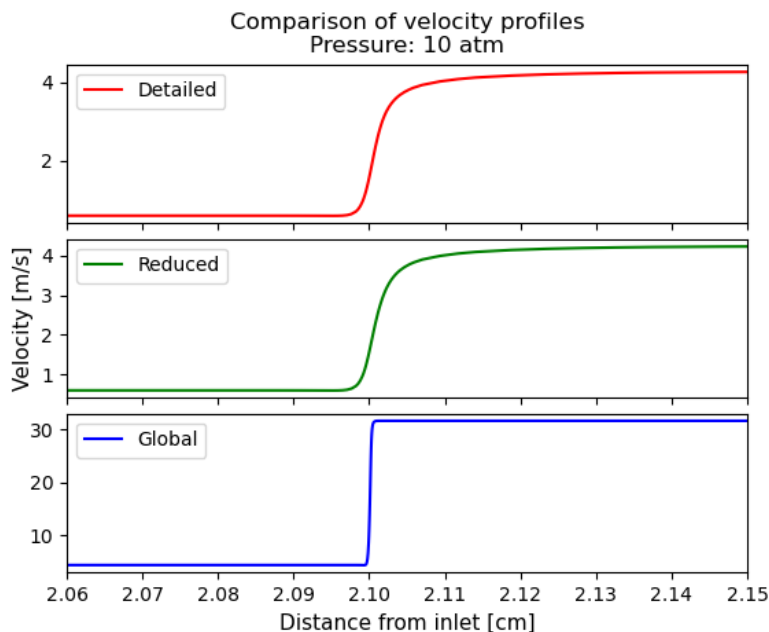
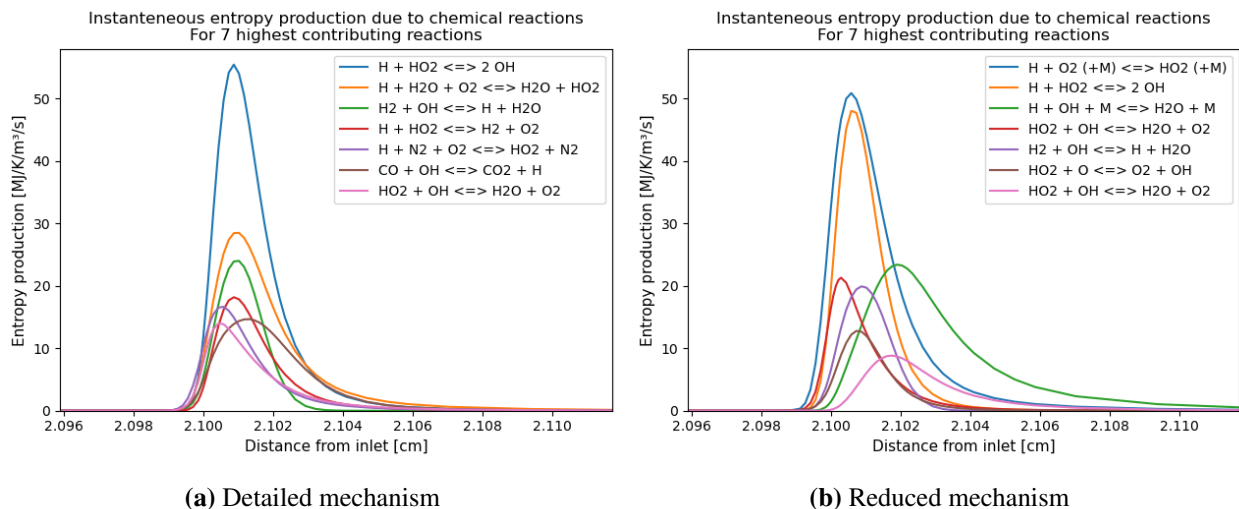


**Figure 61:** Comparison of velocity profiles using detailed, reduced, and global mechanisms for premixed, freely-propagating syngas flame at 10 atm

In Figure 62, the seven highest contributing reactions are compared, using the detailed (Figure 62a), and reduced (Figure 62b) mechanisms. First, it should be noted that the scale on the vertical axis have increased by one order of magnitude. Further, The highest contributing reaction is the same at 10 atm, as it was at 1 atm for the detailed mechanism, while both the highest, and second highest contributing reactions are the same for the reduced mechanism.



(a) Detailed mechanism

(b) Reduced mechanism

**Figure 62:** Comparison of the entropy production due to chemical reactions, from the highest contributing reactions using the detailed (a), and reduced (b) mechanism. Fuel type is syngas in premixed, freely-propagating model at 10 atm pressure.

In Figure 63, the integrated entropy production from the 20 highest contributing reactions, using the detailed mechanism are presented. In contrast to the corresponding results at 1 atm presented in Figure 54, both the highest, and second highest contributing reactions are similar for the local, and integrated production.

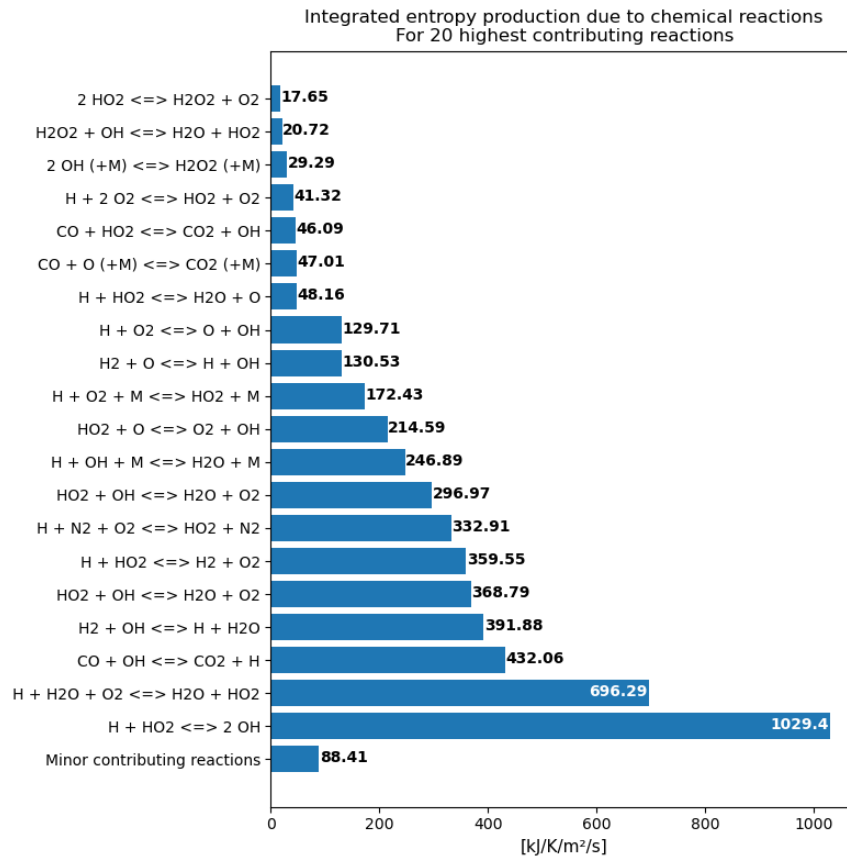


**Figure 63:** Integrated entropy production due to the highest contributing reactions, for detailed mechanism in premixed, freely-propagating syngas flame at 10 atm

The 20 reactions with highest integrated contribution using the reduced mechanism are shown in 64. The reaction with the highest integrated contribution also has the highest local production. The two following reactions have switched places in Figure 64 and Figure 62b. This is logical, as the reaction with the third highest local contribution clearly have a lower peak but more area under its graph, compared with the reaction with the second highest local contribution.

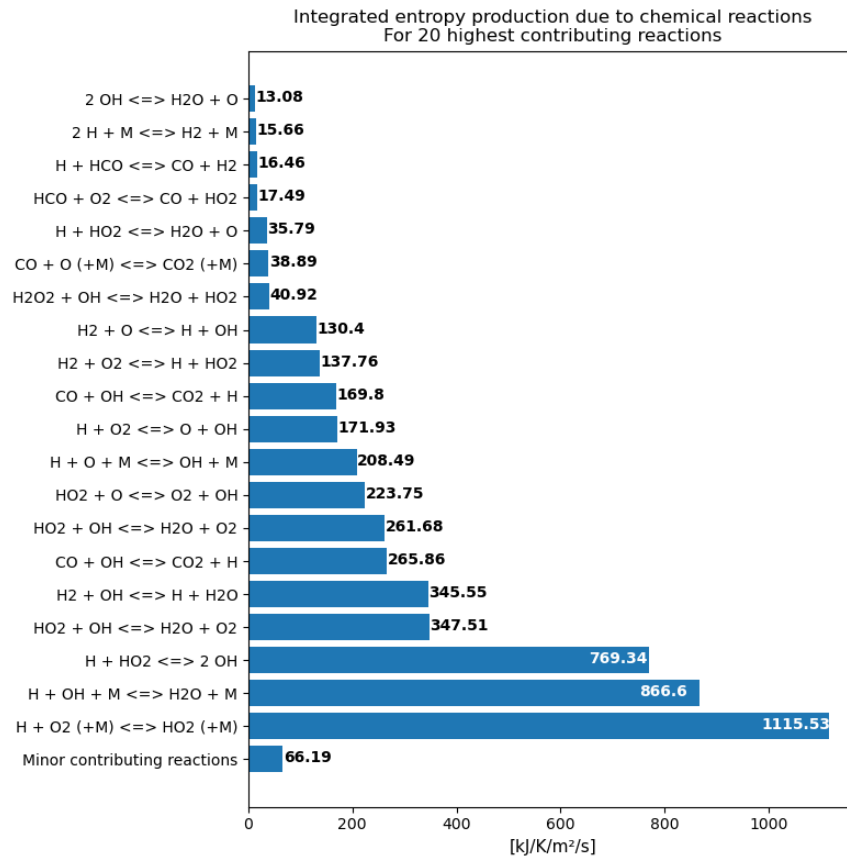


**Figure 64:** Integrated entropy production due to the highest contributing reactions, for reduced mechanism in premixed, freely-propagating syngas flame at 10 atm

The local (Figure 65a), and integrated (Figure 65b) entropy production for each reaction in the global mechanism are displayed in Figure 65. As for the results at 1 atm in Figure 56, the third reaction appears to have no local entropy production, but is included with an integrated production. This was discussed for the results at 1 atm, and will not be repeated here. The graphs are similar in shape, but clearly thinner and taller. The values on both of the scales have changed, and have increased for the vertical axis, and decreased for the horizontal axis.

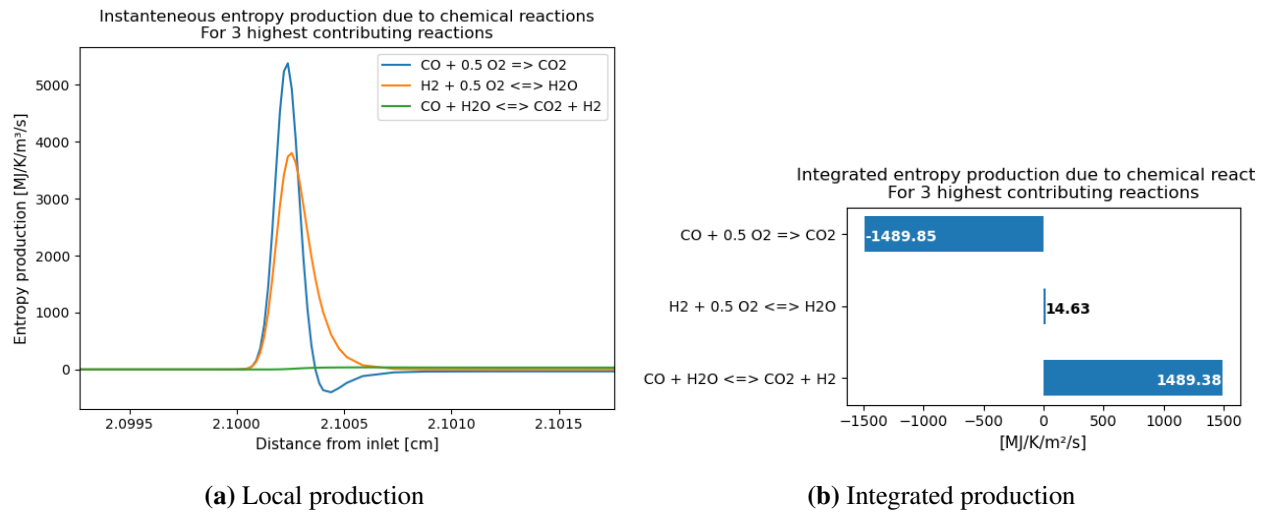


**Figure 65:** Comparison of the local (a), and integrated (b) entropy production due to the chemical reactions, using the global mechanism. Fuel type is syngas in premixed, freely-propagating model at 10 atm pressure.

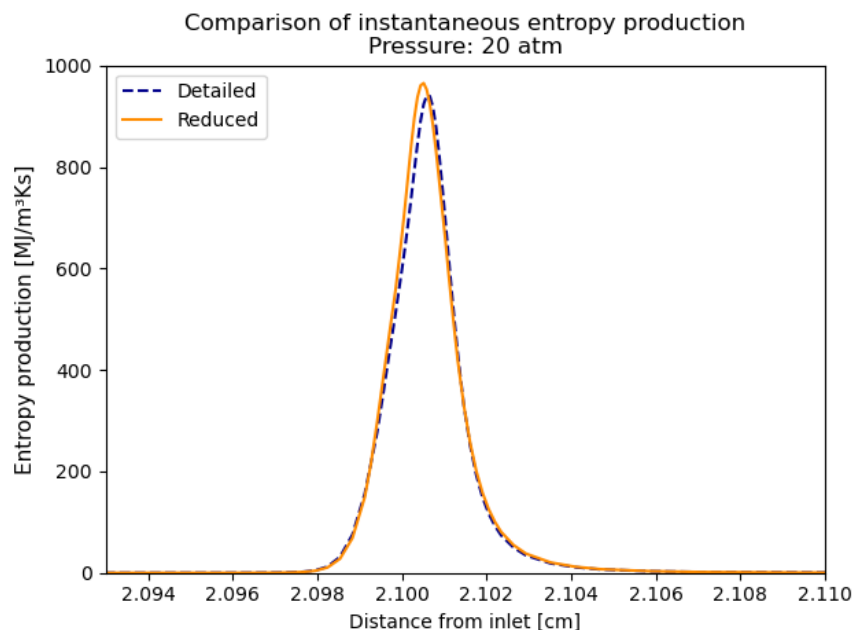
### 5.5.4 20 atm

Table 8 contains details about the integrated entropy production by source at 20 atm. For the detailed and reduced mechanisms, it can be seen that conduction now has an even higher contribution than chemical reactions, compared with Table 7. The contributions from diffusion and chemical reactions have also increased. For the detailed mechanism, the entropy production due to viscosity have decreased again. Meanwhile, it has increased by 2% for the reduced mechanism. Furthermore, the total integrated entropy production using the reduced mechanism is now higher than that of the detailed mechanism. For the global mechanism the entropy production due to all the irreversible processes have increased.

**Table 8:** Integrated entropy production by source for the premixed, freely-propagating syngas flame at 20 atm.

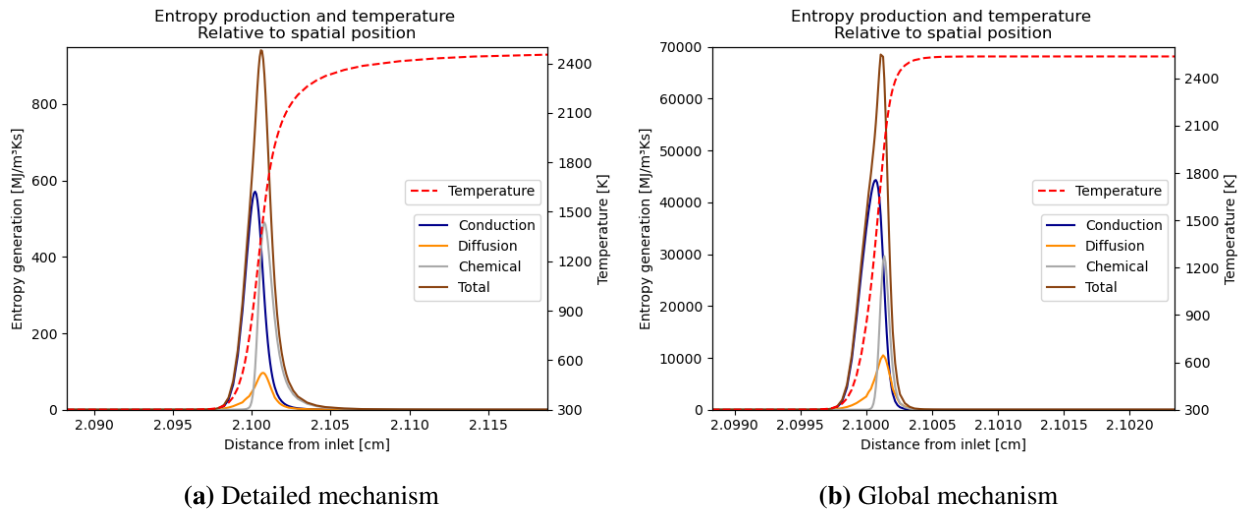
	Integrated entropy production by source [kJ/K/s]		
	Detailed	Reduced	Global
Viscosity	1,02E-02	1,05E-02	8,11E+00
Conduction	8669,78	8660,39	90316,63
Diffusion	1552,77	1552,86	18279,99
Chemical	6356,71	6886,97	27111,00

In Figure 66 the total local entropy production using the detailed and reduced mechanisms are presented. Again it is clear how the entropy production using the reduced mechanism have surpassed that of the detailed mechanism. The profiles follow each other more closely for 20 atm, and it can be seen that both profiles are more narrow with higher peak values. The profiles have a width of approximately 0.006 cm, which is a decrease by a factor of around 2. This compares to the increase in pressure.



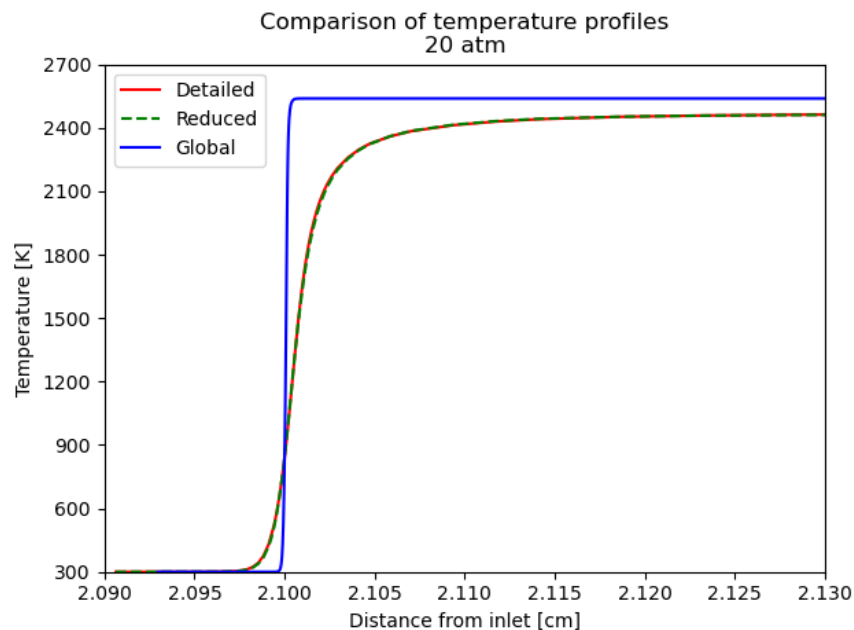
**Figure 66:** Comparison of the entropy production using detailed, and reduced mechanism. Fuel type is syngas in premixed, freely-propagating model with 20 atm pressure.

In Figure 67, the local entropy production by source is shown using the detailed (Figure 67a), and global (Figure 67b) mechanisms. The profiles are more similar in shape than they were at 10 atm (58), but the dimensions on the x- and y-axis show the difference. The y-axis in Figure 67b is an order of magnitude higher than the y-axis in Figure 67a. The profile for total entropy production in Figure 67a is approximately 0.0075 cm wide, while it is approximately 0.0005 cm wide in Figure 67b. Therefore, the global mechanism is still considerably more narrow and higher. One trend that can be seen with the increase in pressure for the detailed mechanism in particular, is that the peak of the profile for chemical reactions move to the right. As a result the steep gradient seen on the left side in Figure 57 becomes more gradual. Another trend that can be mentioned, is the specific profiles for each irreversible process getting more narrow with the increasing pressure. The same trend was observed by Acampora and Marra [4], and is displayed in Figure 10 in their article. However, in the results obtained by Acampora and Marra the contribution from the chemical reactions decrease, which causes the contribution from conduction to exceed it. While the contribution from conduction exceeds that of the chemical reactions in the results in the current project too, it is not because the contribution from the chemical reactions decrease but because the contribution from conduction increases more. The reason for the difference in trends are uncertain, but it should be mentioned that the Soret diffusion and pressure diffusion is not included by Acampora and Marra, while it is in the current project.



**Figure 67:** Instantaneous entropy production by source using the detailed (a), and global (b) mechanism on a premixed, freely-propagating syngas flame at 20 atm.

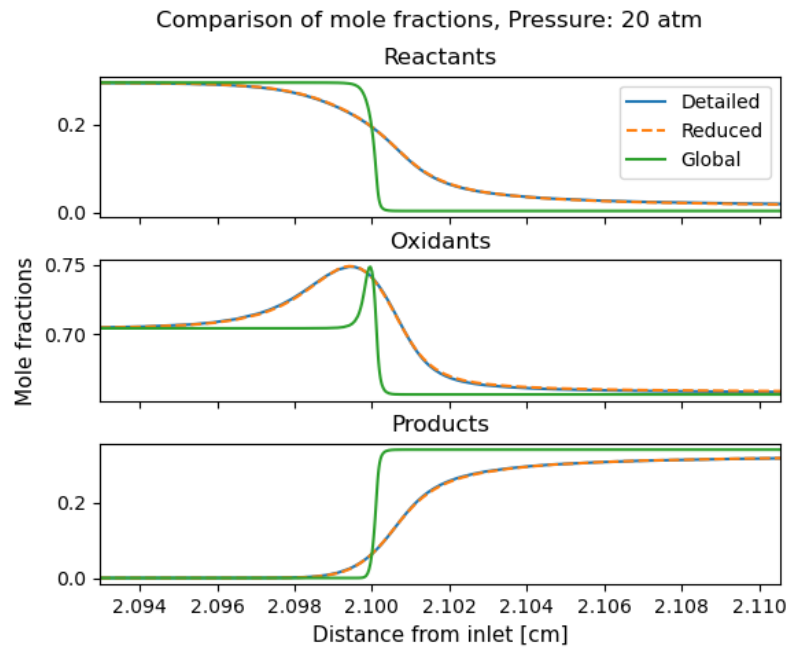
Figure 68 shows the temperature profiles for the different mechanisms at 20 atm. It may be difficult to discover any changes from 10 atm to 20 atm by comparing Figure 59 and Figure 68. Regardless, the detailed and reduced mechanisms calculate a higher peak temperature, with a steeper temperature gradient. The factor of change in pressure from 1 atm to 10 atm, is higher than the factor from 10 atm to 20 atm. As a result, the increase in entropy production from conduction is greater between 1 atm and 10 atm, than between 10 atm and 20 atm.



**Figure 68:** Comparison of temperature profiles using detailed, reduced, and global mechanisms for premixed, freely-propagating syngas flame at 20 atm

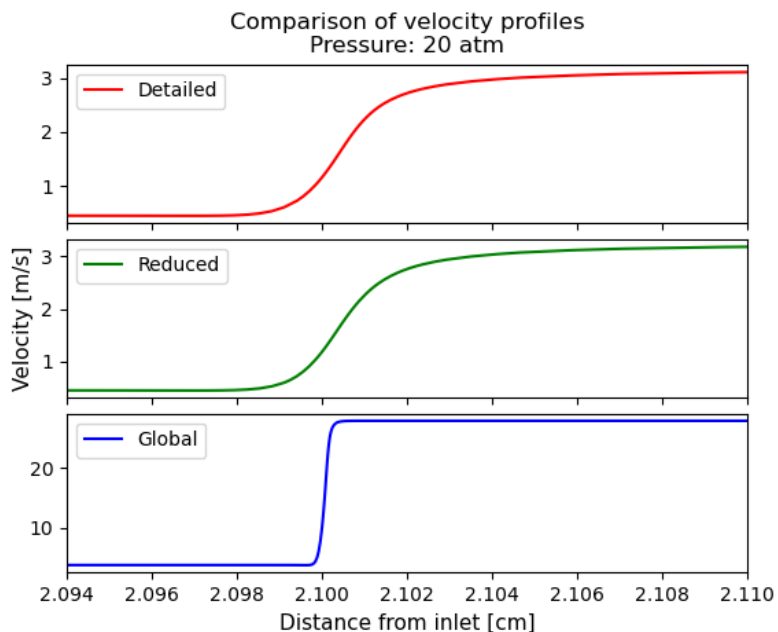


The mole fraction profiles presented in Figure 69 have also changed less from 10 atm to 20 atm, than from 1 atm to 10 atm. Nevertheless, the gradients are steeper, and the mechanisms calculate a final composition that is more similar than seen in Figure 69. The steeper profiles lead to a higher contribution from diffusion and the chemical reactions.



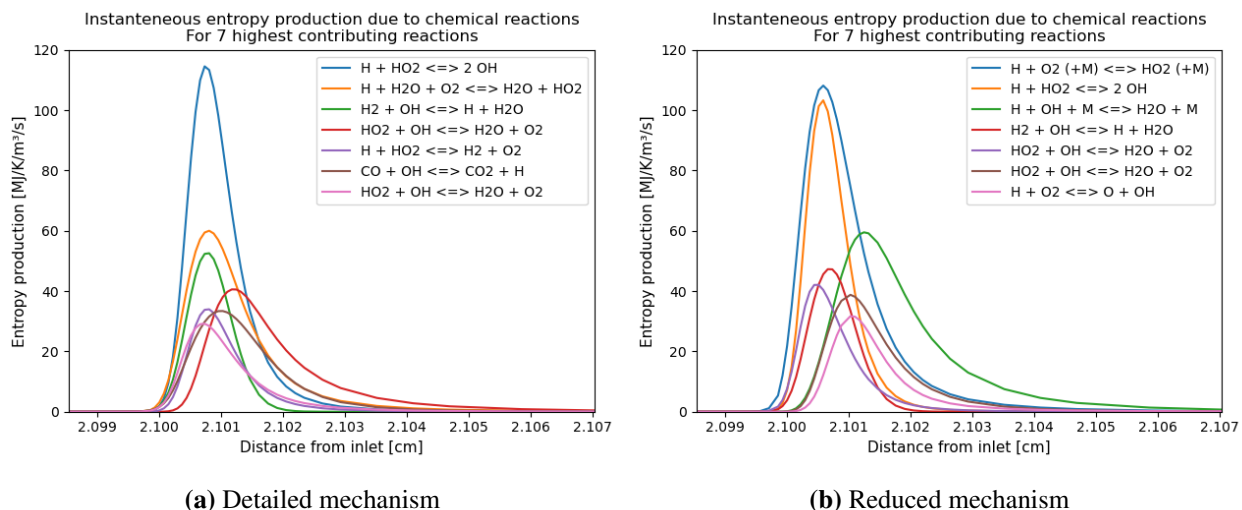
**Figure 69:** Comparison of mole fraction profiles for reactants (CO, H<sub>2</sub>), oxidants (O<sub>2</sub>, N<sub>2</sub>), and products (CO<sub>2</sub>, H<sub>2</sub>O), using detailed, reduced, and global mechanisms for premixed, freely-propagating syngas flame at 20 atm

In Figure 70, the velocity profiles using the different mechanisms are presented. The magnitude of the velocity has decreased compared with Figure 61 for all mechanisms, but the gradients are steeper. It appears that for the reduced and global mechanisms, the effect of steeper gradients outweighs the effects of the lower magnitude, resulting in a higher contribution from viscosity. It also might be that species with greater viscosity than others have gotten higher mole fractions, increasing the viscosity of the solution, which again increase the entropy production due to viscosity.



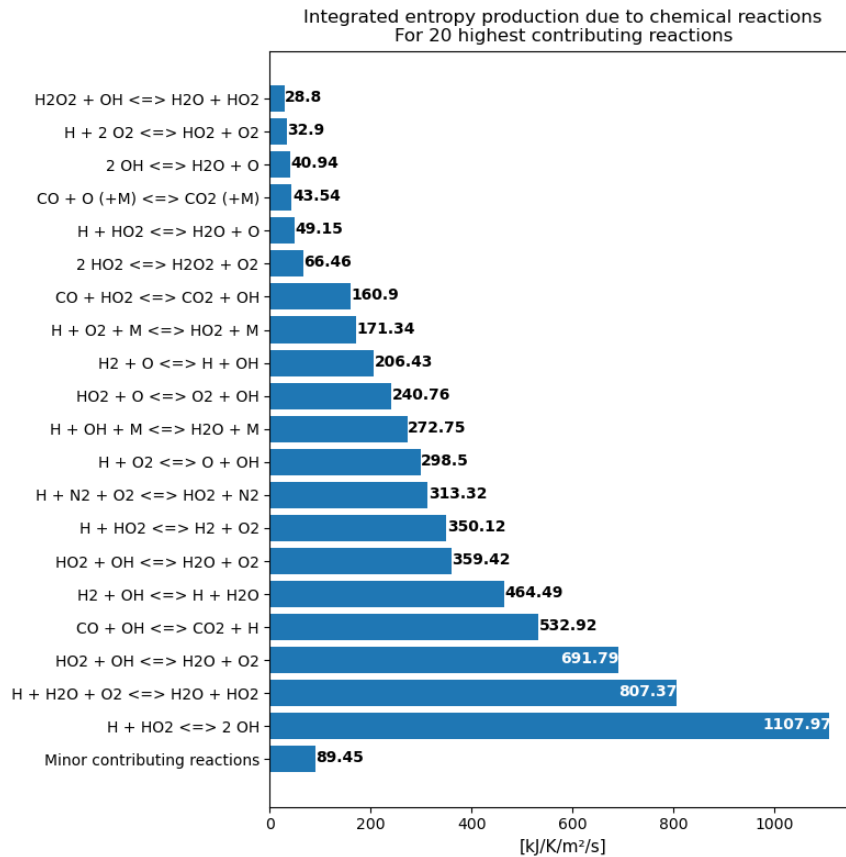
**Figure 70:** Comparison of velocity profiles using detailed, reduced, and global mechanisms for premixed, freely-propagating syngas flame at 20 atm

Figure 71 shows a comparison of the seven reactions with highest local entropy production for the detailed (Figure 71a), and reduced (Figure 71b) mechanisms. The graphs presented are similar in shape to those presented in Figure 62, at 10 atm. For both mechanisms, the three highest contributing reactions are the same, compared with their respective figures at 10 atm



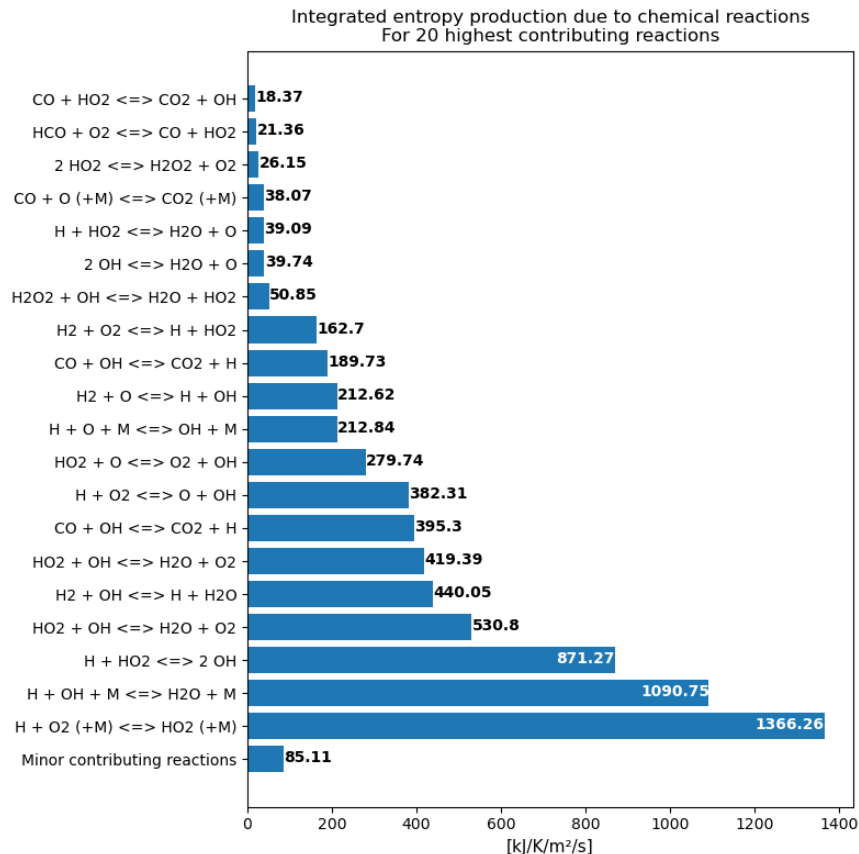
**Figure 71:** Comparison of the entropy production due to chemical reactions, from the highest contributing reactions using the detailed (a), and reduced (b) mechanism. Fuel type is syngas in premixed, freely-propagating model at 20 atm pressure.

Figure 72 presents the 20 reactions with the highest contributions to the integrated entropy production, when the detailed mechanism is used. The two reactions with the highest integrated contributions, also have the highest local contributions. Furthermore, they also had the highest contribution to the integrated production at 10 atm



**Figure 72:** Integrated entropy production due to the highest contributing reactions, for detailed mechanism in premixed, freely-propagating syngas flame at 20 atm

The 20 highest contributing reactions for the integrated production using the reduced mechanism is shown in Figure 73. The reaction with highest contribution to the integrated entropy production, also has the highest local contribution. The second and third highest contributing reactions have switched places for the local and integrated entropy production. If compared with the results at 10 atm in Figure 64, the reactions even up to the fifth highest contributing reaction are the same.



**Figure 73:** Integrated entropy production due to the highest contributing reactions, for reduced mechanism in premixed, freely-propagating syngas flame at 20 atm

In Figure 74, the local (Figure 74a), and integrated (Figure 74b) entropy production are included for the global mechanism. The shapes of the profile agree very well with those presented in Figure 65b, at 10 atm. The scale on the horizontal axis are the same, and it is seen that the profiles are thinner. The scale on the vertical axis have been increased, and the profiles have increased in peak values.

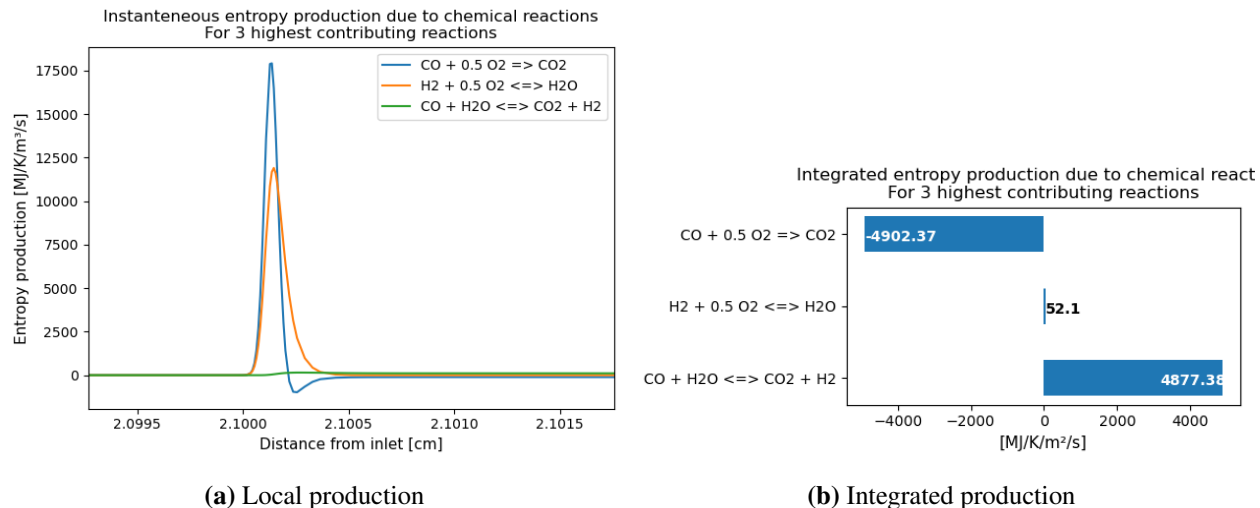


**Figure 74:** Comparison of the local (a), and integrated (b) entropy production due to the chemical reactions, using the global mechanism. Fuel type is syngas in premixed, freely-propagating model at 20 atm pressure.

### 5.5.5 Solution Grid

As for methane, the solution grid was determined by the grid refinement criteria defined in Section 3.3.1. In contrast to methane, the solution grid for the detailed and reduced mechanisms were not identical at 1 atm. The detailed mechanism had the most points (89), followed by the reduced (78), and global (68) mechanisms. The spacing between the grid points were given in meters. For the reduced, and global mechanisms, the last point had a grid spacing with order of magnitude equal to  $10^{-2}$ . If these points are neglected, all mechanisms had a spacing with order of magnitude ranging from  $10^{-3}$  to  $10^{-6}$ . At 10 atm all mechanism have a grid spacing with order of magnitude equal to  $10^{-2}$  in the last grid point. For the remaining grid points, the spacing has an order of magnitude between  $10^{-3}$  and  $10^{-7}$ , for all mechanisms. The detailed mechanism still has the most grid points (90), followed by the reduced (85), and global (83) mechanisms. When the pressure was increased to 20 atm, the reduced and global mechanism had equally many grid points (89), while the detailed mechanism had some more (95). The last point remained for all mechanisms, but if neglected, the order of magnitude of the resolution varied from  $10^{-3}$  to  $10^{-7}$  for the detailed and reduced mechanisms, but from  $10^{-3}$  to  $10^{-8}$  for the global mechanism. The details about the grid spacing are included in the appendix.

## Non-premixed, Counterflow Flame

### 5.6 Methane

As mentioned in Section 3.3.2, the distance between the jets was 3 cm. This was also the width of the solution domain at all pressures. As with the premixed, freely-propagating flame, the graphs in this section will be limited parts of the complete domain. This is to focus on the reaction zone, and clarify small differences in regions with high gradients. Furthermore, when the horizontal axis in graphs are labeled as distance from inlet, it references to the fuel inlet. This was discovered too late, and there was not enough time to correct it because of the large amount of figures. Therefore, it is stated clearly here that the fuel inlet is located at 0 cm, and the oxidizer inlet is located at 3 cm in all cases.

#### 5.6.1 Comparison of Cases.

Figure 75 shows the variation in peak temperature for 1, 10 atm, and 20 atm using detailed, reduced and global mechanisms. The peak temperature calculated by the detailed, and reduced mechanisms increases from 1 atm to 10 atm, but then decreases at 20 atm. Meanwhile, the temperature calculated by the global mechanism decreases for all pressures.

At 1 atm the detailed and reduced mechanisms calculate approximately the same temperature, while the global mechanism overestimates it. At 10 atm the global mechanism still overestimates the temperature, but is much closer to the detailed mechanism, and the reduced mechanism now underestimates the temperature. At 20 atm all mechanisms are close to each other, but both the reduced and global mechanisms slightly underestimate the temperature.

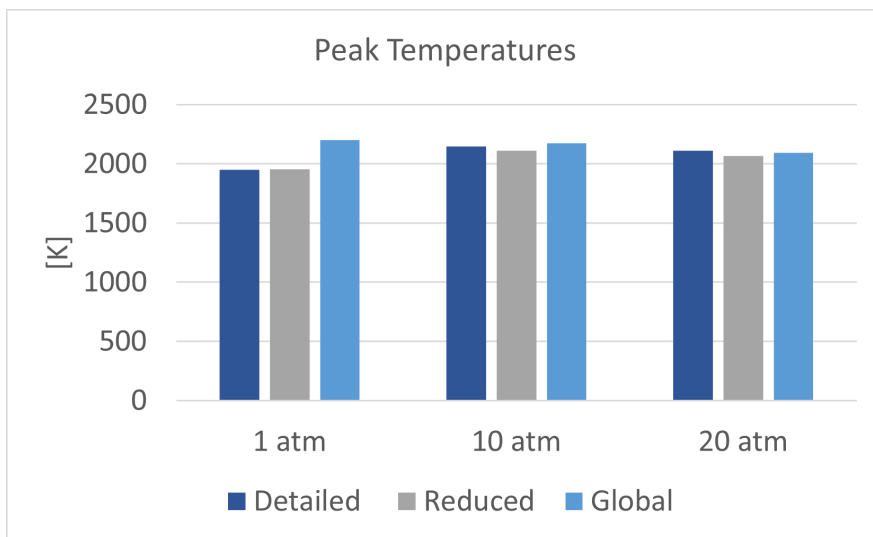


**Figure 75:** Comparison of calculated peak temperatures for detailed, reduced and global mechanisms. Pressure range: 1 atm, 10 atm, and 20 atm. Fuel type is methane in non-premixed, counterflow model.

Figure 76 shows the integrated entropy production by source, with the variation in pressure. The total integrated entropy production decreases with pressure for all mechanisms. Additionally,

the entropy production calculated by the detailed mechanism is larger than the entropy production calculated by the reduced, and global mechanisms. Furthermore, for 1 atm the global mechanism calculate a higher entropy production than the reduced mechanism. However, for 10 atm and 20 atm the reduced mechanism calculates a higher entropy production than the global mechanism.

Something noteworthy can be seen if Figure 76 is compared with Figure 19. The premixed, freely-propagating flame is considerably more affected by the changes in pressure, than the counter-flow flame. Additionally, the entropy production in the premixed flame is increasing with pressure and is substantially higher at all pressures.

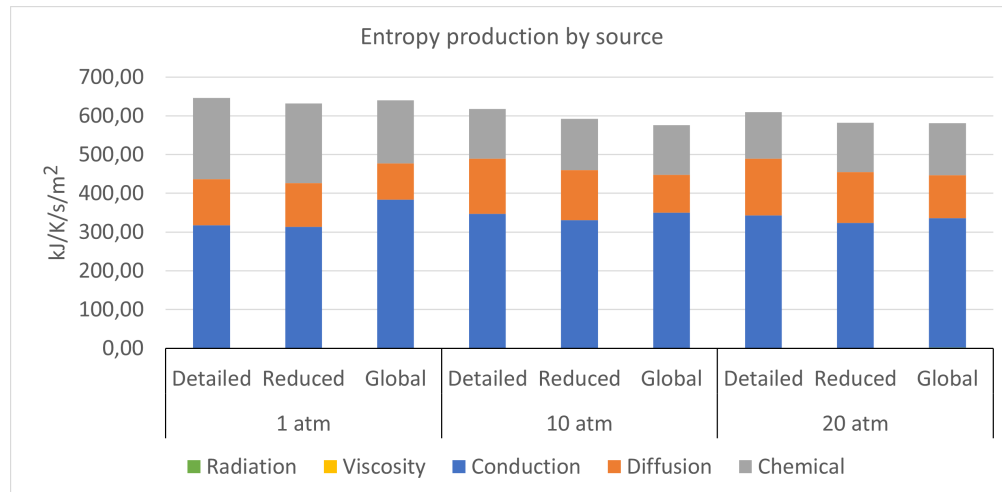


**Figure 76:** Comparison of the entropy production by source for detailed, reduced, and global mechanisms. Pressure range: 1 atm, 10 atm, and 20 atm. Fuel type is methane in non-premixed, counterflow model.

The contribution from radiation and viscosity cannot be seen on the graph in Figure 76 as the contributions are negligible. Nevertheless, the contribution from radiation increases, while it decreases for viscosity for all mechanisms as the pressure increases. The changes in contribution from radiation will be discussed for each pressure, while the contribution from viscosity is only discussed here using the detailed mechanism. The reason is that the entropy production due to viscosity is negligible, and also adequately similar for the different mechanisms at every pressure.

entropy production due to viscous forces is dependent on the viscosity of the fluid  $\mu$ , temperature  $T$ , and velocity gradient  $\frac{\partial u}{\partial x}$ , as can be seen in Equation 6 and Equation 18. Figure 77 presents the velocity profiles for the detailed mechanism at 1 atm, 10 atm, and 20 atm. From the figure it is can be see that the velocity decreases in magnitude with and order of 10 from 1 atm to 10 atm. The velocity then decreases with an order of 2, from 10 atm to 20 atm, which for both cases are the same factor as the pressure increase. Since the shape of the velocity profiles are similar, and the dimensions on the x-axis do not change the velocity gradient must decrease. Therefore, the entropy production due to the viscous forces decrease with pressure, for all mechanisms. This is also explained by the continuity equation (Equation 28) presented with the governing equations for the flame models in Section 2.8.3. The continuity equation indicates that the velocity is inversely proportional to the pressure, which is why it decrease with the same factor as the pressure increases with.

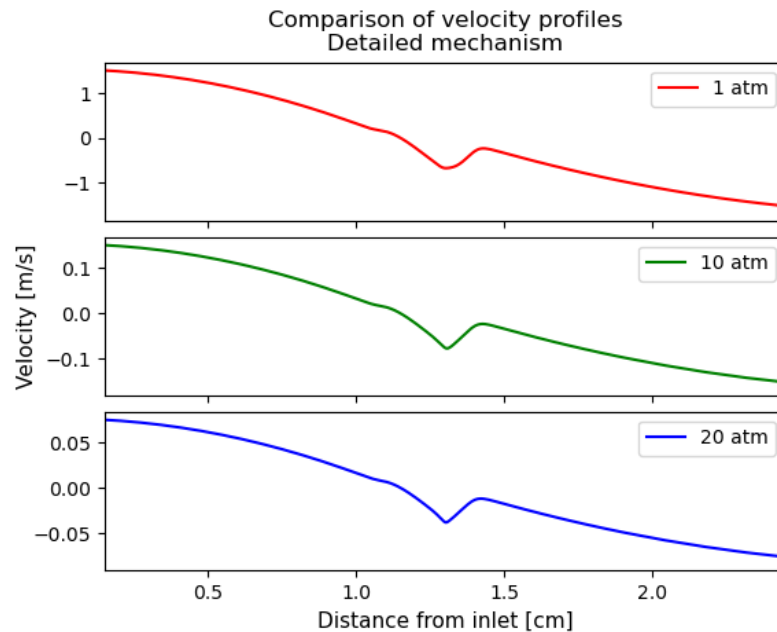


**Figure 77:** Velocity profile at 1 atm, 10 atm, and 20 atm for the non-premixed, counterflow methane flame using detailed mechanism.

### 5.6.2 1 atm

Table 9 shows in more detail the integrated entropy production, by source at 1 atm. It can be seen that conduction is the main contributor, followed by chemical reactions, diffusion, radiation, and lastly viscosity, for all mechanisms. The integrated entropy production due to diffusion and the chemical reactions, is larger when the detailed mechanism is used, follow by the reduced, and global mechanisms. However, the global mechanism overestimates the contributions from radiation, viscosity, and conduction.

**Table 9:** Integrated entropy production by source for the non-premixed, counterflow methane flame at 1 atm.

	Integrated entropy production by source [kJ/K/s/m <sup>2</sup> ]		
	Detailed	Reduced	Global
Radiation	3,35E-02	3,85E-02	0,06
Viscosity	5,47E-05	5,34E-05	6,06E-05
Conduction	317,36	313,25	383,58
Diffusion	118,98	113,27	93,55
Chemical	209,60	205,31	163,25

Figure 78 compares the instantaneous, total entropy production for the detailed, reduced, and global mechanisms at 1 atm. As for the freely-propagating flame model, the system is in steady state, and the entropy production does not change with time. Therefore, local entropy production



could be a more appropriate term than instantaneous entropy production. The graphs for the different mechanisms are similar in shape, with two smaller peaks at each side of one higher peak. The reduced mechanism follows the detailed mechanism closely, but the peaks are lower and slightly shifted to the right. The profile for the global mechanism is even more shifted to the right. The reason may be that the flame in a non-premixed, counterflow model is not located where the fuel- and oxidizer jets momentum cancel each other, but rather where the fuel and oxidizer meet in near-stoichiometric conditions. Furthermore, some of the reactions that are excluded in the reduced and global mechanisms may require less air and will therefore react closer to the fuel inlet.

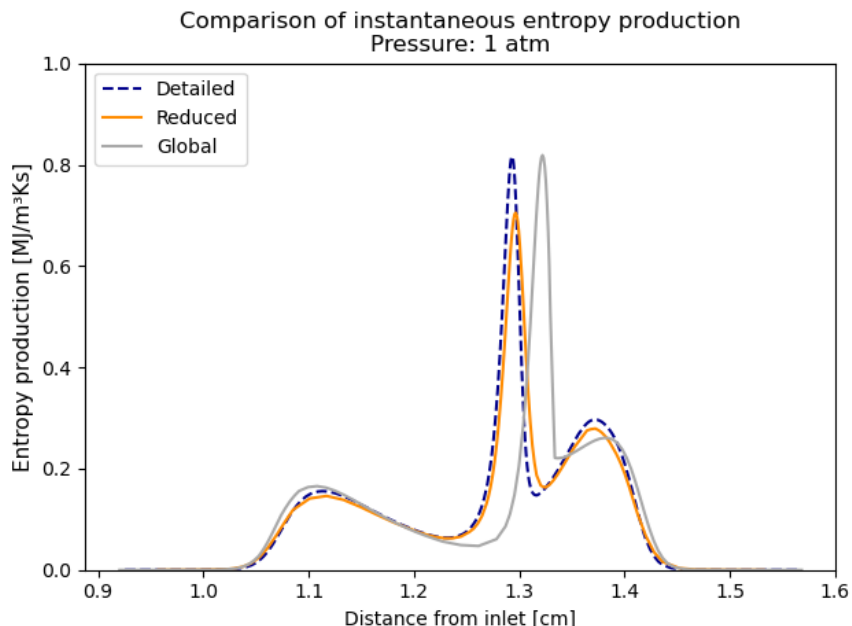


**Figure 78:** Comparison of the entropy production using detailed, reduced, and global mechanism. Fuel type is methane in non-premixed, counterflow model with 1 atm pressure.

In Figure 79 the local entropy production by source is shown for the detailed mechanism. Since the profiles in Figure 78 are adequately similar, the detailed mechanism is assumed to be representative for the reduced and global mechanisms. It can be seen that conduction is the main reason for the peaks at each side. Entropy production from conduction is dependent of the temperature gradient (Equation 19), which is why the peaks are located where the temperature profile is steepest. The right peak is somewhat higher than the left, which is partly because the profile is steeper on this side, but also due to a small peak in entropy production due to chemical reactions. This small peak is due to the reactions mentioned earlier that initiates the chemical reactions. If the same profile for the reduced mechanism is looked at, it can be seen that there is a similar peak, but it is located closer to the main peak. In the global mechanism there are no other reactions, and therefore there is not any peak on the right side. The main peak from the chemical reactions occur at the same location as the temperature peak. This is also true for diffusion, which is logical as it is dependent on the mole fraction gradients, as can be seen in Equation 20. The spatial distribution of the entropy production from the irreversible processes agree with the results in Chen et al. [9]. Even though

the procedures used in this master thesis, and their article are quite different the results in Figure 8a of their article can be compared with Figure 79 in this thesis. It must be noted that in Chen et al. the graphs are the relative entropy production. Nevertheless, the spatial distributions are similar to some degree with a small contribution from diffusion, followed by a peak in contribution from conduction. Lastly, there is a high peak in the contribution from the chemical reactions, in addition to a smaller peak in the contribution from diffusion.

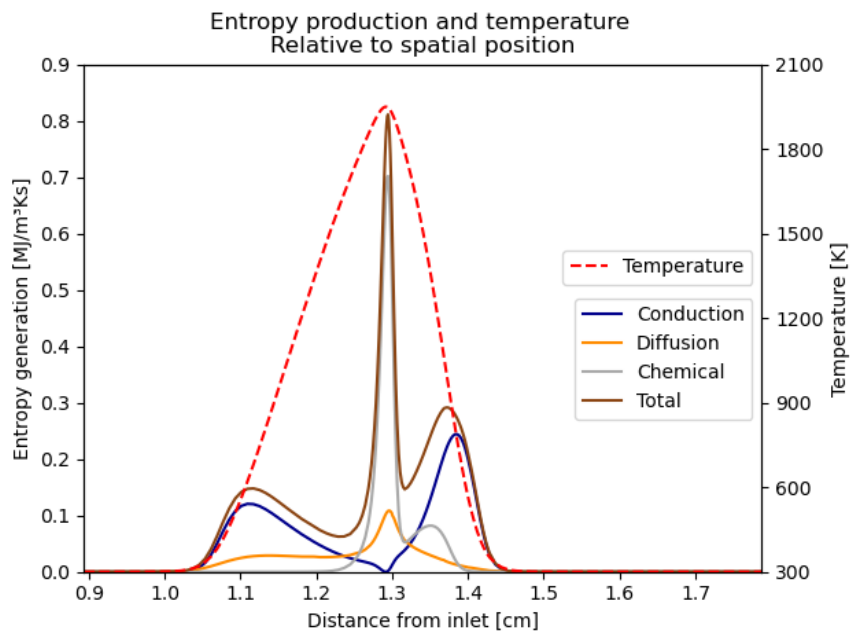


**Figure 79:** Instantaneous entropy production by source for non-premixed, counterflow methane flame at 1 atm, using the detailed mechanism.

As previously stated, the entropy production due to conduction and radiation are dependent on the temperature gradient as shown in Equation 19, and Equation 22, respectively. Therefore, it is reasonable to study the temperature profiles for the chemical mechanisms to see why the contribution using the global mechanism is higher. The temperature profiles are given in Figure 80. The graphs clearly show that the global mechanism overestimates the temperature, which yields a higher contribution from conduction and radiation. Additionally, it can be seen that the reduced mechanism also has a slightly higher peak than the detailed mechanism. However, the detailed mechanism has a steeper profile which gives a higher gradient, and a higher contribution from conduction. Another possible explanation for the higher contribution using the detailed mechanism was given in Section 5.4.2. As the detailed mechanism has more reactions than the reduced mechanism, it is possible that the gas contains more species in point in the flame when the detailed mechanism is used. Furthermore, the thermal conductivity  $\lambda$  of the gas is included in the equation for entropy production due to conduction (Equation 19). Since Cantera [16] accounts for all species when estimating the thermal conductivity, it is possible that when the detailed mechanism is used, the gas has a higher thermal conductivity. Due to time restrictions this was not further investigated.

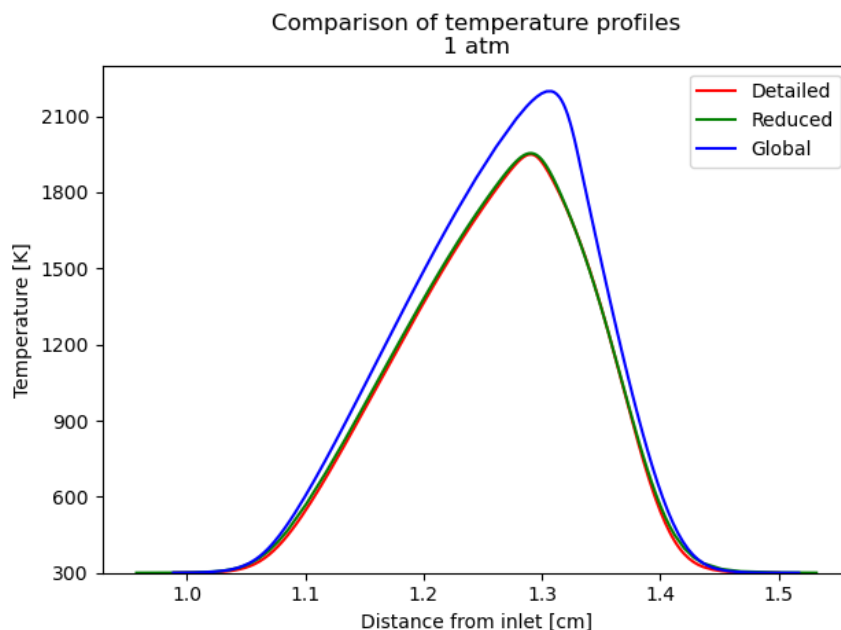


**Figure 80:** Comparison of temperature profiles using the detailed, reduced, and global mechanism for the non-premixed, counterflow flame at 1 atm.

Even though the detailed mechanism has a steeper gradient and thus a higher contribution from conduction, the contribution from radiation is slightly below that of the reduced mechanism. This may be because the radiation model only accounts for radiative heat loss from  $\text{CO}_2$ , and  $\text{H}_2\text{O}$ . As mentioned above, there may be species in the gas when the detailed mechanism is used, that may not be included when the reduced mechanism is used. This leads to a higher mole fraction for  $\text{CO}_2$  and  $\text{H}_2\text{O}$ , and thereby a higher entropy production due to radiation. The same argument can be made for the global mechanism, in addition to the overestimation of the temperature. This is further illustrated in Figure 81. Here, the mole fraction profiles for reactants ( $\text{CO}$ ,  $\text{H}_2$ ), oxidants ( $\text{O}_2$ ,  $\text{N}_2$ ), and products ( $\text{CO}_2$ ,  $\text{H}_2\text{O}$ ), using detailed, reduced, and global mechanisms are included. The peak in products mole fractions are clearly higher for the global mechanism, and incrementally higher for the reduced mechanism, than the detailed mechanism.

Additionally, Figure 81 can give some indications on the contribution from diffusion. With the relation given in Equation 23, the entropy production due to diffusion given in Equation 20 depends on the species mole fraction gradients. In Figure 81 it can be seen that the detailed, and reduced mechanisms use the reactants faster than the global mechanism. Moreover, even though the global mechanism has a higher peak in the mole fraction profile of the products, the effects are outweighed by the lesser gradients and the contribution is lower.

Additionally, it must be mentioned that since the reduced, global mechanisms have fewer reactions, some elementary reaction creating and destroying intermediate species (not included in Figure 81) rapidly may be neglected. These reactions may also be part of the reason that the detail mechanism calculates a higher entropy production due to diffusion. Lastly, the entropy production due to diffusion is given in Equation 20, and is summed over all species. Again, the gas may have fewer species at some points in the flame when the reduced or global mechanisms are used rather

then the detailed mechanism, and this can therefore also be a reason for the lower contribution. These possible explanations were not further pursued due to the limited time.

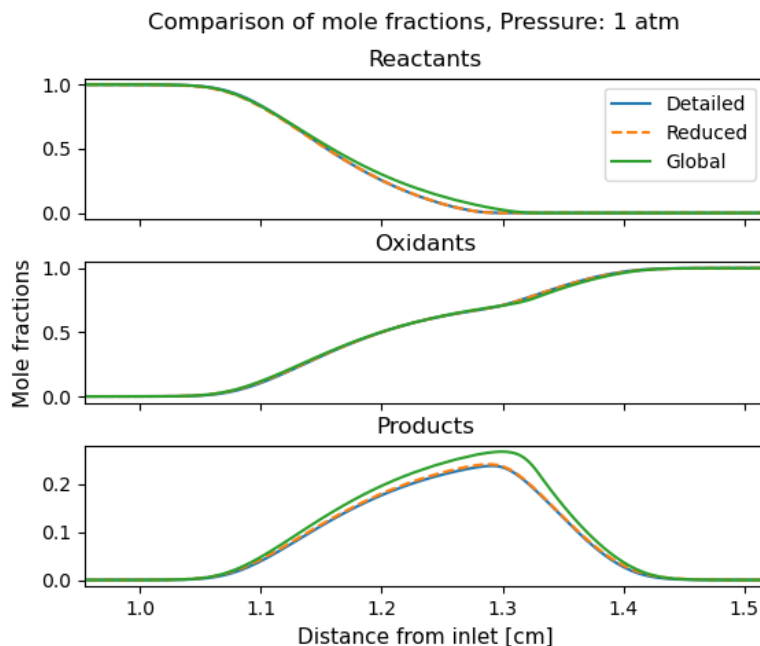


**Figure 81:** Comparison of mole fraction profiles for reactants ( $\text{CO}$ ,  $\text{H}_2$ ), oxidants ( $\text{O}_2$ ,  $\text{N}_2$ ), and products ( $\text{CO}_2$ ,  $\text{H}_2\text{O}$ ), using detailed, reduced, and global mechanisms on non-premixed, counterflow, methane flame at 1 atm.

In Figure 82, the 7 reactions with the highest contribution to the local entropy production are presented, for the detailed (Figure 82a), and reduced (Figure 82b) mechanisms. Seven reactions are considered to be a sufficient number of reactions, as it was for the freely-propagating flame model. If more were included the readability was reduced more than what was gained by information. If Figure 82a is compared with the corresponding graph for the freely-propagating model in Figure 25a, it can be seen that the three reactions with the highest contributions are the same in both models. The remaining four reactions are different. For the reduced mechanism, the results can be compared with those presented in Figure 25b. Here, only the reaction with the highest contribution is the same for both models.

If the graphs in Figure 82 are compared with each other, it can be seen that only the fourth highest contributing reaction is the same for both mechanisms. However, the reaction with the second highest contribution using the detailed mechanism, has the highest contribution when the reduced mechanism is used. Furthermore, the reaction with the highest contribution for the detailed mechanism is not included in the reduced mechanism.

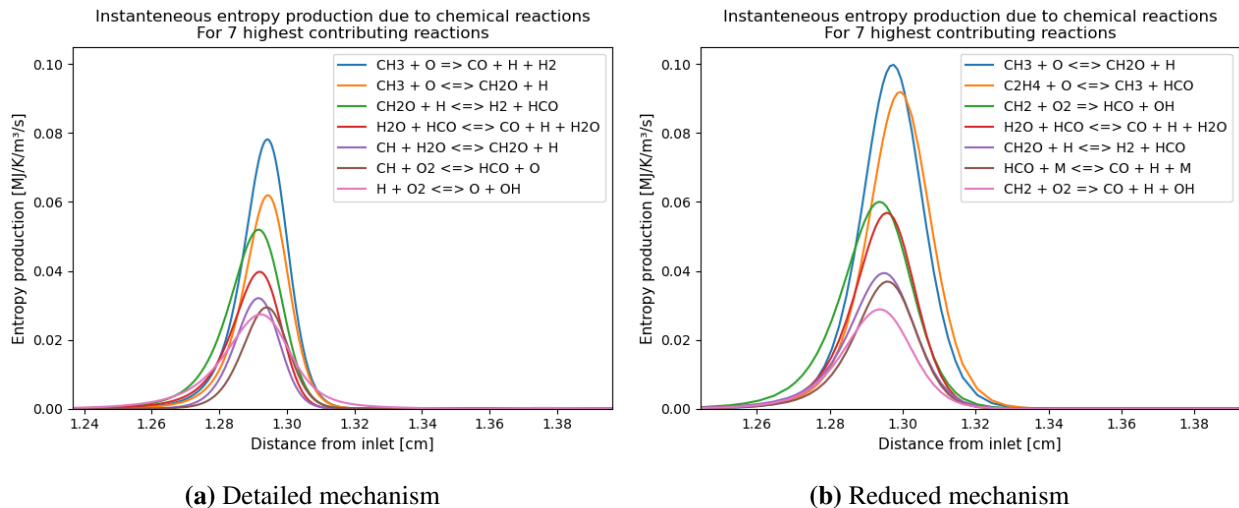


**Figure 82:** Comparison of the entropy production due to chemical reactions, from the seven highest contributing reactions using the detailed (a), and reduced (b) mechanisms. Fuel type is methane in non-premixed, counterflow model at 1 atm.

In Figure 83, the 25 highest contributing reactions for the integrated entropy production are included for the detailed mechanism. Additionally, the sum of the contribution from the remaining reactions are included in the column in the bottom column. The three highest contributing reactions in Figure 83, are also the three highest contributing reactions in Figure 82a.

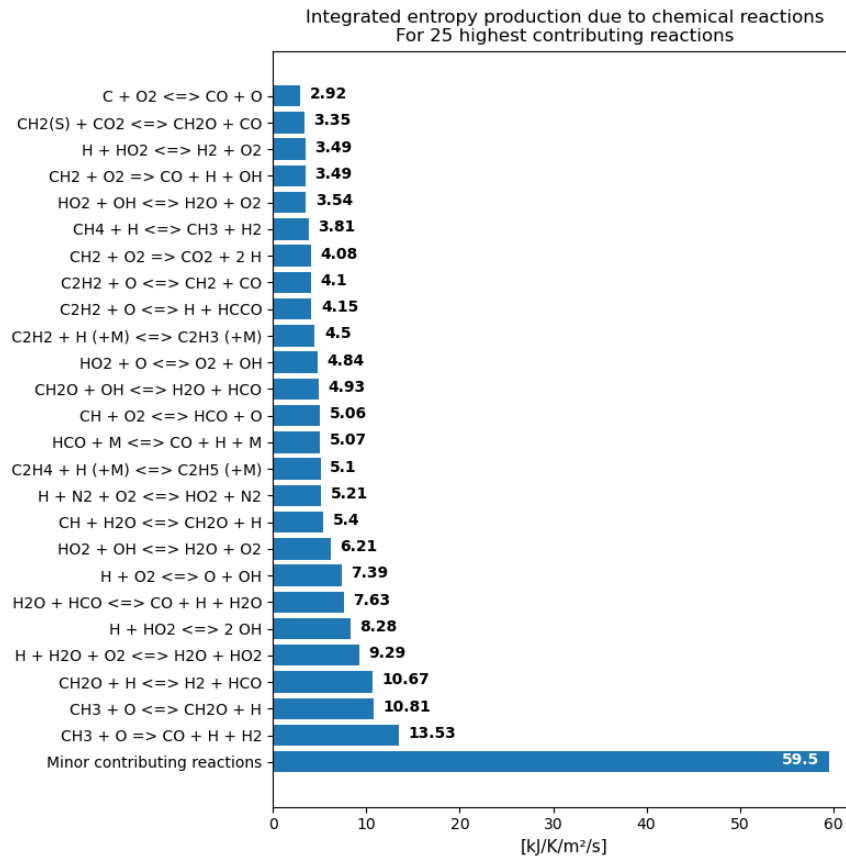


**Figure 83:** Integrated entropy production due to the highest contributing reactions, for detailed mechanism in non-premixed, counterflow model at 1 atm

Figure 84 shows the 25 highest contributing reactions for the integrated entropy production, using the reduced mechanism. For the reduced mechanism all the five highest contributing reactions are the same for the integrated and local entropy production. Furthermore, if the results are compared with those obtained with the detailed mechanism, it may appear that the production is higher. However, it should be reminded that the reduced mechanism contains fewer reactions, and that the total entropy production therefore is distributed over fewer reactions. Additionally, some of the reactions are included in the figures for both the mechanisms, but few have the same rankings.

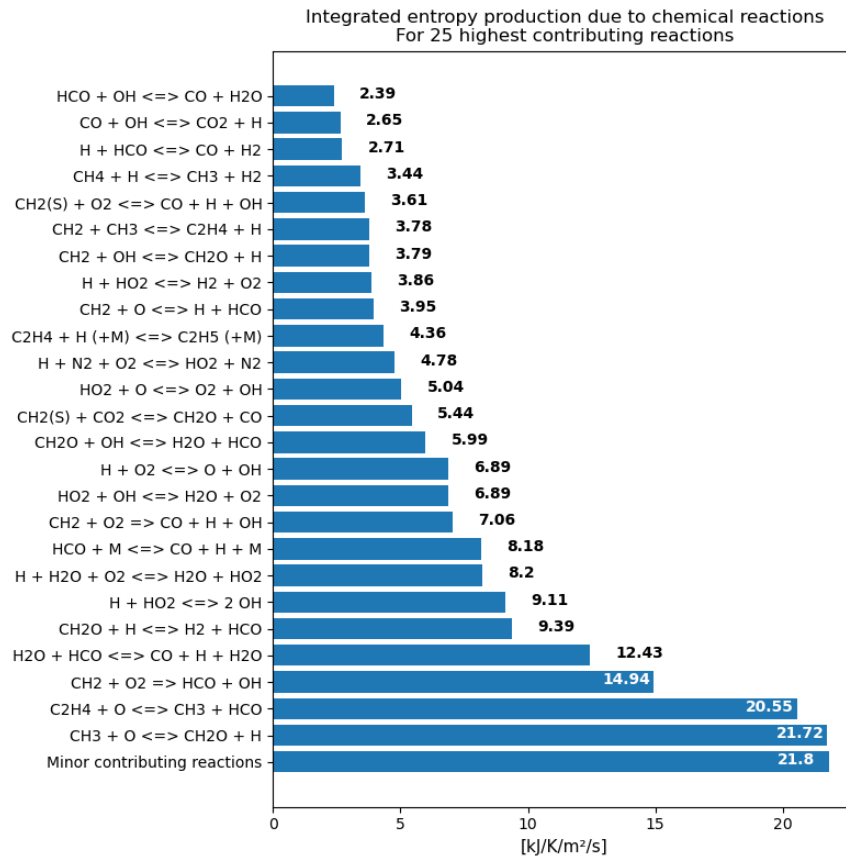


**Figure 84:** Integrated entropy production due to the highest contributing reactions, for reduced mechanism in non-premixed, counterflow model at 1 atm

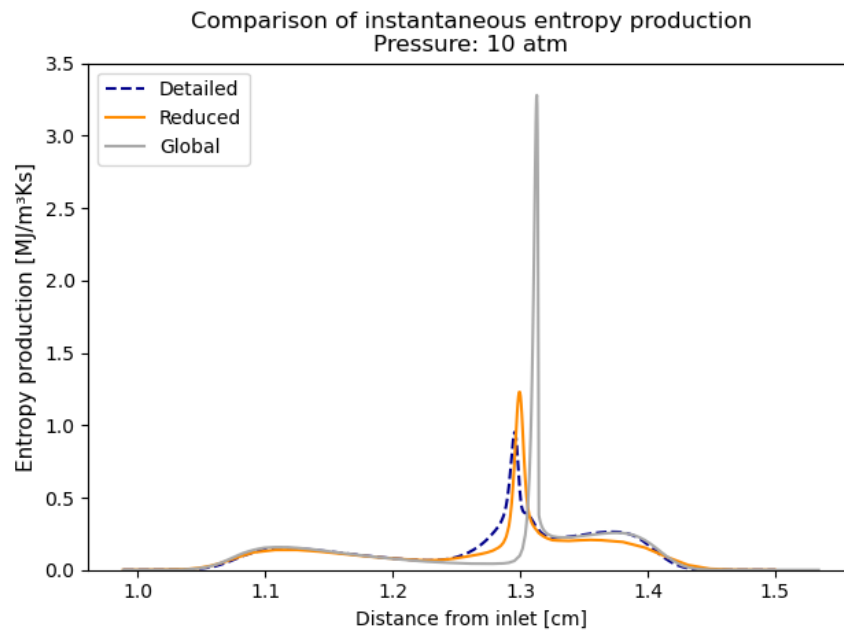
### 5.6.3 10 atm

Table 10 shows the integrated entropy production by source at 10 atm. The contribution from radiation has increase for all mechanisms, and the global mechanism still has the highest contribution. Conduction has an increased entropy production for the detailed and reduced mechanisms, while it has decreased for the global mechanism. The entropy production due to diffusion has increased for all mechanisms, and the detailed mechanism still has the highest value. Lastly, the contribution from the chemical reactions have decreased for all mechanisms, and the reduced mechanism now has a higher contribution, followed by the global mechanism, and finally the detailed mechanism.

**Table 10:** Integrated entropy production by source for the non-premixed, counterflow methane flame at 10 atm.

	Integrated entropy production by source [kJ/K/s]		
	Detailed	Reduced	Global
Radiation	4,23E-01	2,96E-01	0,84
Viscosity	6,16E-07	5,84E-07	5,89E-07
Conduction	347,00	330,58	349,23
Diffusion	142,42	129,62	98,01
Chemical	127,91	132,26	128,14

The comparison of the total local entropy production for the detailed, reduced, and global mechanisms at 10 atm are presented in Figure 85. The most distinct difference from 1 atm is the shape of the profile for the global mechanism. It appears that the entropy production calculated by the global mechanism has been concentrated in one, slightly delayed peak. Also the profile for the reduced mechanism has more discrepancy now, compared with Figure 78. The profile for the detailed mechanism still precedes that of the reduced and global mechanisms.

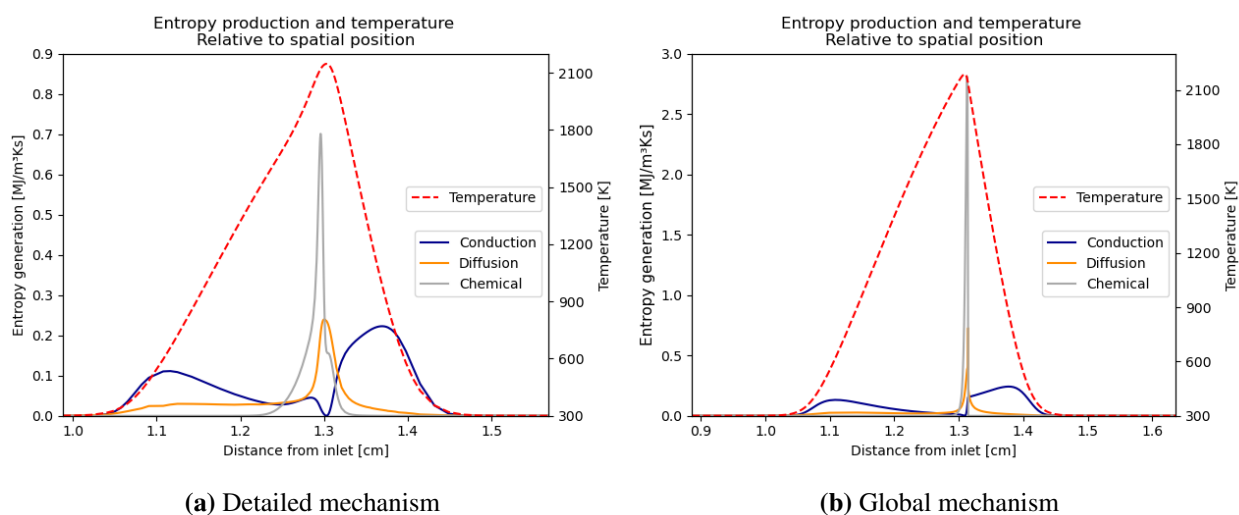
**Figure 85:** Comparison of the entropy production using detailed, reduced, and global mechanisms. Fuel type is methane in non-premixed, counterflow model with 10 atm.

Even though there are more discrepancies in the profile for the reduced mechanism in Figure 78, it still has a similar shape. Therefore, only the instantaneous entropy production by source for the detailed and global mechanisms are included in Figure 86. First, Figure 86a shows that the entropy production due to chemical reactions have not changed much in peak value for the detailed mechanism. However, the peak is more narrow and the lower peak on the right side in Figure



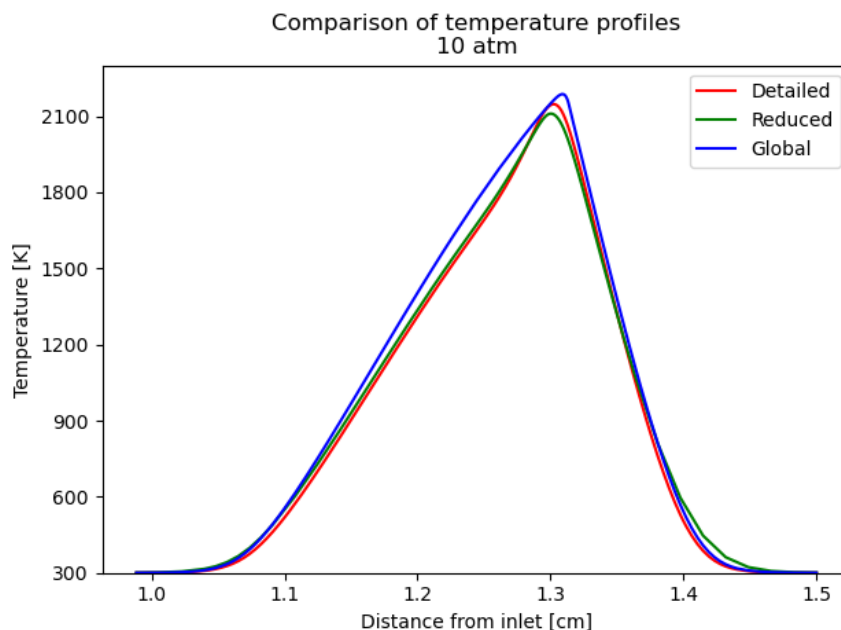
78 is almost completely gone. The peak is lower for conduction, however as shown in Table 10 the entropy production due to conduction has increased which is a result of a wider profile. The contribution from diffusion has a clear increase in peak value, which may be the reason that the smaller peak in entropy production due to chemical reactions have vanished.

Second, the entropy production due to chemical reactions for the global mechanism has been almost entirely focused in one peak. The peak is much higher than the peak for the detailed mechanism, which becomes evident if the difference in scales between Figure 86a and Figure 86b is noticed. The high peak compensates for the narrow profile, and as a result the integrated entropy production due to chemical reactions shown in Table 10 is not very different for the detailed and global mechanisms. Even though it is almost not visible, the contribution from diffusion possesses a similar profile which causes an increase in integrated entropy production from 1 atm.



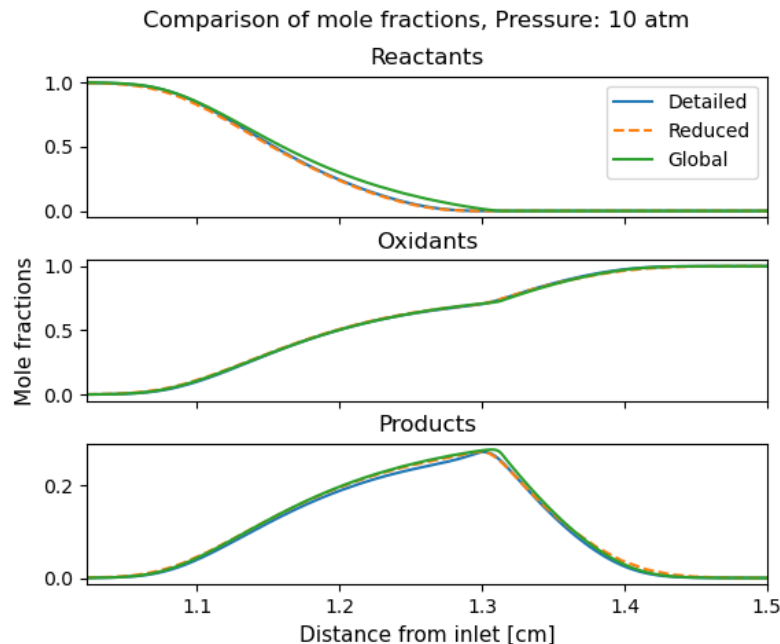
**Figure 86:** Instantaneous entropy production by source for detailed (a), and global (b) mechanisms. Model is non-premixed, counterflow methane flame at 10 atm.

The temperature profiles for all the mechanisms at 10 atm are presented in Figure 87. The profiles have more similar shape than the profiles at 1 atm presented in Figure 80. Moreover, as showed in Figure 75 the peak temperature has increased for the detailed and reduced mechanisms, and decreased for the global mechanism. The profiles of the detailed and reduced mechanism also appear to be thinner, and slightly steeper. This explains the increase in entropy production due to conduction for the detailed and reduced mechanism. The profile of the global mechanism have not gotten any steeper, and with the lower peak this results in a lower entropy production.



**Figure 87:** Temperature profiles for detailed, reduced, and global mechanisms.

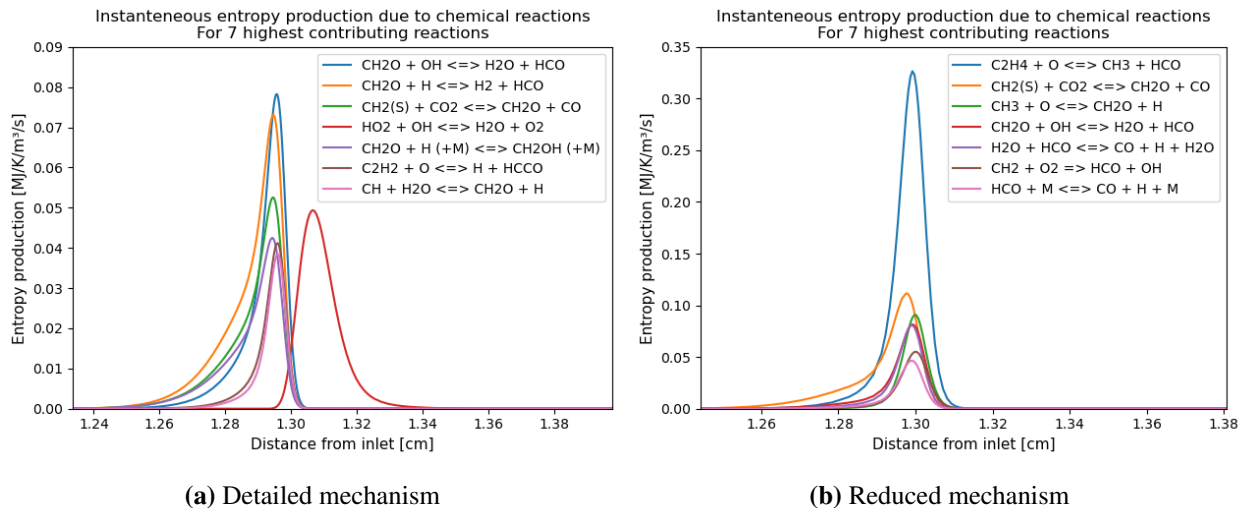
Because the temperature profiles for the detailed and reduced mechanisms became taller, and steeper, while it became lower for the global mechanism the entropy production due to radiation increased for the detailed, and reduced mechanisms and decreased for the global mechanism. Another explanation may be given by the mole fraction profiles presented in Figure 88. For both the detailed and reduced mechanism it can be seen that it is produced more  $\text{CO}_2$  and  $\text{H}_2\text{O}$ , which lead to a higher entropy production due to radiation. For the global mechanism the amount of product is approximately equal to that at 1 atm, however the peak is sharper which indicates higher gradients. The effects of the steeper gradients around the peak is clearly not sufficient to increase the entropy production.



**Figure 88:** Comparison of mole fraction profiles for reactants ( $\text{CO}$ ,  $\text{H}_2$ ), oxidants ( $\text{O}_2$ ,  $\text{N}_2$ ), and products ( $\text{CO}_2$ ,  $\text{H}_2\text{O}$ ), using detailed, reduced, and global mechanisms on non-premixed, counterflow, methane flame at 10 atm.

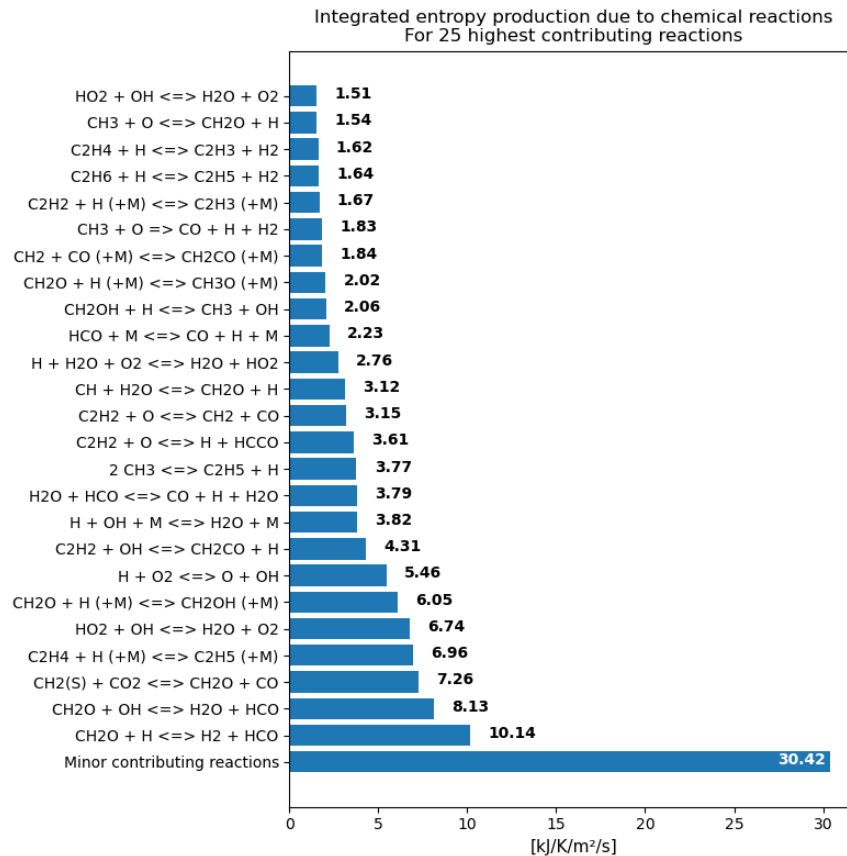
In Figure 89, the seven reactions with the highest contribution to the local entropy production are presented for the detailed (Figure 89a), and reduced (Figure 89b) mechanisms. In Figure 89a the scale on the vertical axis have changed somewhat, but are still in the same order of magnitude. The reactions included have changed, and the profiles have changed noticeably in shape. Furthermore, the profiles have not gotten much lower, but they are thinner. Additionally, the profiles peaks have moved closer to the fuel inlet, except for the fourth highest contributing reactions which have moved further from the inlet.

For the reduced mechanism showed in Figure 89b, the profiles appear to have moved slightly towards the oxidizer inlet. Furthermore, the reactions with the second highest contribution at 1 atm (Figure 82b) had an increased contribution at 10 atm, while the other profiles had approximately the same height.



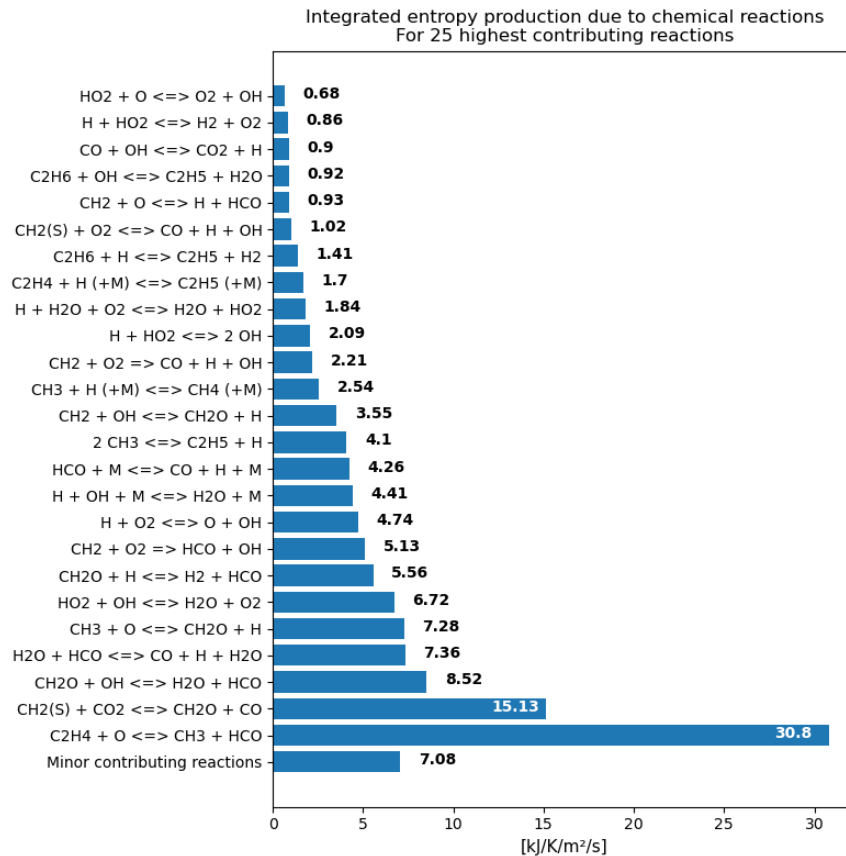
**Figure 89:** Comparison of the entropy production due to chemical reactions, from the highest contributing reactions using the detailed (a), and reduced (b) mechanisms. Fuel type is methane in non-premixed, counterflow model at 10 atm.

Figure 90 presents the 25 highest contributing reactions to the integrated entropy production, using the detailed mechanism. It is seen that the reactions with the highest, and second highest contributions, now have considerably lower contributions. Many reactions are included in the results for the local entropy production as well as the integrated entropy production, but not necessarily with the same ranks.



**Figure 90:** Integrated entropy production due to the 25 highest contributing reactions, for detailed mechanism in non-premixed, counterflow model at 10 atm

In Figure 91 the 25 highest contributing reactions to the integrated entropy production using the reduced mechanism are presented. If compared with the detailed mechanism, the reduced mechanism have less exchange in reactions from 1 atm, to 10 atm. Compared with the local production the two highest contributing reactions are the same.



**Figure 91:** Integrated entropy production due to the 25 highest contributing reactions, for reduced mechanism in non-premixed, counterflow model at 10 atm

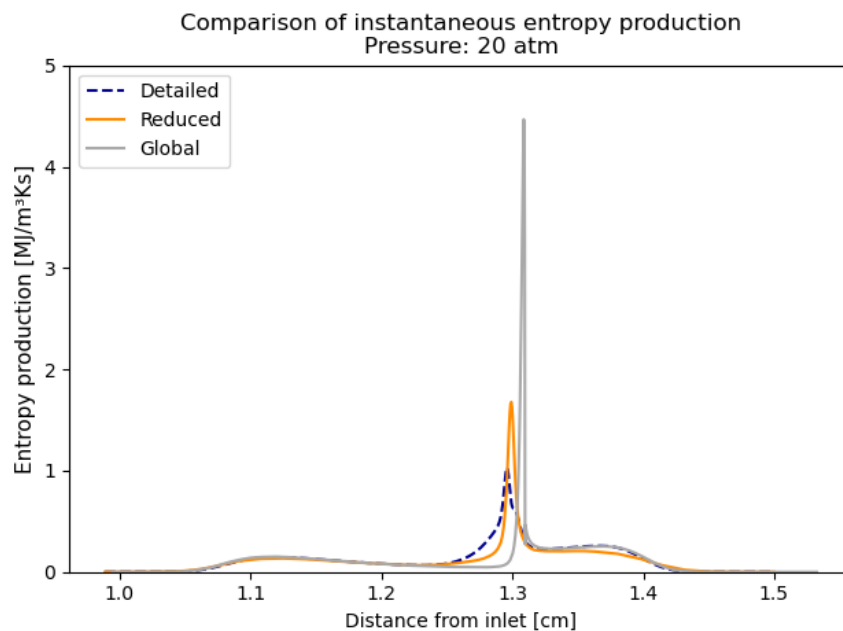
### 5.6.4 20 atm

Table 11 contains the integrated entropy production by source at 20 atm. Radiation has an increased contribution, while viscosity has a decreased contribution, for all mechanisms. Entropy production due to conduction is also lower for all mechanisms, while it is higher for diffusion. For the detailed and reduced mechanisms the entropy production due to chemical reactions are lower, but for the global mechanism it is higher.

**Table 11:** Integrated entropy production by source for the non-premixed, counterflow methane flame at 20 atm.

	Integrated entropy production by source [kJ/K/s/m <sup>2</sup> ]		
	Detailed	Reduced	Global
Radiation	5,13E-01	6,27E-01	1,79
Viscosity	1,52E-07	1,44E-07	1,43E-07
Conduction	342,12	323,36	334,39
Diffusion	147,29	131,16	110,85
Chemical	119,77	127,32	134,47

In figure 92 the total local entropy production for the detailed, reduced, and global mechanisms at 20 atm are shown. The shape of the profiles are similar to the profiles at 10 atm in Figure 85, with the biggest difference being the increase in dimension of the y-axis. The profile for the global mechanism is still concentrated in one peak, which has increased greatly. The profile of the reduced mechanism also appear to be more concentrated in one peak. Contrary to how it looks, the detailed mechanism still has the highest total integrated entropy production. Because, even though the peaks are higher for the global and reduced mechanisms, the total area under their graphs are still less than under the detailed mechanisms graph. The profile for the detailed mechanism still precedes the the profiles for the reduced and global mechanisms. If the graphs for the total local entropy production are compared, it can be seen that the peak do not shift location. This was not the case for the premixed, freely-propagating flame where the peaks clearly moved towards the inlet.



**Figure 92:** Comparison of the entropy production using detailed, reduced, and global mechanism. Fuel type is methane in non-premixed, counterflow model with 20 atm pressure.

Figure 93 shows the local entropy production by source for the detailed mechanism. Both the profile for diffusion and chemical reactions appear to be slimmer. For chemical reactions the peak is not higher, and therefore the integrated value is lower which causes the total integrated entropy production to decrease from 10 atm to 20 atm. Conduction also has a lower contribution, which is mainly because the gradients around 1.3 cm is steeper, making the area under the graph lower. Even though it is not included, the contribution from radiation increases as the temperature gradients are slightly steeper. For diffusion, the effects of a more narrow profile are compensated for by a higher peak which results in a slightly higher integrated entropy production.

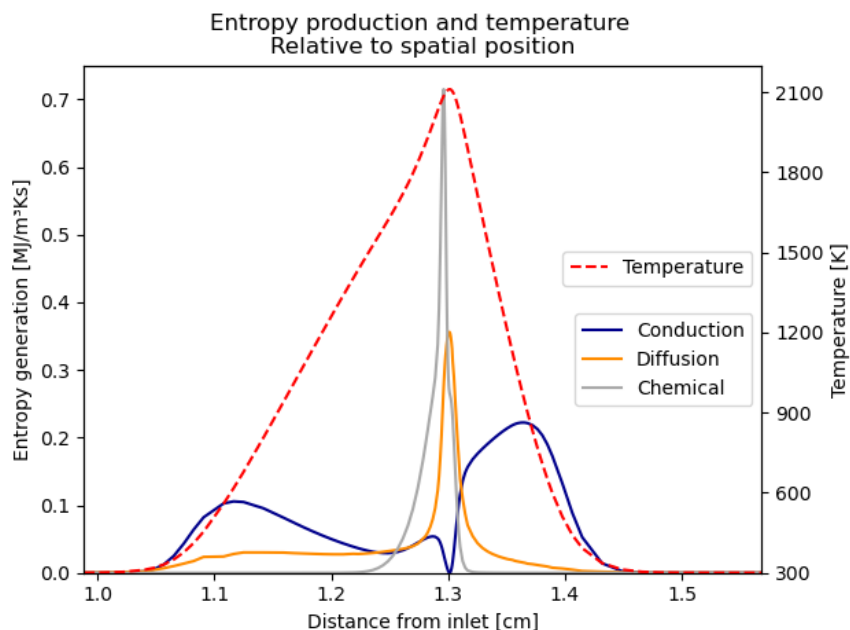


**Figure 93:** Instantaneous entropy production by source for the detailed mechanism at 20 atm, for the non-premixed counterflow methane flame.

Figure 94 displays the local entropy production by source for the reduced and global mechanisms. The profiles for the reduced mechanism, shown in Figure 94a, still have a similar shape to the detailed mechanism, but the profiles for diffusion and conduction are lower. For the global mechanism in Figure 94b, diffusion and conduction also have lower profiles compared with Figure 86b. As a consequence, the integrated value of the entropy production due to conduction is lower for both mechanisms. However, the contribution from diffusion has increased, and it can be assumed that is because the profile is slightly wider. The entropy production due to chemical reactions are for both mechanisms concentrated in one narrow peak. For the reduced mechanism the integrated value is lower than it was at 10 atm, while it is higher for the global mechanism. This indicates that for the global mechanism, the effects of a higher peak outweigh the effects of a more narrow profile, which is not true for the reduced mechanism.



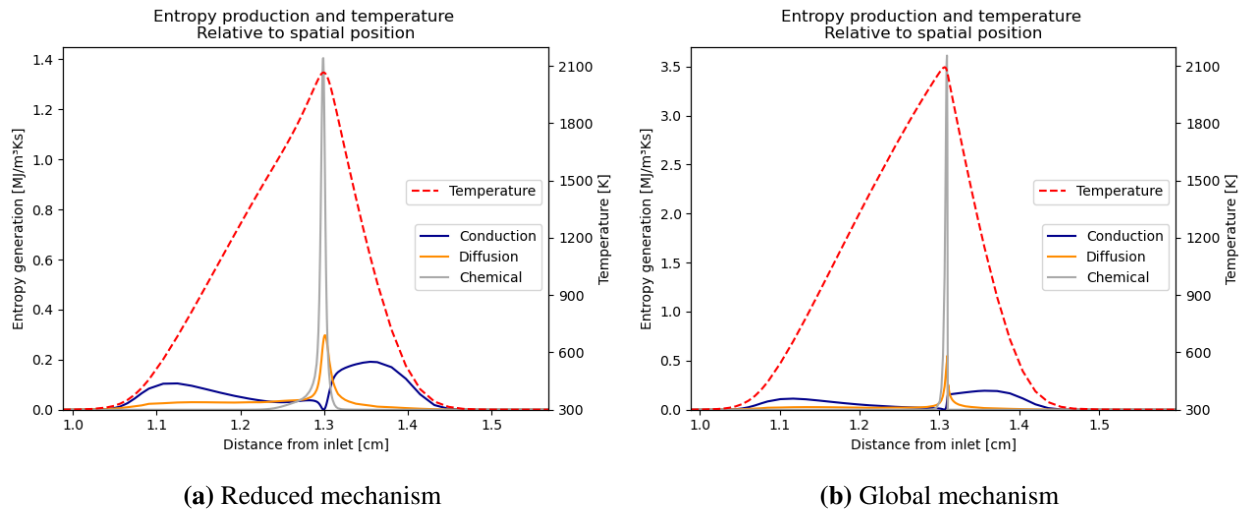


**Figure 94:** Instantaneous entropy production by source for detailed (a), and global (b) mechanisms. Model is non-premixed, counterflow methane flame at 20 atm.

The temperature profiles for all the mechanisms at 20 atm, are presented in Figure 95. As shown in Figure 75 the peak temperature is slightly lower. The mechanisms are even more similar in shape than the profiles at 10 atm, and the peaks are more narrow. Regarding the contribution from conduction, the effects of the narrow profile is outweighed by the effects of the lower peak, which results in a lower entropy production due to conduction for all mechanisms.

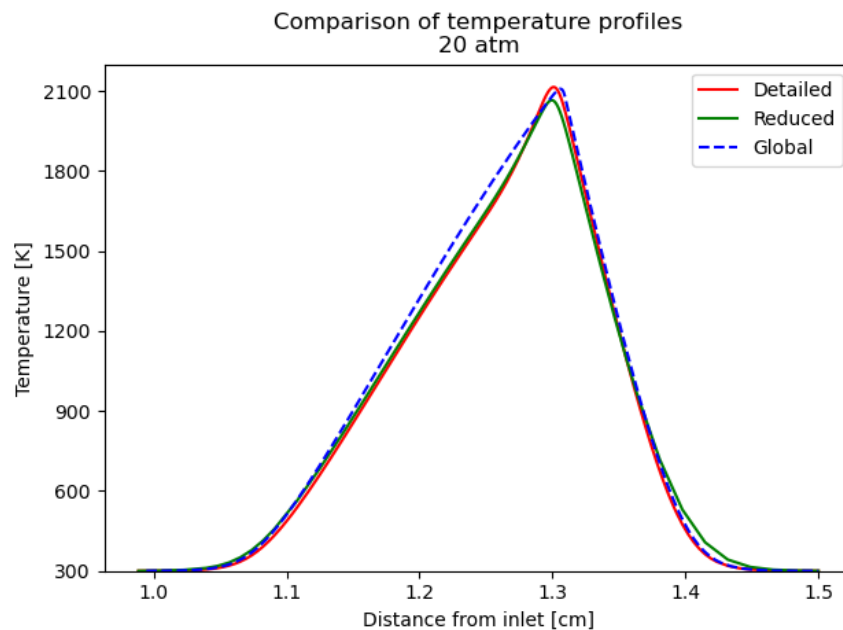


**Figure 95:** Temperature profiles for detailed, reduced, and global mechanisms.

The lower peaks and more narrow temperature profiles also affect the contribution from radia-

tion to entropy production. Even though the peaks are slightly lower, the steeper profiles result in a higher production. However, it is also dependent on the concentration of  $\text{CO}_2$  and  $\text{H}_2\text{O}$ . Even though it is difficult to see from Figure 96, the mole fraction profile for the products are steeper and slightly higher which results in more entropy production due to radiation, for all mechanisms.

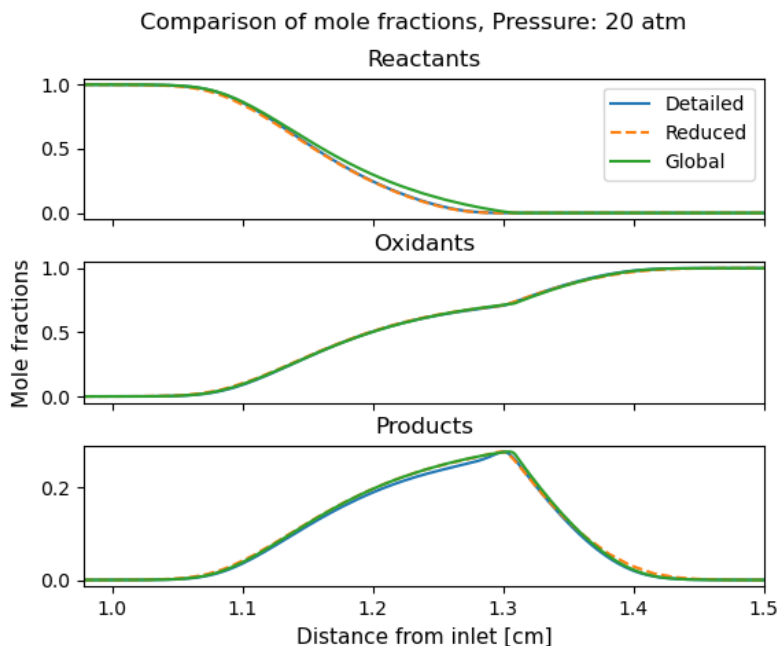


**Figure 96:** Caption

The seven reactions with the highest local entropy production at 20 atm are included in Figure 97a for the detailed, and Figure 97b for the reduced mechanisms. Many of the reactions with high contributions for the detailed mechanism, also had high contributions at 10 atm. However, they do not necessarily have the same ranks. The profiles appear to have divided from 10 atm to 20 atm. The reactions that have peaks closer to the oxidizer inlet are reactions with more radical species, than the reactions closer to the fuel inlet.

For the reduced mechanism, the profiles are similar in shape to the results shown in Figure 89b, at 10 atm. However, the highest contributing reaction have increased further, as have the second highest contributing reaction. However, the profiles are thinner which causes a lower integrated, total entropy production, as mentioned earlier.

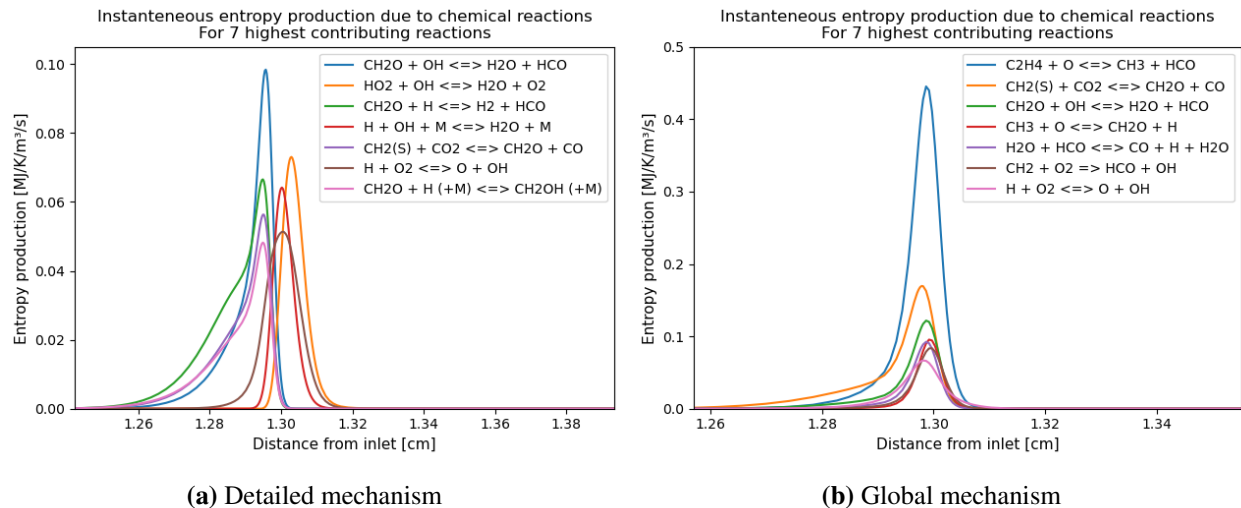


**Figure 97:** Comparison of the entropy production due to chemical reactions, from the highest contributing reactions using the detailed (a), and reduced (b) mechanism. Fuel type is methane in non-premixed, counterflow model at 20 atm pressure.

The 25 reactions with the highest contributions to the total integrated entropy production, using the detailed mechanism, is shown in Figure 98. Compared with the corresponding results at 10 atm, shown in Figure 90 the three highest contributing reactions are the same. Many of the other reactions are also present in both figures, but not necessarily with the same ranking. Furthermore, it can be seen that some of the reactions closer to the fuel inlet have higher integrated contributions than those closer to the oxidizer inlet.

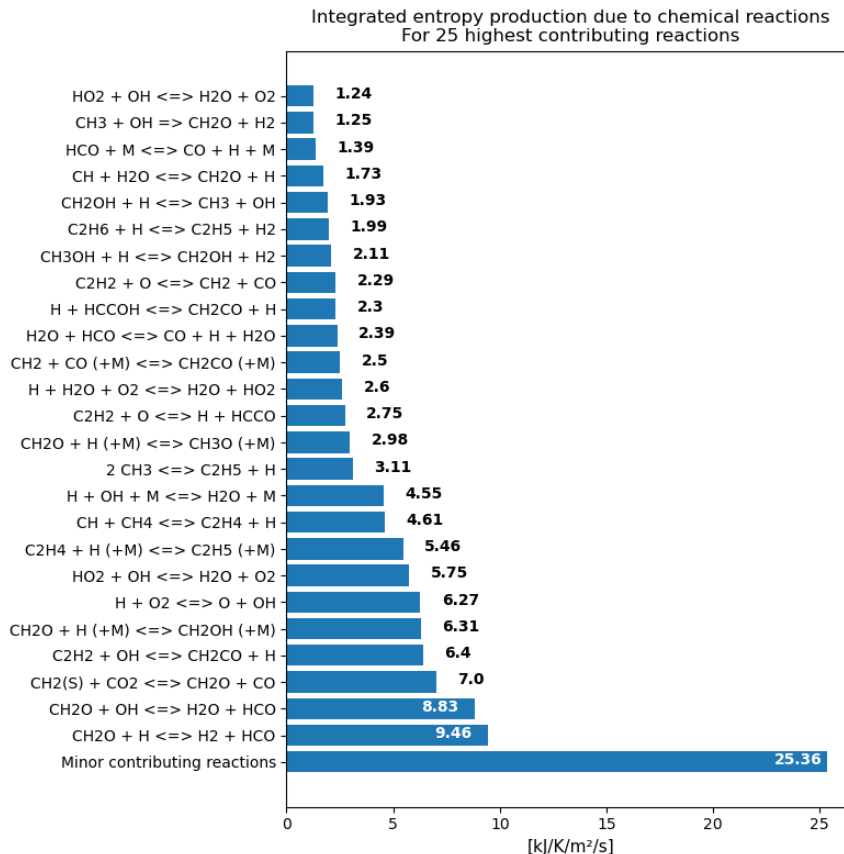


**Figure 98:** Integrated entropy production due to the highest contributing reactions, for detailed mechanism in non-premixed, counterflow model at 20 atm

In Figure 99, the 25 reactions with the highest integrated entropy production, using the reduced mechanism are shown. The three highest contributing reactions are the same as they were at 10 atm (Figure 91), and also have the highest local contribution.

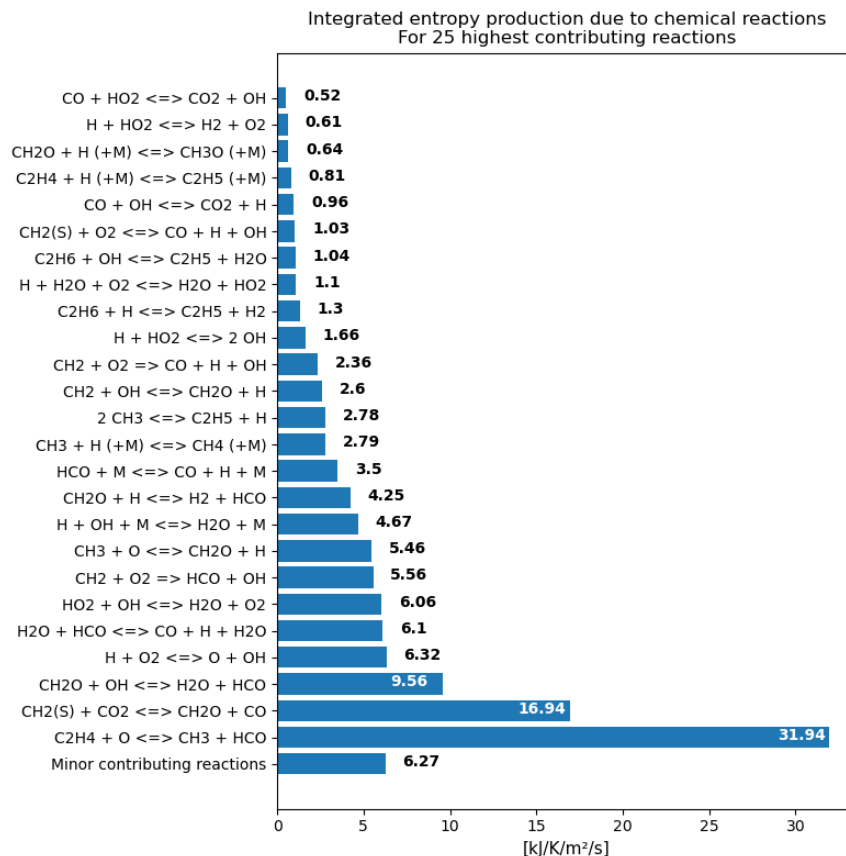


**Figure 99:** Integrated entropy production due to the highest contributing reactions, for reduced mechanism in non-premixed, counterflow model at 20 atm

### 5.6.5 Solution Grid

The details about the solution grid resolution are included in the appendix, while some specifics are stated here too. The solution grid, and its resolution, were determined by the grid refinement criteria presented in Section 3.3.2. At 1 atm, the detailed mechanism had considerably more grid points (259) than the reduced (132), and global (139) mechanisms. The resolution varied in order of magnitude, between  $10^{-4}$  and  $10^{-6}$  for the detailed and reduced mechanisms, and between  $10^{-3}$  and  $10^{-6}$  for the global mechanism. At 10 atm, the detailed mechanism still had the most grid points (248), followed by the global (156), and reduced (109) mechanisms. The grid resolution had an order of magnitude ranging from  $10^{-3}$ , to  $10^{-6}$ . At 20 atm, the number of grid points were 241, 160, and 113, for the detailed, global, and reduced mechanisms, respectively. Furthermore, the resolution still varied in order of magnitude between  $10^{-3}$  and  $10^{-6}$ .

## 5.7 Syngas

The distance between the fuel and oxidizer jets were 0.03 cm, which was also the width of the numerical domain. The graphs presented in this section only show parts of this domain, to focus

on the reaction zone and more easily identify differences between cases.

### 5.7.1 Comparison of Cases.

As it can be seen from Figure 100 the peak temperature calculated by all the mechanisms are similar. The figure also shows that the peak temperature increases from 1 atm to 10 atm, and then decreases at 20 atm, for all mechanisms. At 1 atm both the reduced and global mechanism overestimate the temperature compared with the detailed mechanism, and the global mechanism predicts the highest temperature. At 10 atm, the reduced mechanism predicts the highest temperature, and both the reduced and global mechanism predicts a higher temperature than the detailed mechanism. The reduced mechanism still predicts the highest temperature at 20 atm, but now the global mechanism underestimates the temperature.

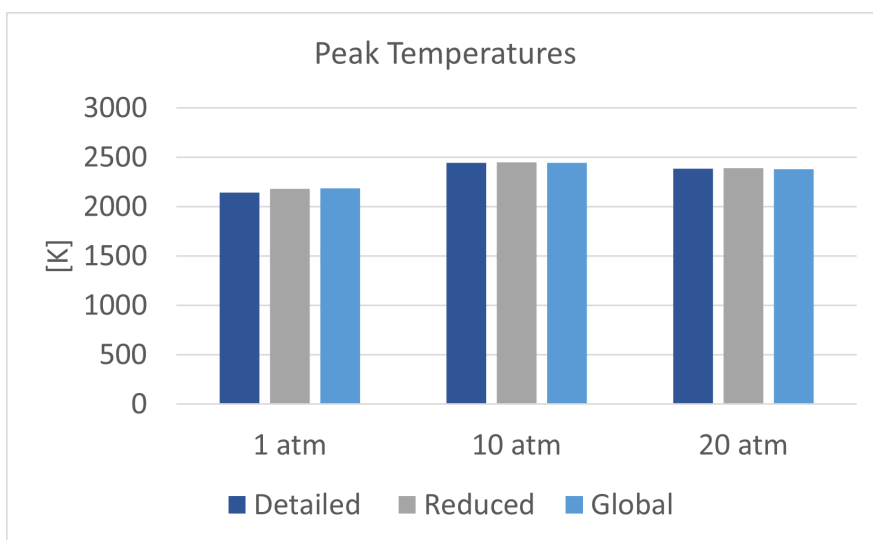


**Figure 100:** Comparison of calculated peak temperatures for detailed, reduced and global mechanism. Pressure range 1 atm, 10 atm, and 20 atm. Fuel type is syngas in non-premixed, counterflow model.

Figure 101 shows a comparison of the integrated entropy production by source for the detailed, reduced, and global mechanisms with variations in the pressure. It is clear that the entropy production using the global mechanism is lower than the detailed and reduced mechanisms for all pressures. All the mechanisms calculate a lower entropy production as the pressure increases. The detailed and reduced mechanisms predicts approximately the same production at each pressure. However, the detailed mechanism calculates a slightly higher production at 1 atm and 20 atm, while the reduced mechanism predicts an incrementally higher entropy production at 10 atm.

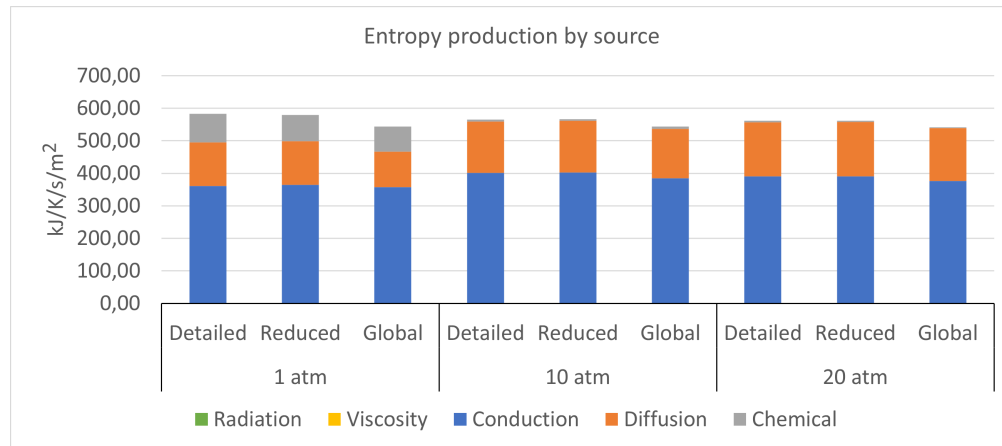


**Figure 101:** Comparison of the entropy production by source and the entropy change, for detailed, reduced, and global mechanisms. Pressure range 1 atm, 10 atm, and 20 atm. Fuel type is syngas in non-premixed, counterflow model.

The entropy production due to radiation and viscosity is negligible for all mechanisms, at all pressures. The contribution from radiation will be discussed for each pressure, while the contribution from viscosity is only discussed here. The entropy production due to viscosity calculated by the mechanisms are close for all pressures. Therefore, it is assumed that the detailed mechanism is representative for the reduced, and global mechanisms also.

The contribution from viscosity decreases with pressure, for all mechanisms. This was mainly due to the velocity gradient  $\frac{\partial u}{\partial x}$  in Equation 18. The effect of varying the pressure on the velocity is presented in Figure 102. From 1 atm to 10 atm, the velocity decreases with a factor of 10. Further, from 10 atm to 20 atm the velocity decreases again, now with a factor of two. The factor of decrease corresponds to the factor of increase in pressure. As the order of magnitude for the velocity decreases, the shape of the profiles, and the dimension on the x-axis remain almost entirely unchanged. Therefore, the velocity gradients will decrease, which leads to a decrease in contribution from viscosity.

Additionally, the global mechanism calculates a slightly lower entropy production due to viscosity than the detailed and reduced mechanism. One explanation for this was given for methane in Section 5.4.2. Here, it was stated that the viscosity  $\mu$  is calculated with regards to the species in the gas at every point in the flame. Furthermore, it was said that since the detailed mechanism contains more reactions than the reduced, and global mechanisms, some species may not be created at some given locations in the flame. If the species that are not included have a high viscosity, neglecting them will result in a lower viscosity for the gas, and thereby a lower entropy production.

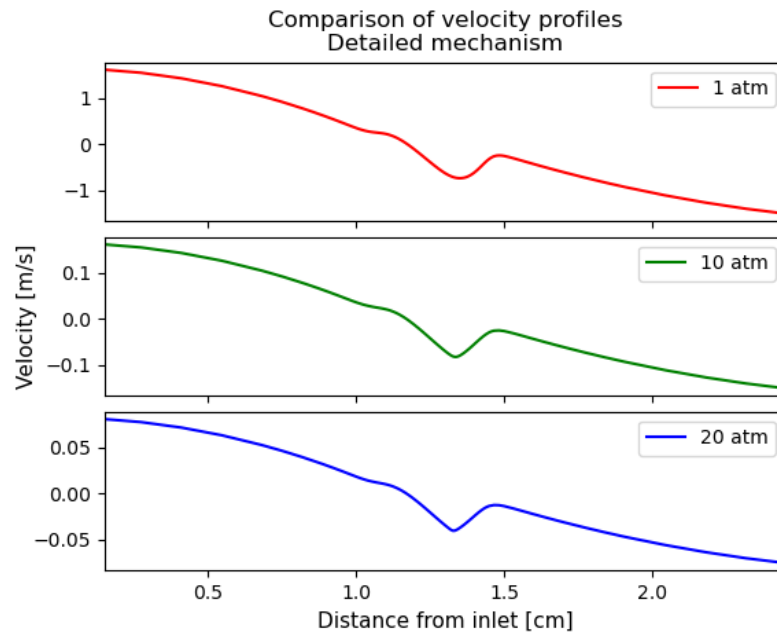


**Figure 102:** Comparison of velocity profiles at different pressures using non-premixed, counterflow flame model with syngas.

### 5.7.2 1 atm

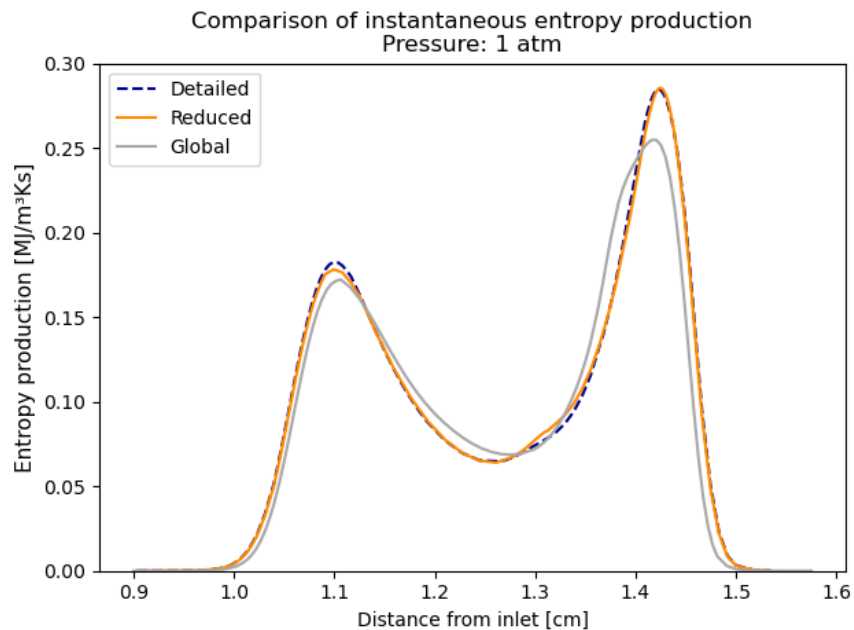
Table 12 contains the integrated entropy production by source at 1 atm. From the table it can be seen that the detailed mechanism calculates a higher entropy production due to viscosity, diffusion, and chemical reactions. The reduced mechanism calculates a slightly higher entropy production from radiation and conduction.

**Table 12:** Integrated entropy production by source for the non-premixed, counterflow syngas flame at 1 atm.

	Integrated entropy production by source [kJ/K/s/m <sup>2</sup> ]		
	Detailed	Reduced	Global
Radiation	4,48E-02	5,93E-02	3,70E-02
Viscosity	6,66E-05	6,61E-05	6,26E-05
Conduction	361,20	364,93	357,25
Diffusion	134,19	133,65	108,67
Chemical	86,83	81,24	78,33

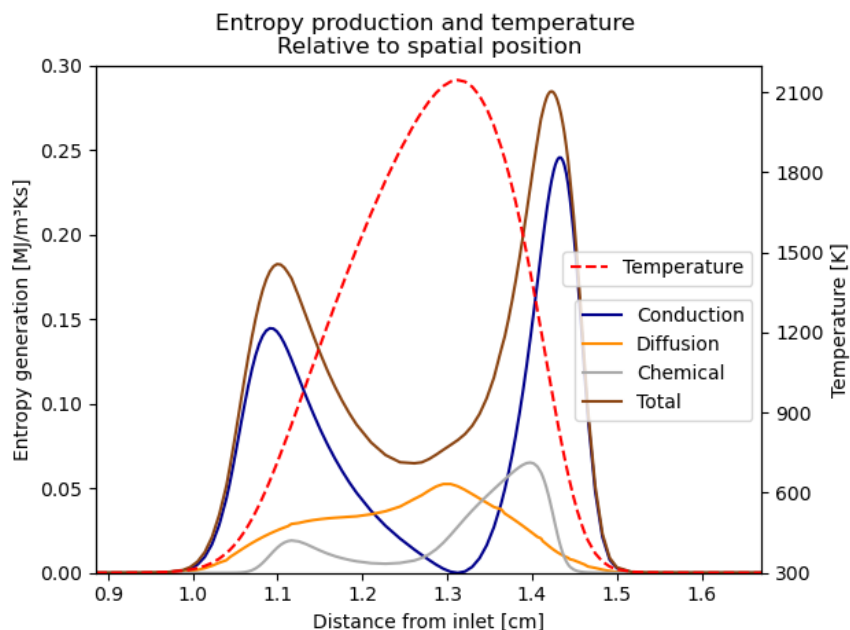
The comparison of the total instantaneous entropy production for detailed, reduced, and global mechanisms at 1 atm is displayed in Figure 103. Again, local entropy production could be a more appropriate term, since the system is in steady state and the production does not change with time. The curves follow each other nicely, with some discrepancy for the global mechanism. On both sides of the graph, the profile of the detailed mechanism is preceding the reduced, an global mechanism slightly.





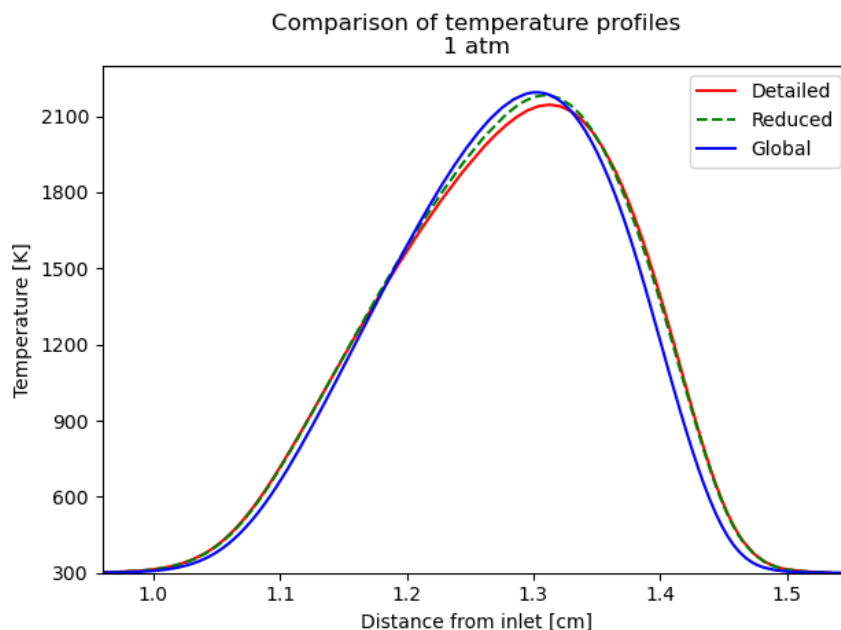
**Figure 103:** Comparison of the entropy production using detailed, reduced, and global mechanism. Fuel type is syngas in non-premixed, counterflow model with 1 atm pressure.

Figure 104 shows the local entropy production by source, for the detailed mechanism at 1 atm. Since the profiles in Figure 103 are similar, it is sufficient to investigate the profile of the detailed mechanism to further understand the shapes of the profiles in Figure 104. First, it can be seen that the peaks are because of the entropy production due to conduction. They are located where the temperature gradients are steep, since the entropy production due to conduction is dependent on the temperature gradient squared (Equation 19). The chemical reactions start to occur when the temperature is sufficient, and the entropy production due to the reactions have a peak on each side right after the peak due to conduction. The contribution from diffusion is initiated when the temperature begins to increase, reaches a peak that is located at the peak of the temperature profile, as the other contributions fall to zero. The profiles of radiation and viscosity are not included as their contributions could not be detected in the graph.



**Figure 104:** Instantaneous entropy production by source, and temperature profile, for counterflow flame at 1 atm, with syngas, using the detailed mechanism GRI-mech 3.0 [41]

To further investigate why the reduced mechanism overestimates the contribution from conduction and radiation, the temperature profiles at 1 atm are displayed in Figure 105. First, it is clearly shown that the reduced and global mechanisms overestimate the peak temperature, as was also shown in Figure 100. Second, the profile for the reduced mechanism is slightly steeper than the profile of the detailed mechanism. As the entropy production due to conduction is dependent on the temperature gradient squared (Equation 19), these two aspects of the profile result in a higher entropy production calculated by the reduced mechanism. Logically, the same arguments should also apply for the profile of the global mechanism as it is even taller and steeper. However, the entropy production is lower. One explanation was given for methane in the premixed, freely-propagating flame in Section 5.4.2. It was stated that Cantera [16] calculates the thermal conductivity  $\lambda$  based on all the species in the gas, and that since a large number of reactions are neglected in the global mechanism, some species may be included by the detailed mechanism but not by the global mechanism. Furthermore, if these neglected species have a high thermal conductivity, the gas will have a lower thermal conductivity.



**Figure 105:** Temperature profiles for detailed, reduced, and global mechanisms.

The higher, and steeper temperature profile is also part of the reason that the reduced mechanism calculates a higher contribution from radiation than the detailed mechanism. However, another reason can be investigated by looking at Figure 106, where the mole fraction profiles for reactants ( $\text{CO}$ ,  $\text{H}_2$ ), oxidants ( $\text{O}_2$ ,  $\text{N}_2$ ), and products ( $\text{CO}_2$ ,  $\text{H}_2\text{O}$ ) are presented. Since the model used by Cantera [16] only accounts for  $\text{CO}_2$  and  $\text{H}_2\text{O}$ , their mole fractions will have an impact on the entropy production due to radiation. In the figure it is clear how the global mechanism underestimates the mole fractions of the products, and the effects outweigh the effects of a steeper and taller temperature profile, resulting in a lower entropy production due to radiation. Furthermore, if one looks closely at the profile for the products it can be seen that the reduced mechanism calculates a slightly higher mole fraction for the products. This overestimation, in addition to the steeper and higher temperature profile results in a higher entropy production due to radiation.

The mole fraction profiles can also be part of the explanation for why the entropy production due to diffusion is higher for the detailed and reduced mechanism, than for the global mechanism. It can be seen that the reactants are used faster for the detailed and reduced mechanisms, which results in higher gradients for the mole fraction profiles, and a higher entropy production. However, the detailed and reduced mechanisms follow each other closely, and yet the detailed mechanism calculates a higher entropy production. This may also be because of the neglected equations. Some of these equations are elementary equations that create and destroy intermediate species rapidly, which leads to steep gradients.

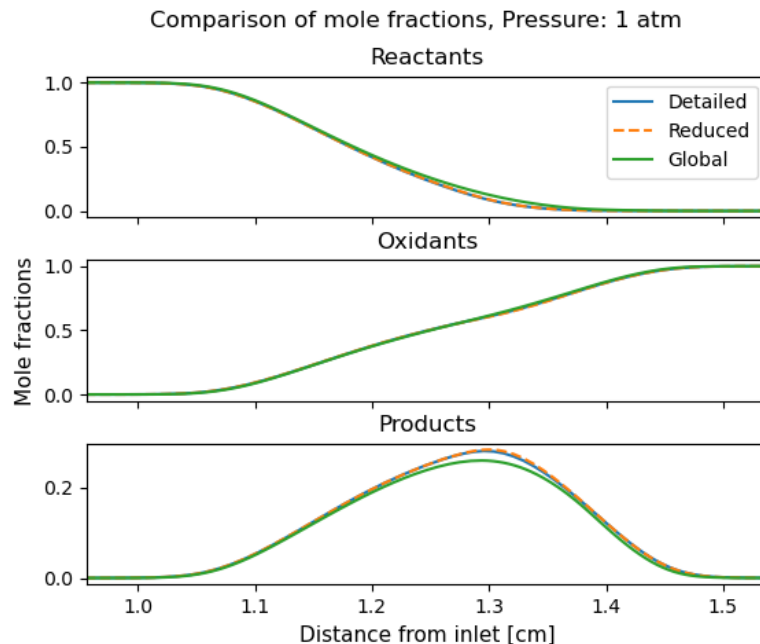
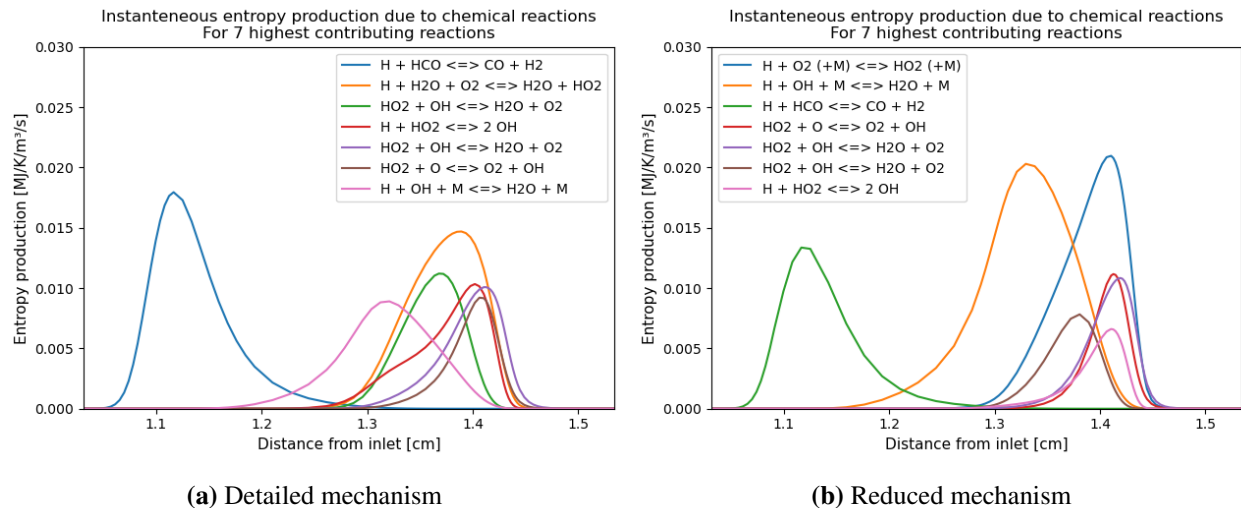


**Figure 106:** Comparison of the mole fraction profiles for reactants ( $\text{CO}$ ,  $\text{H}_2$ ), oxidants ( $\text{O}_2$ ,  $\text{N}_2$ ), and products ( $\text{CO}_2$ ,  $\text{H}_2\text{O}$ ), for the detailed, reduced, and global mechanisms at 1 atm

Figure 107 compares the seven reactions with the highest local entropy production for the detailed (Figure 107a), and reduced (Figure 107b) mechanisms. For both mechanisms, the same reaction have its contribution closer to the fuel inlet than the other reactions. This may be because both the species in the fuel ( $\text{CO}$ ,  $\text{H}_2$ ) are included on the right hand side of the reactions. Something noteworthy is that this reaction is also the only reaction included in the figures where  $\text{CO}$ , or any species with carbon ( $\text{C}$ ) is included.

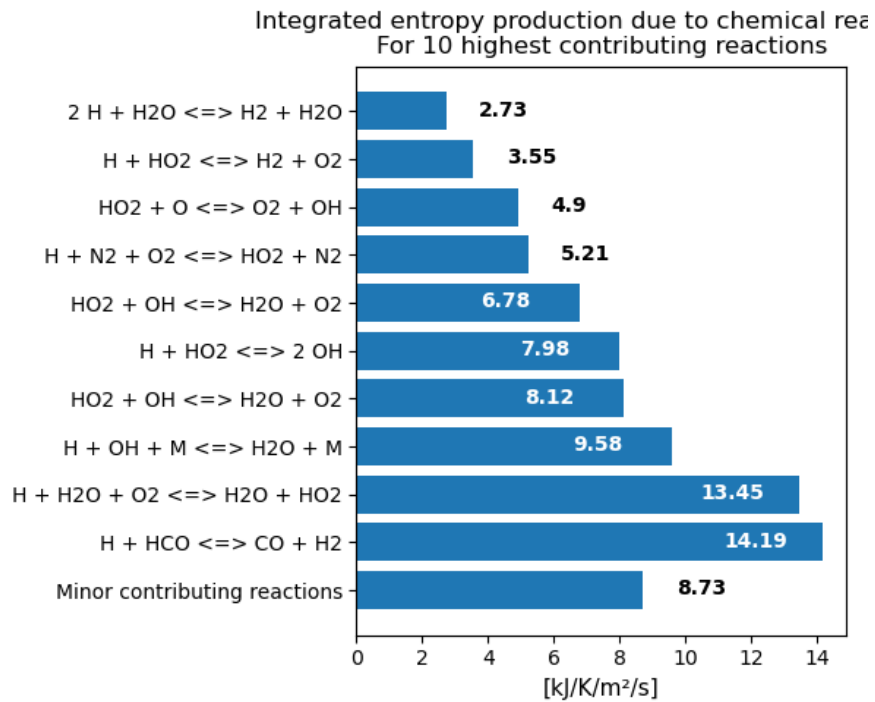
Furthermore, it is worth mentioning that the reaction with the second highest contribution using the detailed mechanism, is similar to the reaction with the highest contribution using the detailed mechanism. This was also experienced with the freely-propagating flame model, but with a different pair of reactions. The reaction in the reduced mechanism contains a variable species  $\text{M}$ , that represents a inert species that do not undergo any changes in the reaction but can contribute through collisions. In the reaction in the detailed mechanism  $\text{H}_2\text{O}$  have this exact same feature. However, since the reaction in the reduced mechanism also can contain other species, it is logical that it has a higher contribution.

Moreover, the two reactions with the fifth, and sixth highest contribution in the figure for the reduced mechanism are duplicates. This is also true for the third, and fifth highest contributing reactions in the figure for the detailed mechanism. In their respective mechanisms, the reactions differ in their parameters used in the Arrhenius function. This could have been investigated further, as it is possible that the contributions from these reactions should have been summed together. Unfortunately, this was discovered too late to correct.



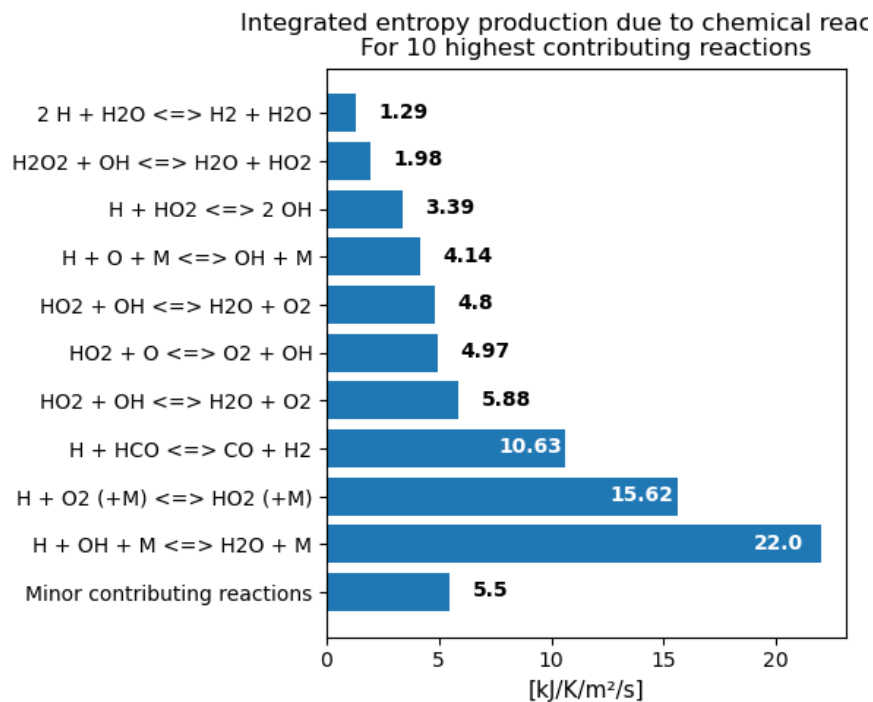
**Figure 107:** Comparison of the entropy production due to chemical reactions, from the highest contributing reactions using the detailed (a), and reduced (b) mechanism. Fuel type is syngas in non-premixed, counter-flow model at 1 atm pressure.

In Figure 108, the ten reactions with highest integrated entropy production, using the detailed mechanism is shown. Additionally, the remaining 315 reactions are included as one contribution in the column at the bottom. The number reactions include was reduced to ten, as the entropy production from the remaining reactions were considerably lower. Regardless, many of the reactions with the highest local entropy production, also have high integrated entropy production. It should be mentioned that there is still only one reaction containing CO included in the figure.



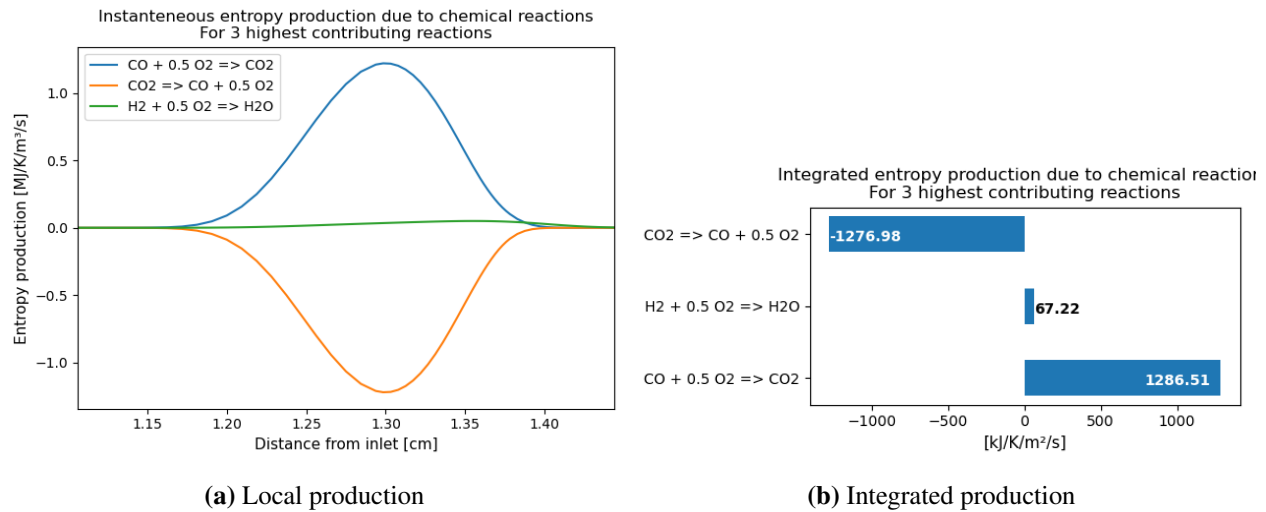
**Figure 108:** Integrated entropy production due to the highest contributing reactions, for detailed mechanism in non-premixed, counterflow model at 1 atm

Figure 109 shows the 10 reactions with highest integrated entropy production, using the reduced mechanism. In this case, the seven reactions with highest local entropy production, also have the highest integrated value. However, not necessarily in the same order.



**Figure 109:** Integrated entropy production due to the highest contributing reactions, for reduced mechanism in non-premixed, counterflow model at 1 atm

Figure 110, presents the local (Figure 110a), and integrated (Figure 110b), entropy production for each reaction included in the global mechanism. This was not included for methane, as the global mechanism for methane only contain one reactions. Compared with reactions 1 and reaction 2 in Figure 110, reactions three has almost a negligible contribution. However, if the contributions from reaction 1 and reaction 2 where combined, reaction 3 would have the highest contribution. It should be noted that the reactions do not appear in the same order in the legend in Figure 110, and on the axis in Figure 110b.



**Figure 110:** Comparison of the local (a), and integrated (b) entropy production due to the chemical reactions, using the global mechanism. Fuel type is syngas in non-premixed, counterflow model at 1 atm pressure.

### 5.7.3 10 atm

Table 13 shows the integrated entropy production by source, at 10 atm. The contribution from radiation, conduction, and diffusion have increased, while the contributions from viscosity and chemical reactions have decreased for all mechanisms. The reduced mechanism still calculates a higher entropy production from radiation and conduction than the detailed, and global mechanism. The reduced mechanism also calculates a higher contribution from viscosity, and diffusion. Meanwhile, the global mechanism now calculates a higher entropy production due to the chemical reactions than the detailed, and reduced mechanisms.

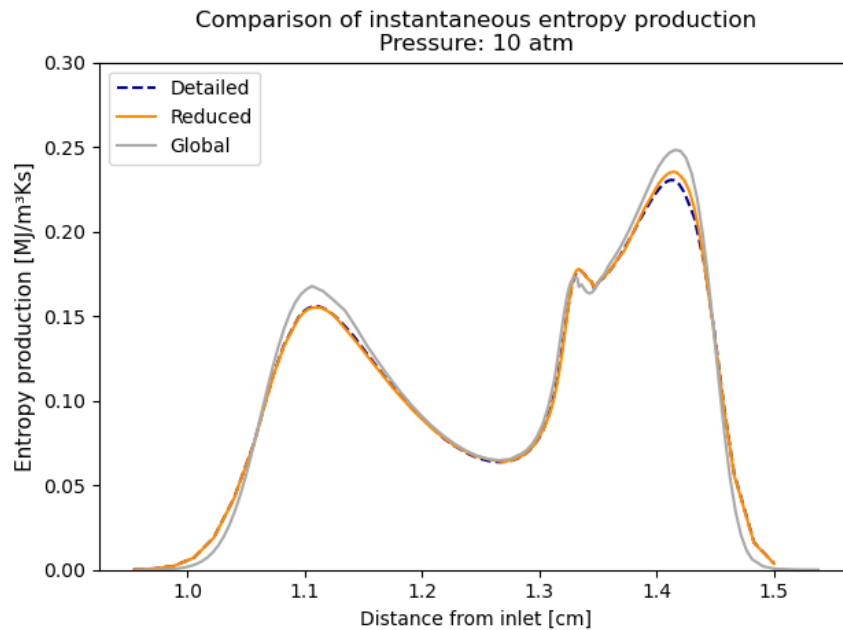
**Table 13:** Integrated entropy production by source for the non-premixed, counterflow syngas flame at 10 atm.

	Integrated entropy production by source [kJ/K/s/m <sup>2</sup> ]		
	Detailed	Reduced	Global
Radiation	3,55E-01	7,05E-01	5,13E-01
Viscosity	7,09E-07	7,10E-07	6,92E-07
Conduction	400,50	401,67	384,51
Diffusion	158,30	158,76	151,92
Chemical	6,09	5,08	7,22

Figure 111 shows the total local entropy production using detailed, reduced, and global mechanisms when the pressure is increased by a factor of ten. There are still two peaks in the entropy profiles, but now there is a new smaller peak just before the last peak. The graphs are similar in shape, and the graphs for the detailed and reduced mechanisms are almost identical. The global mechanism overestimates both of the peaks, and also have steeper gradients at the beginning and end of the profiles. The effects of the higher peaks are cancelled by the effects of the steeper gra-

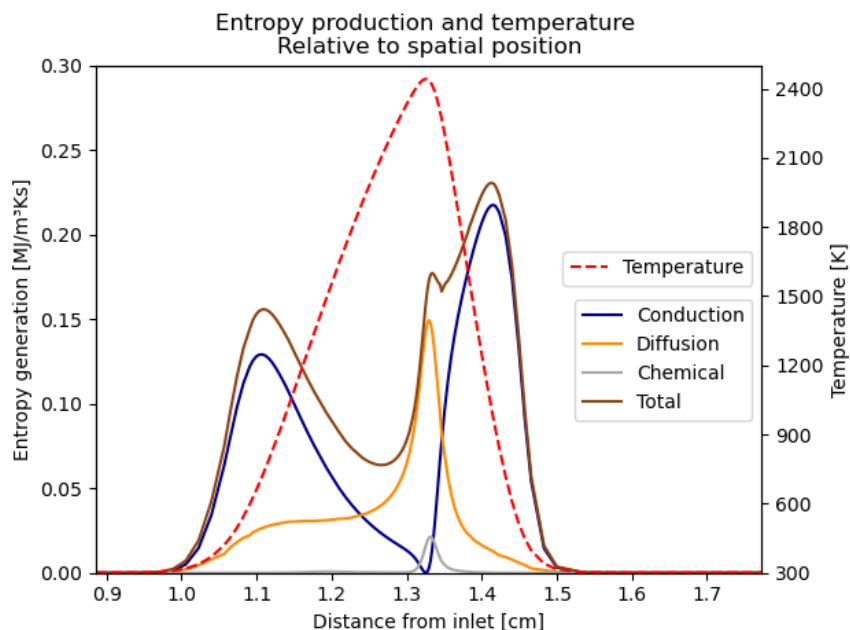


dients, which makes the integrated value of entropy production close to the total value for 10 atm and 20 atm. It can also be noted that the width of the profiles have not changed.



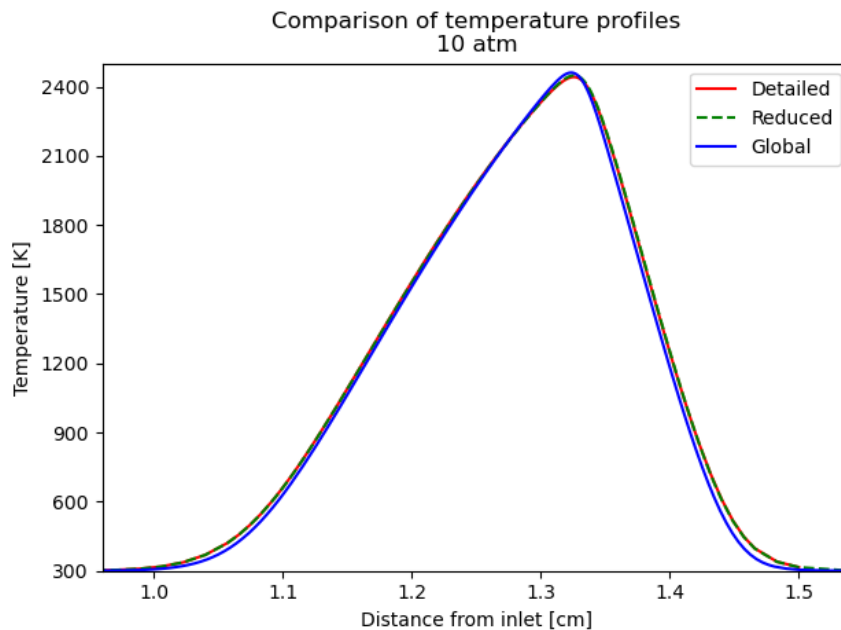
**Figure 111:** Comparison of the entropy production using detailed, reduced, and global mechanism. Fuel type is syngas in non-premixed, counterflow model with 10 atm pressure.

In Figure 112 the local entropy production by source, using the detailed mechanism at 10 atm, is presented. The profiles in Figure 111 are considered to be adequately similar, so that the detailed mechanism also is representative for the reduced, and global mechanisms. From studying the graph it can be seen that the new peaks results from an increase in diffusion. The reason for the increase will be discussed later in this section. The profile of the entropy production due to conduction are wider, with a lower peak value. The effects of the wider profile outweighs the effects of a lower peak, and therefore the integrated entropy production from conduction increases. The entropy production due to the chemical reactions are considerably lower, and is concentrated in a small peak around the same location as the peak in temperature.



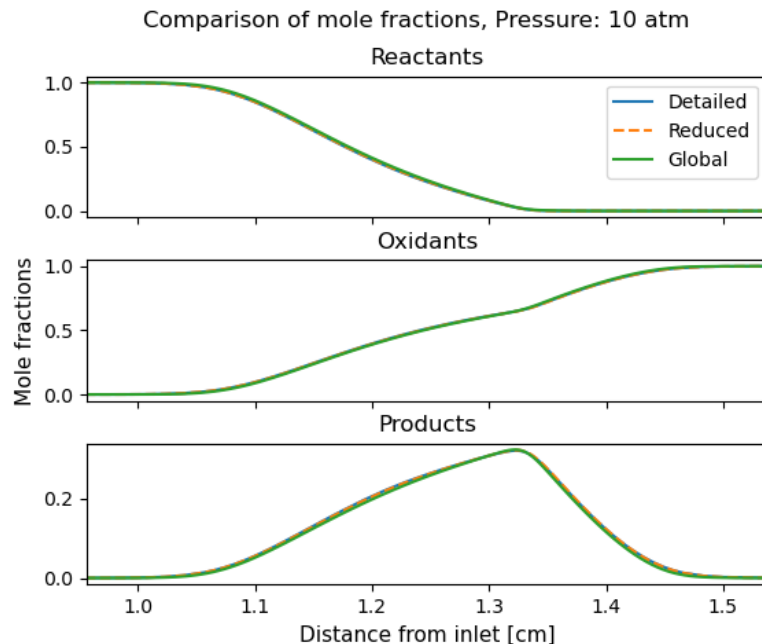
**Figure 112:** Instantaneous entropy production by source for a non-premixed, counterflow flame model with syngas, at 10 atm, using the detailed mechanism GRI-mech 3.0 [41].

The contribution from conduction can be investigated further by studying the temperature profiles, presented in Figure 113. Compared with the profiles in Figure 105, the profiles are higher and steeper. The profiles using the detailed and reduced mechanisms are closer, which is why the calculated integrated entropy production is also closer. However, the global mechanism also have less discrepancy, but the integrated value is actually more erroneous than it was for 1 atm.



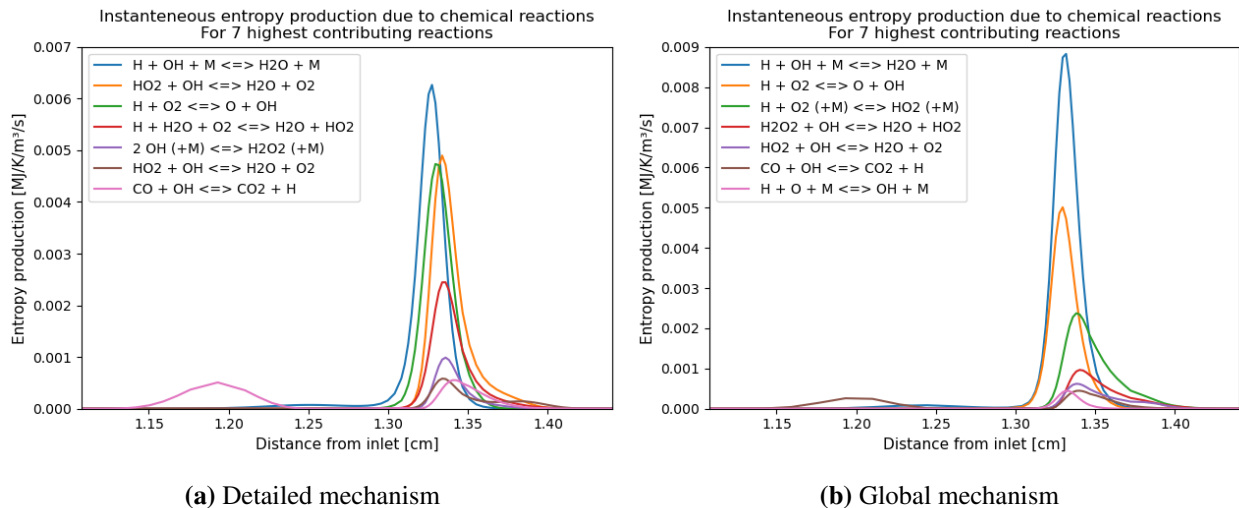
**Figure 113:** Temperature profiles for detailed, reduced, and global mechanisms.

The mole fraction profiles for reactants ( $\text{CO}$ ,  $\text{H}_2$ ), oxidants ( $\text{O}_2$ ,  $\text{N}_2$ ), and products ( $\text{CO}_2$ ,  $\text{H}_2\text{O}$ ) at 10 atm are presented in Figure 114. The profiles for the detailed, reduced, and global mechanisms follow each other more closely, compared with Figure 106. The profiles for the products are steeper at 10 atm, which is the main reason for the increase in entropy production due to radiation, and diffusion.



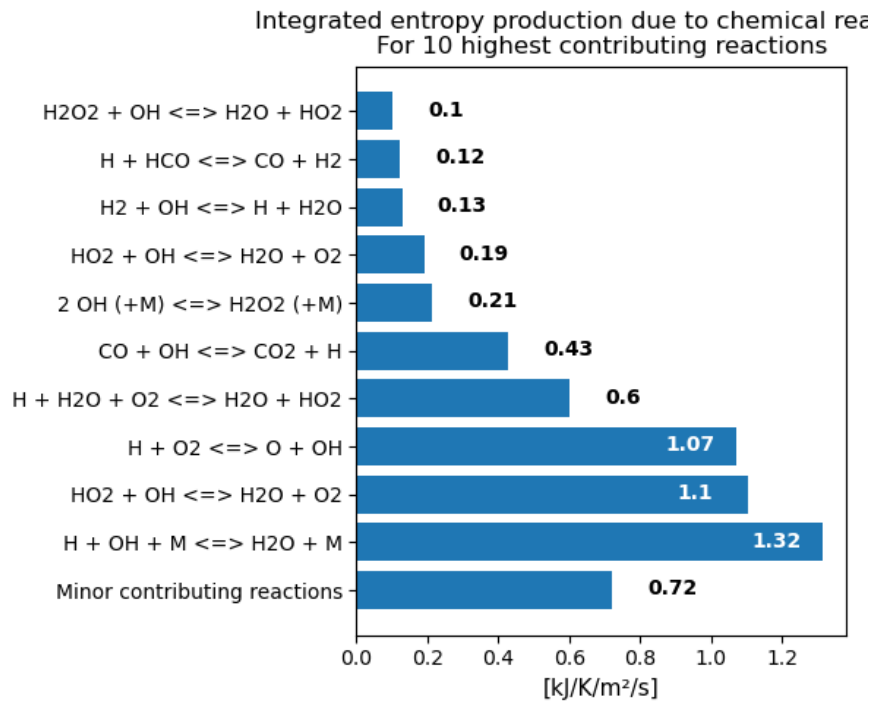
**Figure 114:** Comparison of the mole fraction profiles for reactants ( $\text{CO}$ ,  $\text{H}_2$ ), oxidants ( $\text{O}_2$ ,  $\text{N}_2$ ), and products ( $\text{CO}_2$ ,  $\text{H}_2\text{O}$ ), for the detailed, reduced, and global mechanisms at 10 atm

Figure 115 shows the seven reactions with the highest local entropy production, using the detailed (Figure 115a), and reduced (Figure 115b) mechanisms. First, it should be mentioned that the scales on the vertical axis in the figures are not the same, as they were for 1 atm. The axis have decreased for both mechanisms, as have the horizontal axis. The reaction that had its contribution close to the fuel inlet at 1 atm, is no longer included in the figures of either mechanisms. However, a new reaction is included, that have its contribution close to the fuel inlet and contains CO.



**Figure 115:** Comparison of the entropy production due to chemical reactions, from the highest contributing reactions using the detailed (a), and reduced (b) mechanism. Fuel type is syngas in non-premixed, counter-flow model at 10 atm pressure.

The ten reactions with highest integrated entropy production, using the detailed mechanism are included in Figure 116. The reactions with highest integrated contribution have changes according to the reactions with highest local production, and the reactions included are similar to those included in Figure 115a.



**Figure 116:** Integrated entropy production due to the highest contributing reactions, for detailed mechanism in non-premixed, counterflow model at 10 atm

In Figure 117 the ten reactions with the highest contributions to the total integrated entropy production using the reduced mechanism are included. As for the detailed mechanism, the reactions included have changed according to the reactions with the highest local entropy production. As a result, many of the reactions included are also included in Figure 115b.

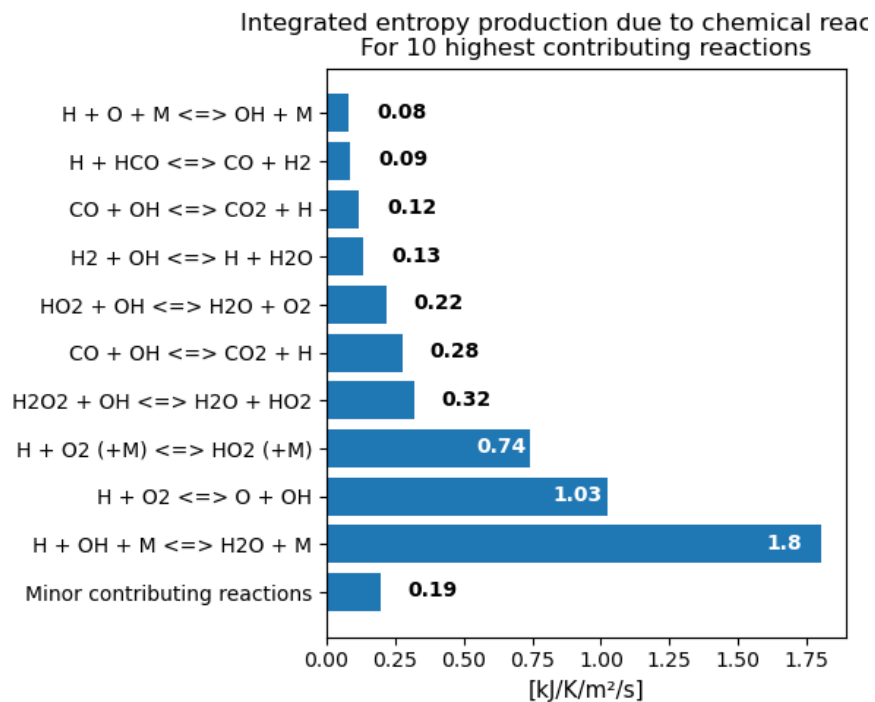


**Figure 117:** Integrated entropy production due to the highest contributing reactions, for reduced mechanism in non-premixed, counterflow model at 10 atm

In Figure 118 results for the local (Figure 118a), and integrated (Figure 118b) entropy production using the global mechanism are shown. Compared with the results at 1 atm (Figure 110), both the local and integrated entropy production have increased for reaction 1 and reaction 2 (in Figure 118a). However, if these contributions are summed the contributions from the two have decreased. The contribution from the remaining reaction has also decreased. Furthermore, the profiles in Figure 118a are shifted towards the oxidizer inlet.

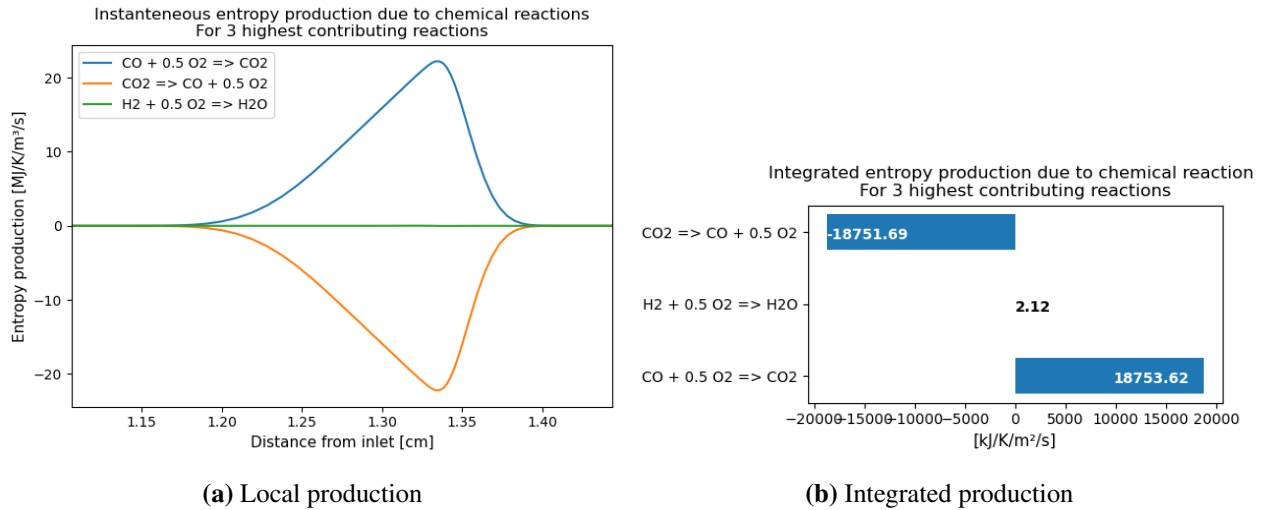


**Figure 118:** Comparison of the local (a), and integrated (b) entropy production due to the chemical reactions, using the global mechanism. Fuel type is syngas in non-premixed, counterflow model at 10 atm pressure.

### 5.7.4 20 atm

Table 14 shows the integrated entropy production by source, for all mechanisms at 20 atm. Entropy production has increased, and the reduced mechanism still predicts the highest value, followed by the global, and the detailed mechanisms. The contribution from viscosity has further decreased, and all the mechanisms calculate approximately the same value. The detailed and reduced mechanism also calculate the same values, with negligible differences for conduction and diffusion, and the global mechanism has a lower contribution for both. For all mechanisms the contribution from conduction has decreased, while it has increased for diffusion from 10 atm to 20 atm. The entropy production due to the chemical reactions have decreased further, and at 20 atm the detailed mechanism calculates the highest contribution, followed by the reduced, and global mechanisms.

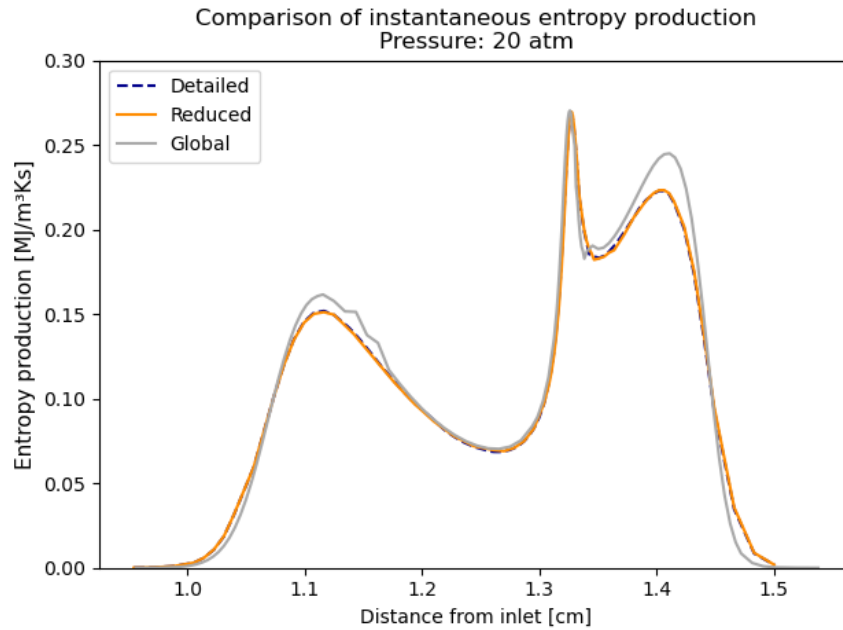
**Table 14:** Integrated entropy production by source for the non-premixed, counterflow syngas flame at 20 atm.

	Integrated entropy production by source [kJ/K/s/m <sup>2</sup> ]		
	Detailed	Reduced	Global
Radiation	5,92E-01	1,42E+00	1,10
Viscosity	1,75E-07	1,75E-07	1,72E-07
Conduction	389,56	389,28	374,92
Diffusion	166,22	166,67	163,18
Chemical	4,78	3,77	2,22

Figure 119 compares the total, local entropy production for detailed, reduced, and global mechanism with 20 atm. The profiles are similar to the profiles at 10 atm, but now the new peaks are higher. The detailed and reduced mechanism have almost identical graphs, while the discrepancy of the global mechanism is worse. The graph of the global mechanism have become even more

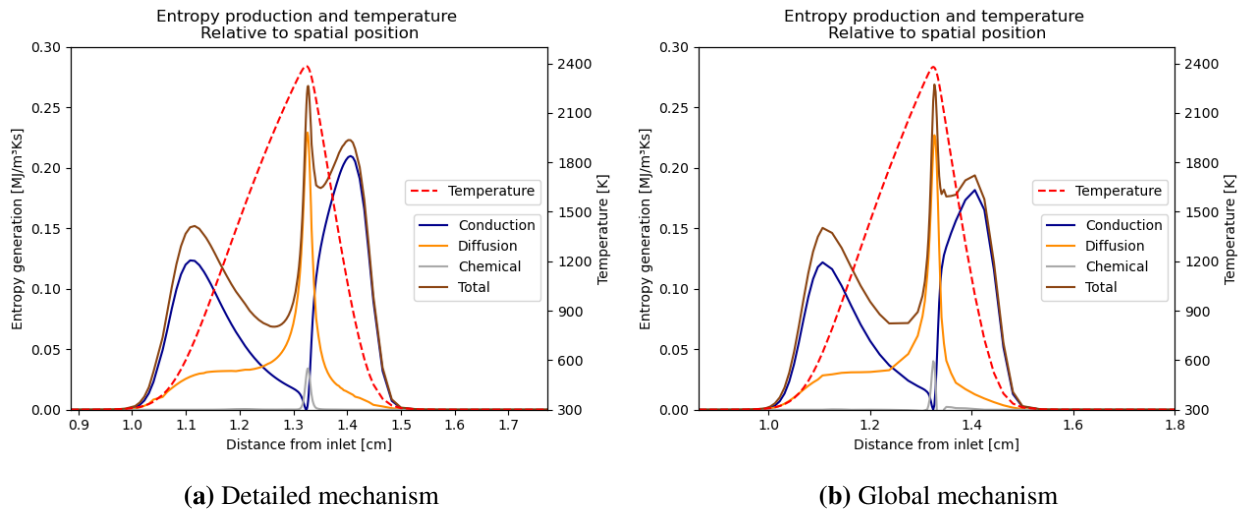


narrow with higher peaks. Again, the effects from the steeper gradients cancel against the effects of the higher peaks and the integrated value do not change much.



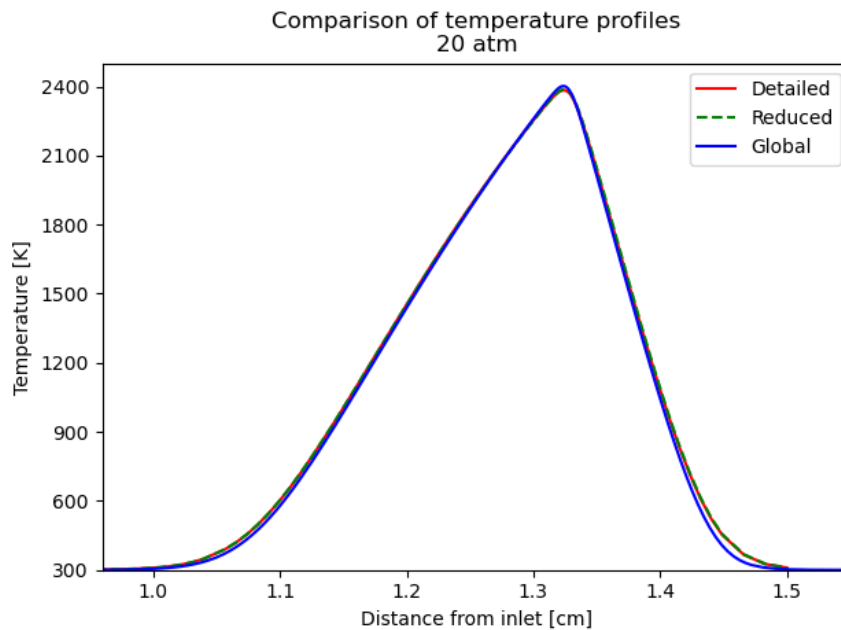
**Figure 119:** Comparison of the entropy production using detailed, reduced, and global mechanism. Fuel type is syngas in non-premixed, counterflow model with 20 atm pressure.

Figure 120 shows the local entropy production by source for the detailed (Figure 120a) and global (Figure 120b) mechanisms. The detailed mechanism is assumed to be representative for the reduced mechanism. The profile for diffusion in Figure 120a has a noticeably higher peak. The profiles for conduction have a similar shape, but are slightly steeper right after 1.3 cm from the fuel inlet. The contribution from chemical reactions have also gotten a more narrow, and taller profile. The profiles of the global mechanism is seen to have a shape that is similar to the profiles of the detailed mechanism. However, it is more uneven, which can be an indication that the grid should have been finer for this solution.



**Figure 120:** Instantaneous entropy production by source for detailed (a), and global (b) mechanisms. Model is non-premixed, counterflow syngas flame at 20 atm.

In Figure 121, the temperature profiles for all the mechanisms at 20 atm are presented. Even though it is barely visible, the profiles are slightly lower, and steeper. Furthermore, it is seen that the profiles are even more similar in shape. These two changes explain why the integrated entropy production calculated by the mechanisms have decreased, and are more equal at 20 atm.



**Figure 121:** Temperature profiles for detailed, reduced, and global mechanisms.

Since the entropy production due to radiation also depend on the temperature profiles, but increase from 10 atm to 20 atm, instead of decreasing as the contribution from conduction does, it

must be investigated further. Therefore, the mole fraction profiles for reactants ( $\text{CO}$ ,  $\text{H}_2$ ), oxidants ( $\text{O}_2$ ,  $\text{N}_2$ ), and products ( $\text{CO}_2$ ,  $\text{H}_2\text{O}$ ) are presented in Figure 122. It is almost not visible, but the profiles are slightly steeper for all mechanisms. Additionally, it is produced slightly more products, and this is the reason for the increase in contribution from radiation and diffusion. With the increasing pressure the mole fraction gradient of the products have gotten steeper. This trend was also seen by Som et al. [42], and is illustrated in Figure 11a and Figure 11b in their article, which is the same graphs used for the validation in Section 4.2. However, it should be noted that Som et al. used a partially premixed mixture of syngas and air, which may be the reason that the mole fraction profiles in their results are steeper.

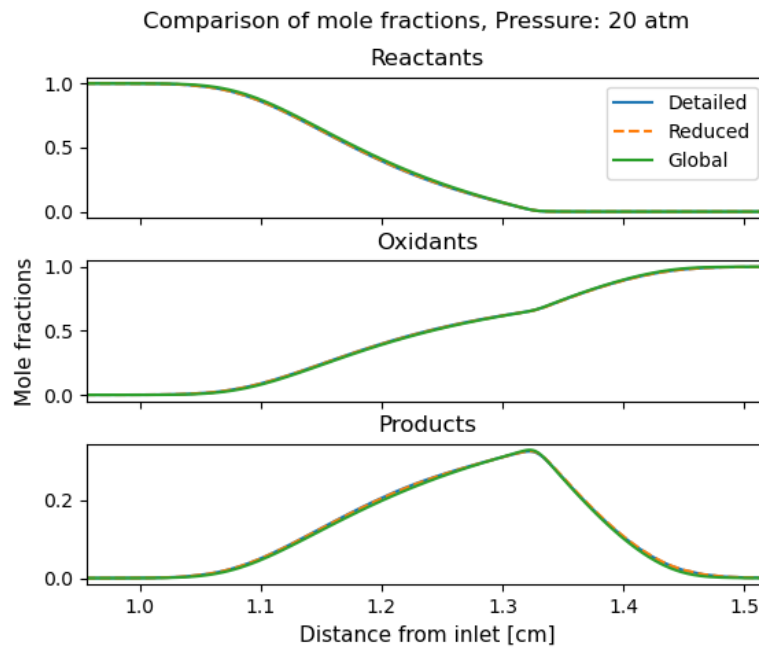


**Figure 122:** Comparison of the mole fraction profiles for reactants ( $\text{CO}$ ,  $\text{H}_2$ ), oxidants ( $\text{O}_2$ ,  $\text{N}_2$ ), and products ( $\text{CO}_2$ ,  $\text{H}_2\text{O}$ ), for the detailed, reduced, and global mechanisms at 20 atm

The local entropy production from the seven highest contributing reactions using the detailed (Figure 123a), and reduced (Figure 123b) mechanisms are presented in Figure 123. For both mechanism, there have been fewer exchanges of reactions from 20 atm to 20 atm, than from 1 atm, to 10 atm. Furthermore, the profiles in both figures have increased peaks, but thinner profiles resulting in lower integrated entropy production. For both mechanisms there are still only one reaction containing  $\text{CO}$ , but it has now a higher contribution.

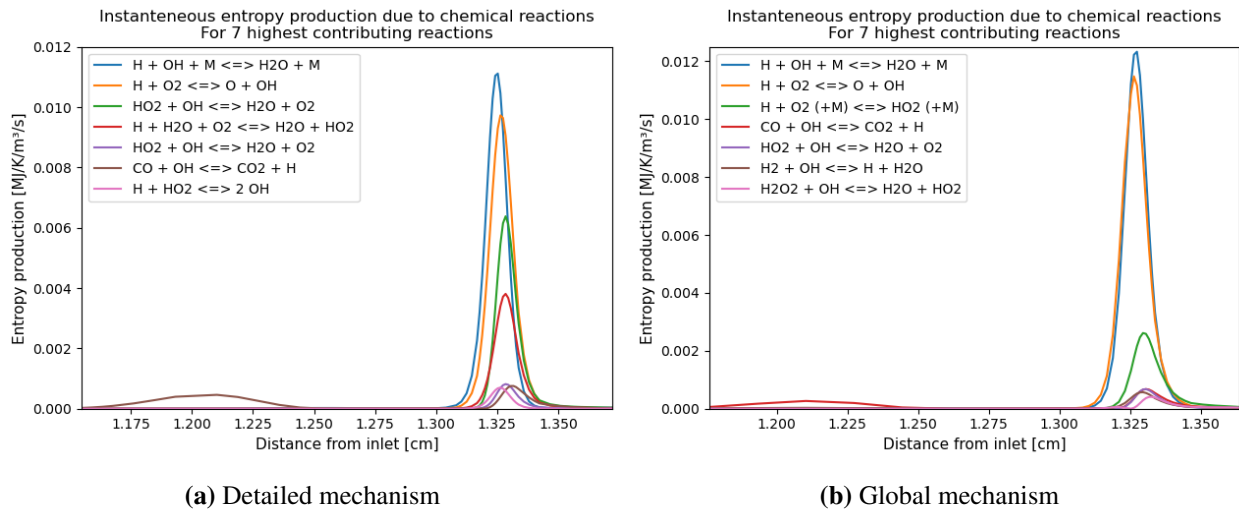


**Figure 123:** Comparison of the entropy production due to chemical reactions, from the highest contributing reactions using the detailed (a), and reduced (b) mechanism. Fuel type is syngas in non-premixed, counterflow model at 20 atm pressure.

The ten reactions with the highest integrated entropy production using the detailed mechanism are displayed in Figure 124. As for 10 atm, most of the reactions with the highest local production also have the highest integrated production.

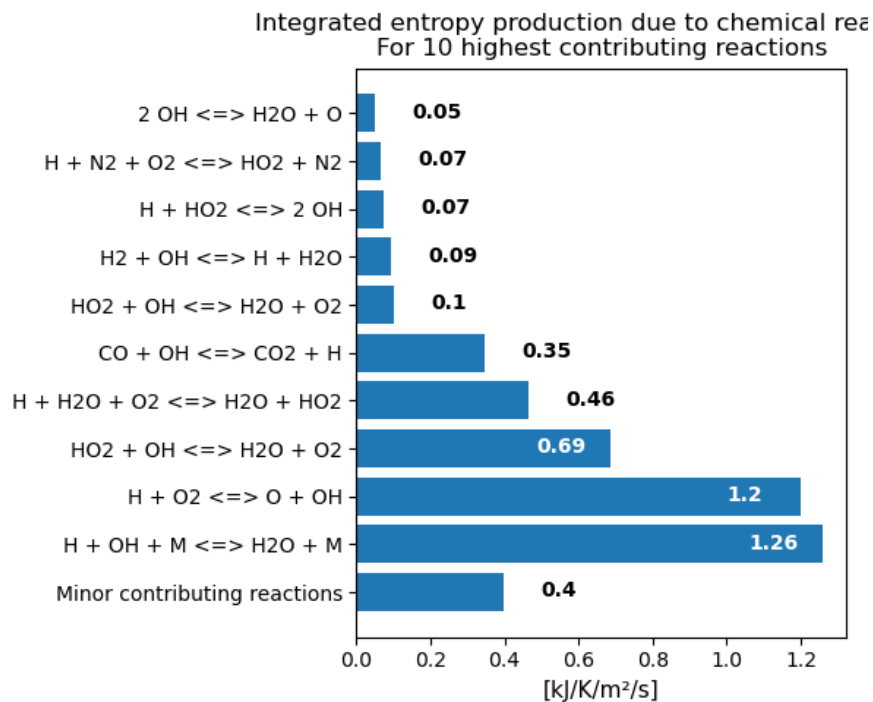


**Figure 124:** Integrated entropy production due to the highest contributing reactions, for detailed mechanism in non-premixed, counterflow model at 20 atm

In Figure 125, the ten reactions with highest integrated entropy production using the reduced mechanism are included. For the reduced mechanism the reactions with the highest integrated production, and the reactions with the highest local production are not as similar as for the detailed mechanism. Moreover, a second duplicate reaction have appeared in Figure 125. The fourth, and sixth highest contributing reactions are duplicates. If the contributions from these two were combined, it would be the third highest contribution.

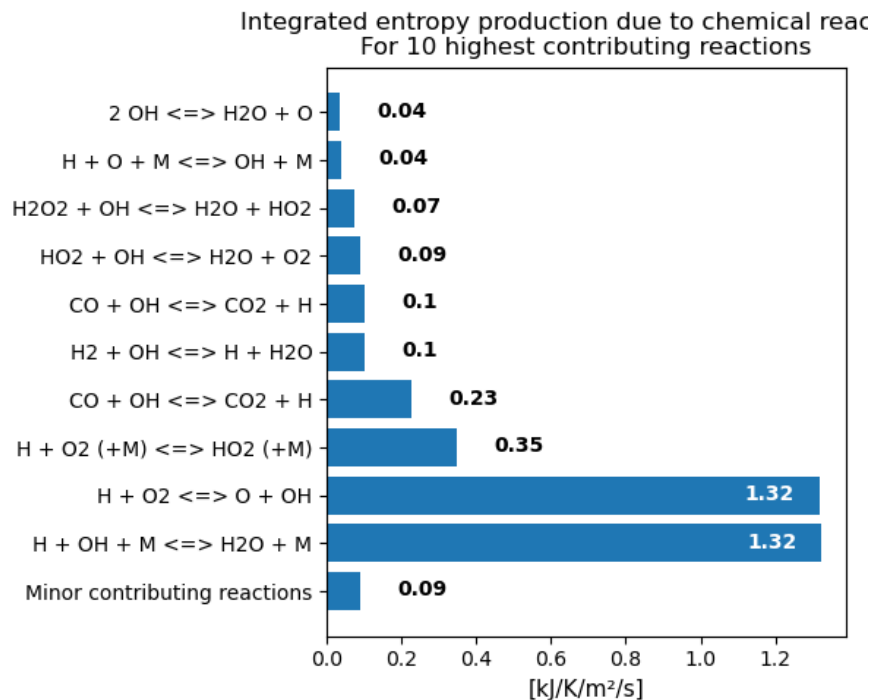


**Figure 125:** Integrated entropy production due to the highest contributing reactions, for reduced mechanism in non-premixed, counterflow model at 20 atm

In Figure 126 the graphs for the local (Figure 126a), and integrated (Figure 126b) entropy production, using the global mechanism are included. The shapes of the profiles have changed compared with the results at 10 atm shown in Figure 118a. The integrated production from reaction 1 and reaction reaction 3 in Figure 126b have increased in magnitude. If summed together their combined contribution have increased, which is in to the change from 1 atm to 10 atm.

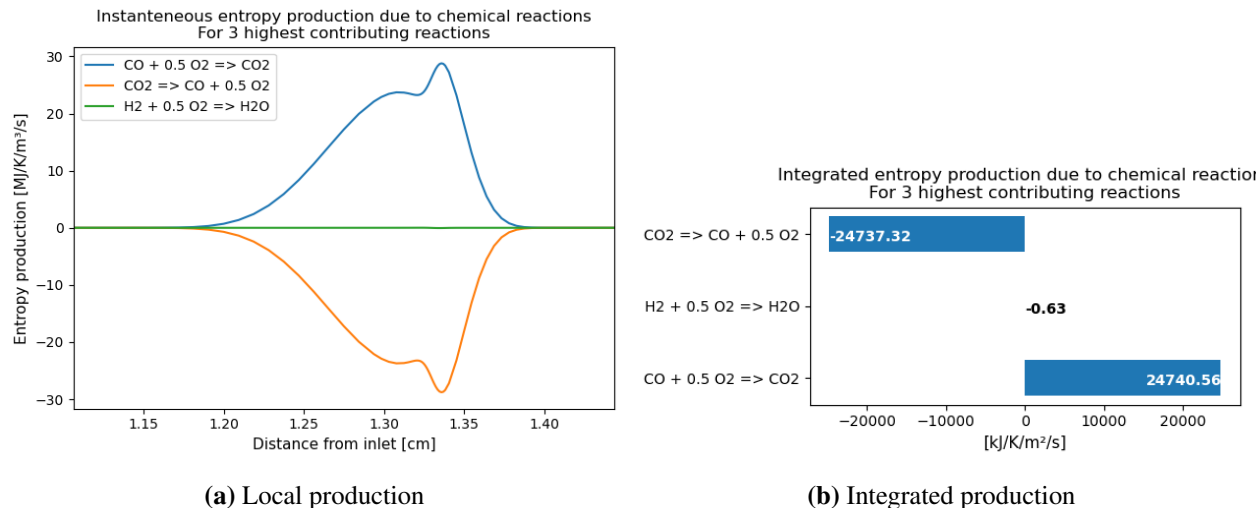


**Figure 126:** Comparison of the local (a), and integrated (b) entropy production due to the chemical reactions, using the global mechanism. Fuel type is syngas in non-premixed, counterflow model at 20 atm pressure.

### 5.7.5 Solution Grid

As for methane, the grid was determined by the grid refinement criteria presented in Section 3.3.2. With a pressure of 1 atm, the resolution varied in order of magnitude, between  $10^{-3}$ , and  $10^{-5}$  for all mechanisms. The resolution, spacing between the grid points, were given in meters. The global mechanism had most grid points (130), followed by the detailed (117), and reduced (109) mechanisms. When the pressure was increased to 10 atm, the resolution still had an order of magnitude, ranging from  $10^{-3}$ , to  $10^{-5}$  for all mechanisms. The number of grid points for the detailed, reduced, and global mechanisms were 128, 107, and 143, respectively. At 20 atm, the number of grid point were 123, 99, and 147 for the detailed, reduced, and global mechanisms respectively. The order of magnitude of the resolution varied between  $10^{-3}$  and  $10^{-5}$  for the detailed and reduced mechanisms, and between  $10^{-3}$  and  $10^{-6}$  for the global mechanism.

## 6 Conclusion

### 6.1 Objective

The objective of the project was determine a way to analyse the entropy production, and its spatial distribution, and thereafter perform such an analysis on the flame models mentioned, with variations in the conditions. In the analyses, methane and syngas were used as fuels. For each fuel one detailed, one reduced and one global mechanism were used. In addition to varying the fuel, and the degree of simplification in the chemical mechanisms, the pressure was varied between 1 atm, 10 atm and 20 atm. This resulted in a total number of 54 individual cases, that could elucidate trends and parameters that increase, or decrease the entropy production.

The purpose of this section is to give an answer to the research question presented in Section 1.3.3, using the results presented in Section 5. It is therefore first explained how the entropy production was calculated. Then the effects of changing pressure and chemical mechanism had in each model is given.

### 6.2 Entropy Production

The entropy production, with its spatial distribution was calculated in a post-process analysis. Cantera [16] was used, with the programming language Python, as the tool to simulate the different cases and obtain the necessary results for the calculations. The entropy production from the irreversible processes of viscous dissipation, heat conduction, mass diffusion, and chemical reactions were included in all cases. Additionally, the entropy production from radiative heat loss was included for the non-premixed, counterflow flame.

Two obstacles was met in the effort to calculate the production. First, in the reactor it was necessary to account for the entropy production due internal heat transfer from the reactions to the fuel-air mixture, in addition to the production from the chemical reactions which initially was thought to be the only source.

Second, Cantera [16] does not provide the multi-component diffusion coefficients in each point. This was solved by iterating through each point in the solution, retrieving the species molar fluxes. The fluxes was then used in the calculation of the contribution from mass diffusion, circumventing the need for the multi-component diffusion coefficients.

### 6.3 Effect of Chemical Mechanism

The reduced mechanism chosen for methane worked well considering the calculation of the integrated entropy production in all models. In the freely-propagating flame model the reduced mechanism also performed well considering the local entropy production by source. With the counterflow flame model the reduced mechanism worked well at 1 atm, but had some discrepancy at the increased pressures with a delayed profile, more concentrated in one peak.

The values for the integrated entropy production calculated by the global mechanism for methane was in well agreement with the values calculated by the detailed mechanism, in all the models. However, the spatial distribution had some discrepancy at 1 atm for the freely-propagating flame model, but the discrepancies decreased with the increase pressure. For the counterflow flame model,

the global mechanism had similar profiles to the detailed mechanism at 1 atm, but had large discrepancies at increased pressures.

The reduced mechanism chosen for syngas worked well to calculate the integrated entropy production in all models. The spatial distribution of the entropy production was also in very good agreement with those calculated by the detailed mechanism.

Lastly, it was used two different global mechanisms for syngas. One was used in the freely-propagating flame, while the other was used in the well-stirred reactor, and counterflow flame. First, the global mechanism used in the freely-propagating flame was not appropriate to use for entropy analysis. It worked well to estimate the steady state temperature in the reactor, and to some degree the molar composition but calculated the entropy production poorly.

Second, the mechanism used in the reactor and counterflow flame obtained results for the integrated entropy production, that were in good agreement with those obtained with the detailed mechanism in the reactor and counterflow flame. However, it was a slight deviation for the reactor. The global mechanism calculated a negative contribution from the chemical reactions at 20 atm. Moreover, the profile for the local total entropy production using the global mechanism was surprisingly similar to the profile using the detailed mechanism.

## 6.4 Effect of Pressure

In the premixed well-stirred reactor model, the entropy production due to the chemical reactions decreased with pressure, while the contribution from the internal heating increased. This trend was seen for both fuels, using all mechanisms. The entropy production calculated was also in good agreement with the entropy change in the system.

When the entropy production was calculated for the premixed freely-propagating model, the integrated entropy production and entropy change increased with pressure for both fuels, with all mechanisms. The difference in production and change also increased with pressure. The profiles of the spatial distribution of the local entropy production showed similar trends for both fuels, where profiles got thinner and taller. However, the shape of the profiles using syngas as fuel was slightly more pressure dependent.

For the non-premixed counterflow model the integrate entropy production decreased with pressure for both fuels, with all mechanisms. The profile for the distribution of the local entropy production was not as sensitive to pressure changes as for the freely-propagating model. But had some unexpected trends worth investigating.



## References

- [1] Acampora, L., Kooshkbaghi, M., Frouzakis, C.E., Marra, F.S., 2019. Generalized entropy production analysis for mechanism reduction. *Combustion Theory and Modelling* 23, 197–209.
- [2] Acampora, L., Marra, F., 2017. Investigation by thermodynamic properties of methane combustion mechanisms under harmonic oscillations in perfectly stirred reactor. *Chemical Engineering Transactions* 57, 1459–1464.
- [3] Acampora, L., Marra, F., Martelli, E., 2016. Comparison of different CH<sub>4</sub>-air combustion mechanisms in a perfectly stirred reactor with oscillating residence times close to extinction. *Combustion Science and Technology* 188, 707–718.
- [4] Acampora, L., Marra, F.S., 2020. Second law thermodynamic analysis of syngas premixed flames. *International Journal of Hydrogen Energy* 45, 12185–12202.
- [5] Bejan, A., 1996. The equivalence of maximum power and minimum entropy generation rate in the optimization of power plants. *Journal of Energy Resources Technology* 118, 98–101.
- [6] Cantera, a. Cantera documentation. <https://cantera.org/documentation/index.html>. (Accessed on 05/03/2021).
- [7] Cantera, b. Cantera science. <https://cantera.org/science/index.html>. (Accessed on 12/04/2020).
- [8] Chen, S., Han, H., Liu, Z., Li, J., Zheng, C., 2010a. Analysis of entropy generation in non-premixed hydrogen versus heated air counter-flow combustion. *International Journal of Hydrogen Energy* 35, 4736–4746.
- [9] Chen, S., Liu, Z., Liu, J., Li, J., Wang, L., Zheng, C., 2010b. Analysis of entropy generation in hydrogen-enriched ultra-lean counter-flow methane–air non-premixed combustion. *International Journal of Hydrogen Energy* 35, 12491–12501.
- [10] Chen, S., Mi, J., Liu, H., Zheng, C., 2012. First and second thermodynamic-law analyses of hydrogen-air counter-flow diffusion combustion in various combustion modes. *International Journal of Hydrogen Energy* 37, 5234–5245.
- [11] Cuoci, A., Frassoldati, A., Faravelli, T., Ranzi, E., 2009. Accuracy and flexibility of simplified kinetic models for cfd applications, in: *Combust. Colloq*, pp. 1–6.
- [12] Dagaut, P., 2002. On the kinetics of hydrocarbons oxidation from natural gas to kerosene and diesel fuel. *Physical Chemistry Chemical Physics* 4, 2079–2094.
- [13] Datta, A., 2000. Entropy generation in a confined laminar diffusion flame. *Combustion Science and Technology* 159, 39–56.

- [14] Datta, A., 2005. Effects of gravity on structure and entropy generation of confined laminar diffusion flames. *International Journal of Thermal Sciences* 44, 429–440.
- [15] Davis, S.G., Joshi, A.V., Wang, H., Egolfopoulos, F., 2005. An optimized kinetic model of H<sub>2</sub>/CO combustion. *Proceedings of the Combustion Institute* 30, 1283–1292.
- [16] Goodwin, D.G., Speth, R.L., Moffat, H.K., Weber, B.W., 2018. Cantera: An object-oriented software toolkit for chemical kinetics, thermodynamics, and transport processes. <https://www.cantera.org>. doi:10.5281/zenodo.1174508. version 2.4.0.
- [17] IEA, 2020a. World energy balances. <https://www.iea.org/reports/world-energy-balances-overview#world>. (Accessed on 02/16/2021).
- [18] IEA, 2020b. World Energy Outlook 2020. Technical Report. IEA, Paris. <https://www.iea.org/reports/world-energy-outlook-2020>, (Accessed on 02/16/2021).
- [19] Jejurkar, S.Y., Mishra, D.P., 2011. Effects of wall thermal conductivity on entropy generation and exergy losses in a H<sub>2</sub>-air premixed flame microcombustor. *International Journal of Hydrogen Energy* 36, 15851–15859.
- [20] Jejurkar, S.Y., Mishra, D.P., 2013. Numerical analysis of entropy generation in an annular microcombustor using multistep kinetics. *Applied Thermal Engineering* 52, 394–401.
- [21] Johannessen, E., Kjelstrup, S., 2004. Minimum entropy production rate in plug flow reactors: An optimal control problem solved for SO<sub>2</sub> oxidation. *Energy* 29, 2403–2423.
- [22] Jones, N.H., Cizmas, P.G., Slattery, J.C., 2015. Creating reduced kinetics models that satisfy the entropy inequality. *Journal of Engineering for Gas Turbines and Power* 137.
- [23] Jones, W., Lindstedt, R., 1988. Global reaction schemes for hydrocarbon combustion. *Combustion and Flame* 73, 233–249.
- [24] Kazakov, A., Frenklach, M., . Reduced reaction sets based on gri-mech 1.2. <http://combustion.berkeley.edu/drm/>. (Accessed on 10/09/2020).
- [25] Kee, R.J., Coltrin, M.E., Glarborg, P., Zhu, H., 2005. *Chemically Reacting Flow: Theory and Practice*. 2nd ed., John Wiley & Sons.
- [26] Kooshkbaghi, M., Frouzakis, C.E., Boulouchos, K., Karlin, I.V., 2014. Entropy production analysis for mechanism reduction. *Combustion and Flame* 161, 1507–1515.
- [27] Lieuwen, T., Yang, V., Yetter, R., 2009. *Synthesis Gas Combustion: Fundamentals and Applications*. CRC press.
- [28] Liu, Y., Chen, S., Yang, B., Liu, K., Zheng, C., 2015. First and second thermodynamic-law comparison of biogas mild oxy-fuel combustion moderated by CO<sub>2</sub> or H<sub>2</sub>O. *Energy Conversion and Management* 106, 625–634.

- [29] Liu, Y., Rogg, B., 1991. Modelling of thermally radiating diffusion flames with detailed chemistry and transport, in: *Heat Transfer in Radiating and Combusting Systems*. Springer, pp. 114–127.
- [30] Lorentzen, S.J., 2020. Understanding energy conversion in combustion. Project assignment, preparation work for the master thesis submitted to NTNU.
- [31] Marra, F.S., Acampora, L., Martelli, E., 2015. Non-linear response to periodic forcing of methane-air global and detailed kinetics in continuous stirred tank reactors close to extinction conditions. *International Journal of Spray and Combustion Dynamics* 7, 175–208.
- [32] Marzouk, O.A., Huckaby, E.D., 2010. A comparative study of eight finite-rate chemistry kinetics for CO/H<sub>2</sub> combustion. *Engineering Applications of Computational Fluid Mechanics* 4, 331–356.
- [33] Mohammadi, I., Ajam, H., 2019. A theoretical study of entropy generation of the combustion phenomenon in the porous medium burner. *Energy* 188, 116004.
- [34] Moran, M.J., Shapiro, H.N., 2006. *Fundamentals of Engineering Thermodynamics*, SI Version. 5th ed., John Wiley & Sons.
- [35] Nishida, K., Takagi, T., Kinoshita, S., 2002. Analysis of entropy generation and exergy loss during combustion. *Proceedings of the Combustion Institute* 29, 869–874.
- [36] Nummedal, L., Kjelstrup, S., Costea, M., 2003. Minimizing the entropy production rate of an exothermic reactor with a constant heat-transfer coefficient: the ammonia reaction. *Industrial & Engineering Chemistry Research* 42, 1044–1056.
- [37] Porras, S., Bykov, V., Gol'dshtein, V., Maas, U., 2017. Joint characteristic timescales and entropy production analyses for model reduction of combustion systems. *Entropy* 19, 264.
- [38] Puri, I.K., 1992. Second law analysis of convective droplet burning. *International Journal of Hechenat and Mass Transfer* 35, 2571–2578.
- [39] Salimath, P.S., Ertesvåg, I.S., 2021. Local entropy generation and entropy fluxes of a transient flame during head-on quenching towards solid and hydrogen-permeable porous walls. *International Journal of Hydrogen Energy* (Accepted).
- [40] Slattery, J.C., Cizmas, P.G., Karpetis, A.N., Chambers, S.B., 2011. Role of differential entropy inequality in chemically reacting flows. *Chemical Engineering Science* 66, 5236–5243.
- [41] Smith, G.P., Golden, D.M., Frenklach, M., Moriarty, N.W., Eiteneer, B., Goldenberg, M., Bowman, C.T., Hanson, R.K., Song, S., Gardiner Jr, W., Lissianski, V.V., Qin, Z., . [https://me.berkeley.edu/gri\\_mech/](https://me.berkeley.edu/gri_mech/). (Accessed on 10/09/2020).
- [42] Som, S., Ramirez, A., Hagerdorn, J., Saveliev, A., Aggarwal, S., 2008. A numerical and experimental study of counterflow syngas flames at different pressures. *Fuel* 87, 319–334.

- [43] Sonntag, R.E., Van Wylen, G.J., 1991. Introduction to Thermodynamics: Classical and Statistical. Wiley New York.
- [44] Terzi, R., 2018. Application of exergy analysis to energy systems, in: Taner, T. (Ed.), Application of Exergy. IntechOp. chapter 6, pp. 109–125.
- [45] Turns, S.R., 1996. An Introduction to Combustion Concepts and Applications. 3rd ed., McGraw-Hill.
- [46] Watanabe, H., Otaka, M., 2006. Numerical simulation of coal gasification in entrained flow coal gasifier. Fuel 85, 1935–1943.
- [47] Westbrook, C.K., Dryer, F.L., 1981. Simplified reaction mechanisms for the oxidation of hydrocarbon fuels in flames. Combustion Science and Technology 27, 31–43.
- [48] Westbrook, C.K., Dryer, F.L., 1984. Chemical kinetic modeling of hydrocarbon combustion. Progress in Energy and Combustion Science 10, 1–57.
- [49] Zuo, W., Zhang, Y., Li, J., Li, Q., He, Z., 2019. A modified micro reactor fueled with hydrogen for reducing entropy generation. International Journal of Hydrogen Energy 44, 27984–27994.

# Appendices



5,86E-06	5,86E-06	4,69E-05	1,76E-05	9,38E-05	5,86E-06
8,79E-06	8,79E-06	4,69E-05	2,34E-05	9,38E-05	8,79E-06
1,17E-05	1,17E-05	7,03E-05	2,34E-05	0,000141	1,17E-05
1,17E-05	1,17E-05	9,38E-05	2,34E-05	0,000188	1,76E-05
1,17E-05	1,17E-05	0,000141	2,34E-05	0,000188	2,34E-05
1,17E-05	1,17E-05	0,000188	3,52E-05	0,000281	2,34E-05
1,17E-05	1,17E-05	0,000188	4,69E-05	0,000563	3,52E-05
1,17E-05	1,17E-05	0,000281	7,03E-05	0,001125	4,69E-05
1,17E-05	1,17E-05	0,000563	9,38E-05	0,001875	7,03E-05
1,17E-05	1,17E-05	0,00075	0,000141	0,002625	9,38E-05
8,79E-06	8,79E-06	0,00075	0,000188	0,00375	9,38E-05
5,86E-06	5,86E-06	0,00075	0,000188	0,00525	0,000141
8,79E-06	8,79E-06	0,001125	0,000281	0,006	0,000188
1,17E-05	1,17E-05	0,00225	0,000563		0,000188
1,17E-05	1,17E-05	0,00375	0,00075		0,000281
1,17E-05	1,17E-05	0,00525	0,00075		0,000563
1,17E-05	1,17E-05	0,006	0,00075		0,00075
1,17E-05	1,17E-05		0,001125		0,00075
1,17E-05	1,17E-05		0,0015		0,00075
1,17E-05	1,17E-05		0,0015		0,001125
1,76E-05	1,76E-05		0,0015		0,0015
2,34E-05	2,34E-05		0,00225		0,0015
2,34E-05	2,34E-05		0,0045		0,0015
2,34E-05	2,34E-05		0,006		0,00225
3,52E-05	3,52E-05				0,0045
4,69E-05	4,69E-05				0,006
7,03E-05	7,03E-05				
9,38E-05	9,38E-05				
0,000141	0,000141				
0,000188	0,000188				
0,000281	0,000281				
0,000563	0,000563				
0,00075	0,00075				
0,00075	0,00075				
0,00075	0,00075				
0,001125	0,001125				
0,0015	0,0015				
0,0015	0,0015				
0,0015	0,0015				
0,00225	0,00225				
0,0045	0,0045				
0,006	0,006				

Comparison of spatial resolution dx, for premixed, freely-propagating syngas flame

1 atm			10 atm			20 atm		
Reduced	Detailed	Global	Reduced	Detailed	Global	Reduced	Detailed	Global
0,006	0,006	0,006	0,006	0,006	0,006	0,006	0,006	0,006
0,0045	0,0045	0,0045	0,0045	0,0045	0,0045	0,0045	0,0045	0,0045
0,003	0,003	0,003	0,003	0,003	0,003	0,003	0,003	0,003
0,003	0,003	0,003	0,003	0,003	0,003	0,003	0,003	0,003
0,002625	0,002625	0,002625	0,002625	0,002625	0,002625	0,002625	0,002625	0,002625
0,001875	0,001875	0,001875	0,001875	0,001875	0,001875	0,001875	0,001875	0,001875
0,001125	0,001125	0,001125	0,001125	0,001125	0,001125	0,001125	0,001125	0,001125
0,000563	0,000563	0,000563	0,000563	0,000563	0,000563	0,000563	0,000563	0,000563
0,000375	0,000375	0,000375	0,000375	0,000375	0,000375	0,000375	0,000375	0,000375
0,000281	0,000281	0,000328	0,000328	0,000328	0,000328	0,000328	0,000328	0,000328
0,000141	0,000141	0,000211	0,000211	0,000211	0,000211	0,000211	0,000211	0,000211
9,38E-05	9,38E-05	0,000117	0,000117	0,000117	0,000141	0,000117	0,000117	0,000141
7,03E-05	7,03E-05	7,03E-05	7,03E-05	7,03E-05	0,000105	7,03E-05	7,03E-05	0,000105
4,69E-05	4,69E-05	4,69E-05	4,69E-05	4,69E-05	5,86E-05	4,69E-05	4,69E-05	5,86E-05
4,69E-05	4,69E-05	3,52E-05	3,52E-05	3,52E-05	3,52E-05	3,52E-05	3,52E-05	3,52E-05
3,52E-05	3,52E-05	2,34E-05	2,34E-05	2,34E-05	1,76E-05	2,34E-05	2,34E-05	1,76E-05
2,34E-05	2,34E-05	2,34E-05	2,34E-05	2,34E-05	1,17E-05	2,34E-05	2,34E-05	1,17E-05
1,76E-05	2,34E-05	1,76E-05	1,76E-05	1,76E-05	8,79E-06	1,76E-05	1,76E-05	8,79E-06
1,17E-05	1,76E-05	1,17E-05	1,17E-05	1,17E-05	4,39E-06	1,17E-05	1,17E-05	5,86E-06
1,17E-05	1,17E-05	8,79E-06	8,79E-06	8,79E-06	2,93E-06	8,79E-06	8,79E-06	4,39E-06
1,17E-05	1,17E-05	5,86E-06	5,86E-06	5,86E-06	2,93E-06	5,86E-06	5,86E-06	2,2E-06
1,17E-05	1,17E-05	5,86E-06	5,86E-06	5,86E-06	2,2E-06	5,86E-06	5,86E-06	1,46E-06
1,17E-05	1,17E-05	5,86E-06	5,86E-06	5,86E-06	1,1E-06	4,39E-06	4,39E-06	1,1E-06
8,79E-06	8,79E-06	5,86E-06	5,86E-06	5,86E-06	7,32E-07	2,93E-06	2,93E-06	7,32E-07
5,86E-06	5,86E-06	5,86E-06	4,39E-06	4,39E-06	7,32E-07	2,93E-06	2,93E-06	7,32E-07
5,86E-06	5,86E-06	5,86E-06	2,93E-06	2,93E-06	7,32E-07	2,93E-06	2,93E-06	5,49E-07
5,86E-06	5,86E-06	4,39E-06	2,93E-06	2,93E-06	7,32E-07	2,93E-06	2,93E-06	3,66E-07
5,86E-06	5,86E-06	2,93E-06	2,2E-06	2,2E-06	7,32E-07	2,93E-06	2,93E-06	3,66E-07
5,86E-06	5,86E-06	2,93E-06	1,46E-06	1,46E-06	7,32E-07	2,93E-06	2,93E-06	3,66E-07
5,86E-06	5,86E-06	2,93E-06	1,46E-06	1,46E-06	7,32E-07	2,2E-06	2,93E-06	3,66E-07
5,86E-06	5,86E-06	2,2E-06	1,46E-06	1,46E-06	7,32E-07	1,46E-06	2,2E-06	3,66E-07
8,79E-06	8,79E-06	1,46E-06	1,46E-06	1,46E-06	5,49E-07	1,46E-06	1,46E-06	3,66E-07
1,17E-05	1,17E-05	1,46E-06	1,1E-06	1,1E-06	3,66E-07	1,46E-06	1,46E-06	3,66E-07
1,17E-05	1,17E-05	1,46E-06	7,32E-07	7,32E-07	3,66E-07	1,46E-06	1,1E-06	3,66E-07
1,17E-05	1,17E-05	1,46E-06	7,32E-07	7,32E-07	2,75E-07	1,1E-06	7,32E-07	3,66E-07
1,17E-05	1,17E-05	1,46E-06	7,32E-07	7,32E-07	1,83E-07	7,32E-07	7,32E-07	2,75E-07
1,17E-05	1,17E-05	1,46E-06	7,32E-07	7,32E-07	1,83E-07	7,32E-07	7,32E-07	1,83E-07
1,17E-05	1,17E-05	1,46E-06	7,32E-07	7,32E-07	1,83E-07	7,32E-07	7,32E-07	1,37E-07
1,17E-05	1,17E-05	1,46E-06	1,1E-06	1,1E-06	1,83E-07	7,32E-07	7,32E-07	9,16E-08
1,17E-05	1,17E-05	1,46E-06	1,46E-06	1,46E-06	1,83E-07	7,32E-07	7,32E-07	9,16E-08
1,17E-05	1,17E-05	1,46E-06	1,46E-06	1,46E-06	1,83E-07	7,32E-07	7,32E-07	9,16E-08
1,17E-05	1,17E-05	1,46E-06	1,46E-06	1,46E-06	1,83E-07	7,32E-07	7,32E-07	9,16E-08
1,17E-05	1,17E-05	2,2E-06	1,46E-06	1,46E-06	1,83E-07	7,32E-07	7,32E-07	9,16E-08
1,76E-05	1,17E-05	2,93E-06	1,46E-06	1,46E-06	1,83E-07	7,32E-07	7,32E-07	9,16E-08
2,34E-05	1,17E-05	4,39E-06	1,46E-06	1,46E-06	1,83E-07	7,32E-07	7,32E-07	9,16E-08
2,34E-05	1,17E-05	5,86E-06	1,46E-06	1,46E-06	1,83E-07	7,32E-07	7,32E-07	1,37E-07
2,34E-05	1,76E-05	5,86E-06	1,46E-06	1,46E-06	1,83E-07	7,32E-07	7,32E-07	1,37E-07
2,34E-05	2,34E-05	8,79E-06	1,46E-06	1,46E-06	1,83E-07	7,32E-07	7,32E-07	9,16E-08
2,34E-05	2,34E-05	1,17E-05	1,46E-06	1,46E-06	1,83E-07	1,1E-06	7,32E-07	9,16E-08
2,34E-05	2,34E-05	1,76E-05	1,46E-06	1,46E-06	1,83E-07	1,1E-06	7,32E-07	9,16E-08
2,34E-05	2,34E-05	2,34E-05	1,46E-06	1,46E-06	1,83E-07	7,32E-07	7,32E-07	9,16E-08
2,34E-05	2,34E-05	2,34E-05	1,46E-06	1,46E-06	1,83E-07	7,32E-07	7,32E-07	9,16E-08
2,34E-05	2,34E-05	3,52E-05	2,2E-06	2,2E-06	1,83E-07	7,32E-07	7,32E-07	9,16E-08
2,34E-05	2,34E-05	4,1E-05	2,93E-06	2,93E-06	1,83E-07	1,1E-06	7,32E-07	9,16E-08
3,52E-05	2,34E-05	7,03E-05	2,93E-06	2,93E-06	2,75E-07	1,46E-06	7,32E-07	1,37E-07
4,69E-05	3,52E-05	0,000117	2,93E-06	2,93E-06	3,66E-07	1,46E-06	1,1E-06	1,83E-07
4,69E-05	4,69E-05	0,000211	2,93E-06	2,93E-06	3,66E-07	1,46E-06	1,46E-06	1,83E-07
4,69E-05	4,69E-05	0,000328	2,93E-06	2,93E-06	5,49E-07	1,46E-06	1,46E-06	2,75E-07
4,69E-05	4,69E-05	0,000469	4,39E-06	4,39E-06	1,1E-06	1,46E-06	1,46E-06	3,66E-07
7,03E-05	4,69E-05	0,000563	5,86E-06	5,86E-06	1,46E-06	1,46E-06	1,46E-06	3,66E-07
9,38E-05	7,03E-05	0,000656	5,86E-06	5,86E-06	2,2E-06	2,2E-06	1,46E-06	5,49E-07
0,000141	9,38E-05	0,001125	8,79E-06	8,79E-06	4,39E-06	2,93E-06	2,2E-06	7,32E-07
0,000188	0,000141	0,00225	1,76E-05	1,76E-05	5,86E-06	4,39E-06	2,93E-06	7,32E-07
0,000281	0,000188	0,00375	2,34E-05	2,34E-05	8,79E-06	5,86E-06	4,39E-06	1,1E-06
0,000375	0,000281	0,00675	2,34E-05	2,34E-05	1,17E-05	5,86E-06	5,86E-06	1,46E-06
0,000375	0,000375	0,0075	3,52E-05	3,52E-05	1,76E-05	8,79E-06	5,86E-06	2,2E-06
0,000563	0,000375	0,009	4,69E-05	4,69E-05	3,52E-05	1,17E-05	8,79E-06	4,39E-06
0,001125	0,000563	0,012	4,69E-05	4,69E-05	5,86E-05	1,76E-05	1,17E-05	5,86E-06
0,0015	0,001125		4,69E-05	4,69E-05	8,2E-05	2,34E-05	1,76E-05	8,79E-06
0,0015	0,0015		4,69E-05	4,69E-05	0,000117	2,34E-05	2,34E-05	1,17E-05
0,0015	0,0015		7,03E-05	7,03E-05	0,000141	3,52E-05	2,34E-05	1,76E-05
0,00225	0,0015		9,38E-05	9,38E-05	0,000164	4,69E-05	3,52E-05	2,93E-05
0,003	0,00225		0,000141	0,000141	0,000281	4,69E-05	4,69E-05	3,52E-05



0,003	0,003	0,000188	0,000188	0,000469	4,69E-05	4,69E-05	4,1E-05
0,003	0,003	0,000188	0,000188	0,000563	4,69E-05	4,69E-05	7,03E-05
0,0045	0,003	0,000281	0,000281	0,000656	7,03E-05	4,69E-05	0,000117
0,009	0,0045	0,000563	0,000375	0,001125	9,38E-05	7,03E-05	0,000141
0,012	0,0045	0,00075	0,000375	0,00225	0,000141	9,38E-05	0,000164
	0,00225	0,001125	0,000563	0,00375	0,000281	0,000141	0,000281
	0,0015	0,00225	0,001125	0,00675	0,000375	0,000188	0,000469
	0,0015	0,00375	0,0015	0,0075	0,000563	0,000188	0,000563
	0,0015	0,00525	0,0015	0,009	0,00075	0,000281	0,000656
	0,001125	0,0075	0,0015	0,012	0,001125	0,000563	0,001125
	0,00075	0,0105	0,00225		0,00225	0,00075	0,00225
	0,000563	0,012	0,003		0,00375	0,001125	0,00375
	0,000375		0,003		0,00675	0,0015	0,00675
	0,000375		0,003		0,0075	0,0015	0,0075
	0,000375		0,0045		0,009	0,0015	0,009
	0,000375		0,009		0,012	0,00225	0,012
			0,012			0,003	
						0,003	
						0,003	
						0,0045	
						0,009	
						0,012	

Comparison of spatial resolution dx, for counterflow methane flame

1 atm			10 atm			20 atm		
Reduced	Detailed	Global	Reduced	Detailed	Global	Reduced	Detailed	Global
0,000638	0,000638	0,000682	0,001364	0,000682	0,000682	0,001364	0,000682	0,000652
0,000638	0,000638	0,000682	0,001364	0,000682	0,000682	0,001364	0,000682	0,000652
0,000638	0,000638	0,000682	0,001364	0,000682	0,000682	0,001364	0,000682	0,000652
0,000638	0,000638	0,000682	0,001364	0,000682	0,000682	0,001364	0,000682	0,000652
0,000638	0,000638	0,000682	0,001023	0,000682	0,000682	0,001023	0,000682	0,000652
0,000638	0,000638	0,000682	0,000682	0,000682	0,000682	0,000682	0,000682	0,000652
0,000638	0,000638	0,000682	0,000682	0,000682	0,000682	0,000682	0,000682	0,000652
0,000638	0,000638	0,000682	0,000511	0,000682	0,000682	0,000511	0,000682	0,000652
0,000638	0,000638	0,000682	0,000341	0,000682	0,000682	0,000341	0,000682	0,000652
0,000638	0,000638	0,000682	0,000256	0,000682	0,000682	0,000256	0,000682	0,000652
0,000638	0,000638	0,000682	0,00017	0,000682	0,000682	0,00017	0,000682	0,000652
0,000638	0,000638	0,000682	0,00017	0,000682	0,000682	0,00017	0,000682	0,000652
0,000638	0,000479	0,000511	0,00017	0,000511	0,000511	0,00017	0,000511	0,000489
0,000638	0,000319	0,000341	0,00017	0,000341	0,000341	0,00017	0,000341	0,000326
0,000479	0,000319	0,000256	0,000128	0,000256	0,000256	0,000128	0,000256	0,000326
0,000239	0,000319	0,00017	8,52E-05	0,00017	0,00017	8,52E-05	0,00017	0,000326
0,00016	0,000239	0,00017	8,52E-05	0,00017	0,00017	8,52E-05	0,00017	0,000245
0,00012	0,00016	0,000128	8,52E-05	0,000128	0,000128	8,52E-05	0,000128	0,000163
7,98E-05	0,00012	8,52E-05	8,52E-05	8,52E-05	8,52E-05	8,52E-05	8,52E-05	0,000122
7,98E-05	7,98E-05	8,52E-05	8,52E-05	8,52E-05	8,52E-05	8,52E-05	8,52E-05	8,15E-05
7,98E-05	7,98E-05	6,39E-05	0,000128	8,52E-05	6,39E-05	0,000128	8,52E-05	8,15E-05
7,98E-05	7,98E-05	4,26E-05	0,00017	6,39E-05	4,26E-05	0,00017	6,39E-05	8,15E-05
7,98E-05	7,98E-05	4,26E-05	0,00017	4,26E-05	4,26E-05	0,00017	4,26E-05	6,11E-05
7,98E-05	5,98E-05	4,26E-05	0,00017	4,26E-05	4,26E-05	0,00017	4,26E-05	4,08E-05
7,98E-05	3,99E-05	4,26E-05	0,00017	4,26E-05	4,26E-05	0,00017	4,26E-05	4,08E-05
0,00012	3,99E-05	3,2E-05	0,00017	4,26E-05	4,26E-05	0,00017	4,26E-05	4,08E-05
0,00016	3,99E-05	2,13E-05	0,00017	3,2E-05	3,2E-05	0,00017	3,2E-05	3,06E-05
0,00016	3,99E-05	2,13E-05	0,000128	2,13E-05	2,13E-05	0,000128	2,13E-05	2,04E-05
0,00016	3,99E-05	2,13E-05	6,39E-05	2,13E-05	2,13E-05	6,39E-05	2,13E-05	2,04E-05
0,00016	3,99E-05	2,13E-05	4,26E-05	2,13E-05	2,13E-05	4,26E-05	2,13E-05	2,04E-05
0,00016	3,99E-05	2,13E-05	4,26E-05	2,13E-05	2,13E-05	4,26E-05	2,13E-05	2,04E-05
0,00016	3,99E-05	2,13E-05	4,26E-05	2,13E-05	2,13E-05	4,26E-05	2,13E-05	2,04E-05
0,00012	3,99E-05	2,13E-05	4,26E-05	2,13E-05	2,13E-05	4,26E-05	2,13E-05	2,04E-05
7,98E-05	3,99E-05	2,13E-05	4,26E-05	2,13E-05	2,13E-05	4,26E-05	2,13E-05	2,04E-05
7,98E-05	3,99E-05	2,13E-05	4,26E-05	2,13E-05	2,13E-05	4,26E-05	2,13E-05	2,04E-05
7,98E-05	3,99E-05	3,2E-05	4,26E-05	2,13E-05	2,13E-05	4,26E-05	2,13E-05	2,04E-05
7,98E-05	3,99E-05	4,26E-05	4,26E-05	3,2E-05	2,13E-05	4,26E-05	2,13E-05	2,04E-05
7,98E-05	3,99E-05	4,26E-05	4,26E-05	4,26E-05	2,13E-05	4,26E-05	2,13E-05	2,04E-05
7,98E-05	3,99E-05	4,26E-05	4,26E-05	4,26E-05	3,2E-05	4,26E-05	2,13E-05	3,06E-05
5,98E-05	3,99E-05	6,39E-05	4,26E-05	4,26E-05	4,26E-05	4,26E-05	2,13E-05	4,08E-05
3,99E-05	3,99E-05	8,52E-05	4,26E-05	4,26E-05	4,26E-05	4,26E-05	2,13E-05	4,08E-05
3,99E-05	3,99E-05	8,52E-05	4,26E-05	4,26E-05	4,26E-05	4,26E-05	2,13E-05	4,08E-05
3,99E-05	3,99E-05	8,52E-05	4,26E-05	4,26E-05	6,39E-05	4,26E-05	3,2E-05	6,11E-05
2,99E-05	3,99E-05	8,52E-05	3,2E-05	4,26E-05	8,52E-05	3,2E-05	4,26E-05	8,15E-05
1,99E-05	3,99E-05	8,52E-05	2,13E-05	4,26E-05	8,52E-05	2,13E-05	4,26E-05	8,15E-05
1,99E-05	3,99E-05	8,52E-05	2,13E-05	4,26E-05	8,52E-05	2,13E-05	4,26E-05	8,15E-05
1,99E-05	3,99E-05	8,52E-05	2,13E-05	4,26E-05	8,52E-05	2,13E-05	4,26E-05	8,15E-05
1,99E-05	3,99E-05	8,52E-05	1,6E-05	4,26E-05	8,52E-05	1,6E-05	4,26E-05	8,15E-05
1,99E-05	3,99E-05	8,52E-05	1,07E-05	4,26E-05	8,52E-05	1,07E-05	4,26E-05	8,15E-05
1,99E-05	3,99E-05	8,52E-05	1,07E-05	4,26E-05	8,52E-05	1,07E-05	4,26E-05	8,15E-05
1,99E-05	3,99E-05	8,52E-05	1,07E-05	6,39E-05	8,52E-05	1,07E-05	4,26E-05	8,15E-05
1,99E-05	5,98E-05	8,52E-05	1,07E-05	8,52E-05	8,52E-05	7,99E-06	4,26E-05	8,15E-05
1,99E-05	7,98E-05	8,52E-05	1,07E-05	8,52E-05	8,52E-05	5,33E-06	4,26E-05	8,15E-05
1,5E-05	7,98E-05	8,52E-05	7,99E-06	8,52E-05	8,52E-05	5,33E-06	6,39E-05	8,15E-05
9,97E-06	7,98E-05	8,52E-05	5,33E-06	8,52E-05	8,52E-05	4E-06	8,52E-05	8,15E-05
9,97E-06	7,98E-05	0,000128	5,33E-06	8,52E-05	8,52E-05	2,66E-06	8,52E-05	8,15E-05
9,97E-06	7,98E-05	0,00017	5,33E-06	8,52E-05	8,52E-05	2,66E-06	8,52E-05	8,15E-05
9,97E-06	7,98E-05	0,00017	5,33E-06	8,52E-05	0,000128	2,66E-06	8,52E-05	0,000122
9,97E-06	5,98E-05	0,000128	5,33E-06	6,39E-05	0,00017	4E-06	6,39E-05	0,000163
9,97E-06	3,99E-05	6,39E-05	5,33E-06	3,2E-05	0,00017	5,33E-06	4,26E-05	0,000163
9,97E-06	3,99E-05	4,26E-05	5,33E-06	2,13E-05	0,000128	5,33E-06	4,26E-05	0,000122
9,97E-06	3,99E-05	4,26E-05	7,99E-06	2,13E-05	6,39E-05	5,33E-06	4,26E-05	6,11E-05
9,97E-06	3,99E-05	4,26E-05	1,07E-05	2,13E-05	4,26E-05	5,33E-06	4,26E-05	4,08E-05
9,97E-06	3,99E-05	4,26E-05	1,07E-05	2,13E-05	4,26E-05	5,33E-06	4,26E-05	3,06E-05
9,97E-06	3,99E-05	3,2E-05	1,07E-05	2,13E-05	3,2E-05	5,33E-06	4,26E-05	2,04E-05
1,5E-05	3,99E-05	2,13E-05	1,07E-05	2,13E-05	2,13E-05	5,33E-06	4,26E-05	2,04E-05
1,99E-05	3,99E-05	2,13E-05	1,07E-05	2,13E-05	1,6E-05	5,33E-06	4,26E-05	2,04E-05
1,99E-05	3,99E-05	1,6E-05	1,07E-05	2,13E-05	1,07E-05	5,33E-06	4,26E-05	2,04E-05
1,99E-05	3,99E-05	1,07E-05	1,07E-05	2,13E-05	1,07E-05	5,33E-06	3,2E-05	2,04E-05
1,99E-05	3,99E-05	1,07E-05	1,07E-05	2,13E-05	1,07E-05	5,33E-06	2,13E-05	1,53E-05
1,99E-05	2,99E-05	1,07E-05	1,07E-05	2,13E-05	7,99E-06	5,33E-06	2,13E-05	1,02E-05
1,99E-05	1,99E-05	1,07E-05	1,07E-05	2,13E-05	5,33E-06	5,33E-06	2,13E-05	1,02E-05

1,99E-05	1,99E-05	1,07E-05	1,07E-05	2,13E-05	5,33E-06	5,33E-06	2,13E-05	7,64E-06
2,99E-05	1,99E-05	1,07E-05	1,6E-05	2,13E-05	5,33E-06	7,99E-06	2,13E-05	5,1E-06
3,99E-05	1,99E-05	1,07E-05	2,13E-05	2,13E-05	4E-06	1,07E-05	2,13E-05	5,1E-06
3,99E-05	1,99E-05	1,07E-05	2,13E-05	2,13E-05	2,66E-06	1,07E-05	2,13E-05	5,1E-06
3,99E-05	1,99E-05	1,07E-05	2,13E-05	2,13E-05	2,66E-06	1,07E-05	2,13E-05	5,1E-06
3,99E-05	1,99E-05	1,07E-05	2,13E-05	2,13E-05	2,66E-06	1,6E-05	2,13E-05	5,1E-06
3,99E-05	1,99E-05	1,07E-05	3,2E-05	2,13E-05	2,66E-06	2,13E-05	2,13E-05	3,82E-06
3,99E-05	1,99E-05	1,07E-05	4,26E-05	2,13E-05	2,66E-06	2,13E-05	2,13E-05	2,55E-06
3,99E-05	1,99E-05	1,07E-05	4,26E-05	2,13E-05	2,66E-06	3,2E-05	2,13E-05	2,55E-06
3,99E-05	1,99E-05	1,6E-05	6,39E-05	2,13E-05	2,66E-06	4,26E-05	2,13E-05	2,55E-06
3,99E-05	1,5E-05	2,13E-05	8,52E-05	2,13E-05	2,66E-06	4,26E-05	2,13E-05	2,55E-06
5,98E-05	9,97E-06	2,13E-05	8,52E-05	2,13E-05	2,66E-06	4,26E-05	2,13E-05	2,55E-06
5,98E-05	9,97E-06	2,13E-05	0,000128	2,13E-05	2,66E-06	4,26E-05	2,13E-05	2,55E-06
3,99E-05	9,97E-06	2,13E-05	0,00017	2,13E-05	2,66E-06	6,39E-05	2,13E-05	2,55E-06
2,99E-05	9,97E-06	2,13E-05	0,00017	2,13E-05	2,66E-06	8,52E-05	2,13E-05	1,91E-06
1,99E-05	9,97E-06	3,2E-05	0,00017	2,13E-05	2,66E-06	8,52E-05	2,13E-05	1,27E-06
1,99E-05	9,97E-06	4,26E-05	0,00017	2,13E-05	2,66E-06	0,000128	2,13E-05	1,91E-06
1,99E-05	9,97E-06	4,26E-05	0,00017	1,6E-05	2,66E-06	0,00017	2,13E-05	2,55E-06
1,99E-05	9,97E-06	4,26E-05	0,00017	1,07E-05	2,66E-06	0,00017	2,13E-05	2,55E-06
1,99E-05	9,97E-06	4,26E-05	0,00017	1,07E-05	2,66E-06	0,00017	2,13E-05	2,55E-06
1,99E-05	9,97E-06	4,26E-05	0,000256	1,07E-05	2,66E-06	0,00017	1,6E-05	2,55E-06
1,99E-05	9,97E-06	4,26E-05	0,000341	1,07E-05	2,66E-06	0,00017	1,07E-05	2,55E-06
2,99E-05	9,97E-06	4,26E-05	0,000341	1,07E-05	2,66E-06	0,00017	1,07E-05	2,55E-06
3,99E-05	7,48E-06	4,26E-05	0,000341	1,07E-05	2,66E-06	0,00017	1,07E-05	2,55E-06
3,99E-05	4,99E-06	4,26E-05	0,000341	1,07E-05	2,66E-06	0,000256	1,07E-05	2,55E-06
3,99E-05	4,99E-06	4,26E-05	0,000341	1,07E-05	2,66E-06	0,000341	1,07E-05	2,55E-06
3,99E-05	4,99E-06	4,26E-05	0,000511	1,07E-05	4E-06	0,000341	1,07E-05	2,55E-06
3,99E-05	4,99E-06	4,26E-05	0,000682	7,99E-06	5,33E-06	0,000341	1,07E-05	2,55E-06
5,98E-05	4,99E-06	4,26E-05	0,000682	5,33E-06	7,99E-06	0,000341	1,07E-05	2,55E-06
7,98E-05	4,99E-06	4,26E-05	0,001023	5,33E-06	1,07E-05	0,000341	1,07E-05	2,55E-06
7,98E-05	4,99E-06	4,26E-05	0,001364	5,33E-06	1,07E-05	0,000511	1,07E-05	2,55E-06
0,00012	4,99E-06	4,26E-05	0,001364	5,33E-06	1,6E-05	0,000682	1,07E-05	3,82E-06
0,00016	4,99E-06	4,26E-05	0,001364	5,33E-06	2,13E-05	0,000682	7,99E-06	5,1E-06
0,000239	4,99E-06	4,26E-05	0,002045	5,33E-06	3,2E-05	0,001023	5,33E-06	5,1E-06
0,000319	4,99E-06	4,26E-05	0,002727	4E-06	4,26E-05	0,001364	5,33E-06	5,1E-06
0,000479	4,99E-06	4,26E-05	0,002727	2,66E-06	4,26E-05	0,001364	4E-06	7,64E-06
0,000638	4,99E-06	4,26E-05		2,66E-06	4,26E-05	0,001364	2,66E-06	1,02E-05
0,000638	4,99E-06	4,26E-05		2,66E-06	4,26E-05	0,002045	2,66E-06	1,53E-05
0,000638	4,99E-06	4,26E-05		2,66E-06	4,26E-05	0,002727	2,66E-06	2,04E-05
0,000638	4,99E-06	4,26E-05		2,66E-06	4,26E-05	0,002727	2,66E-06	3,06E-05
0,000638	4,99E-06	6,39E-05		2,66E-06	4,26E-05		2,66E-06	4,08E-05
0,000638	4,99E-06	8,52E-05		2,66E-06	4,26E-05		2,66E-06	4,08E-05
0,000638	4,99E-06	8,52E-05		2,66E-06	4,26E-05		2,66E-06	4,08E-05
0,000638	4,99E-06	8,52E-05		2,66E-06	4,26E-05		2,66E-06	4,08E-05
0,000638	4,99E-06	8,52E-05		2,66E-06	4,26E-05		2,66E-06	4,08E-05
0,000638	4,99E-06	8,52E-05		2,66E-06	4,26E-05		2,66E-06	4,08E-05
0,000638	4,99E-06	0,000128		2,66E-06	4,26E-05		2,66E-06	4,08E-05
0,000638	4,99E-06	0,00017		2,66E-06	4,26E-05		2,66E-06	4,08E-05
0,000638	4,99E-06	0,000256		2,66E-06	4,26E-05		2,66E-06	4,08E-05
0,000638	4,99E-06	0,000341		2,66E-06	4,26E-05		2,66E-06	4,08E-05
0,000638	4,99E-06	0,000341		2,66E-06	4,26E-05		2,66E-06	4,08E-05
0,000638	4,99E-06	0,000341		2,66E-06	4,26E-05		2,66E-06	4,08E-05
0,000638	4,99E-06	0,000341		2,66E-06	4,26E-05		2,66E-06	4,08E-05
0,000638	4,99E-06	0,000341		2,66E-06	4,26E-05		2,66E-06	4,08E-05
0,000638	4,99E-06	0,000511		2,66E-06	4,26E-05		2,66E-06	4,08E-05
0,000638	4,99E-06	0,000682		2,66E-06	4,26E-05		2,66E-06	4,08E-05
0,000638	4,99E-06	0,000682		2,66E-06	4,26E-05		2,66E-06	4,08E-05
0,000638	4,99E-06	0,001023		2,66E-06	4,26E-05		2,66E-06	4,08E-05
0,000638	4,99E-06	0,001364		2,66E-06	4,26E-05		2,66E-06	4,08E-05
0,000638	4,99E-06	0,001364		2,66E-06	4,26E-05		2,66E-06	4,08E-05
	4,99E-06	0,001364		2,66E-06	4,26E-05		2,66E-06	4,08E-05
	4,99E-06	0,001364		2,66E-06	6,39E-05		2,66E-06	4,08E-05
	4,99E-06	0,001364		2,66E-06	8,52E-05		2,66E-06	4,08E-05
	4,99E-06	0,001364		2,66E-06	8,52E-05		2,66E-06	4,08E-05
	7,48E-06	0,001364		2,66E-06	0,000128		2,66E-06	4,08E-05
	9,97E-06	0,001364		4E-06	0,00017		2,66E-06	4,08E-05
	9,97E-06			5,33E-06	0,000256		4E-06	6,11E-05
	9,97E-06			5,33E-06	0,000341		4E-06	8,15E-05
	9,97E-06			5,33E-06	0,000341		2,66E-06	8,15E-05
	9,97E-06			5,33E-06	0,000341		2,66E-06	8,15E-05
	9,97E-06			5,33E-06	0,000341		2,66E-06	8,15E-05
	9,97E-06			5,33E-06	0,000341		2,66E-06	0,000122
	9,97E-06			5,33E-06	0,000511		2,66E-06	0,000163
	9,97E-06			5,33E-06	0,000682		2,66E-06	0,000245
	9,97E-06			5,33E-06	0,000682		2,66E-06	0,000326
	9,97E-06			5,33E-06	0,001023		2,66E-06	0,000489
	9,97E-06			5,33E-06	0,001364		2,66E-06	0,000652









